GAMMA-RAY COMPTON SCATTERING STUDIES

by

Ronald S. Holt, B.Sc., M.Sc.

A thesis submitted for the degree of
Doctor of Philosophy of the University
of Warwick

Dept. of Physics,
University of Warwick

September, 1978

GAMMA-RAY COMPTON SCATTERING STUDIES

by

Ronald S. Holt, B.Sc., M.Sc.

A thesis submitted for the degree of
Doctor of Philosophy of the University
of Warwick

Dept. of Physics,
University of Warwick

September, 1978

To my wife and parents

CONTENTS

		page
CHAPTER 1	GENERAL INTRODUCTION	
1.1	Introduction	1
1.2	The Compton Profile and Momentum Distributions	4
1.2.1	Electron Behaviour in Momentum Space	7
1.3	Experimental Methods	13
1.3.1	Energy Limitations	17
1.3.2	Gamma-ray Sources	19
1.4	Aims of the Present Work	21
1.5	Plan of Thesis	24
CHAPTER 2	THEORY OF THE COMPTON PROCESS	
2.1	General Theory of Scattering Processes	25
2.2	Non-relativistic Compton Cross Section	27
2.3	Relativistic Compton Cross Section	29
2.4	Validity of the Impulse Approximation	33
2.5	Multiple Scattering Processes	34
CHAPTER 3	GAMMA-RAY DATA REDUCTION	
3.1	Introduction	38
3.2	Preliminary Calculations and Corrections	39
3.2.1	Energy Calibration	39
3.2.2	Background	40
3.2.3	Detector Efficiency	41
3.3	Deconvolution	42
3.4	Energy Dependent Corrections	46
3.4.1	Absorption	46
3.4.2	Cross Section Transformation	47
3.4.3	Normalisation	48
3.5	Multiple Scattering Correction	50
3.6	Computational Considerations	52
CHAPTER 4	^{241}Am COMPTON SPECTROMETERS	
4.1	Introduction	53
4.2	Disc Source Spectrometer	55
4.3	Annular Source Spectrometer	56
4.3.1	Design Considerations	56

4.3.2 Construction 58
4.3.3 Detection System 61
4.3.4 Geometrical Energy Broadening 62
4.4 Initial Test Results 64
4.4.1 Linearity of the Energy Scale 64
4.4.2 Detector Resolution 65
4.4.3 Sample Location 67
4.5 Initial Test Profiles 67
4.5.1 Statistical Accuracy and Reproducibility 68
4.5.2 Symmetry of the Profile 69
4.5.3 Qualitative Comparisons 71

CHAPTER 5 MOLECULAR COMPTON PROFILES: GASEOUS HYDROCARBONS

5.1 Introduction 73
5.1.1 Self-Consistent-Field Calculations 74
5.1.2 Localised Molecular Orbitals 76
5.1.3 Experimental Evidence 78
5.1.4 Aims of the Present Work 80
5.2 Initial Experimental Study 80
5.2.1 Experimental Method 82
5.2.2 Theoretical Profiles 83
5.3 Results and Discussion 85
5.3.1 Propene and Cyclopropane 85
5.3.2 2-Butene 87
5.3.3 Conclusions 88

CHAPTER 6 MOLECULAR COMPTON PROFILES: LIQUID HYDROCARBONS

6.1 Introduction 89
6.2 Experimental Details 90
6.3 Bond Compton Profiles 91
6.4 Group Compton Profiles 98
6.5 Absolute Compton Profiles 101
6.6 General Conclusions 105

CHAPTER 7 MEASUREMENTS WITH ^{198}Au

7.1 Introduction 108
7.2 Experimental Technique 110
7.2.1 Apparatus 110
7.2.2 Resolution Measurement 111
7.2.3 Detector Efficiency 113

7.2.4 Compton Profile Measurements 114
7.3 Compton Profiles of Nb and $NbH_{0.76}$ 115
7.3.1 Experimental Details 117
7.3.2 Results and Discussion 119
7.4 Compton Profile of Lead 122
7.4.1 Experimental Details and Results 123
7.5 General Discussion 124

CHAPTER 8 CONSTRUCTION OF A HIGH INTENSITY 412 KeV COMPTON SPECTROMETER

8.1 Background 128
8.2 Design and Construction Considerations 129
8.2.1 Compton Scattering Requirements 129
8.2.2 Gold Source Spectra 131
8.2.3 Shielding Materials 132
8.3 Details of the Design 134
8.3.1 The Source Block 134
8.3.2 The Source Holder 137
8.3.3 Collimators and Shielding 138
8.3.4 Sample Chamber 139
8.4 Detector and Electronics 140
8.5 Results of Trial Irradiation 141

CHAPTER 9 CURRENT DEVELOPMENTS AND FUTURE EXPERIMENTS

9.1 General Conclusions 144
9.2 Developments in Experimentation 147
9.2.1 Gamma-ray Sources 147
9.2.2 X-ray Sources 148
9.2.3 Synchrotron Radiation 149
9.2.4 Alternative Techniques 152
9.3 Future Experiments 153
9.4 Summary 156

REFERENCES 158

APPENDICES 165

ACKNOWLEDGEMENTS

I would like to thank my supervisor Dr. Malcolm Cooper for his help and encouragement throughout my period of research. I am also indebted to Dr. Phillip Pattison who introduced me to this field and for his continual interest and encouragement.

Thanks are due to Dr. Jochen Schneider for his valuable knowledge and help in the design of the ^{198}Au gamma-ray Compton spectrometer-diffractometer system, and to members of the Rutherford Laboratory particularly Dr. Bruce Forsyth, Mr. Terry Jones and Miss Kate Knight for their considerable contribution. I would also like to thank members of the mechanical workshop (Warwick) especially Mr. Malcolm Gutteridge and Mr. Bill Jones for their skill and effort in constructing both the ^{198}Au and ^{241}Am systems.

I would like to thank Dr. Wolf Weyrich who assisted me in understanding molecular Compton profiles, and Dr. David Hirst who kindly carried out several molecular orbital calculations.

Appreciation is also due to Prof. Jim DuBard and Dr. Dick Weiss for their assistance given in many ways during the past year.

I would also like to thank Prof. A. J. Forty and Prof. P. N. Butcher for allowing me to use the facilities of the Physics Department, and the Science Research Council for providing me with a Research Studentship.

Finally, I wish to thank my wife Lynne for her careful typing of the manuscript and for her patience and support throughout this period of research.

MEMORANDUM

This dissertation is submitted to the University of Warwick in support of my application for the admission to the degree of Doctor of Philosophy. It contains an account of my own work performed at the Department of Physics of the University of Warwick in the period from October 1975 to September 1978 under the supervision of Dr. M. J. Cooper. No part of it has been used previously in a degree thesis submitted to this or any other University. The work described in this thesis is the result of my own independent research except where acknowledged in the text. An account of the work on molecular Compton profiles has been published in Chem. Phys. Lett., 43, 606, and Chem. Phys. Lett., 55, 284. The study of the Compton profile of niobium and niobium hydride has been published in Zeits. Phys. B27, 205

September 1978

R. S. Holt.

ABSTRACT

The method of measuring ground state electron momentum densities using Doppler broadening of Compton scattered radiation, is reviewed. The principles of Compton profile measurements with gamma-ray sources used with energy dispersive photon detectors, are introduced.

Particular emphasis is shown in the design and construction of two gamma-ray Compton spectrometers using a 5 Ci ^{241}Am (59.54 KeV) annular source, and a 120 Ci ^{198}Au (411.8 KeV) source. The application of the gamma-ray techniques to a number of molecular and metallic systems and comparison with theoretical profiles, highlights the sensitivity of the Compton profile to subtle changes in the bonding and conduction electron density.

Measurements of the momentum density of isotropic hydrocarbons with ^{241}Am provide a method of assessing the reliability and validity of the localised molecular orbital and self-consistent-field descriptions of these molecules. It is shown that an average set of localised bond orbitals obtained theoretically are not sufficiently accurate to describe the Compton profile of highly strained cyclic molecules, conjugated molecules and resonant structures.

Directional Compton profiles for niobium and niobium hydride using ^{198}Au show the sensitivity of the profile to subtle changes in the band electron profile following the introduction of hydrogen into the metallic lattice. Overall qualitative changes in the directional profiles are understood within the rigid band approximation.

Momentum density studies with the two gamma-ray techniques show that in general, the usefulness of these methods lies not in a determination of an absolute Compton profile but in measurements where intepretation is focussed on the difference between similar profiles.

AUTHOR'S NOTE

Units

Throughout this thesis atomic units (a.u.) have been used unless otherwise stated. These are chosen so that $\hbar = m = 1$ and $c = 137.036$. It follows that 1 a.u. of momentum = 1.993×10^{-24} kgms^{-1}; 1 a.u. of energy = 27.212 eV, and 1 a.u. of length = 5.292×10^{-11} m.

Notation

Electron momentum is denoted by q or p_z depending on whether the Compton profile describes the spherical average (isotropic) or directional property of the system.

CHAPTER 1

GENERAL INTRODUCTION

1.1 Introduction

In 1923 A.H.Compton described in a clear and direct way the essential duality of a classical wave description and a corpuscular or quantum description of radiation (Compton, 1923). X-ray photons whose properties had accounted for their diffraction by gratings and crystals were shown to possess corpuscular properties of energy and momentum, and to be capable of utilizing their entire energy and momentum in a single collision with one particular electron. The effect named after him, gave rise to an expression for the energy change upon scattering in terms of the incident photon energy and angle of scattering. It was sometime later however, before DuMond (1929) showed that instead of the unique X-ray energy predicted by the Compton formula for a stationary electron, the energy of the Compton scattered photon is Doppler shifted by the momentum of the scattering electron, an effect first recognised by Jauncey (1924).

The intensity at any point in the modified Compton line was shown to be proportional to the probability of an X-ray photon being scattered with that energy. This in turn was proportional to the probability of encountering an electron in the scattering material having a corresponding linear momentum specified by the modified Compton formula given by DuMond (1929). The Compton line shape or Compton profile as it is more commonly called, therefore describes the electron momentum distribution in the scattering material.

The consequences of measuring a momentum distribution instead of the more usual position distributions commonly associated with X-ray diffraction studies, can be seen via the Fourier transform between position and momentum space. The significance of such a transform makes the Compton

profile particularly sensitive to the behaviour of the outer electrons. Compton profile measurements therefore provide a significant amount of detail, complementary to X-ray diffraction techniques, about the loosely bound electrons and particularly those responsible for the interatomic effects which lead to the formation of solids and molecules. Furthermore, because the Compton scattering process is incoherent, i.e. there is no phase relationship between the scattering amplitudes of the individual electrons, all points in reciprocal space are spanned. This allows measurements to be readily undertaken on solids, liquids and gaseous samples. Measurements which determine the Compton profile of a scattering material provide detailed information about the electronic structure of a wide range of physical and chemical systems.

The impetus provided by these discoveries further advanced the study of Compton scattering in the 1930's through the experimental work of Ross and Kirkpatrick (1934), Kappeler (1936), DuMond and Kirkpatrick (1937) and Hicks (1937). Unfortunately the experimental difficulties encountered, which stemmed primarily from the weakness of the Compton scattered radiation, eventually led to a dormant experimental period of over thirty years. Interest remained however, largely due to the theoretical work of Coulson and Duncanson (1941), March (1954) and Kilby (1963).

The revival of interest in momentum density studies began in the mid 1960's with the initial experimental efforts of Cooper et. al. (1965), and Weiss (1966), and the theoretical stimulus provided by Platzman and Tzoar (1965) and later by Eisenberger and Platzman (1970). The early experimental work began to explain the anomolous experimental result in lithium obtained by Kappeler (1936). These researches employed X-ray tubes of much greater power than those available to DuMond, Kappeler and co-workers. and coupled with crystal spectrometers provided a high intensity system with good resolution. The initial studies which followed the measurements on lithium were, however, directed at a qualitative rather than quantitative

understanding of momentum space properties. Consequently the initial efforts were largely uncoordinated and developed rather haphazardly. Moreover, for many experimental results no relative theory was available to provide the means of assessing the accuracy of the measurements.

Despite the much improved quality of the X-ray generators available at that time, the X-ray technique still required long measuring times to obtain a statistically accurate Compton profile. Furthermore, the low energies gave rise to a significant amount of photoelectric absorption even for samples of low atomic number. It was not until the commercial introduction of high resolution, high efficiency solid state detectors based on germanium and silicon semiconductor crystals, at the beginning of this decade, that high energy gamma-rays could be used to measure momentum densities. These detectors together with their associated electronics have effectively replaced the X-ray crystal spectrometer. The major advantages of using gamma-ray sources in conjunction with solid state detectors are, significant improvements in the reliability, accuracy and speed with which Compton profiles can be measured, albeit at lower resolution, and the ability to investigate effectively all elements in the periodic table rather than a limited number as in the case of X-rays.

The gamma-ray Compton scattering method is therefore a comparatively young and still relatively unknown technique. However, during the past few years considerable advances have been made in interpreting and understanding momentum density properties. Investigations with these sources have been undertaken in well defined areas and experiments performed in a more systematic manner. The gamma-ray technique has therefore emerged with its scope and limitations fairly well defined. Because of the recent and rapid developments in Compton scattering most of the early literature on the subject is largely of historic interest and often not reliable. The theoretical and experimental progress in Compton scattering up to 1971 has been reviewed in an excellent article by Cooper (1971). Recently a second

review article by the same author (Cooper, 1977) describes the current state of the art and the progress that has been made over the past five years. A more comprehensive account of the developments in Compton scattering can be found in a recent monograph edited by Williams (1977).

In the following sections of this introductory chapter a brief review is given of the properties and behaviour of the Compton profile in relation to the recent experimental and theoretical progress that has been made. Particular emphasis is shown in the current gamma-ray techniques that are available and which are the subject of this thesis.

1.2 The Compton Profile and Momentum Distributions

The electron momentum distribution or momentum density in a scattering material $n(\bar{p})$, can be obtained directly from the momentum space wavefunction $\chi(\bar{p})$, where

$$n(\bar{p}) = |\chi(\bar{p})|^2 \qquad 1\text{-}1$$

and $\bar{p}$ denotes the initial electron momentum. A determination of $n(\bar{p})$ therefore provides an alternative method of describing the electronic structure of matter. The experimental methods used to measure the momentum density, described briefly in the following sections, do not usually measure $n(\bar{p})$ directly but a quantity which is proportional to the integral of $n(\bar{p})$ over two (or one) of the components of $\bar{p}$, i.e.

$$J(p_z) = \iint_{-\infty}^{\infty} n(\bar{p})\,dp_x\,dp_y \qquad 1\text{-}2$$

$J(p_z)$ is the Compton profile and p_z is the projection of the initial electron momentum $\bar{p}$ onto the scattering vector. From eqn. 1-2 it can be seen that the Compton profile does not yield directly any single physical parameter but instead provides a powerful tool for testing electronic wavefunction calculations.

Momentum space wavefunctions can be determined by solving the Schrödinger equation directly in the momentum space. McWeeny and Coulson

(1949) attempted this almost thirty years ago for the simplest one-electron, one-nucleus case. Unfortunately attempts to extend this by introducing electron correlation made the calculation exceedingly difficult and the problem soon became intractable. Since then there has been considerable advances in numerical and computational techniques, and a renewed attack on the problems associated with this method may well prove rewarding.

An alternative method, and by far the most successful, is to calculate the position space wavefunction and to Fourier transform them to momentum space, i.e.

$$\chi(\bar{p}) = (2\pi)^{-3/2}\int\psi(\bar{r})e^{-i\bar{p}\cdot\bar{r}}\,d\bar{r} \qquad 1\text{-}3$$

Using eqn. 1-1 the momentum space wavefunction can be used to obtain the momentum density and hence the Compton profile. The success of this method depends on the level and degree of approximation used to obtain the position space wavefunctions. This in turn depends on the nature of the calculation and whether it is concerned with a metal, ionic crystal, molecule or an atom. Some of the theoretical models are discussed in the following section.

An immediate consequence of the Fourier relationship between position and momentum space (eqn. 1-3) is that measurements of the Compton profile provide an accurate and sensitive test of the quality of theoretical wavefunction calculations. Furthermore, the profile is particularly sensitive to the behaviour of the more loosely bound electrons which are involved in bonding and conduction processes. The outer electrons of an atom, molecule or solid possess an extensive spatial wavefunction which leads, after transformation, to a wavefunction which is highly localised in momentum space, giving sharply peaked contributions to the Compton profile. Hence, the entire contribution of these electrons to the profile is confined to regions of low momenta. Conversely, the contribution from the inner electrons, which are more localised around the atomic cores in

position space, spread out on transformation to give only a slowly varying background to the profile extending to high values of momenta.

To illustrate the basic features of the Compton profile Fig. 1-1 shows the profile of calcium derived from the free atom wavefunctions calculated by Biggs et. al. (1975). The contributions from the separate electron shells (each normalised to the number of contributing electrons) is clearly shown. The superposition of core and valence Compton profiles is also depicted. Because the core electrons possess a relatively flat profile, it may be expected that this contribution will be unaffected by the transition to a solid state or molecular environment. These results contrast sharply with those of an X-ray diffraction experiment, where the intensity of the Bragg peaks depend primarily upon the spatial electron density which is proportional to $|\psi(\bar{r})|^2$. Since the atomic electron density distributions are concentrated around the core, the outer electrons make little contribution to the Bragg scattering. The complementary nature of position and momentum density distributions are therefore clearly reflected in the sensitivity of the two techniques.

In a material where the scatterers are randomly oriented, e.g. gas, liquid and powder samples, the momentum density must be averaged over the full solid angle. Using eqn. 1-2 and transforming to cylindrical coordinates, the isotropic Compton profile is given by

$$J(q) = 2\pi \int_{|q|}^{\infty} p\langle n(\bar{p})\rangle \, d\bar{p} \qquad 1\text{-}4$$

where $\langle n(\bar{p})\rangle$ is the spherical average of $n(\bar{p})$, ($J(p_z)$ defines the directional Compton profile). Moreover, in an analogous way to the radial charge density of X-ray diffraction, a radial momentum density $I(\bar{p})$ can be defined, where

$$I(\bar{p})d\bar{p} = 4\pi\bar{p}^2\langle n(\bar{p})\rangle \qquad 1\text{-}5$$

With this definition the isotropic Compton profile can be expressed in

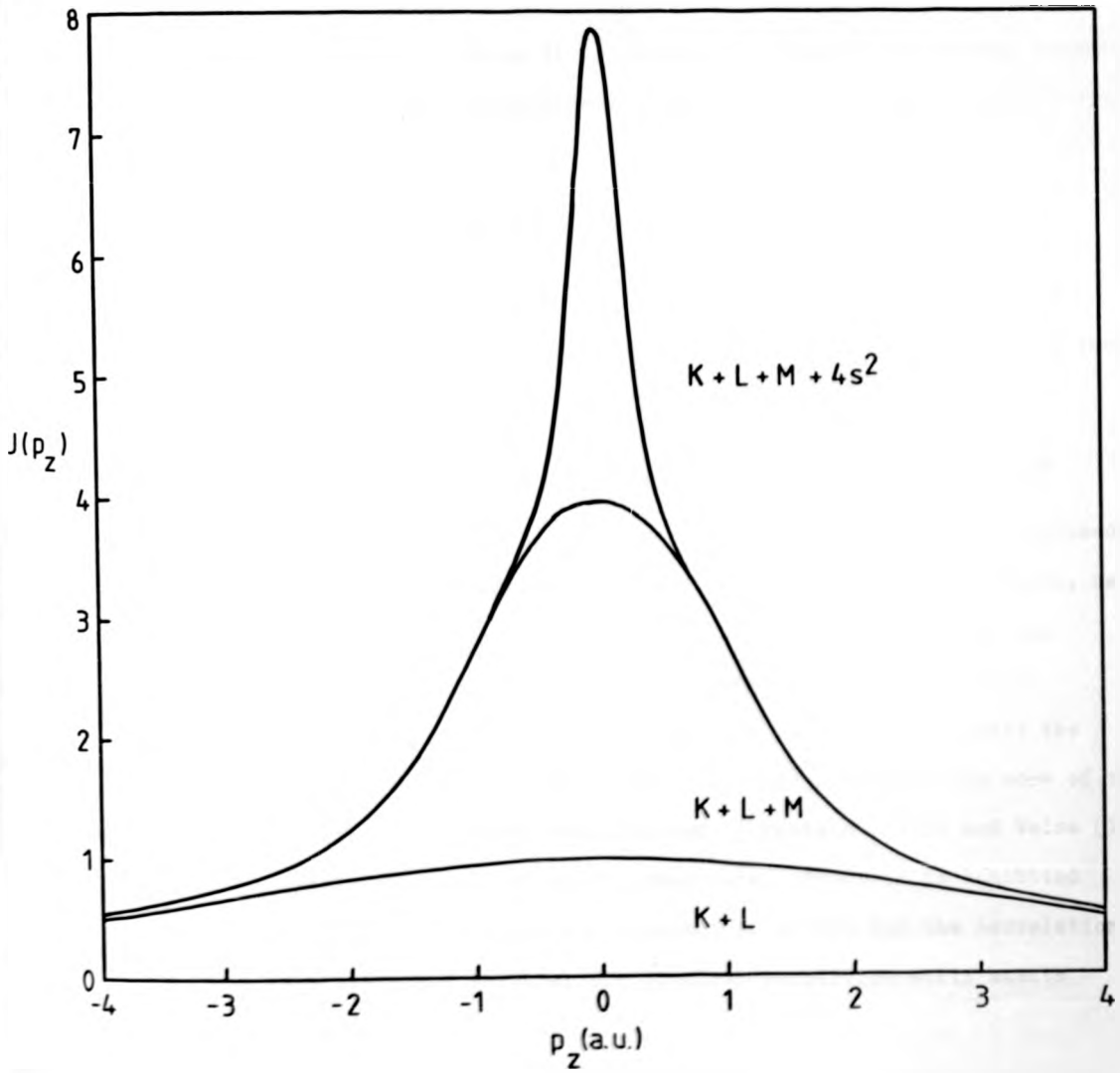

Fig. 1-1: Free-atom Compton profile of calcium.

terms of the radial momentum density as follows

$$J(q) = \frac{1}{2} \int_{|q|}^{\infty} \frac{I(\bar{p})}{p} \, d\bar{p} \qquad 1\text{-}6$$

By inverting this expression it is possible to extract the radial momentum density directly from a measurement of the isotropic Compton profile via a differentiation step,

$$I(\bar{p})d\bar{p} = -2p \frac{dJ(q)}{dp} \qquad p>0 \qquad 1\text{-}7$$

Epstein (1973) has shown that a significant amount of information is contained in the radial momentum density, particularly in evaluating the principal momentum expectation values given by

$$\langle p^n \rangle = \int_c^{\infty} p^n I(\bar{p}) \, d\bar{p} \qquad 1\text{-}8$$

Cooper (1967), Coulson (1973) and Benesch and Smith (1973) have independently shown that the total energy of an atom or molecule can, in principle, be obtained experimentally using eqn. 1-8 with n=2. Unfortunately the statistical errors are amplified by the differentiation procedure, particularly in the tails of the profile, and this severly limits the accuracy and reliability of the result. Methods circumventing some of these practical difficulties have been proposed by Epstein (1973) and Weiss (1978) although little progress has so far been made. Progress is inhibited because the interpretation of the expectation values and the correlation between them and other physical and chemical properties still awaits development.

1.2.1 Electron Behaviour in Momentum Space

Since the revival of experimental work in 1965 a large number of experimental and theoretical Compton profiles covering a multitude of materials have been published. In order to illustrate the essential features and properties of the profile it is only possible to refer to a small part of the total work. In this section the work pertaining to the

electron behaviour in momentum space with particular emphasis to molecular and solid state systems is reviewed.

In recent years considerable interest has been shown in molecular systems, particularly the organic molecules which have been subject to several extensive studies (Hennecker and Cade, 1968, Epstein and Lipscomb, 1970, Roux and Epstein, 1973, Smith and Whangbo, 1974). A more comprehensive review of molecular momentum space properties can be found with reference to Epstein and Tanner (1977). For the present an appreciation of the nature of the information which can be extracted can be gained from a consideration of the simplest molecule, the H_2^+ molecule-ion.

The molecular wavefunction for this molecule can be written as

$$\Psi_{\pm}(\bar{r}) = (\psi(\bar{r}) \pm \psi(\bar{r}-\bar{R}))/(2 \pm 2S) \qquad 1\text{-}9$$

where $\psi(r)$ is the isolated atomic orbital, S is the overlap integral between the two atomic orbitals, and $\bar{R}$ is the internuclear vector. The positive sign corresponds to a bonding orbital and the negative sign to an antibonding orbital. Fourier transforming and squaring the result enables the momentum density to be obtained (see eqn. 1-1),

$$n(\bar{p}) = |\chi(\bar{p})|^2 (1 \pm \cos\bar{p}.\bar{R})/(2 \pm 2S) \qquad 1\text{-}10$$

where $\chi(\bar{p})$ is the momentum orbital associated with the isolated atomic orbital $\psi(\bar{r})$. Equations 1-9 and 1-10 can be generalised to incorporate a larger number of basis functions, and a larger number of atoms. The contours of bonded electron density for the H_2^+ molecule-ion in both position and momentum space representations are shown in Fig. 1-2. The most obvious difference between the two density maps is the single centre associated with the momentum density map. The importance and significance of momentum space wavefunction calculations can now be seen in that the problem reduces to a calculation involving only a single centre, instead of the multicentre integrals which have to be evaluated in position space

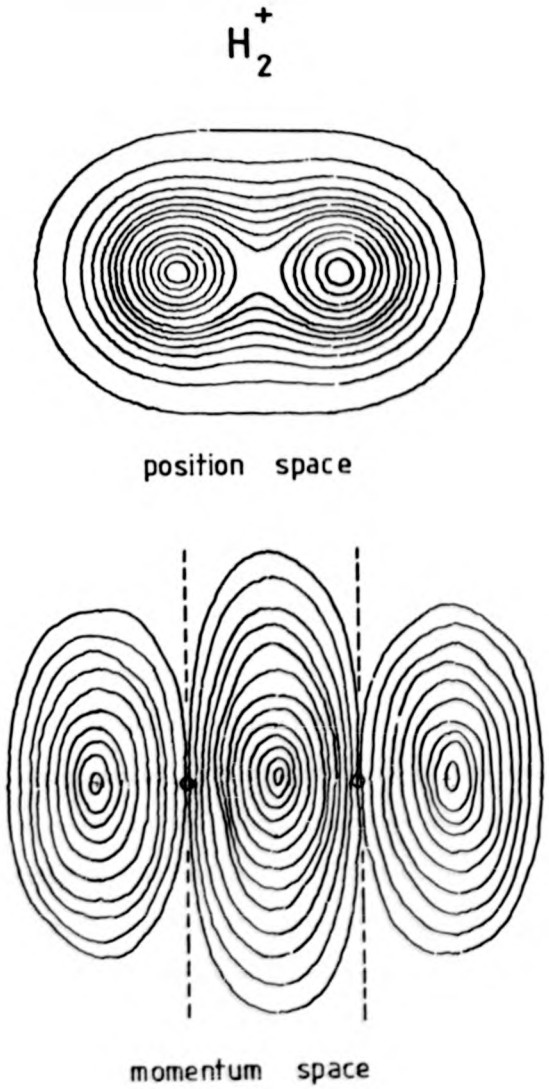

Fig. 1-2: The contours of bonded electron density for the H_2^+ molecule-ion in position and momentum space.

wavefunction calculations. The difficulties encountered in momentum space are a result of solving many differential equations which are less tractable than integrals.

To explain these maps reference will be made to a study of the roles of kinetic and potential energies in bond formation by Feinberg and Rudenberg (1971). These authors suggested that as two isolated atoms approached one another, bonding arises not from a lowering of the potential energy but from a lowering of the component of the kinetic energy parallel to the bond axis. In their view the ultimate decrease in potential and increase in kinetic result from the orbital contraction (in position space) which occurs at the equilibrium distance. The Variation Principle requires that the virial theorem be satisfied, i.e.

$$E = -T = \frac{1}{2}V \qquad 1\text{-}11$$

where E is the total, T the kinetic and V the potential energies. This is achieved through a redistribution of the kinetic and potential energies which is accompanied by a contraction of the wavefunction, i.e. the orbital exponent in the basis function changes from unity (free atom case) to a slightly higher value (~1.2 for H_2^+). This contraction of the atomic orbitals has the effect of expanding the momentum density in all directions. The accumulation of charge in regions centred about the nuclei causes the wavefunction to change less rapidly there than it did in the absence of the bond. Since the gradient of the wavefunction is equivalent to the momentum, the component of momentum along the bond is decreased. Conversely, the momentum perpendicular to the bond axis is increased as shown in the figure, a result which could also be predicted from the Fourier transform principle.

The anisotropy of the bond momentum density must vanish for large momenta since such regions correspond to position space regions close to the nuclei where the charge distribution may be expected to be spherically

symmetric (Fig. 1-2). The profile at high momenta can therefore be represented to a good approximation by a free atom profile. The effects of bonding will however, dominate the low momentum region of the profile. The expansion of the momentum density upon bonding means that the isotropic profile is always broader than the corresponding free atom profile. The same effect may also be seen from the point of view of using an improved wavefunction to describe the molecule. The principle follows from the virial theorem which requires that systems of lower total energy (improved wavefunction) have higher kinetic energy. Since $T = \langle p^2 \rangle / 2$ (see eqn. 1-11), lowering a systems energy increases the average value of the momentum and consequentely will tend to shift momentum density from regions of lower to regions of higher momenta.

The oscillations in the momentum density predicted by eqn. 1-10, and illustrated in Fig. 1-2, can only be detected in Compton profiles of oriented molecules. Although these oscillations have been observed in theoretical studies of diatomic molecules (Kaiser and Lindner, 1975, Langhoff and Tawil, 1975) experimental verification is difficult, owing to the problems of measuring and analysing single crystals of oriented molecules (Reed et. al., 1978).

Consideration of atomic behaviour has led to several experimental and theoretical studies of the inert gases. He, Ne, Ar and Kr have been studied using X-rays (Eisenberger, 1970) and gamma-rays (Eisenberger and Reed, 1972). Comparison with theoretical profiles calculated using non-relativistic Hartree-Fock wavefunctions (Clementi, 1965) has resulted in large discrepencies which have been attributed to electron correlation effects. Correlated profiles are now available (Benesch, 1978) which give good agreement with the experimental profiles at low momenta.

For simple diatomic molecules and some simple, i.e. small, organic ones, it is possible to compare the experimental results with theoretical ab initio calculations on the self-consistent Hartree-Fock level, or by

means of configuration interaction (electron correlation) techniques. For larger, more complex molecules the computational labour involved in these calculations is prohibitive, and many approximate methods have been developed to circumvent these problems. The localised molecular orbital approach taken by Epstein (1970), Smith and Whangbo (1974) is one way. In this method, which is described more fully in Chapter 5, the momentum density is fragmented into bonding and inner shell distributions which are regarded as transferable from one molecule to another. In this way the momentum density and Compton profile of very large molecules can be built up merely from considering calculations based on a limited number of smaller molecules (for which SCF-MO calculations are readily available). Such an approach to molecular momentum densities has been by far the most closely investigated of the techniques available, although semi-empirical molecular orbital methods are also being examined (Ahlenius and Lindner, 1975). The former method has been applied with considerable success to the hydrocarbons although it does not appear to be , at present, extendible to molecules containing oxygen and nitrogen (Epstein, 1970). The effect of molecular vibrations on the Compton profile has also been studied. For some diatomic molecules the effects have been found to be small (Braun-Keller and Epstein, 1976), suggesting that an extension to larger systems would indicate a negligible effect on the profile.

In crystalline solids the situation is more complex. The isotropic Compton profiles of the alkali halides have been comprehensively studied by Paakkari et. al. (1974), Manninen et. al. (1973), Weyrich (1975) and Berggren et. al. (1976), both experimentally and theoretically. It has been found that in some ionic solids Hartree-Fock free-ion wavefunctions adequately describe the momentum density. In others, e.g. LiH, it is necessary to go beyond just nearest neighbour interactions and consideration must be given to overlap effects between ion pairs (Berggren and Martino,

(1971). The effect of including overlap in the calculation leads to a build-up of charge at these ion sites and a consequent broadening of the momentum density. For some ionic solids such as NaF, it is also necessary to include the effects due to the crystalline field in the calculation of the wavefunction in order to achieve good agreement with experiment (Fukamachi and Hosoya, 1970). Directional Compton profiles have also been reported for LiF and LiH (Reed et. al., 1975, Reed, 1978), and compared to calculations based on the linear-combination-of-atomic-orbitals (LCAO) method. The overall agreement between theory and experiment is found to be satisfactory for all three principal directions. For covalent solids, such as diamond, Si, Ge (and graphite), the theoretical anisotropy (Wepfer et. al. 1973, Reed and Eisenberger, 1972) is much larger than that experimentally determined (Reed and Eisenberger, 1972, Paakkari, 1974, Weiss, 1972) although their is qualitative agreement.

For metals, the simplest theoretical model is the core plus free conduction electrons. These non-interacting electrons occupy a set of states in momentum space uniformly filling the three-dimensional Fermi sphere (see for example Kittel, 1971). This model is a reasonable first approximation for the alkali metals, such as Li, Be and Na, where the resulting Compton profiles contain a discontinuity in the line shape which locates the Fermi surface. However, even in these 'simple' systems, deviations from free electron behaviour arise through inter-electron Coulomb interactions, i.e. electron correlations, which promote electrons to momentum states above the Fermi surface. Consequently, the Compton profile contains a high momentum tail that is more pronounced for materials with a high conduction electron density. The behaviour of the momentum density and Compton profile due to electron correlation is shown in Fig. 1-3. Correspondingly, the correlated profile is much flatter at low momenta and good agreement with experiment has been found for Na and Al.

In heavier metals, e.g. the transition series, the momentum density

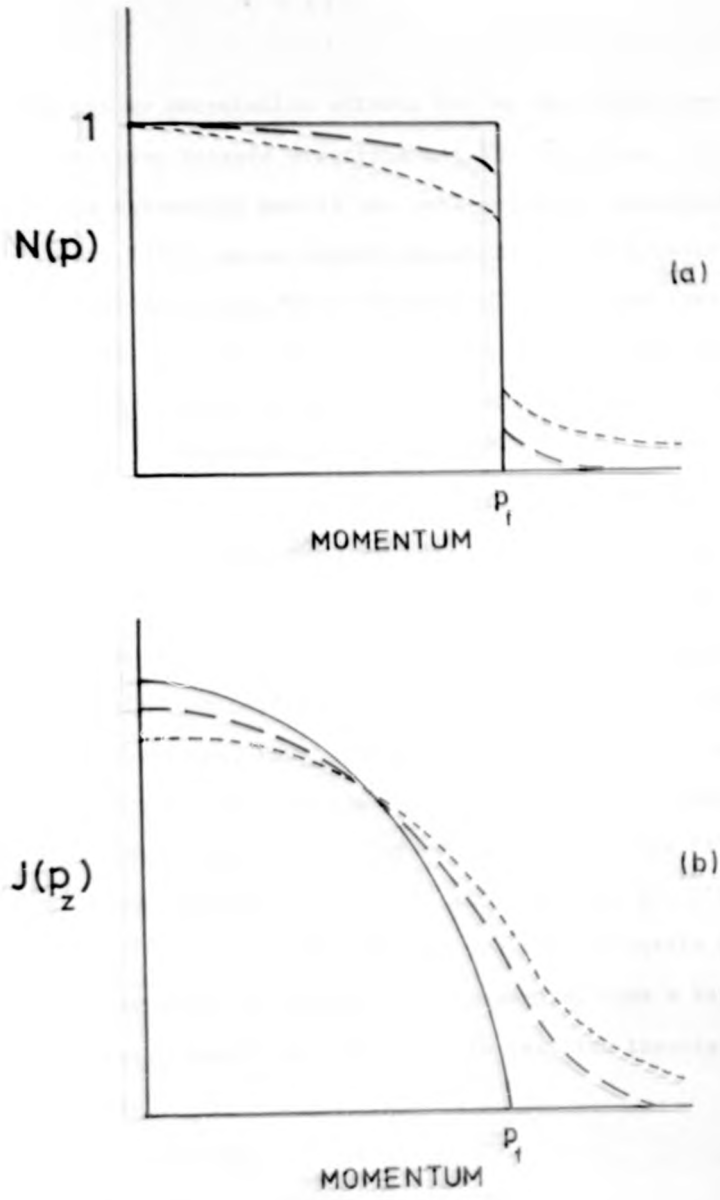

Fig. 1-3: Effects of electron correlation on the momentum density and Compton profile of an electron gas.

is dominated not by correlation effects but by band structure effects, i.e. Coulomb interactions between electrons and the ion cores. For isotropic profiles of the transition metals the semi-empirical renormalised free atom model (Berggren, 1972), gives results which are in reasonable agreement with experimental data (the first transition series have free atom-like 3d bands)(Paakkari et. al., 1975, 1976). For many metals, however, directional Compton profiles have been measured and the anisotropy in the momentum density is therefore available. Directional profiles allow a more stringent test of the quality of the wavefunctions used, and indicates the limitations of the renormalised free atom model. In order to obtain accurate anisotropy behaviour an explicit calculation of the electron wavefunction throughout the bands is required. The complex and formidable task has consequently only been performed on a few materials, e.g. vanadium (Wakoh and Yamashita, 1973, KKR, Wakoh et. al., 1976, APW), chromium (Wakoh and Yamashita, 1973, APW), and niobium (Wakoh et. al., 1975, APW). In contrast there is a wealth of experimental information, e.g. Weiss (1973), Ohara et. al. (1974), Eisenberger and Reed (1974) and Wakoh et. al. (1975). The overall policy of obtaining experimental profiles in metals (and alloys) is to test the accuracy of wavefunctions generated from a band structure and less complete calculations, and also to test the theories of many electron effects.

1.3 Experimental Methods

(i) X-ray and Gamma-ray Compton Scattering

Scattering experiments preceeding Comptons' eludication of the effect frequently employed radioactive sources of gamma-rays, and utilized the rapid variation of absorption coefficient with energy to determine the nature of the scattered radiation. However, the need to perform a line shape analysis prevented the use of gamma radiation for which energy sensitive detectors had not been invented. The discovery of X-rays and

the development of the Coolidge form of the X-ray tube offered much higher fluxes of incident radiation; coupled with a crystal spectrometer the system was capable of achieving very good resolution. Despite the high fluxes the Compton scattered intensity was still very weak. For example, a measurement of the Compton profile of hydrogen by DuMond and Kirkpatrick (1937) took over 2000 hours to complete. Fortunately, the overall qualitative agreement with a theoretical profile confirmed the potential of the photon scattering technique as a method of studying the electronic wavefunction, albeit with difficulty. Such practical problems were certainly prominant in leading to the long period of inactivity in momentum density studies between 1940 and 1965.

When the revival in studying momentum densities began through the efforts of Cooper et. al. (1965), it was not surprising that the X-ray tube and crystal spectrometer were used to produce and analyse the scattered radiation. It soon became apparent that the background radiation (bremsstrahlung) and also the doublet nature of the K_α peak led to uncertainties in the results especially in the tails of the profile. Despite the power available from commercial X-ray generators the technique was still slow requiring long measuring times, even for relatively light materials. It was not too long however, before gamma-rays were beginning to emerge as an alternative source following the introduction of energy sensitive solid state detectors. An early demonstration of the technique was forthcoming from McIntyre et. al. (1967), using a lithium-drifted germanium detector with gamma-rays emitted from a ^{60}Co source. This was followed three years later by measurements involving a 300 mCi ^{241}Am source which has a primary gamma line at 59.54 KeV (Felsteiner et. al., 1970). The advantages of this technique were demonstrated with momentum distributions being given for aluminium and graphite samples. The results and conclusions drawn from these exploratory studies showed clearly the considerable

advantages gamma-rays had compared with the usual X-ray method. The peak-to-background ratio is very much smaller and the incident radiation is monochromatic. With the introduction of solid state detectors the energy loss spectrum can be measured at one time although the momentum resolution is somewhat lower than that of an X-ray experiment (0.5 a.u. cf. 0.2 a.u.) The rapid development of the gamma-ray technique and the progress made so far has rendered the conventional method as a specialised tool for detailed investigations on low atomic number systems only.

Recently several Compton profile measurements have been reported using synchrotron radiation produced by the NINA electron synchrotron (Cooper et. al.,1976, Holt et. al., 1978), and the technique has been described in detail in the authors M.Sc. thesis (Holt, 1976). At present the experimental technique and the problems associated with it are akin to those usually found with the gamma-ray method. As such the X-ray, gamma-ray and synchrotron methods are relatively straightforward in terms of experimental technique and are probably the most versatile of the methods which are currently available. There are at least three alternatives to photon Compton scattering for measuring electron momentum distributions. These are positron annihilation, high energy electron scattering and (e,2e) angular correlation, and each of these different techniques are briefly outlined in the remaining part of this section.

(ii) Positron Annihilation

When high energy positrons are injected into a sample they quickly thermalise and annihilate with an electron resulting in the emission of two photons. The angle between the two photons deviates from 180° by p_x/mc, where p_x is the momentum component. This angular deviation, although of the order of milliradians, is easily measured and the angular correlation of the photons detected in coincidence. Recent advances in the experimental technique have allowed two-dimensional projections to be measured, i.e.

the projection of the momentum density onto certain planes. The positron annihilation apparatus has a good resolution exceeding that of current gamma-ray methods by an order of magnitude or so. The excellent resolution provides accurate determination of the sharp discontinuity on the momentum density due to the Fermi surface, and is therefore, most suitable for measurements on metals and alloys. Despite its versatility, the technique is not without its problems. The question of the exact form of the positron wavefunction and how it disturbs the electron distribution still present problems (Carbotte and Salvadori, 1967). Positrons also show preference for annihilating in vacancies, and although this allows a method for studying vacancies themselves, complicates the interpretation of the profiles measured on 'perfect' materials. For excellent reviews on this method see West (1973) and Berko and Mader (1975).

(iii) High Energy Electron Impact Spectroscopy (HEEIS)

Like photon Compton scattering, the use of electron scattering underwent a lengthy period of dormancy after the initial studies by Hughes and Mann (1938), only to reappear in a more powerful form. Details of the present experimental as well as the theoretical aspects of electron scattering have been given by Wellenstein and Bonham (1973), and Bonham and Fink (1974), respectively. The technique is only suited to high resolution measurements in gaseous samples composed of light elements ($Z \leqslant 10$). The limitation is imposed because of corrections for relativistic effects, as well as electron exchange and interference between the incident and scattered beams. Despite these rather severe restrictions the method does yield accurate Compton profiles very quickly, and with good statistical accuracy. Furthermore, the resolution is an order of magnitude better than the present X-ray (or gamma-ray) technique.

(iv) (e,2e) Angular Correlation

This is a relatively new technique in which an electron is scattered

from the sample and both the scattered and recoil electrons are detected in coincidence. Initial measurements have been reported by Ehrhardt et. al. (1969) and Weigold et. al. (1975). Unfortunately, there are practical limitations which result in poor resolution, relatively low count rates and, as in the case of HEEIS, restriction to gases. However, despite these difficulties a compensating and attractive feature is the capability of measuring the momentum density of each electron orbital separately.

However, this thesis is only concerned with the gamma-ray Compton scattering technique although the future experimental development of these alternative methods are described in Chapter 9. In the following sections attention is focussed on the experimental aspects of the gamma-ray method.

1.3.1 Energy Limitations

There are a number of experimental conditions which together limit the energy of a gamma-ray source that can be profitably used in Compton scattering experiments. The first of these concern the possible interactions between photons and electrons. The interaction can be with the entire atom (photoelectric effect and Rayleigh scattering), or with one electron in the atom (Compton effect), or with the atomic nucleus (pair production). The relative cross section for each interaction depending primarily upon the photon energy and the atomic number Z of the material. In the energy range for which gamma-ray sources are available (typically 0.01 to 10 MeV), the predominate interactions are the photoelectric effect, Compton scattering and pair production, and the approximate boundaries between them are shown in Fig. 1-4.

The onset of pair production only occurs when the incident photon energies are in excess of $2mc^2$ ($\geq$ 1.023 MeV). When this condition is satisfied the photon decays into a positron-electron pair, and both particles subsequently lose energy in the form of bremsstrahlung radiation as they decelerate. Furthermore, the positron can annihilate with any electron

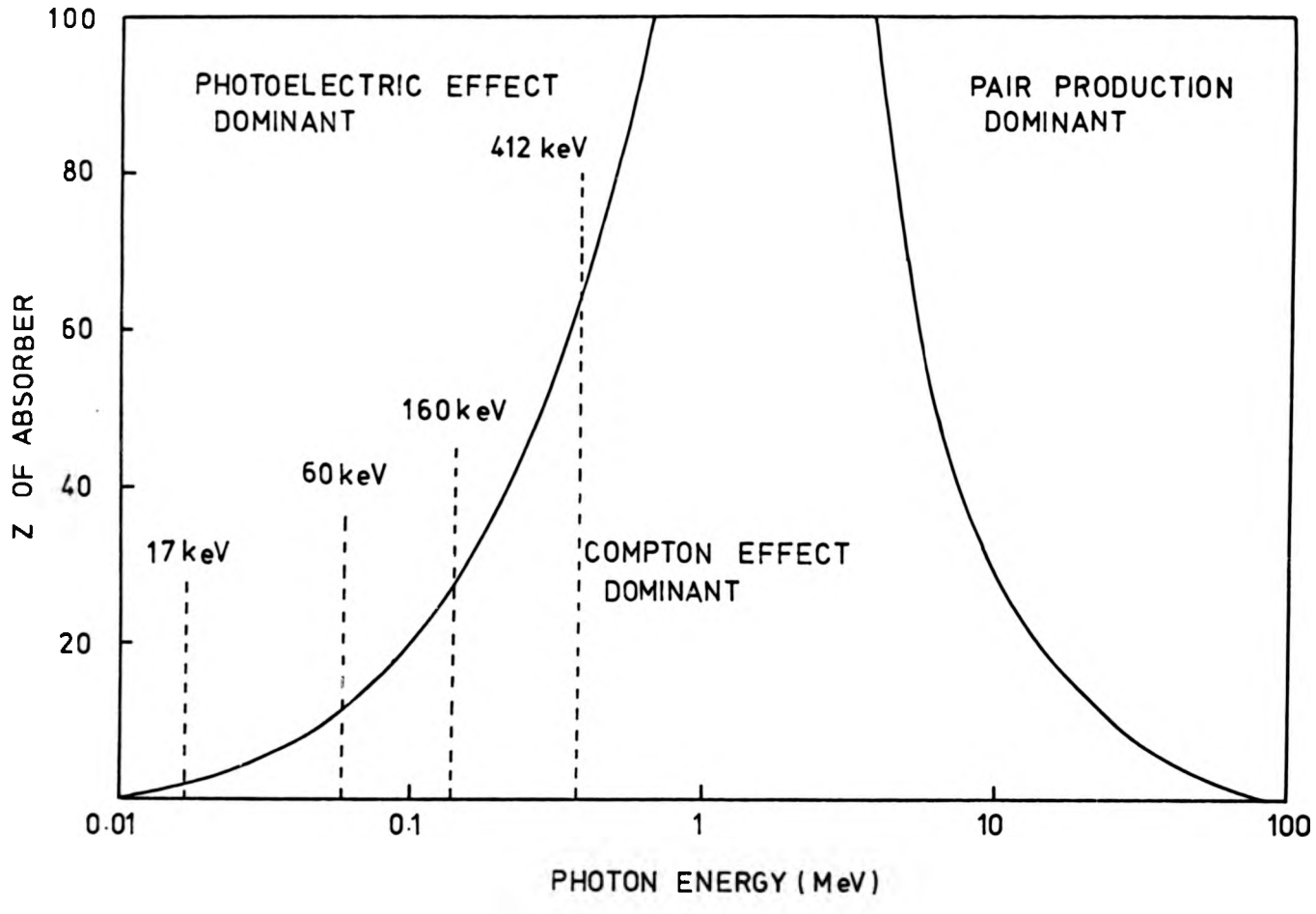

Fig. 1-4: Relative cross sections for photoelectric absorption, Compton scattering and pair production as a function of energy and atomic number.

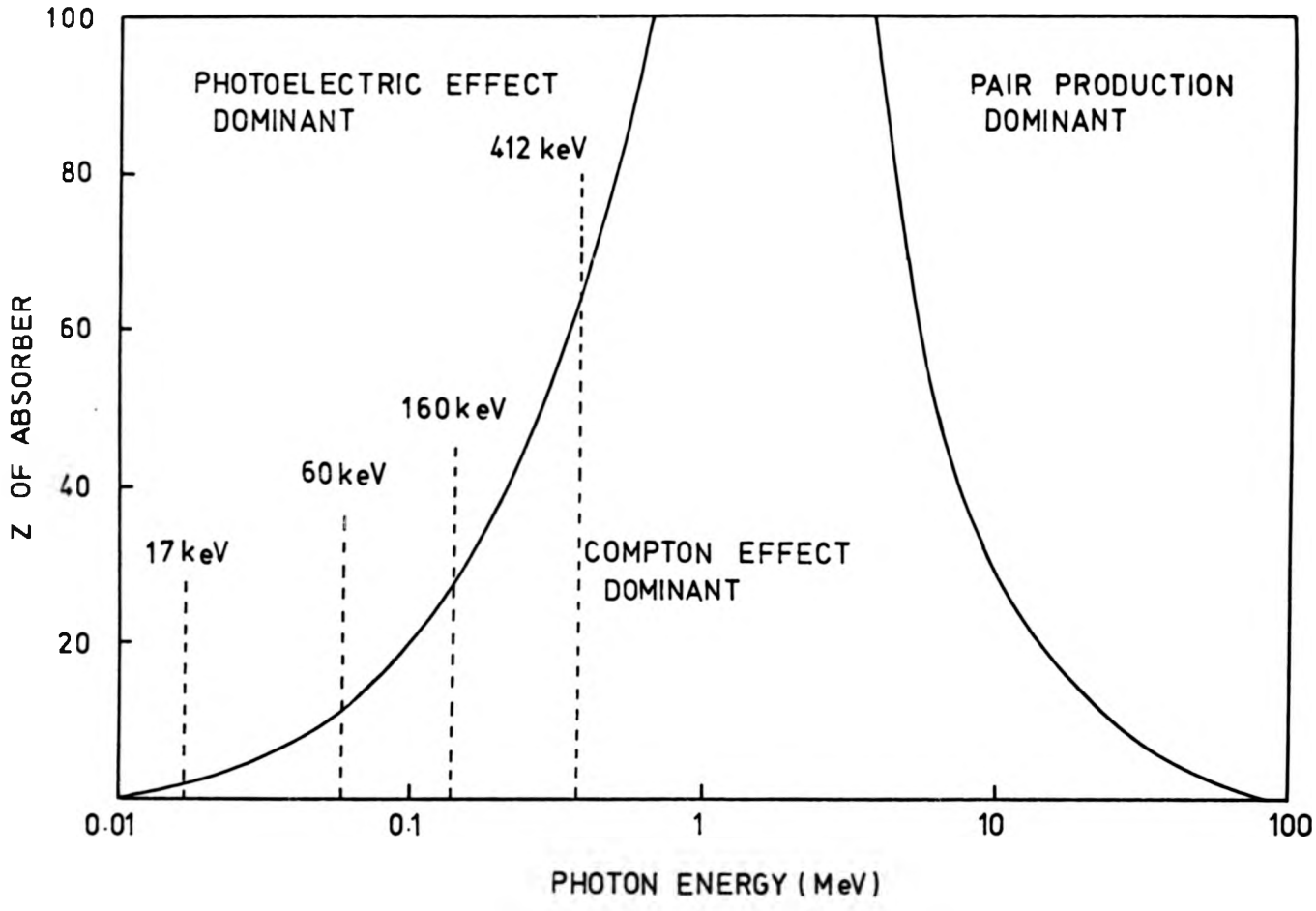

Fig. 1-4: Relative cross sections for photoelectric absorption, Compton scattering and pair production as a function of energy and atomic number.

to produce two 512 KeV photons. However, experimental difficulties particularly shielding the detector from stray radiation, coupled with the rapid deterioration of detector efficiency with increasing energy, presents many problems in allowing photon Compton scattering studies to be performed in this energy range.

For the range of energies and materials which are of interest in Compton scattering (see Fig. 1-4) the greatest cause of beam attenuation is photoelectric absorption. For low photon energies (~60 KeV) only materials with relatively low atomic numbers can be studied. Beyond the 3d transition elements photoelectric absorption becomes the dominant process. Furthermore, for materials with $Z > 70$ the photon energy loss in Compton scattering is less than the K shell binding energy. Under these conditions extra corrections are necessary which result in an overall loss of accuracy. In order to study the momentum density of materials of high atomic number requires gamma-ray sources of very high energies with an upper limit being placed around 500 KeV.

The intensity of the Compton scattered radiation is simply proportional to the Compton profile only when certain approximations in the derivation of this relationship are valid. The energy limitations imposed by one of these approximations - the impulse approximation (Eisenberger and Platzman, 1970) severely limits the range of materials that can be studied by Compton scattering. The essential feature of the impulse approximation is simply that an electron which is bound to its parent atom may be regarded as a free electron with the same momentum distribution. The necessary conditions for treating an electron in this manner are well fulfilled when the recoil energy is much larger than the binding energy of the electron. For 60 KeV radiation this condition imposes an upper limit on the materials that can be studied to around $Z=30$.

The third consideration to the energy limitations imposed on Compton

scattering is the momentum resolution. In Fig. 1-1 it was shown that the width of the Compton profile of bonding and conduction electrons was of the order of half an atomic unit. Electron momentum resolutions at least of this order are therefore required in an experiment if the fine details on the profile are to be resolved. According to McIntire (1976) there is a significant improvement in the momentum resolution (by a factor of 2) as the incident photon energy increases from 60 to 200 KeV. Above 200 KeV there is only a small improvement due to the increased contribution to the resolution arising from beam divergence effects. The contribution from this effect becomes dominant, i.e. greater than that from the detector alone, when energies in excess of 450 KeV are used.

From the above arguements gamma-ray sources which can be used to study the momentum density have an upper limit on their energy of around 500 KeV. Several high energy sources in this energy range (60 - 500 KeV) have been used and several others are currently under investigation. Some of these sources together with their basic properties are summarised in the following section.

1.3.2 Gamma-ray Sources

The most widely used radiation source for gamma-ray Compton profile measurements is ^{241}Am. It is a 'permanent' radiation source with a half-life of 458 years, and is obtainable at moderate cost. It has a principal gamma-ray line at 59.54 KeV with a less intense line at 26.36 KeV. Strong self-absorption limits the effective 59.54 KeV gamma activity to about 0.8 Ci per cm^2 of surface area. Typical activities that have been used in Compton scattering experiments range from 300 mCi to 900 mCi for a cylindrical source geometry. Recently a 1 Ci annular source has been investigated (Weyrich, 1975) which alleviates some of the experimental problems encountered with cylindrical sources. The author has designed and constructed a Compton spectrometer that uses a 5 Ci annular source,

and a detailed description of this system can be found in Chapter 4.

The advantages associated with higher primary radiation energy sources led to the use of ^{123m}Te (159 KeV) (Eisenberger and Reed, 1972). This nuclide is produced by the neutron capture reaction on ^{122}Te, and because of its metastable state has a short half-life of only 120 days. Furthermore, it is relatively expensive which severely limits the use of this type of source. Activities of the order of 1 Ci are typical.

The next high energy source that has been used to measure Compton profiles is ^{203}Hg (279.2 KeV). This nuclide, like Te, is produced by neutron capture and is relatively expensive. The half-life is only 46.6 days and activities of the order of 1 Ci have been used.

The 411.8 KeV primary line from ^{198}Au has been used to perform Compton profile measurements (Cooper et. al., 1976), and the results of some of these initial studies will be presented in Chapter 7. The source normally consists of a small strip of gold foil activated by the neutron capture reaction on ^{197}Au, and has a half-life of 2.7 days. Initial activities in excess of 70 Ci are possible, but periodic activation in a reactor is necessary because of the very short half-life.

Finally, the highest energy gamma-ray source that has been used to obtain high resolution Compton profiles is the 661.6 KeV radiation emitted from ^{137}Cs (DuBard, 1978). This source is a fission product that is available commercially, and at moderate cost. With a half-life of 30 years it is a 'permanent' radiation source. Activities of the order of 150 - 200 Ci can be contained within a cylindrical capsule of 1 cm diameter.

Each of these gamma-ray sources has its own advantages and disadvantages depending on the nature of the experiment. Many of these important points will be mentioned throughout this thesis in connection with the ^{241}Am and ^{198}Au spectrometers used in the present study.

1.4 Aims of the Present Work

The aims of the present work are twofold and can be summarised as follows: to use existing low and high energy Compton spectrometers (^{241}Am, ^{198}Au) to study the momentum density in a variety of molecular and metallic systems, respectively; and to design and construct improved systems based on the results and conclusions drawn from the previous studies, and to use these new systems to observe more subtle bonding and conduction effects.

A large number of different materials (gases, liquids and solids) have received attention from the various experimental groups using both the X-ray and gamma-ray techniques. Some of these experiments have been made in the absence of any comparable theoretical work. In the case of molecular Compton scattering however, this has not been the case. A considerable amount of theoretical work has been done (Henneker and Cade, 1968, Roux and Epstein, 1973) concerning the potential of characterising bonding effects with very little experimental support. Particular interest has been shown (and evidence mounted) in support of a localised molecular orbital model. Using this model the profiles of relatively complex molecules can be approximated by summing the contributions due to highly localised momentum distributions, e.g. inner shells, lone pairs and bonding orbitals. These fragments of momentum density are usually determined from a small set of simple molecular profiles. Experimental evidence (Eisenberger and Marra, 1971, Epstein et. al., 1973) has indicated that such individual bond profiles are to a very good approximation transferable from one molecule to another.

From an experimental viewpoint however, both of these early studies were made using the X-ray technique and were conducted at a time when the full extent of the effects of multiple photon-electron scattering were not understood, and in some instances entirely neglected. The development

of the gamma-ray technique has uncovered and eliminated the major sources of systematic error. At the present level of accuracy and reliability it was desirable to undertake a comprehensive study of molecular Compton profiles.

The initial work would involve the original low energy gamma-ray system which uses a 300 mCi ^{241}Am source. The majority of the measurements would however, be obtained using an improved spectrometer, designed and constructed to house a 5 Ci ^{241}Am annular source. The benefits of this system should be expressed in a substantial increase in the Compton scattered intensity as well as an improvement in the momentum resolution. This would allow high quality measurements to be performed on a daily rather than weekly basis. The system would be designed to study only materials containing low atomic number elements and would be particularly suited to study hydrocarbon molecules. With the increased quality of the results it is hoped to look more closely at the localised molecular orbital model, and in particular the question of ideal transferability.

For the above study differential experiments,where attention is focussed on the difference between two similar profiles measured under near identical conditions, can provide a very sensitive technique. The use of such an approach can minimise the effects of almost all the systematic errors and has already been used to study molecular systems (Epstein et. al., 1973). A similar approach can be used to study solid state systems where measurements can be made on single crystals in various crystallographic directions. This method is rather more sensitive to the accuracy of the wavefunctions used since the profile contains directional information and not a result of integration over all solid angles akin to isotropic profiles. Differential experiments therefore provide a measure of the anisotropy in the electron momentum distribution.

Measurements of this kind have already been reported for a number of

metals and ionic crystals using ^{241}Am and ^{123m}Te radiation. In order to increase the scope of the measurements to include high atomic number elements it is necessary to use a high energy source other than those indicated. A ^{198}Au source has recently been used (Cooper et. al., 1976) to obtain the Compton profiles of aluminium and germanium (Z=32). The comparative success of these measurements has allowed a further investigation of the transition metal niobium, where attention could be focussed on the anisotropy in the momentum density and where a detailed comparison could be made with a recent Augmented Plane Wave (APW) band structure calculation (Wakoh et. al., 1975). Furthermore, the electronic properties of metal hydrides is currently of interest and it is hoped that by looking at the directional properties of a particular hydride of niobium ($NbH_{0.76}$) some interesting and detailed structurally information can be obtained.

The study of very high Z elements does however raise another important question concerning atomic calculations at the non-relativistic Hartree-Fock level. Such calculations will fail to take proper account of the relativistic effects in the wavefunction, especially of the inner s and p orbitals. Recent relativistic Hartree-Fock calculations (Mendelsohn et. al., 1974) have revealed significant effects particularly in lead (Z=82). The ^{198}Au system could therefore be used to investigate such effects while at the same time provide a method of assessing the potential of the current high energy system. However, results already obtained with this system although establishing the method as a valid and useful technique have shown that a new spectrometer could provide more intensity and thus allow even shorter measuring times than those attainable with the present system. The design and construction of a new ^{198}Au source facility was also initiated.

1.5 Plan of Thesis

The contents of this thesis are divided into nine chapters and are listed on pages preceding this introductory Chapter 1.

Chapter 2 of this thesis contains a summary of the theoretical aspects of the Compton scattering process, culminating in a relativistic Compton cross section expression appropriate to describe experiments undertaken with gamma-ray sources.

The third Chapter contains the general procedures necessary for processing gamma-ray Compton profile data.

The fourth Chapter deals specifically with the experimental techniques associated with the ^{241}Am gamma-ray sources, and with the design and construction of a Compton spectrometer housing a 5 Ci annular source.

In Chapter 5 the experimental and theoretical approaches to Compton scattering in molecules is reviewed. Measurements on gaseous hydrocarbon molecules are also presented in this chapter. The results of an extensive series of measurements on liquid hydrocarbons are presented in Chapter 6.

Anisotropy measurements with ^{198}Au on single crystals of niobium and niobium hydride are presented in Chapter 7, together with a measurement of the Compton profile of lead.

In Chapter 8 details of the development of an improved ^{198}Au source facility are described and compared with similar sources past and present.

Finally, in Chapter 9 the main conclusions, scope and limitations of each technique are discussed and contrasted with established methods. Future experiments with gamma-ray sources as well as with the established techniques are described.

CHAPTER 2

THEORY OF THE COMPTON PROCESS

2.1 General Theory of Scattering Processes

In a scattering experiment where the incident radiation is scattered weakly by the target, the scattering process may be treated in the lowest order Born approximation (Messiah, 1961). In this instance the spectrum of scattered radiation reflects the properties of the medium i.e. a correlation function. For incident photons of energy ω_1 and wavevector $\bar{k}_1$ impinging on a target, the scattering cross section contains information about the momentum $\bar{k} = \bar{k}_1 - \bar{k}_2$ and energy $\omega = \omega_1 - \omega_2$, where ω_2, $\bar{k}_2$ are the energy and wavevector of the scattered photon, respectively. The expression for the cross section can then be obtained via the Golden Rule,

$$\frac{d\sigma}{d\Omega\, d\omega} = \left(\frac{d\sigma}{d\Omega}\right)_e S(\bar{k},\omega) \qquad 2\text{-}1$$

$$S(\bar{k},\omega) = \sum_f \sum_i \left| \langle f | \sum_j \exp(i\bar{k}.\bar{r}_j) | i \rangle \right|^2 \delta(E_f - E_i - \omega) \qquad 2\text{-}2$$

Equations 2-1 and 2-2 contain three physically distinct pieces of information. The energy delta function contains all the relevant frequency information and expresses explicitly the conservation conditions. The matrix element is evaluated between the final $\langle f|$ and initial $\langle i|$ states of a many body system, and the factor $\exp(i\bar{k}.\bar{r}_j)$ simply gives the phase of the scattering amplitudes. The amplitudes from different scatterers are added and then squared so that in general there will be interference between scattering amplitudes. Finally, the term $(d\sigma/d\Omega)_e$ characterizes the basic coupling; for non-relativistic X-rays, for example, it is represented by the Thompson cross section, i.e. scattering from a single free electron.

The scattering formula defined by equation 2-1 is a general

scattering expression which can be subdivided further by specifying the nature of the final states $\langle f |$ which are involved. The following theory is strictly treated in the non-relativistic limit.

When the final and initial states are the same, i.e. $\langle f | = \langle i |$, the electron makes no transition and the atom as a whole takes up the electron recoil momentum. Since the atomic mass is relatively large their is negligible energy absorption. Under these conditions $\omega_1 = \omega_2$ and constructive interference exists between the scattering from individual electrons (the process is called elastic, coherent or Rayleigh scattering). In a crystal where there is spatial structure for example, this elastic scattering gives rise to intense diffraction in particular directions (Bragg scattering). The high intensity obtained in Bragg scattering makes the technique of X-ray diffraction particularly attractive. The intensity associated with the Bragg peaks depends upon the structure factor which describes the phase relationship between the scattering from different atoms. However, the scattering from each atom, the atom form factor, depends principally upon the electronic spatial density distribution, i.e.

$$f(\bar{k}) = \sum_n \int \left| \psi_n(\bar{r}_n)\, e^{i\bar{k}.\bar{r}_n} \right| d\bar{r}_n \qquad 2\text{-}3$$

Since atomic electron density distributions are concentrated around the core, the outer electrons make little contribution to the Bragg scattering. Although structure factor measurements have been successfully used to establish the crystal structure, the overall electron distribution in a solid is fairly close to that of the appropriate free atoms. The technique has since developed to include measurements on molecular crystals. Most of the work has been related to molecules formed with first row atoms for which good theoretical calculations are available. An excellent review of the experimental and theoretical developements in this field have been given by Ecker (1977) and Smith (1977), respectively.

During the scattering process the electron may also be raised to a

discrete excited state, i.e. $\langle f | = \langle n |$, and this process is called Raman scattering. Raman experiments using X-rays have yet to be performed although theoretical calculations in this energy range have been made (Doniach et. al., 1971). The majority of Raman experiments have been made using soft X-ray emission particularly at optical wavelengths (Crisp and Williams, 1960, Mahan, 1967).

The final possibility is that the scattered photon will leave the atom in an ionized state, i.e. $\langle f |$ = continuum, and this process is called Compton scattering. Compton collisions involve only incoherent scattering in which each electron acts entirely independently. The remainder of this chapter is devoted to the details of this process.

2.2 Non-relativistic Compton Cross Section

The energy losses suffered by X-ray photons in their passage through atomic systems will be typically small. To a first approximation therefore, $|\bar{k}_1| \simeq |\bar{k}_2|$, so that the momentum transfer $\bar{k}$ ($= |\bar{k}_1 - \bar{k}_2|$) will be determined to a high degree of accuracy by the scattering angle θ,

$$k = 2k_1 \sin \theta/2 \qquad 2\text{-}4$$

By scanning θ, it is possible to go from zero momentum transfer in the forward direction to a maximum in the backward direction of $2k_1$. The Compton scattering process can then be divided into two physically distinct regimes depending on the size of the momentum transfer.

For $k\lambda_c \ll 1$ (where λ_c is a characteristic wavelength approximately given by the interatomic spacing) there is interference between the scattering amplitudes from many electrons. In such a region the features of the spectrum tend to be dominated by the collective motion of a large number of electrons, i.e. plasmons. At the other extreme (the single particle regime), where $k\lambda_c \gg 1$, i.e. large momentum transfers, the scattering amplitudes do not interfere with one another, and it is this region of the $(\omega, \bar{k})$ space which is the subject of this study and the basis

of X-ray (and gamma-ray) Compton scattering (Platzman and Tzoar, 1977).

The Compton interaction process is shown schematically in Fig. 2-1. For an electron with an initial momentum $\bar{p}$, the energy transfer ω, is given by

$$\omega = \frac{(\bar{p} + \bar{k})^2}{2m} - \frac{p^2}{2m} = \frac{k^2}{2m} + \frac{\bar{k}.\bar{p}}{m} \qquad 2\text{-}5$$

The first term on the right hand side of the equation is the recoil or Compton shift term, and the second term is the so-called Doppler shift which depends on the momentum of the scattering electron. The interaction has been focussed however, only on a single scattering event, from one free electron with a momentum $\bar{p}$. Generally electrons in atoms have a momentum distribution given by $n(\bar{p})$, and defined by

$$n(\bar{p}) = \left| \int \exp(i\bar{p}.\bar{r})\psi(\bar{r})d^3\bar{r} \right|^2 \qquad 2\text{-}6$$

where $\psi(\bar{r})$ is the ground state position wavefunction, i.e. the Fourier transform of the momentum space wavefunction. If the scattering amplitudes from different electrons do not interfere, it follows that the cross section for the Compton scattering process may be given by (Platzman and Tzoar, 1965)

$$\frac{d\sigma}{d\Omega d\omega} = \left(\frac{d\sigma}{d\Omega}\right)_o \left(\frac{\omega_1}{\omega_2}\right) \int \frac{d^3\bar{p}}{(2\pi)^3} n(\bar{p}) \delta(\omega - \frac{k^2}{2m} - \frac{\bar{k}.\bar{p}}{m}) \qquad 2\text{-}7$$

or equivalently

$$\frac{d\sigma}{d\Omega d\omega} = \left(\frac{d\sigma}{d\Omega}\right)_o \left(\frac{\omega_1}{\omega_2}\right) J(\bar{q}) \qquad \bar{q}=\bar{k}.\bar{p} \qquad 2\text{-}8$$

where $J(q)$ is the Compton profile.

In order to arrive at this result Platzman and Tzoar (1965) assumed that the scattering had taken place from a single free electron possessing the same momentum distribution as a bound electron. The impulse approximation, partly defined above, therefore assumes that the binding energy of the electron (B_K, B_L, etc.) is much smaller than the electrons recoil energy gained in the scattering process ($\Delta\omega$). It has been pointed

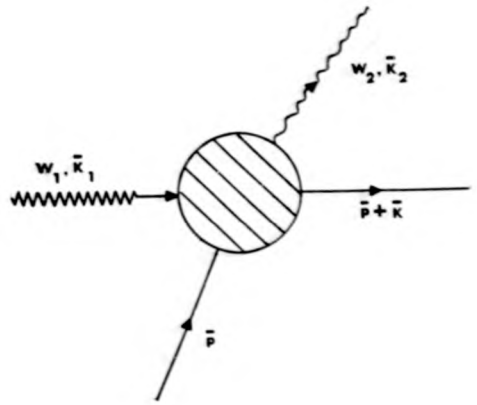

$$W = \frac{(\bar{p} + \bar{K})^2}{2m} - \frac{p^2}{2m} = \frac{K^2}{2m} + \frac{\bar{K} \cdot \bar{p}}{m}$$

Recoil Doppler

Fig. 2-1: The kinematics of free-particle electron-photon 'Compton' scattering.

out (Eisenberger and Platzman, 1970) that this is equivalent to assuming that the electron is moving in a constant potential and can therefore be regarded as free. Detailed calculations (Eisenberger and Reed, 1972) have led to the conclusion that this approximation is accurate to terms of order $(\Delta\omega/B_K)$.

However, when the incident photon energy is low, or the scattering angle small, the energy of the recoil electron is close to the binding energy, i.e. $\Delta\omega \sim B_K$ and the collective regime is entered with the result that the impulse approximation breaksdown. This partly explains why measurements with conventional X-ray sources ($\omega_1 \sim 15$ - 20 KeV) have concentrated on measuring systems in the first row of the periodic table where the impulse approximation has been shown to hold reasonably well (Eisenberger and Reed, 1974). The Compton profile of these low atomic number elements is rather insensitive to the core electrons (where B_K is greatest) and where the major contribution is attributed to the more lightly bound valence electrons. Therefore some breakdown in the impulse approximation can be tolerated for the core electrons without the introduction of serious errors.

2.3 Relativistic Compton Cross Section

The introduction of gamma-rays and the higher energies afforded by them have the advantage that the energy transfers are large enough to allow for investigations of a wider class of materials. For photon energies in the range 15 - 150 KeV the Compton cross section is roughly proportional to the atomic number Z, and the photoelectric cross section to Z^4/ω_1^3. For example, the use of ^{123m}Te gamma-rays produces a gain of about a factor of 10^3 in the Compton scattered intensity over Mo X-rays. At the same time they have reduced the uncertainties in using the impulse approximation for interpreting Compton profile data. However, a serious implication of the gamma-ray technique is the relativistic effect which is introduced because of the extremely large energy transfers. Typically $\omega_1/mc \sim 0.12$ for ^{241}Am, and ~ 0.88 for ^{198}Au. Therefore, in order to obtain

a more relevant cross section expression, for which the Compton profile is the momentum dependent part, consideration must be given to these relativistic effects.

The principal objective of a Compton scattering experiment is to extract from a measured differential cross section a description of the momentum distribution which is independent of the particular experimental conditions. Experimental factors such as initial photon energy and the scattering angle modify the energy distribution of the differential cross section and these must be eliminated from the final result which should contain only that part of the cross section which depends on the electron momentum. The differential scattering cross section should therefore be described in the following form,

$$\frac{d\sigma}{d\Omega d\omega} = C(\omega_1,\omega_2,\theta,p_z)\ J(p_z) \qquad 2\text{-}9$$

where the profile is given by

$$J(p_z) = \iint_{-\infty}^{\infty} n(\bar{p})dp_x dp_y \qquad 2\text{-}10$$

The mathematical details involved in determining this factor $C(\omega,\theta,p_z)$ can be found elsewhere (Manninen et. al., 1974, Eisenberger and Reed, 1974): only a summary of the important points are outlined in this section to clarify the approximations made.

If an electron is assumed to be initially free and at rest, the differential scattering cross section is given by the Klein-Nishina formula (Klein and Nishina, 1929). For the case of unpolarised incident radiation the cross section is given by

$$\left(\frac{d\sigma}{d\Omega}\right)_{KN} = \frac{r_o^2}{2}\left(\frac{\omega_2}{\omega_1}\right)^2\left(\frac{\omega_1}{\omega_2} + \frac{\omega_2}{\omega_1} - \sin^2\theta\right) \qquad 2\text{-}11$$

where r_o is the classical electron radius, and θ is the scattering angle. The incident and scattered photon energies, ω_1 and ω_2, respectively, are related by the expression

$$\frac{\omega_1}{\omega_2} = 1 + \frac{\omega_1}{mc^2}(1 - \cos\theta) \qquad 2\text{-}12$$

In the non-relativistic limit of Compton scattering, $\omega_1 \simeq \omega_2$ and the Klein-Nishina formula reduces to the classical Thompson cross section.

The Klein-Nishina formula has been generalised by Jauch and Rohrlich (1955) to include the case of moving, relativistic electrons, and is given by

$$\frac{d\sigma}{d\Omega d\omega} = \frac{r_0^2 m^2 \omega_2}{2E_2} \int \frac{d^3\bar{p}_1 n(\bar{p}_1)}{\omega_1 E_1} \int d^3\bar{p}_2 \, X \, \delta^4(k_1 + p_1 - k_2 - p_2) \qquad 2\text{-}13$$

where $(E,\bar{p})$ are the electronic properties, the subscripts 1 and 2 referring to the initial and final states, respectively, X is the flux factor, and the delta function arises from energy and momentum conservation. However, before the cross section can be applied to Compton scattering several modifications are necessary which involve a number of further approximations. Both the methods of Eisenberger and Reed (1974) and Manninen et. al., (1974) approached the problem in a similar manner. In reducing equation 2-13 to a form more suitable for Compton scattering two major problems were encountered:-

(i) E_1 depends on $\bar{p}_1$ rather than $\bar{p}_2$

(ii) X depends on both E_1 and $\bar{p}_1$

Without further approximations it is not possible to remove X from the integral and obtain the Compton profile as defined in equation 2-8.

Eisenberger and Reed (1974) and Manninen et. al. (1974) were able to obtain the cross section in closed analytical form by replacing E_1 by mc^2, i.e. neglecting terms of order p^2/m^2, and choosing a scattering angle of 180°. At this angle the expression for the flux factor $X_{180^\circ}(X(\theta = 180^\circ))$ becomes a constant, and can therefore be removed from inside the integrand. In this way the differential cross section can be written in the form defined by equation 2-7, i.e. a form akin to the non-relativistic expression.

Prior to 1975 this was the usual form of the cross section used by experimentalists to analyse their data. However, the question still remained as to the validity of the expression for scattering angles other than 180°. This is a relatively important question since experiments are necessarily performed at lower angles, typically 150°, to avoid the coincidence of the scattering volume with the walls of the sample chamber. Moreover, as the accuracy and reliability of the experimental technique improves, the angular dependence of the relativistic cross section becomes important. Ribberfors (1975) has recently studied this problem theoretically, elaborating on the approaches used by Eisenberger and Reed (1974) and Manninen et. al. (1974). The resulting expression for the differential cross section involved a series expansion of which the zeroth order was accurate enough to describe the Compton profile in its usual form for all angles of scattering,

$$\frac{d\sigma}{d\Omega d\omega} = \frac{m^2 r_o^2 \omega_2}{2\omega_1 kE} \; X \; J(p_z) \qquad 2\text{-}14$$

Here the flux factor is a more complicated expression than that used previously, now depending on E, p and θ, i.e.

$$X = \frac{R}{R'} + \frac{R'}{R} + 2m^2\left(\frac{1}{R} - \frac{1}{R'}\right) + m^4\left(\frac{1}{R} - \frac{1}{R'}\right)^2 \qquad 2\text{-}15$$

$$R = \omega\left[E + (\omega_1 - \omega_2 \cos\theta)p_z/k\right] \qquad 2\text{-}15$$

$$R' = R - \omega_1\omega_2(1-\cos\theta)$$

and

$$E = (p_z + m^2)^{1/2}$$

Despite the improvement in describing the cross section, both the Ribberfors (1975) expression and that derived by Eisenberger and Reed (1974) and Manninen et. al. (1974) are still in use. It was of some importance therefore to compare the effects of using each cross section in analysing Compton profile data for varying angles of scattering θ, and incident

energy ω_1. Fig. 2-2 shows the effect of the differences as a function of θ and ω_1 commonly used in experiments using gamma-ray sources. The ordinate represents differences in the proportionality factor which relates the cross section to the Compton profile. The largest discrepancies are obtained for high energy gamma-ray sources, particularly at large angles of scattering. The opposite effect is obtained for 60 KeV radiation whereas 160 KeV gamma-rays produce only a small difference. The Ribberfors (1975) expression is a more general equation that is clearly more appropriate for Compton scattering studies undertaken at lower angles. Because of the significant differences between the two cross section relations particularly at 60 KeV and 412 KeV, the Ribberfors (1975) expression has been used throughout this thesis to analyse all experimental results.

2.4 Validity of the Impulse Approximation

In the above analysis of the differential scattering cross section the use and validity of the impulse approximation has been implicitely assumed. Developments in the experimental technique, both in photon Compton scattering and electron scattering, have resulted in an overall improvement in the quality and accuracy of the profiles reported. This has led several experimental groups to publish results which appear to refute the accuracy of the impulse approximation and its validity in constructing the cross section expressions. Experimental evidence for this defect obtained using X-rays (Weiss, 1975, Weiss et. al., 1977) and electron scattering (Barlas et. al., 1977,1978, Tavard, 1978), have shown that the Compton profile of loosely bound electron systems have their profiles centred around a shifted energy that is some 10 - 20 eV smaller than the Compton shift for a free stationary electron.

The early theoretical calculations of Currat et. al. (1971) and Bloch and Mendelsohn (1974) however, demonstrated that the corrections to the impulse approximation were negligible. The main difficulties

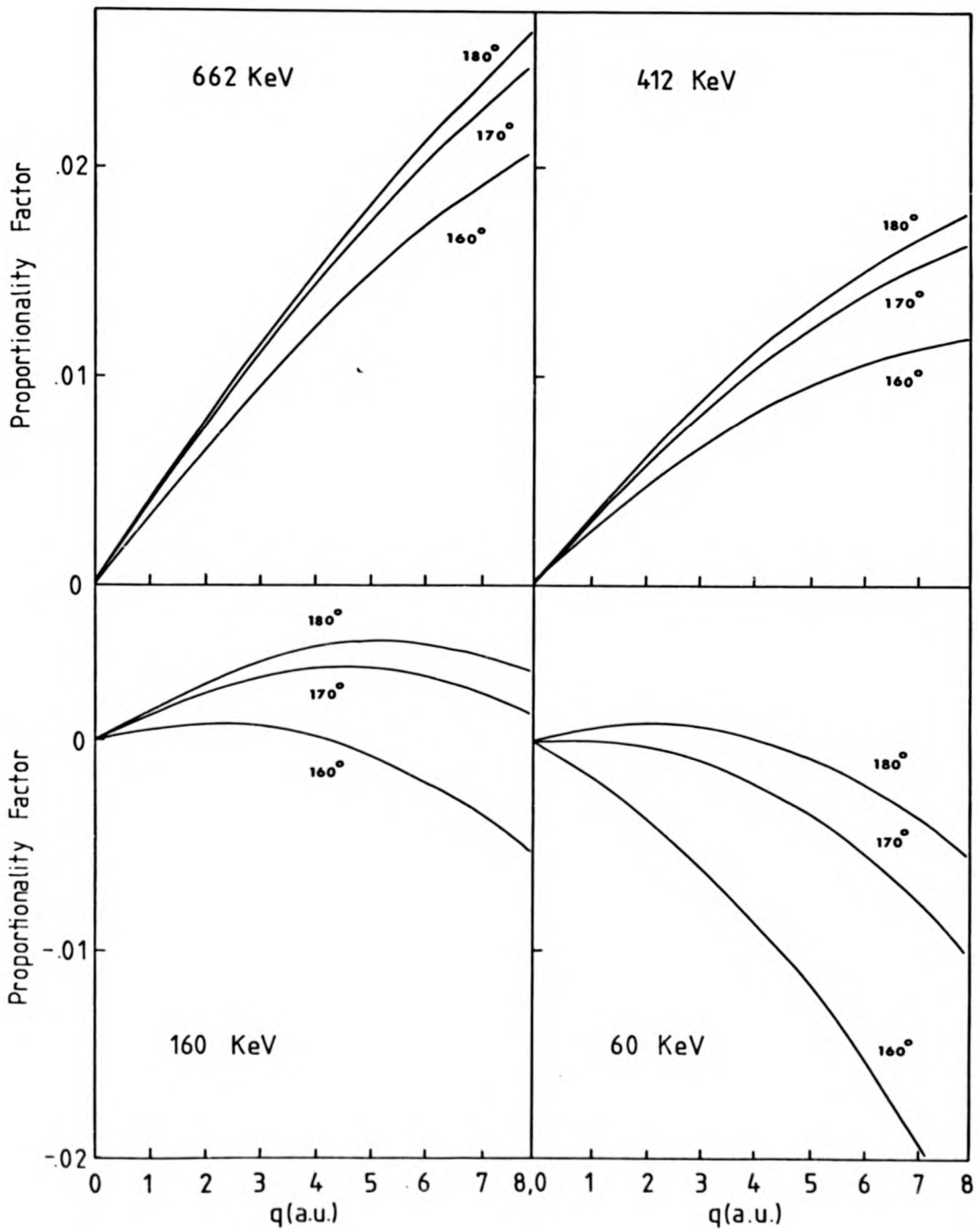

Fig. 2-2: Comparison of the relativistic Compton cross sections as a function of incident photon energy and angle of scattering.

which have been encountered in the calculations are in evaluating the total final state wavefunction when one electron has been ejected from the atom. Currat et. al. (1971) have calculated the core contribution to several Compton profiles, employing excited state one-electron continuum wavefunctions evaluated in the ground state potential of the nucleus, and the remaining electrons. They obtained good agreement with an impulse approximation calculation, and this was verified experimentally. Eisenberger and Platzman (1970) obtained analytic 'exact hydrogenic' profiles for K-shell electrons and compared them with the profiles calculated within the impulse approximation. The results showed clearly that the low energy recoil portion of the spectrum was defined very accurately by the impulse approximation, deviations becoming apparent only when the threshold was reached, i.e. $\Delta\omega \sim B_K$. Mendelsohn and Bloch (1975) have extended the previous calculations to cover a wider range of incident photon energies, and scattering angles for both K and L shell electrons with similar results.

However, recent calculations by Mendelsohn and Grossman (1977) and Mendelsohn (1978) using exact Hartree-Slater equations at X-ray and gamma-ray energies have resulted in defects which are in qualitative agreement with experiment. The largest defect was found for the M-shell electrons. The calculations undertaken at 60 KeV are also in reasonable agreement with recent measurements made by the author on aluminium. These recent results are discussed more fully in Appendix A.

2.5 Multiple Scattering Processes

In the derivation of the cross section expression a single photon-electron collision has been investigated and the final result has described the energy distribution of photons scattered at an angle θ. However, it is possible that a photon may have suffered more than one collision before leaving the sample, and the question arises as to what extent the spectral distribution of scattered photons is affected by these multiple scattering events. The severity of the problem was highlighted by Reed and Eisenberger

(1972) in measurements on silicon. They reported that the measured line shape was strongly dependent on the sample scattering volume, and attributed their results to the effects of multiple photon-electron collisions. Although the problems are clearly confined to experimental profiles the methods which have been used to determine the multiple scattered photon energy distribution have been confined predominantly to theoretical calculations. However, experimental techniques do exist, and these together with theoretical methods fall naturally into three categories.

The first method is to change the dimensions of the scattering body in such a way that the probability of occurence of events involving more than one photon-electron scattering is reduced. With this method the most obvious approach is to use a series of thin samples and extrapolate the results to zero thickness. Although this approach has been attempted the extrapolation is complicated because the distortion has been found to vary either linearly (Manninen et. al., 1974) or as the square root (Paakkari et. al., 1974). Measurements on samples of varying thickness are therefore not only time consuming but can lead to results which are possibly unreliable.

The second method is to study the amount of multiple scattering directly by only measuring the intensity of those collisions due to multiple scattering using a displaced beam technique (Phillips and Chin, 1973). Although the probability of obtaining a given pair of scattering angles is altered by displacing the beam, the measured profile of multiple scattered events may still be used to correct the observed Compton profile. The experimental uncertainties in this method are however still too large for a reliable, corrected profile to be extracted.

Finally, the intensity and spectral distribution of multiple scattering events can be calculated for a given sample thickness and geometry, and the results applied directly to the measured Compton profile. It is variations of this approach which have been used by experimentalists

because of the flexibility which can be built into the technique.

The first attempt to obtain a theoretical understanding of the multiple scattering process was made by DuMond (1930) who calculated analytically the intensity of twice scattered radiation. DuMonds work was extended by Williams et. al. (1974) to include the case of moving electrons. This gave rise to some of the basic ideas which were subsequently used in more advanced studies of the collision process. One such effect, recognised by DuMond (1930) and later verified by Reed and Eisenberger (1972), was that the shape of the scattering body plays an important part in determining the energy distribution of multiple scattered radiation. Unfortunately a purely analytical formulation of the problem was impossible. McIntire (1974) was, however, able to calculate the spectral distribution of double scattering of 60 KeV photons scattered at 180°, partly analytically and partly using numerical integration. Fortunately, at this angle of scattering the multiple scattered profile is centred at the same energy location as the single scattered profile. It was clear, therefore, that a study of the interaction process on a more general basis would require a more sophisticated method of approach.

Felsteiner et. al. (1974) have applied a Monte Carlo technique to estimate the amount of multiple scattering for a specific experimental condition. The principal of the procedure, described in more detail in Chapter 3, is to simulate using a computer a real experiment by following a large number of photon paths in the sample under rigid, specified conditions. They took into account the nature of attenuation by using cross section expressions for elastic and inelastic scattering, and also allowed for the possibility of photoelectric absorption.

A similar and alternative procedure developed by Halonen and Williams (1975) uses a theoretical single scattered profile to generate the multiple scattering contribution. The intensity of the multiple scattered

contribution is obtained from a Monte Carlo calculation. A major advance in using this procedure was the introduction of a binding energy cut-off which is essential when undertaking corrections in materials of high atomic number. Modifications were soon made by Felsteiner and Pattison (1975) in their Monte Carlo approach, to take account of electron binding energies.

A series of papers by Tanner and Epstein (1976) have reformulated the ideas of McIntire (1974) and undertaken a complete analytical investigation of single and double scattering from cylindrical samples. They found that by taking a sufficiently thin sample one may obtain the angular distributions for single and double scattering, and the total intensity of single scattering exactly. In order to achieve this they found it necessary to ignore the change in the absorption coefficient with photon energy and to employ the Thompson cross section with stationary electrons. They were also able to show that sample geometry is more important than the form of the cross section in determining the intensity, spectral and angular distributions. This latter point is in agreement with the results of Williams (1977) who showed that although the magnitudes of the various cross sections are significantly different, the energy dependence of each one is essentially the same.

At the present time the Monte Carlo technique developed by Felsteiner and Pattison (1975) is currently the most widely used method for correcting experimental profiles. The method has therefore been used by the author to correct all experimental data presented in this thesis. A full and more detailed description of the Monte Carlo technique has been given by Pattison (1975).

CHAPTER 3

GAMMA-RAY DATA REDUCTION

3.1 Introduction

The standard arrangement for a gamma-ray Compton scattering experiment consists of a radioactive source and a high resolution solid state detector linked to a multichannel analyser (MCA). A schematic diagram of a typical gamma-ray apparatus is shown in Fig. 3-1. The MCA in conjunction with the solid state detector measures all points on the profile simultaneously, instead of sequentially as in the X-ray method. Such a system enables the scattered radiation to be energy analysed at a fixed angle of scatter θ. By collimating the incident and scattered beams, the Compton scattered intensity is reduced considerably since the solid angle is severly restricted. However, even this experimental geometry allows a significant proportion of the scattered photons to scatter twice or even more times before leaving the sample. These multiple scattering events also have to be contended with.

When enough Compton counts have been accumulated, a series of important corrections must be made in order to obtain the Compton cross section and hence the Compton profile from the scattered intensity. The relation between the cross section and the Compton profile for X-rays and gamma-rays has already been considered. In this chapter the procedures adopted to obtain the Compton profile from a scattered intensity are described.

The observed intensity $I(\omega)$ can be expressed in a general equation which relates $I(\omega)$ to the cross section $d\sigma/d\Omega d\omega$,

$$C(\omega) = G(\omega)A(\omega)\frac{d\sigma}{d\Omega\, d\omega}\left[I(\omega) - B(\omega)\right] \qquad 3\text{-}1$$

where $B(\omega)$ is the background, $A(\omega)$ is an absorption correction and $G(\omega)$ is

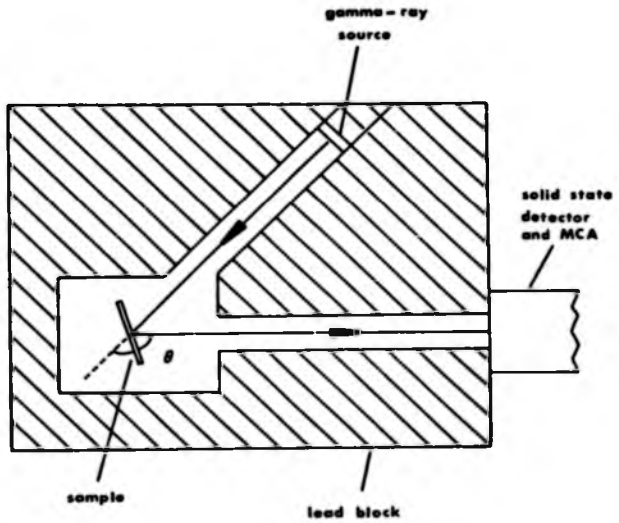

Fig. 3-1: Schematic arrangement of a typical gamma-ray apparatus.

an efficiency correction for the solid state detector. The corrected data $C(\omega)$, is then deconvoluted to remove the effects of instrumental resolution, $R(\omega)$, and normalised such that the area under the Compton profile is equal to the number of electrons per atom, i.e.

$$\int_{-\infty}^{\infty} J(p_z)dp_z = \frac{1}{T}\int_{-\infty}^{\infty} \left[C(\omega) * R(\omega)\right] d\omega \frac{dp_z}{d\omega} = N \qquad 3\text{-}2$$

where T is a normalisation constant, N is the number of electrons per atom, and * denotes convolution. Both of these expressions are general, and are applicable to any gamma-ray Compton profile data. The large amount of data which is collected, coupled with some complicated correction procedures, necessitates the use of a computer which can cope with the large data arrays. The final section of this chapter considers the computational aspects of undertaking the following corrections to Compton profile data.

3.2. Preliminary Calculations and Corrections

3.2.1 Energy Calibration

The energy calibration of the channels in the MCA is usually determined before an experiment is begun. The peak positions of several gamma-ray lines produced by a number of different, low activity radioactive sources, are determined by fitting a parabola over a restricted range of data covering each peak. The linear energy-channel relation is found by making a least squares fit to obtain the coefficients 'a' and 'b' in the expression for the energy,

$$\omega_i = a + bk_i \qquad 3\text{-}3$$

where ω_i is the energy (in KeV) corresponding to the MCA channel number k_i, $(k_i \geq 0)$. The slope of the line, b, gives a measure of the channel spacing in KeV. The maximum deviation from linearity across the energy ranges typically used in gamma-ray experiments, e.g. ^{241}Am(26 -74 KeV), ^{198}Au(140 - 190 KeV), are usually less than 0.04%. From equation 3-3 the value of scattered gamma-ray energy at any point in the experimental Compton

profile can be obtained by linear interpolation between the energy locations, specified above.

3.2.2 Background

The removal of the background from the energy loss spectrum is necessary before the remaining data processing procedures can be used. The background consists of three main components:

(i) a part due to Compton scattering of the radiation from the walls of the sample chamber.

(ii) a random part due to the natural radioactivity, i.e. cosmic rays.

(iii) a part due to radiation detected directly from the source.

For most experimental situations, particularly those of short duration, the second contribution is of little importance and can be safely neglected. The remaining contributions have to be measured and subtracted from the Compton scattering data.

The measurements are accomplished by recording the energy loss spectrum from the sample chamber after the removal of the sample. If the sample was contained in a holder, then this to is included in the background spectrum. For samples containing light elements, or for high energy incident radiation, the effect of absorption in the sample on the background can be neglected.

The background determined in this way can be subtracted from the raw data on a point-by-point basis only after applying an appropriate normalisation procedure. For measurements conducted with gamma-ray sources having long half-lives (e.g. ^{241}Am, ^{137}Cs) the procedure involves normalising the background relative to the elapsed time over which the data was collected. For measurements using short half-life sources (e.g. ^{123m}Te, ^{198}Au) a second correction is necessary to take account of the decay of the source and the exponential decrease in signal.

3.2.3 Detector Efficiency

Once the energy scale is established, and the background subtracted, it may be necessary to undertake a correction for the energy dependence of the detector efficiency. For Compton profiles measured in the energy range 30 - 60 KeV with a germanium solid state detector, the efficiency curve for this detector is almost 100%, and constant over this range. An efficiency correction for profiles measured with ^{241}Am sources is therefore not necessary. However, above 60 KeV the efficiency curve falls rapidly, decreasing to 20% at 160 KeV, and only 5% at 412 KeV, necessitating the use of a correction for all other gamma-ray sources presently in use. The form of correction must be represented by some analytical function of the gamma-ray energy in order to correct the measured intensity at each point in the profile.

The form of this analytical expression is obtained experimentally by measuring selected gamma-ray lines over the region of interest. Although the appropriate absorption coefficients should be included in the fit, i.e. elastic, inelastic and photoelectric, in practice it is only necessary to use the photoelectric mass absorption coefficient appropriate to germanium (Cooper et. al., 1976). The discrepancy between the measured efficiency and the calculated curve using the photoelectric absorption coefficients only (using eq. 3-4) was within the quoted experimental error of $\pm$ 2%. The analytical expression for the detector efficiency correction used in the data analysis is given by

$$G(\omega) \propto \int_0^d e^{-\mu(\omega)t}\, dt = \frac{1 - e^{-\mu(\omega)d}}{\mu(\omega)} \qquad 3\text{-}4$$

where d represents the thickness of the active region of the germanium crystal, and μ is the absorption coefficient.

An absolute determination of the form of this correction is not required, only its behaviour as a function of energy. It is necessary, however, that this behaviour is known as accurately as possible since

corrections to the data are large, and consequently small errors in the efficiency curve will be amplified when the data is normalised.

3.3 Deconvolution

(i) The Resolution Function

Before the next stage in the processing can be undertaken, i.e. the deconvolution of the measured line shape, a measurement of the instrument resolution function is required. The full-width-at-half-maximum height (FWHM) of the detector resolution function varies as $\omega_1^{1/2}$, while for low energies ($\omega_1 < mc^2$) the Compton profile width varies as ω_1. Although the energy resolution of the detector therefore varies over the range of energy in which the Compton profile is measured, it is not possible in practice to experimentally determine this variation at each point on the profile. Furthermore, it is only possible to obtain a resolution measurement close to the centre of the profile, and this criterion depends upon the availability of radioactive sources possessing isolated gamma lines close to the energy of the profile centre. Fortunately experience has shown that neither of these conditions impose any real serious constraints on the analysis of Compton profile data. In Chapters 4 and 7 the methods used to obtain an accurate measurement of the resolution function for ^{241}Am and ^{198}Au Compton spectrometers are described.

Measurements of the resolution function have shown that it can be well represented by a Gaussian line shape with a small (~1% of the peak height) low energy tail. The tail arises from incomplete absorption of the incoming radiation in the detector crystal and also from multiple Compton air scattering between the source and detector (if the experimental system is not completely evacuated). The latter effect which has only recently been recognised (Cooper et. al., 1978) plays an important part in the deconvolution of the profile and effects dramatically the final symmetry of the profile. Such effects are described in Chapter 4.

The aim of the deconvolution procedure is to remove the effects of instrumental resolution from the measured spectrum. In principle this objective can be achieved exactly if the experimental data is divided by the resolution function in the frequency domain. However, the measured spectrum inevitably contains high-frequency components which arise from the random statistical errors on the raw data. The noise is therefore treated in the same way as the spectrum to be deconvoluted i.e. as if it was subject to the same detector function. There are several procedures available which have been used with Compton profile measurements: Fourier analysis based on Stokes' method (Stokes, 1948, Cheng et. al., 1971); the method of successive approximations (Phillips and Weiss, 1968, Reed and Eisenberger, 1972); the method of graphical reconstruction (Lloyd, 1969, Pattison, 1975); and finally the generalised least squares method (Paatero et. al., 1974). For a general review of deconvolution methods reference should be made to a recent article by Cooper (1977).

The above mentioned methods were designed to suppress the over-amplification of the high-frequency oscillations by encorporating a filtering procedure. The filtering is designed to produce a deconvoluted profile as close to the 'true' profile as possible, and this is achieved by making a sharp cut-off in the frequency spectrum of the data. This operation is particularly important when the theory itself predicts some high-frequency components arising for example from a sharp change in slope in a profile, e.g. a break in the profile of a metal at the Fermi momentum. The importance of the filter function has already been stressed by Paatero et. al. (1974) who called it the 'Residual Instrumental Function' (RIF). However, in order to make a reliable comparison between the deconvoluted measured profile and any given theory it is necessary to make a similar filtering of the theoretical profile. Unfortunately, a sharp cut-off in the Fourier coefficients leads to a complex RIF in momentum.

space and this makes the comparison between experiment and theory rather difficult.

(ii) The Filtering Procedure

The approach used in the present data processing is a little different since here the RIF is chosen so as to simplify as much as possible the comparison between theory and experiment. If $f(\bar{k})$, $g(\bar{k})$ and $h(\bar{k})$ represent the true Compton profile, experimental resolution function and measured Compton profile in the channel domain, respectively, then the measured profile is the convolution of $f(\bar{k})$ with $g(\bar{k})$, i.e.

$$h(\bar{k}) = f(\bar{k}) * g(\bar{k}) \qquad 3\text{-}5$$

In principle the Fourier transforms $H(\bar{\nu})$ and $G(\bar{\nu})$ can be calculated, and the Fourier transform of the true Compton profile $F(\bar{\nu})$, obtained by Stokes' method of Fourier deconvolution as

$$F(\bar{\nu}) = \frac{H(\bar{\nu})}{G(\bar{\nu})} \qquad 3\text{-}6$$

In this ideal situation the true profile can be obtained by Fourier synthesis of $F(\bar{\nu})$, i.e.

$$\left\{F(\bar{\nu})\right\} = f(\bar{k}) \qquad 3\text{-}7$$

where $\{\ \}$ denotes Fourier synthesis. In reality, however, the computation requires the application of some filter function $s(\bar{k})$ from which it follows

$$f^{\circ}(\bar{k}) = \left\{F^{\circ}(\bar{\nu})\right\} = \left\{\frac{H(\bar{\nu})}{G(\bar{\nu})} S(\bar{\nu})\right\} \qquad 3\text{-}8$$

$$f^{\circ}(\bar{k}) = \left\{F(\bar{\nu}) S(\bar{\nu})\right\} \qquad 3\text{-}9$$

and hence

$$f^{\circ}(\bar{k}) = f(\bar{k}) * s(\bar{k}) \qquad 3\text{-}10$$

The RIF of Paatero et. al. (1974) makes $s(\bar{k})$ a complex function, but leads to an $f^{\circ}(\bar{k}) \simeq f(\bar{k})$, the true profile. The present processing follows the procedure first introduced by Weyrich (1975) and later used by

Cooper et. al. (1976), and uses a Gaussian filter function. This has the advantage of possessing an analytical counterpart in the channel domain. Moreover, if the Gaussian filter function is chosen to have the same FWHM as the measured resolution function, then any features which remain after processing can be reliably interpreted as physical rather than some statistical error amplified by the deconvolution process. This method therefore affords a relatively simple comparison between experiment and theory provided that the theoretical profiles are convoluted with the same Gaussian function. Making $s(\bar{k})\equiv g(\bar{k})$ it follows from eqns. 3-5 and 3-10 that $f^{\circ}(\bar{k})=h(\bar{k})$. The final profile after deconvolution and filtering is therefore a tail corrected profile equivalent to the true profile convoluted with a Gaussian of known width.

The Fourier transform of the experimental data and measured resolution function are performed using a Fast Fourier transform routine. Simultaneous division, filtering, and Fourier synthesis of the deconvoluted experimental data are also carried out in this routine. The Gaussian filter function in the channel domain is chosen to be represented by an expression of the form

$$s(\bar{k}) = \exp\left(-\frac{k^2}{b^2}\right) \qquad 3\text{-}11$$

where k is the channel number, and b the filter function parameter specified by

$$b = \frac{N2\sqrt{\ln 2}}{\pi\Delta\omega_{\tau}(k)} \qquad 3\text{-}12$$

where N is the total number of channels subject to the Fourier transformation and $\Delta\omega_{\tau}(k)$ is the total FWHM of the resolution function expressed in the number of channels. The calculation of $\Delta\omega_{\tau}(k)$ depends on the experimental conditions which vary from one experiment to another. Details of its determination can be found in Chapter 4.

3.4 Energy Dependent Corrections

3.4.1 Absorption

The sample absorption correction is necessary because the intensity of the photon beam is diminished as the incident beam enters the sample and as the scattered beam leaves. Photoelectric absorption is the main process which has in the past restricted the scope of Compton scattering to elements in the first two or three rows of the periodic table. Fortunately, the use of gamma-rays has lifted some of the restrictions on the materials that can be profitably studied.

In the data processing the analytical expression for a plate sample geometry is given by

$$A(\omega) = \frac{\mu(\omega)\csc\eta_1 + \mu(\omega_1)\csc\eta_2}{1-\exp\left[-t(\mu(\omega)\csc\eta_1 + \mu(\omega_1)\csc\eta_2)\right]} \qquad 3\text{-}13$$

where t is the sample thickness, μ the total mass absorption coefficients, and η_1 , η_2 are the angles between the sample face and the incident and scattered beams, respectively ($\eta_1+\eta_2+\pi=\theta$, where θ is the angle of scattering). The mass absorption coefficients for elastic (μ_{el}), inelastic (μ_{inel}) scattering and photoelectric absorption (μ_a) were calculated using the empirical formula derived by McMaster et. al. (1969),

$$\ln u_n(\omega) = \sum_{i=0}^{1,2,3} A_{ij} \left[\ln(\omega) \right]^{1/2} \qquad 3\text{-}14$$

where $u_n(\omega)=(u_{el}, u_{inel}, u_a)$, and A_{ij} are the ln-ln coefficients given in tabulated form by McMaster et. al. (1969) for each process and for each element in the periodic table. The total absorption coefficient for the sample is then calculated via the equation

$$u_{total} = u_{el} + u_{inel} + u_a \qquad 3\text{-}15$$

An absolute value of the correction term is not required only its dependence on the energy over the region of interest in which the Compton profile is measured.

A second absorption correction, albeit small, is also required to make allowance for the loss of intensity caused by air absorption between the source, sample and detector. However, for high energy incident radiation or for systems that are continuously evacuated, such a correction is not necessary since air absorption is negligible.

Inherent in the calculation of $A(\omega)$ is a knowledge of the scattering angle, θ. A preliminary value is obtained by fitting a parabola over the peak of the Compton profile data, to obtain the energy at the centre of the profile ω_c. The scattering angle is then given by

$$\cos\theta = 1 - \left(\frac{\omega_1 - \omega_c}{\omega_1 \omega_c}\right) \qquad 3\text{-}16$$

and it is this angle which is used to correct for absorption in the sample.

3.4.2 Cross Section Transformation

An accurate location of the profile centre (corresponding to the origin of the electron momentum scale) is of major importance in the data reduction (Williams, 1976) particularly in performing the cross section to Compton profile transformation. After correcting the data for sample absorption the peak position is located again using the same method of fitting a parabola over the profile centre. This is necessary especially when high Z samples are being analysed, because the absorption correction causes a small shift in the position of the peak, and hence a small change in the scattering angle. The angle obtained by this method is used to convert the abscissa from an energy scale to a momentum scale. The Compton profile is subsequentely extracted from the measured cross section using eqn. 2-14 (Ribberfors, 1975) in the limited range $\pm$ 0.5 a.u. The centre of the profile is relocated by fitting a quartic polynomial to $J(q)$ and a more accurate value of the scattering angle deduced. Using this more precise value the entire Compton profile is recalculated.

The momentum scale is simultaneously calculated at selected values

of energy, ω_2, using the expression given by Ribberfors (1975),

$$p_z = \frac{\omega_1\omega_2(1-\cos\theta) - (\omega_1 - \omega_2)}{(\omega_1^2 + \omega_2^2 - 2\omega_1\omega_2\cos\theta)^{1/2}} \qquad 3\text{-}17$$

where p_z is defined such that $p_z > 0$ lies on the high energy side of the profile.

3.4.3 Normalisation

The rather elaborate method involved in defining the momentum scale is critical since a small error in q will have a significant effect on the profile after normalisation. Ideally the Compton profile is normalised according to the number of electrons in a formula unit, i.e.

$$\int_{-\infty}^{\infty} J(p_z)dp_z = N \qquad 3\text{-}18$$

where N is the number of electrons. In practice the normalisation is carried out over a limited momentum range up to p_z^m, where p_z^m is a maximum value of the momentum over which the experimental data can be accurately measured. The normalisation condition is then given by

$$\int_{o}^{p_z^m} J(p_z)dp_z = \frac{N^*}{2} \qquad N^* < N \qquad 3\text{-}19$$

This implies that beyond p_z^m the experimental profiles can be described to a high degree of accuracy by a free atom model. Fortunately it is just this region where the major contribution to the Compton profile arises from the non-bonding core electrons. The approximation is certainly justified provided that the cut-off point is accurately determined. The position of p_z^m depends on the energy (momentum) transfer which is governed by the incident energy and angle of scattering. In these outer momentum regions there is also a greater influence of errors where the profile is small and where the signal-to-noise is appreciably lower. For ^{241}Am $p_z^m \sim 5$ a.u., and for ^{198}Au, $p_z^m \sim 7$-10 a.u.

In defining the normalisation condition in this way (eqn. 3-19) only the high energy side of the profile has been considered. The low energy

side is not normally considered because it is more heavily weighted by the uncertainties in the processing procedures particularly the removal of the tail contribution in the deconvolution step. Although the tail is small it extends for many KeV below the incident photon energy, and accounts for some 20% of the total area under the resolution function. When this asymmetric resolution function is convoluted with a symmetric profile it produces a progressive asymmetric broadening on the low energy side of the line, leaving the high energy side virtually unaffected. While the removal of the tail is formally part of the deconvolution procedure the correction on the low energy side is very sensitive to the exact form of the resolution function, the statistical accuracy of the data, and the precise location of the profile peak (see Chapter 4.).

The value of N^* is obtained by calculating the area under a free atom profile over the same range of momenta using either the non-relativistic (for low-medium Z elements), or the relativistic (for high Z elements) free atom profiles tabulated by Biggs et. al. (1975). The area under the atomic profiles are determined by interpolating them at intervals of 0.1 a.u. with cubic spline functions (Reinsch, 1967) which are accurate to $\pm$ 0.003 a.u. and then integrating using the trapezoidal method. After normalising the high energy side of the experimental profile to this value, a linear interpolation is made between the data points to calculate $J(q)$ at regular intervals of momentum, i.e. 0.1 a.u. up to p_z^m. Since the experimental profile has earlier been filtered with a Gaussian function some fifteen times broader than the channel spacing (channel spacing $\Delta k \sim 0.03$ a.u., Gaussian function FWHM $\sim$ 0.4 a.u.) a linear interpolation is quite satisfactory. Finally, the tabulated profile is again integrated to check on the normalisation and to compare areas under the high and low energy sides of the profile.

3.5 Multiple Scattering Correction

Unfortunately in all experimental arrangements a significant amount of the scattered intensity is a result of multiple photon-electron scattering events which play an important part even in relatively thin samples (Halonen, 1975). The complex problem of multiple scattering has stimulated considerable effort directed at a general understanding of the interaction process. A summary of these efforts from an experimental and theoretical viewpoint was given in the latter part of the previous chapter. For the experimentalists it is the Monte Carlo method, developed specifically for Compton scattering by Felsteiner and Pattison (1975) which has provided an approach which is versatile enough to cater for the wide range of experimental variables, e.g. photon energy, sample geometry, atomic weight of sample etc. An analysis of the Monte Carlo procedure has been the subject of another thesis (Pattison, 1975) to which reference should be made for a detailed discussion. It is the purpose of this section to give only a summary of the procedure.

The Monte Carlo method consists of simulating, following and tabulating the paths of a large number of photons ($\sim 10^{5-6}$) through a sample using a high speed computer. The paths are generated by choosing random numbers to simulate the probabilities of various events, e.g photoelectric absorption, elastic scattering. Since all the calculations are performed numerically the various photon-electron interaction processes can be specified in as much detail as desired. The procedure can be summarized as follows:-

(a) Choose the point of entrance of the photon on the sample face.

(b) Choose the point of the first photon-electron collision, forcing it to occur within the sample for increased efficiency.

(c) Choose the nature of the scattering event, i.e. elastic, inelastic, photoelectric absorption, according to the relative

cross sections for the various processes.

(d) Input the angle of scattering (determined previously to obtain p_z=0) and change the photon energy accordingly.

(e) Calculate the distance to the next collision.

(f) Determine the direction of the scattered photon and using the distance (part (e)) and sample geometry, determine whether or not the next collision will occur within the sample. If it occurs within the sample return to step (c) and continue. If outside the sample the photon has escaped and proceed to step (g).

(g) On leaving the sample, the quantities desired, such as the observed scattering angle, number of collisions, and energy of the photon, are stored in appropriate registers.

In order to calculate the spectrum of multiple scattered radiation an iterative technique is employed. The normalised experimental profile is taken as a first approximation to the true profile. This assumes that the actual multiple scattered profile may be written as the convolution of the unknown single scattered profile with the multiple scattered profile calculated by the Monte Carlo technique. The calculated multiple scattered profile (using the Klein-Nishina cross section for a stationary, free electron) is subtracted from the experimental profile, the corrected profile being renormalised and the result used as a new approximation to the single scattered profile. The procedure can be recycled until self-consistency is reached, but usually convergence is very rapid and only one iteration is usually required.

The above condition only applies to profiles of relatively light materials which have been measured on low energy gamma spectrometers, e.g. ^{241}Am. In this case only 5.10^5 photon paths are usually required to be followed and where only double Compton scattering events are considered. Recently, however, measurements with high energy sources e.g. ^{198}Au have

resulted in a considerable amount of multiple scattering (~30% of the total scattered intensity) even for relatively thin samples. For these cases triple and higher order multiple scattering events have to be considered. Here convergence may only be attained if two or more iterations are used.

3.6 Computational Considerations

The programs and subroutines used throughout this thesis to analyse gamma-ray Compton profile data are modified versions of those introduced by Weyrich and Pattison (1975). Some of the codes have been translated from Algol 60 to Fortran IV. The results of some early measurements reported in Chapter 5 have been processed on an ICL 4130 computer at the Computer Centre, University of Warwick. However, the majority of the results have been processed on a recently acquired Burroughs B6700 at the Centre. There were little difficulties in adapting the programs to run on the more efficient computer. The only exception to this general rule concerns the application of the Monte Carlo program, which by its very nature requires a substantial amount of core space. Although the program was initially run on the Manchester Regional Computer because of time and efficiency, it has been possible to run a more updated and more efficient program on the departmental computer, a GEC 4080. This was only possible because of the availability of disc space and more importantly unlimited time.

In table 3-1 a summary of the main running conditions for each stage of the processing is given. The program results are stated for the Burroughs B6700.

Program Function	Program Length (lines)	Process Time (sec.)	Core storage requirement (kb)
Preliminary calculations and corrections	100	2.4	2.2
Deconvolution and filtering	437	6.1	4.4
Energy dependent corrections	536	7.8	7.7
Multiple scattering*	1261	16.0	8.3

* For 9×10^3 photons

Table 3-1

Data processing program attributes stated for a Burroughs B6700 computer.

CHAPTER 4

^{241}Am COMPTON SPECTROMETERS

4.1 Introduction

Compton scattering studies of electron momentum density using low energy gamma-ray sources have been performed with increasing frequency during the last five years. This followed the development of high resolution, high efficiency solid state detectors, based on the use of lithium drifted germanium and intrinsic (high purity) germanium crystals. The 'new' technique replaced the earlier and more conventional X-ray method which suffered from several, rather severe limitations. A detailed discussion of the relative advantages and disadvantages of the X-ray technique has already been given by Eisenberger and Reed (1972) and Reed (1976). Before describing the low energy gamma-ray method it is useful to briefly outline the main advantages of this technique. These advantages arise from:-

(i) The use of a monochromatic source rather than an X-ray doublet superimposed on the bremsstrahlung background.

(ii) The higher energy photons available from gamma-ray sources have small photoelectric absorption cross sections ($\propto Z^4/\omega_1^3$) and hence the Compton scattered intensities are increased significantly for materials of high atomic number (Compton cross section $\propto$ Z).

(iii) The larger energy transferred to the recoil electrons (~12 KeV ^{241}Am, cf. 1.5 KeV X-rays) in the Compton interaction extends the validity of the impulse approximation.

(iv) A solid state detector allows the simultaneous acquisition of data throughout the whole of the energy loss spectrum, compared with the step by step mode of analysis of an X-ray crystal spectrometer. This compensates for the relative weakness of

gamma-ray sources vis-a-vis X-rays.

The main disadvantage of the gamma-ray experiment lies in its low resolution in momentum space. In general X-ray crystal spectrometers have two or three times the resolution of a gamma-ray detector. This is, however, offset to a large degree by the reliability and greater statistical accuracy which the gamma-ray method provides. The increasing frequency with which gamma-ray sources have been used, and the success of the results clearly indicates the significance and importance of these sources in Compton scattering experiments.

Americium-241 with a principal gamma-ray energy of 59.54 KeV is a very convenient low energy isotope because of its long half-life (458 years), freedom from spectral contamination, and commercial availability. Several groups have used 300 mCi and 900 mCi disc sources and lithium-drifted germanium detectors (Ge(Li)). The energy of 60 KeV is easily absorbed in thin shielding ($t_{\frac{1}{2}}$=10^{-4}m) and the experiment can be housed in a fairly normal laboratory environment. For these reasons, including the advantages given above, ^{241}Am is established as the standard source for Compton scattering studies.

In its present configuration, however, the output is limited to around 1 Ci because of the heavy self-absorption in americium. Disc sources of high intensity are therefore effectively impossible. The problems associated with self-absorption have to some degree been alleviated by using a source which has an annular configuration. Such a geometry, first explored by Ross and Kirkpatrick (1934) as a means for obtaining increased X-ray intensities, has recently been used by Weyrich (1975) for gamma-ray Compton scattering work. The initial strength of the ^{241}Am source used by Weyrich (1975) was ~1 Ci.

In this chapter details of the design and construction of a gamma-ray Compton spectrometer which uses a 5 Ci ^{241}Am annular source and an intrinsic germanium detector are described. The performance of the spectrometer is

assessed by comparison with the equipment it replaced which used a 300 mCi disc source and a Ge(Li) detector. Since some measurements have been made with this earlier system, and described in Chapter 5, a brief summary of the experimental arrangement has also been included. The performance and potential of the new system is made with specific reference to data taken on a 'standard' aluminium sample.

4.2 Disc Source Spectrometer

The experimental arrangement for the disc source geometry is shown schematically in Fig. 4-1. Details of the system have been described elsewhere (Pattison, 1975); only the more salient points are outlined here. In this system 59.54 KeV gamma-rays from a 300 mCi ^{241}Am source are first collimated by a lead tunnel of length 13 cm and diameter 1.2 cm. The active diameter of the source is 1.2 cm. After scattering in a cylindrical sample chamber through a mean angle of 150°, the scattered gamma-rays are collimated further by a second lead tunnel of length 15 cm and diameter 1.2 cm. The scattering angle of 150° was the maximum angle possible, and was chosen so that no part of the walls of the sample chamber could be seen by both source and detector. This configuration therefore allowed only the sample to be contained within the scattering volume. As a further precaution the inside of the chamber was lined with lead, and was evacuated to reduce the contribution from air scattering. A typical signal-to-noise ratio at the Compton peak is around 100:1. Both the incident and scattered beam ports on the scattering chamber were covered with 100 μm thick aluminized mylar foil, giving a negligible contribution to the scttered intensity.

Several measurements with this system on metallic and molecular samples clearly highlighted the need for an improved system. The main disadvantages arise from:-

(i) The lack of intensity caused by strong self-absorption. ^{241}Am possesses an upper limit of photon flux from its surface which is roughly

assessed by comparison with the equipment it replaced which used a 300 mCi disc source and a Ge(Li) detector. Since some measurements have been made with this earlier system, and described in Chapter 5, a brief summary of the experimental arrangement has also been included. The performance and potential of the new system is made with specific reference to data taken on a 'standard' aluminium sample.

4.2 Disc Source Spectrometer

The experimental arrangement for the disc source geometry is shown schematically in Fig. 4-1. Details of the system have been described elsewhere (Pattison, 1975); only the more salient points are outlined here. In this system 59.54 KeV gamma-rays from a 300 mCi ^{241}Am source are first collimated by a lead tunnel of length 13 cm and diameter 1.2 cm. The active diameter of the source is 1.2 cm. After scattering in a cylindrical sample chamber through a mean angle of 150°, the scattered gamma-rays are collimated further by a second lead tunnel of length 15 cm and diameter 1.2 cm. The scattering angle of 150° was the maximum angle possible, and was chosen so that no part of the walls of the sample chamber could be seen by both source and detector. This configuration therefore allowed only the sample to be contained within the scattering volume. As a further precaution the inside of the chamber was lined with lead, and was evacuated to reduce the contribution from air scattering. A typical signal-to-noise ratio at the Compton peak is around 100:1. Both the incident and scattered beam ports on the scattering chamber were covered with 100 μm thick aluminized mylar foil, giving a negligible contribution to the scttered intensity.

Several measurements with this system on metallic and molecular samples clearly highlighted the need for an improved system. The main disadvantages arise from:-

(i) The lack of intensity caused by strong self-absorption. ^{241}Am possesces an upper limit of photon flux from its surface which is roughly

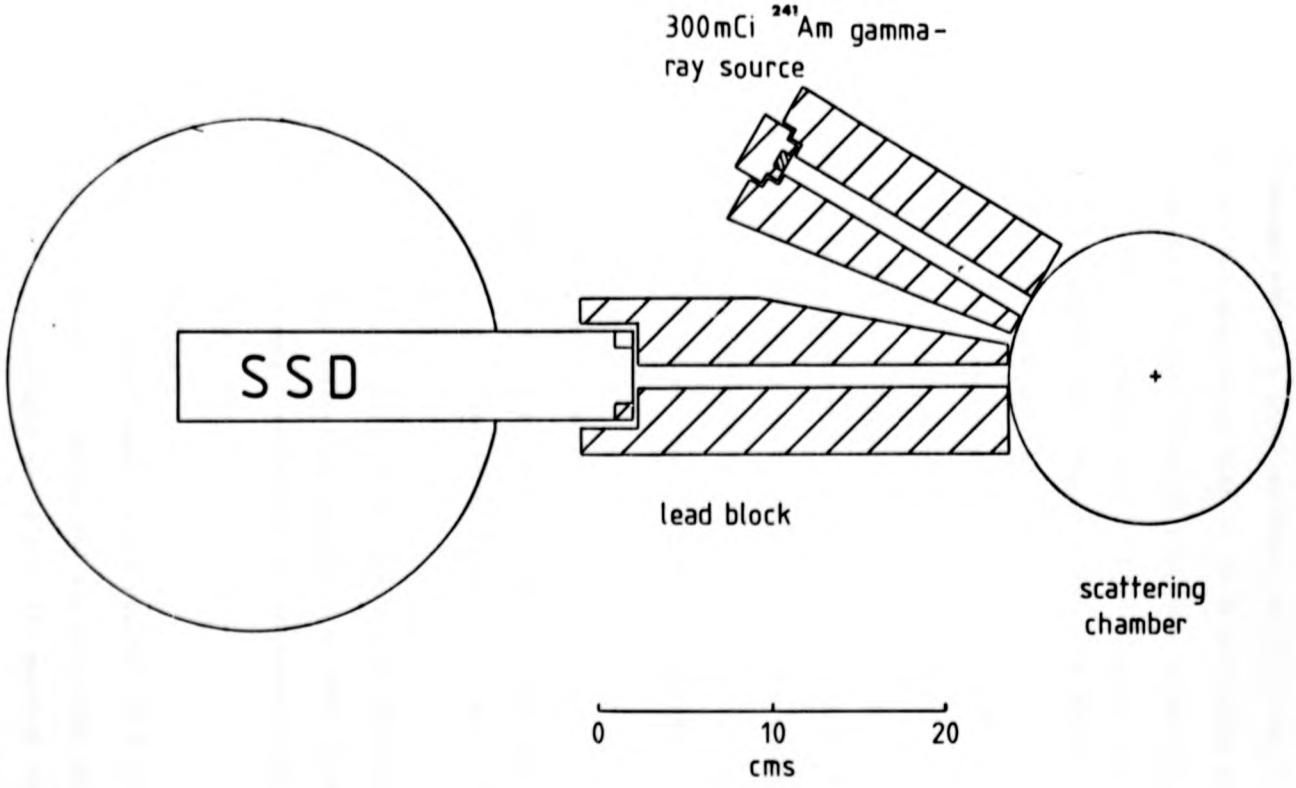

Fig. 4-1: Experimental arrangement of the 300 mCi ^{241}Am disc source spectrometer.

equivalent to 0.4 Ci/cm^2. This means, for example, that for a disc source 1.2 cm × 0.5 cm and having a total strength of about 0.9 Ci, only 30% or approximately 300 mCi will be emitted at 59.54 KeV along the cylinder axis.

(ii) The weakness of the incident radiation results in long measuring times in order to obtain adequate statistical accuracy over the entire Compton profile. A second experimental difficulty which is exacerbated by long experimental times, is the inevitable 'drift' in the electronics due principally to long term temperature fluctuations. The additional smearing of the energy loss spectrum caused by this drift may be as much as 5% of the full-width-at-half-maximum (FWHM) of the total resolution function.

(iii) The simple experimental geometry limits the scattering angle to 150° to reduce the background count and increase the signal-to-noise ratio. However, the small gain in the signal-to-noise ratio is offset by the deterioration in the momentum resolution which only improves for higher scattering angles.

(iv) The weakness of the source prohibits the use of thin samples (for intensity reasons) which would minimize the parasitic effect of multiple scattering and the additional errors that necessarily accompany the correction process.

Clearly, from a consideration of these basic features that underline all experimental Compton scattering systems, the need for an improved system using a more intense source would be extremely beneficial.

4.3 Annular Source Spectrometer

4.3.1 Design Considerations

The ideal Compton spectrometer would consist of a well collimated beam of photons impinging on a sample and the scattered photons detected at an angle of 180°. This angle would give the maximum shift in the Compton profile and therefore the best ratio of the profile width to the detector resolution. It would also mean that the incident and scattered photon momenta, $\bar{k}_1$ and $\bar{k}_2$ are antiparallel, and therefore $\bar{k}$ is fixed in

direction relative to the sample axes. Such an ideal situation is clearly impossible although scattering angles as high as 177° have been obtained (Weyrich, 1975). With $\theta \to 180$, $|\bar{k}_2|$ changes across the profile and consequently $\bar{k}$ also changes both in direction as well as in magnitude. Since a Compton profile measures the projection of the initial momentum of the electron $\bar{p}_i$ onto the scattering vector, i.e.

$$p_z = \frac{\bar{p}_i \cdot \bar{k}}{|\bar{k}|} \qquad 4\text{-}1$$

The direction of p_z relative to the sample axes will not be the same at the centre of the profile as it is in the tails, and this variation becomes greater as the angle θ decrease from 180°. In order to minimize this effect it is desirable to design a system which incorporates a scattering angle as close to 180° as possible.

The width of the detector resolution function is effectively fixed whereas the width of the Compton profile is roughly proportional to $\sin\theta/2$. As mentioned above an improvement in the momentum resolution can be realized for high scattering angles with $\theta \sim 180°$. At these high angles a larger beam divergence can be tolerated. The broadening due to the variation in the scattering angle is proportional to $\cot\theta/2$, so that an increase in the intensity can be obtained for $\theta \sim 180°$. Moreover, the impulse approximation and the interpretive theory developed from it hold more accurately at higher angles.

Another consideration when designing a spectrometer is the background contribution in the data due to photons being scattered from the walls of the sample chamber. The collimation and sample chamber should be designed so that the scattering volume contains only the sample. This will usually mean a much lower angle θ. Furthermore, the sample chamber should be evacuated to reduce the measurable contribution to the scattered intensity arising from air scattering surrounding the sample. At the same time the correct amount of shielding should be placed between the source and

detection system to protect the latter from receiving direct radiation. The amount of shielding will depend on the materials avialable, the cost and their absorption properties. The effect of the shielding in this part of the spectrometer should also help to reduce the background intensity and therefore aid the signal-to-noise ratio. The length of the collimators should be balanced by the need to minimize $1/r^2$ intensity losses.

Finally, solid state detectors that are commercially available and having good energy resolution are limited to a detection surface of approximately 2 cm^2 (16 mm diameter). The above general conditions are imposed on the design of any gamma-ray Compton spectrometer system.

4.3.2 Construction

The design of the new spectrometer was centred around the use of a 5 Ci ^{241}Am annular source. The source was specifically manufactured by the Radiochemical Centre, Amersham, along similar lines to low activity annular sources (~1 Ci) commercially available. The source, with an inner diameter of 2.6 cm and an outer diameter of 3.4 cm, has due to self-absorption an effective specific activity of approximately 3 Ci.

The positioning of the source with respect to the sample and detector is governed principally by the intensity-resolution requirements described above. However, there is one further consideration which arises when an annular source is used. The scattering vector is not uniquely defined but lies anywhere on the surface of a cone of semi-angle $\sim 1/2(180^\circ - \theta)$. While the degree of imprecision is irrelevant in the study of isotropic materials such as polycrystalline and liquid samples, it can present problems for studies of oriented single crystals (Pattison, 1978). This effect can only be diminished by increasing the beam path lengths, which in turn produces disproportionate intensity lossess. In the equipment described here a scattering angle of 170.5° was chosen as a compromise between the above considerations.

The collimation and shielding materials were made from high purity

lead, chosen because it can easily be cast into large blocks which are free from voids. It is easily machined, is a good radiation shield and is available at moderate cost. The resulting design is shown schematically in Fig. 4-2.

The source is held in a conical lead labyrinth, which is itself housed in a large lead block 10 cm × 10 cm × 5 cm thick, and illustrated in Fig. 4-3. The tight push-fit of the source holder in the cylindrical hollow of the lead block was achieved with four thin teflon runners. Directly behind the source are three tungsten alloy 'knockout' pins, which are used to remove the source if required. The source was handled with special tongs and the radiation levels continuously monitored until the conical section was correctly located in its block.

Behind the source block (A, see Fig. 4-2) are two further lead blocks (B and C) of similar size, which act as a shield to the radiation and as collimators to the direct and scattered radiation, respectively. Both blocks contain a 8 cm long tunnel with a diameter of 10 mm. The size of the collimator aperture and the length of the tunnels were governed by the additional contribution to the resolution function arising from beam divergence, and the calculations involved in this effect are discussed further in section 4.3.4. Block C also contains a cut-out in which the detector window is placed. Apart from acting as a protective device in the case of damage to the beryllium window (and hence the crystal), it also shields the detector from stray radiation which could contribute to the background.

On the opposite side of the source block is the lead sample chamber, D, and shutter mechanism. To further reduce the background contribution (particularly from the rear wall of the chamber) a lead lined steel cylinder (E) was added to the chamber doubling its length. The sample chamber (D+E) has a small 100 μm thick mylar window and is continuously evacuated using a Genevac rotary pump enabling pressures less than

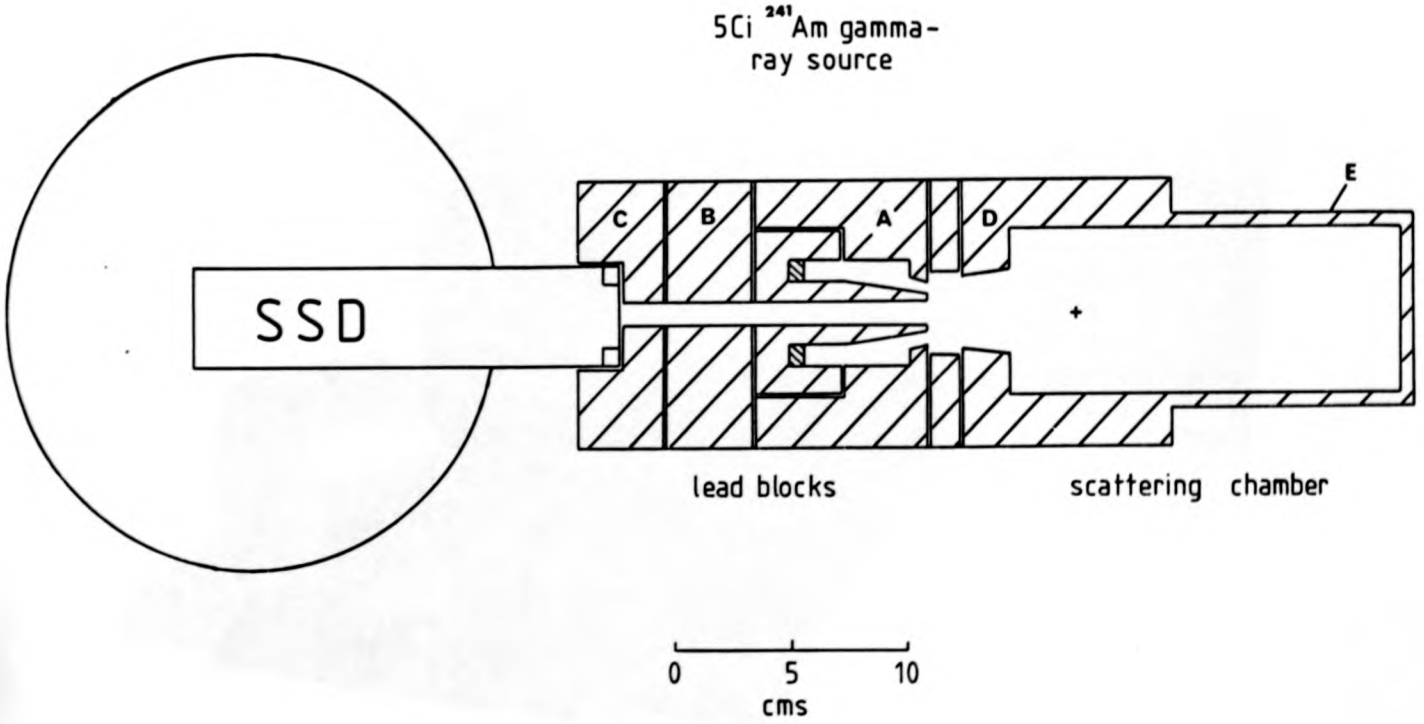

Fig. 4-2: Experimental arrangement of the 5 Ci ^{241}Am annular source spectrometer.

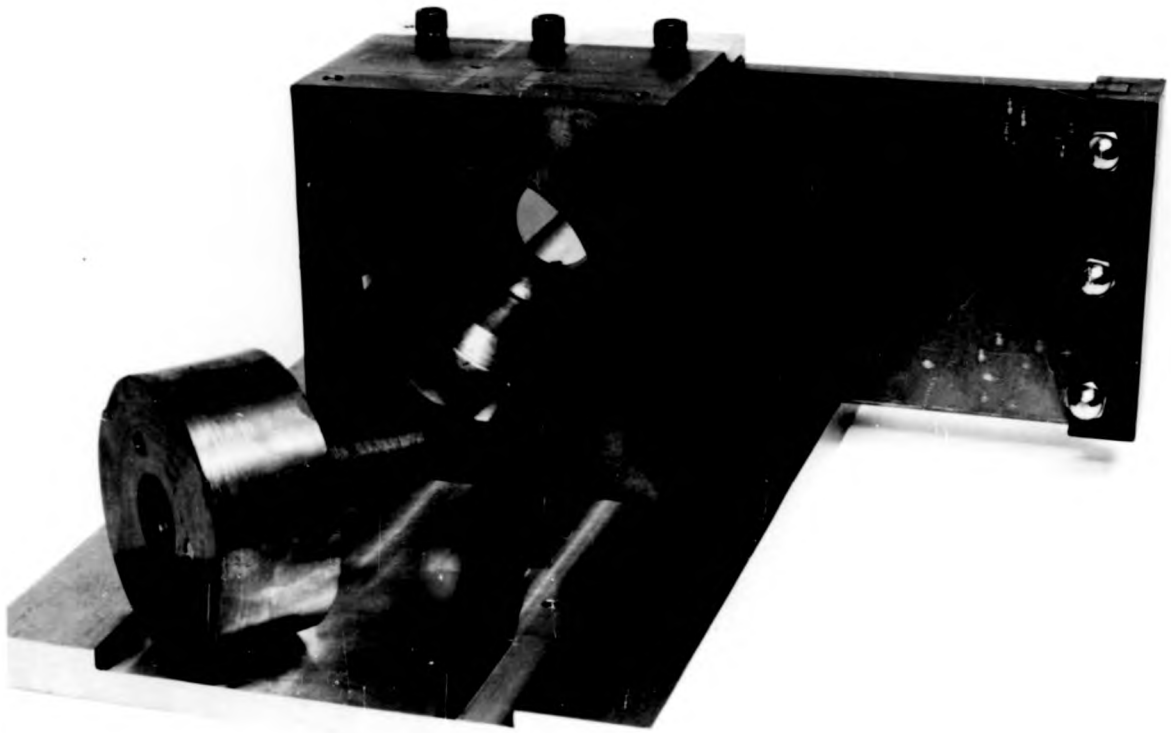

Fig. 4-3: Illustration of the conical lead source holder and collimator arrangement, with shutter.

10^{-4} T to be readily maintained. The large rotary pump is an integral part of the vacuum system which also includes an oil-diffusion pump. Such equipment allows a liquid nitrogen cryostat with a small vertical cold-finger to be mounted on top of the scattering chamber, enabling Compton scattering studies to be undertaken on materials at low temperature.

The shutter mechanism runs between two teflon strips positioned in-between the source block A, and sample chamber D. The window is held in place by two brass support plates affixed above and below the window. The complete system is mounted on an aluminium base plate. On two sides of the apparatus a large lead screen is erected for personnel safety, and the whole equipment is mounted on top of a specially consructed steel bench.

The 5 Ci ^{241}Am source also produces weak gamma-ray lines at 99 KeV and 103 KeV, as well as other lines below 30 KeV including Neptunium X-rays (L series). Fortunately all of these lines are well away from the Compton line. The gamma-ray transition processes are, however, accompanied by a simultaneous emission of high energy neutrons. Neutron absorption in the active region of the detector crystal knock-out germanium nuclei from their regular sites by elastic-inelastic scattering, causing a severe deterioration in the energy resolution capabilities of the detector. For a 5 Ci source the neutron flux is about 10^4/s over 4π. Considering the average absorption cross section of germanium for thermal neutrons, together with the experimental geometry, means that the detector crystal is exposed to ~50 n/s, which is an acceptable level. However, this figure is based on thermal neutron absorption and not fast neutron absorption. Paraffin wax (which has a large absorption cross section for fast neutrons) approximately 8 cm thick was used to surround the whole system and act as a moderator. To protect the detector crystal a small piece of cadmium sheet was placed just in front of the beryllium window. Cadmium has a neutron absorption cross section some ten times that of paraffin wax.

4.3.3 Detection System

The general layout of the detection system, comprising of a germanium solid state detector and the associated electronics, is shown schematically in Fig. 4-4.

Gamma-ray photons entering the detector interact with the semiconductor crystal to produce electron-hole pairs. These are swept to the detector electrodes by a large, negative bias voltage. The charge collected at the electrodes is converted to a voltage pulse in the preamplifier; the amplitude of the integrated voltage pulse being a measure of the energy lost by the incoming radiation in the detector. The detector resolution width $\Delta\omega_{FWHM}$ for scattered photons at final energy ω_f is given by

$$\Delta\omega_{FWHM} = (\sigma^2_{NOISE} + \alpha\omega_f)^{1/2} \qquad 4\text{-}2$$

where σ_{NOISE} is the preamplifier noise contribution, and $\alpha\omega_f$ is the detector crystal contribution given by

$$\alpha\omega_f = 2.355F\bar{\varepsilon}\omega_f \qquad 4\text{-}3$$

The factor F is the Fano factor, and $\bar{\varepsilon}$ is the average energy needed for producing an electron-hole pair. Typically $F \sim 0.09$ and $\bar{\varepsilon} = 2.95$ eV. In order to keep the value of $\bar{\varepsilon}$ as low as possible, detector crystals are cooled to liquid nitrogen temperature, the cryostat being an integral part of the detector. This helps to reduce both the electronic noise in the preamplifier and the leakage current at the surface of the detector crystal.

The detector resolution function is well represented by a Gaussian line shape with a small (~1% of the peak height), slowly decaying tail on the low energy side. A typical resolution function is shown in Fig. 4-5; the intensity is given in logarithmic scale to clearly illustrate the shape and structure of the tail. The tail arises primarily from incomplete absorption due to other interactive processes. Compton scattering in air between the source and detector and within the crystal itself, as well as electron escape (particularly from the surface) and electron-hole

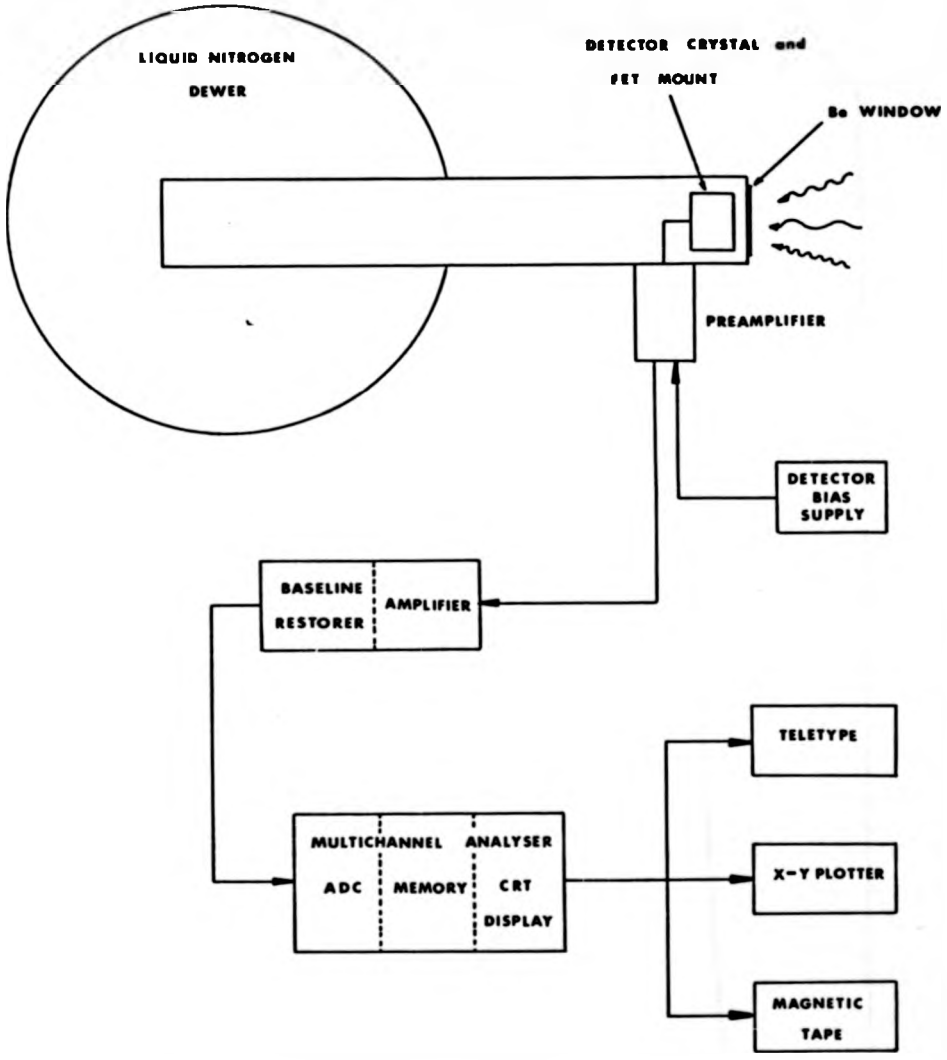

Fig. 4-4: Solid state detector system and associated electronics.

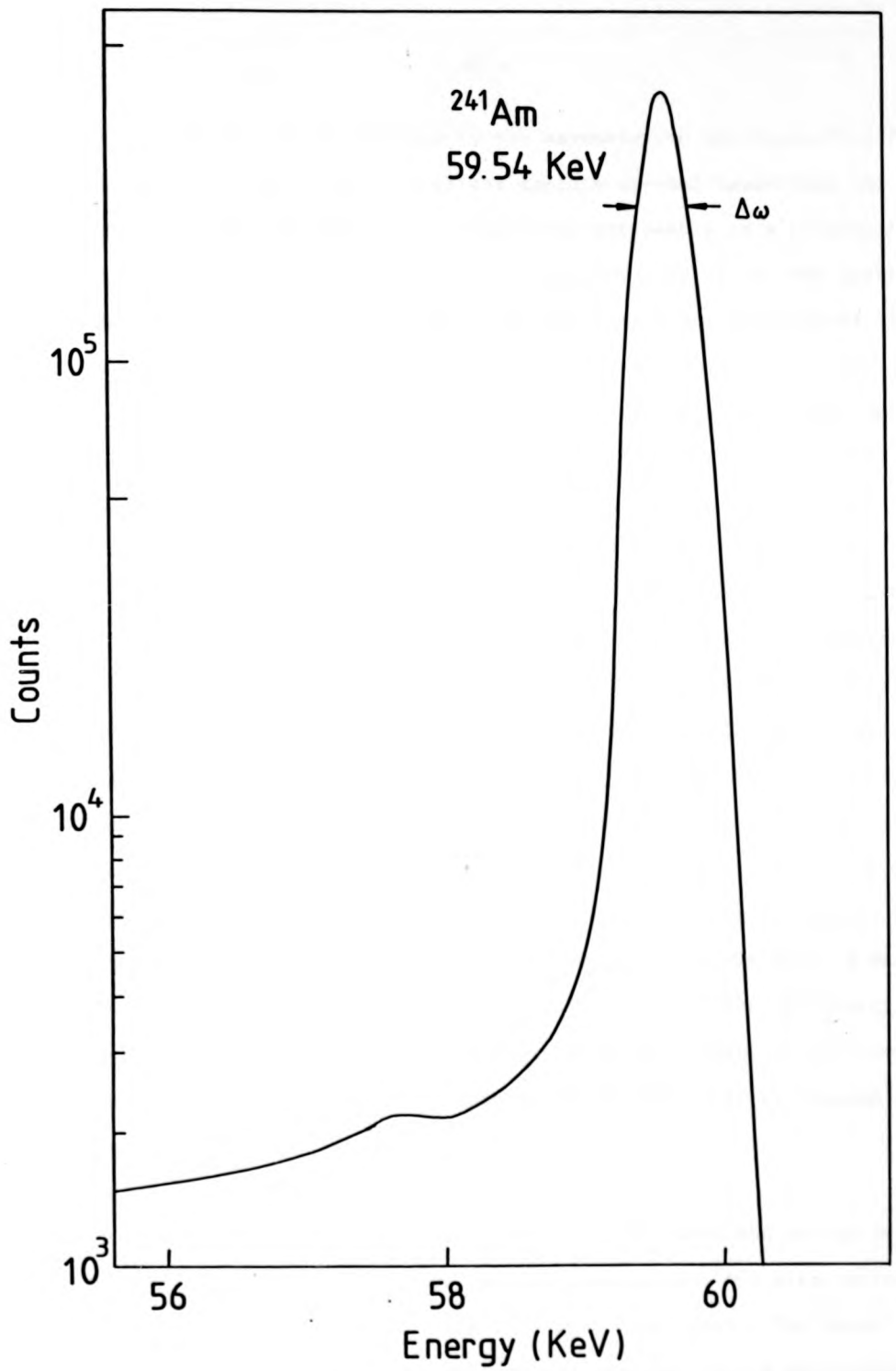

Fig. 4-5: Instrumental resolution function.

recombination, all contribute to the asymmetry in the resolution function. Other factors which have an effect include crystal impurities and imperfections and these are particularly noticeable in a lithium-drifted detector as opposed to an intrinsic detector used in the new system. The advantages of these latter detectors apart from the improvement in the resolution are their ability to be periodically warmed-up without damage to the crystal. For Ge(Li) detectors the crystal must always remain at liquid nitrogen temperature to prevent the lithium from diffusing out of the crystal. The intrinsic germanium detectors are at the current technological limit for photon detection at these energies.

The output pulses from the preamplifier are fed to the main amplifier where they are reshaped and transmitted to the analogue to digital converter (ADC). The periodic pulses are subsequently scaled into an address scalar and the accumulated count is stored in the ferrite core memory of a multichannel analyser (MCA). The eventual count is displayed on an oscilloscope as a histogram of the number of counts accumulated versus input voltage pulse amplitude. A teletype is also linked to the MCA which enables the data to be transfered onto paper tape for processing using the data analysis procedures described in the previous chapter. A magnetic tape facility is also available for archiving the recorded energy loss spectrum enabling a detailed analysis to be undertaken at a later date whilst allowing the current contents of the memory to be cleared for the next experiment.

4.3.4 Geometrical Energy Broadening

In conducting a Compton scattering experiment the energy resolution is not just a function of the detector resolution, but also includes the additional contribution arising from beam divergence. The amount of beam divergence depends upon the collimation employed in the experimental arrangement, and is a measure of the imprecision in the scattering angle θ.

It is important that an accurate estimate of this effect is determined since the additional smearing of the resolution function will adversely affect the deconvolution and filtering procedure.

An accurate estimate of this additional smearing in θ can be obtained by considering the Compton formula with the scattered energy at the Compton peak, i.e. $\omega_2 = \omega_c$. The uncertainty in θ is given by

$$|\Delta\omega| = \frac{\omega_c^2}{mc^2} \sin\theta \, \Delta\theta \qquad 4\text{-}4$$

The geometrical divergence $\Delta\theta$ is well approximated by

$$(\Delta\theta)^2 = (\Delta\theta_S)^2 + (\Delta\theta_D)^2 + (\Delta\theta_T)^2 \qquad 4\text{-}5$$

where $\Delta\theta_S$, $\Delta\theta_D$ and $\Delta\theta_T$ depend on the size of the incident beam collimation, scattered beam collimation, and sample size, respectively. The contribution from $\Delta\theta_T$ has a functional dependence on θ itself, and can therefore be neglected for $\theta > 140^\circ$. The remaining two terms are given by

$$(\Delta\theta_S) = \left(\frac{S}{R_{TS}}\right)$$
$$(\Delta\theta_D) = \left(\frac{D}{R_{TD}}\right) \qquad 4\text{-}6$$

where S and D are the source and detector collimator diameters, and R_{TS} R_{TD} are the target-source and target-detector distances, respectively. A precise value of $\Delta\theta$, and hence $\Delta\omega_c$ therefore depends on the experimental conditions and will therefore vary accordingly. The overall detector resolution, including beam divergence is therefore well represented by

$$\Delta\omega_T = (\Delta\omega^2_{FWHM} + \Delta\omega_c^2)^{1/2} \qquad 4\text{-}7$$

Inserting the appropriate experimental values for both disc and annular source spectrometers results in a similar value for $\Delta\theta$ of about ± 0.04 rads, or $\pm 2.2^\circ$. The effect on $\Delta\omega_c$ however, is very different amounting to 177 eV for the disc source arrangement and only 58 eV for the annular source arrangement compared with a $\Delta\omega_{FWHM}$ of $\sim$380 eV. This difference arises primarily from the significant difference in scattering angles,

viz. 150° (disc) and 170.5° (annular), and hence in ω_c. The effect on the energy resolution is equally apparent with an increase in $\Delta\omega_{FWHM}$ of over 11% for the disc geometry and only 1.4% increase for the annular geometry. These calculations clearly show a considerable advantage in attempting to undertake experiments at high angles of scattering whilst showing the improvements in the gamma-ray technique that can be gained by using an annular source.

4.4 Initial Test Results

As with any new experimental system, before an energy loss spectrum can be accumulated and analysed several important checks are required and the results known, since these will govern the future working conditions of the system. The three most important checks are the linearity of the energy scale, the detector resolution, and the optimum sample position for maximum intensity. Each one of these conditions is dealt with in this section before the results of an accumulated spectrum on a 'standard' aluminium sample are presented.

4.4.1 Linearity of the Energy Scale

A test of the system calibration is a test of the linearity in the energy versus channel relationship, and is designed to investigate the behaviour of the detector and its associated electronics. It is important that the Compton profile data is accumulated in a linear region of the MCA spectrum. Non-linearity will present additional problems in the processing and analysis of the results.

A variable X-ray source containing target materials of Cu, Rb, Mo, Ag, Ba and Tb was used to investigate the energy range from 6.24 KeV (Tb L_{α_2}) to 51.74 KeV (Tb K_{β_2}). A low activity (~1 μCi) ^{241}Am source provided additional information at 59.54 KeV and 26.36 KeV. The peak positions of several of the predominant X-ray lines in each material and the gamma-ray lines from ^{241}Am were determined by fitting a parabola over the data around the centre of each line (or lines in the case of X-ray

doublets which could not be resolved). In this way the centre of each peak could be located to within ± 0.25 channels or ± 5 eV.

A plot of energy (KeV) against channel number revealed excellent linearity from 59.54 KeV to around 21.5 KeV where the first signs of deviations outside the experimental error of the least squares fit were found. These deviations from linearity increased at lower energies. At 6.24 KeV the discrepency amounted to over 7%. Fortunately the lower energy limit is still well away from the Compton profile which for 170.5° scattering has its peak at 48.35 KeV.

4.4.2 Detector Resolution

It has been shown in the previous sections that the detector resolution is dependent primarily upon the size and perfection of the germanium crystal, and also on the associated electronics e.g. amplifier and preamplifier. However, several detrimental effects that may result in poor resolution are always present and must either be eliminated or suppressed. Poor resolution may result from:-

(a) Electronic drift caused by long term temperature fluctuations.

(b) Mechanical vibration transmitted to the detector and cryostat through the floor and also acoustical vibration through the air.

(c) Analyser electromagnetic interference due to the detector being positioned too close to the ferrite core of the MCA.

(d) Ground loops and power line frequency interference which can be caused by long cable connections between detector, preamplifier and main amplifier.

(e) High count rates causing pulse pile-up and misshapen peaks.

Several precautions were therefore taken when the system was initially installed. The electronics rack comprising the MCA, ADC, oscilloscope and magnetic tape deck were placed in a separate room from the spectrometer. Although the electronics room did not contain any temperature control devices, measurements recorded over long periods of time indicated a

temperature stability to within $\pm 2^{\circ}C$, thereby minimizing the electronic drift. The large distance between the electronics and spectrometer also reduced affects arising from interference caused by the ferrite core memory of the MCA. Standard BNC Ortec cables were used to connect the preamplifier to the main amplifier and MCA. To suppress mechanical and acoustical vibration being transmitted to the detector, particularly the cryostat containing the crystal, the detector was placed on a large, thick neoprene mat.

Once the detector and electronics were set up an investigation was undertaken to ascertain the optimum energy resolution, $\Delta\omega_{\text{Pulser}}$ by varying the characteristics of the main (pulse shaping) amplifier. Three energy ranges were chosen by observing the spectrum produced by the three sources ^{55}Fe (5.89 KeV), ^{241}Am (59.54 KeV), and ^{57}Co (121.94 KeV). The gain of the main amplifier was adjusted to place the predominant X-ray and gamma-ray lines at a convenient location in the MCA spectrum. Throughout these measurements the overall count rate into the detector was not allowed to exceed 1000 counts/s to reduce the probability of pulse pile-up. The main amplifier time constant settings were adjusted to maintain a low system noise while maintaining a good overall resolution. Optimization was achieved by using the pole-zero cancellation control which greatly reduces distortion of the pulse, and the resulting pulse widths verified on an oscilloscope before being fed to the MCA. When optimum shaping conditions were met, the resolution of the system was recorded and found to be 173 eV (^{55}Fe), 352 eV (^{241}Am) and 490 eV (^{57}Co). These figures are slightly better than those guaranteed by Ortec particularly at the lower energy. For Compton profile measurements it is the figure at 59.54 KeV which is important. In terms of resolution in momentum space this figure is equivalent to a value of 0.58 a.u. This figure must be augmented with a small contribution from beam divergence which brings it up to 0.59 a.u. (cf. 0.72 a.u. disc source geometry). The equivalent FWHM resolution

figure at the Compton peak energy (48.35 KeV) is ~332 eV or 0.53 a.u.

Although count rates in excess of 10^3 counts/s were unlikely in a Compton experiment, a check was made of the dependence of the FWHM of both the 59.54 KeV and 26.36 KeV lines from a 1 μCi ^{241}Am source as a function of the count rate. A small deterioration (~2% of the FWHM) was found for count rates up to $5 . 10^3$ counts/s.

4.4.3 Sample Location

The precise location of the sample with respect to the source and detector was verified experimentally by undertaking a series of Compton scattering measurements using a thin (0.064 cm thick) slice of aluminium foil. The sample was positioned at various locations throughout the scattering chamber, and the integrated Compton intensity recorded as a function of this position (measured with respect to the fixed position of the detector). In order to achieve a significant statistical accuracy each spectrum was measured for a period of over 24 hours. The total number of Compton counts between ± 5 a.u. on the momentum scale expressed on a 'per second' basis was plotted as a function of sample position. The result shown in Fig. 4-6, shows clearly that the optimum sample position agrees extremely well with the designed position within the thickness of the sample, i.e. ± 0.032 cm.

4.5 Initial Test Profiles

A complete test of the system required the accumulation and analysis of a Compton profile spectrum. In this section measurements of the Compton profile of an aluminium sample are described, with the view to estimating the reliability and reproducibility of the Compton scattering data obtained with this new system. Apart from testing the limits of accuracy of Compton measurements the performance of the spectrometer is also assessed by comparison with the equipment it replaced, a 300 mCi disc source and a Ge(Li) detector, described earlier.

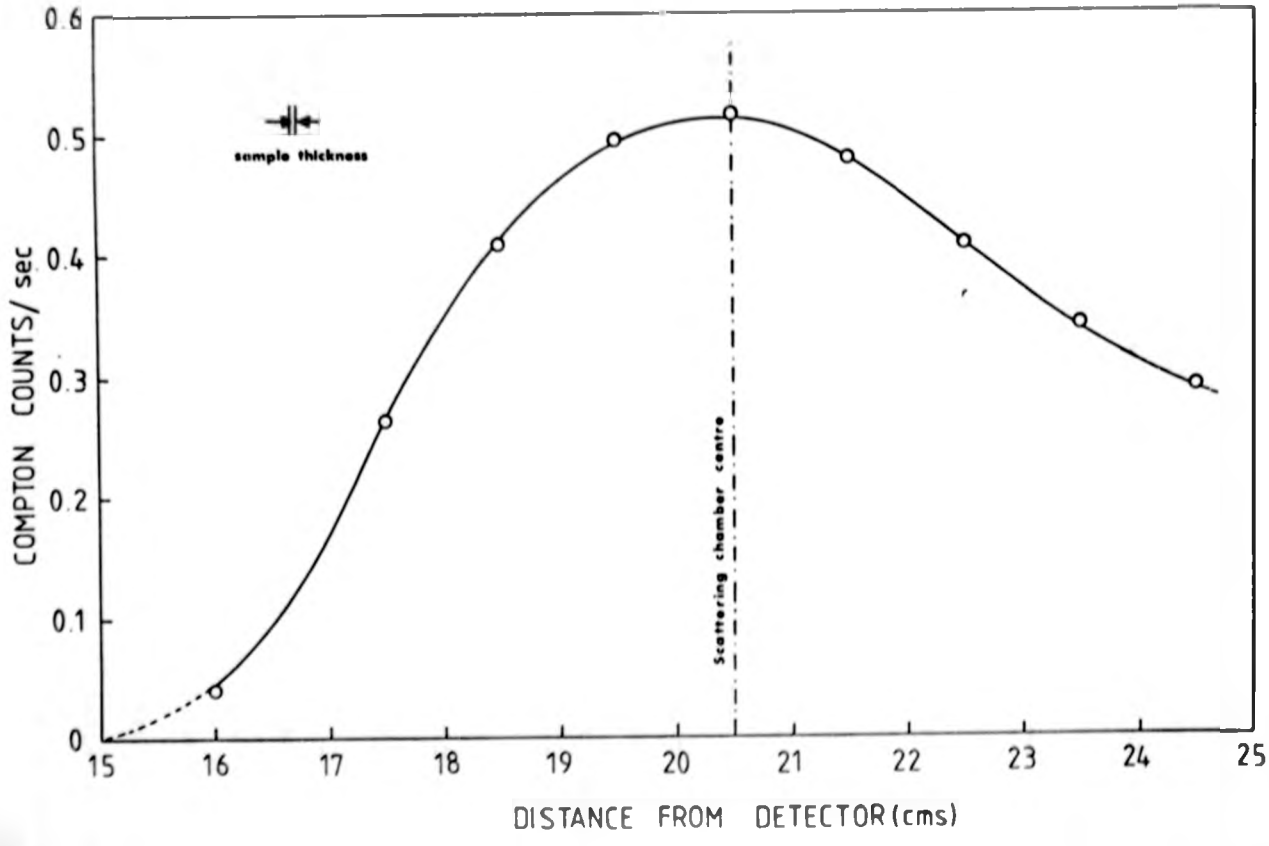

Fig. 4-6: Compton scattered intensity as a function of the sample position.

4.5.1 Statistical Accuracy and Reproducibility

Measurements on the old and new systems with the same aluminium sample have established a gain in intensity of some sixteen times whilst maintaining the previous signal-to-noise ratio of approximately 100 to 1. The increase in intensity is greater than the ratio of the source strengths (~10 to 1) because ot the changes in geometry. A good estimate of the level of residual random errors is provided by comparing two sets of data obtained on the same sample. The results of the reproducibility tests on aluminium are shown in Fig. 4-7, were in each case the data has been processed to obtain the Compton profile (multiple scattering has not been included). The statistical accuracy of the raw data sets is similar, with peak counts in excess of 10^5, and the reproducibility, expressed as a percentage of the Compton peak value J(0), is typically less than $\pm 0.2\%$. By way of comparison the comparable figure for the old system is~$\pm 0.5\%$.

Measurements on hydrocarbons, reported in Chapter 6, which only require measuring times of about 20 hours to obtain a similar statistical accuracy, have resulted in a reproducibility of better than $\pm 0.1\%$ of J(0). The superior reproducibility can probably be ascribed to the diminished effects of instabilities and drifts in the electronics over the shorter measuring period. Although the effects are extremely small they do illustrate a secondary advantage of using more intense sources.

The increased speed with which measurements can now be carried out, especially on the lighter materials, means that extensive series of measurements on related compounds can be contemplated. Such measurements have been undertaken with this system on hydrocarbons and the results are reported in Chapter 6. Moreover, the improved statistical accuracy can be achieved on thinner samples thereby reducing the parasitic effect of multiple scattering.

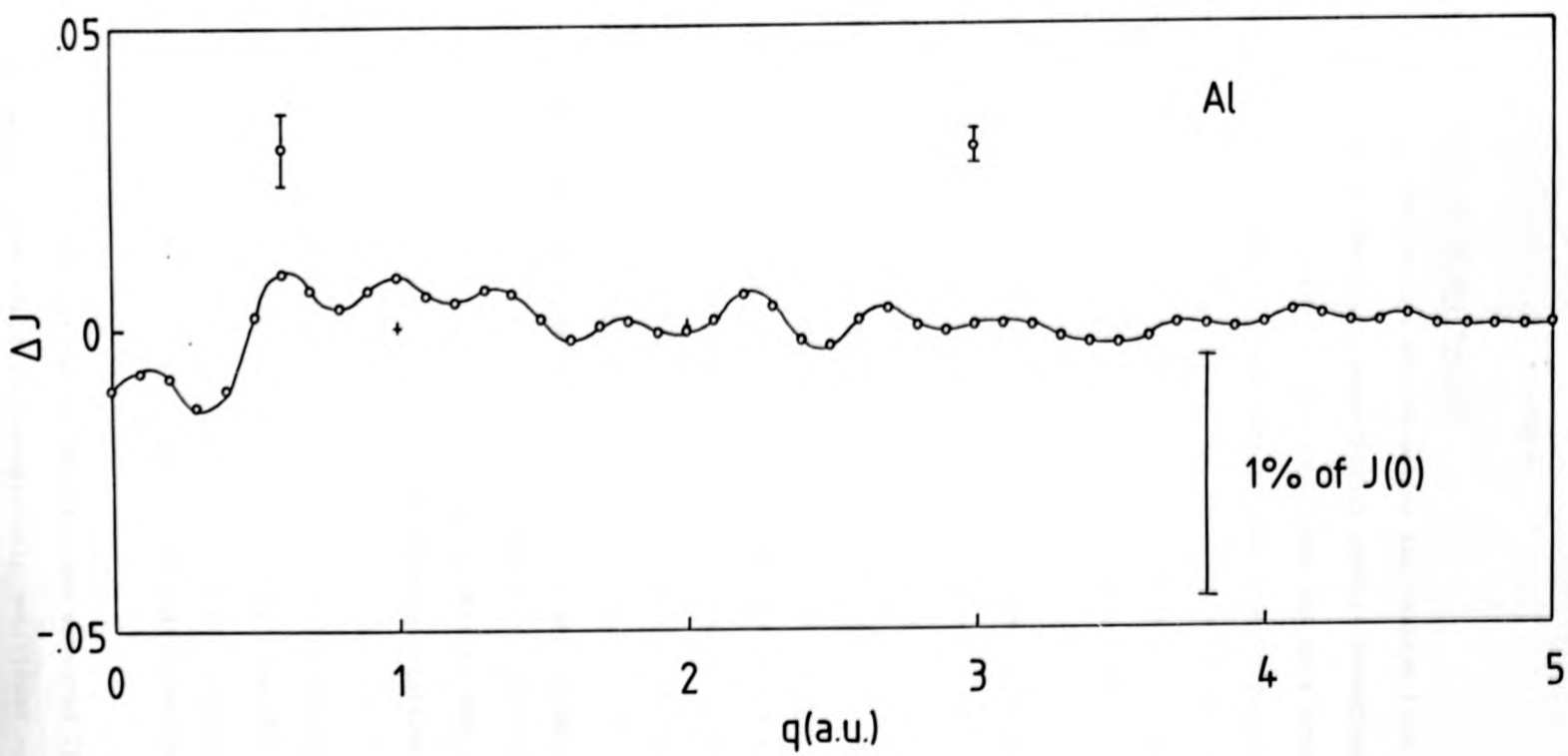

Fig. 4-7: Reproducibility of the Compton profile of aluminium.

4.5.2 Symmetry of the Profile

Within the impulse approximation the Compton line must be symmetric. The symmetry of the final experimental profile therefore gives an indication of the systematic errors in the experiment and data processing. After processing any features which are present symmetrically are likely to be real whereas asymmetric 'bumps' in the profile may be treated as spurious. Whilst undertaking the data processing on aluminium, two particular aspects of the processing procedure were shown to be extremely important, since both seriously affected the profile symmetry. They were the low energy tail on the resolution function, and the location of the profile centre. The effect each has on the symmetry of the profile has indicated that to a large degree each part can be treated independently.

(i) Low Energy Tail on the Resolution Function

In all previous studies with ^{241}Am radiation the low energy side of the line has been discarded because of the difficulty of correcting data of limited statistical accuracy for the asymmetry in the detector resolution function. The new system, however, with its increased intensity and statistical accuracy allows a more stringent test of the profile symmetry to be investigated. The uncertainties in the low energy side of the line arise from the tail on the response function of the detector. While the removal of the tail is formally part of the deconvolution process, the correction on the low energy side is very sensitive to the exact form of the resolution function. Although the tail is small ($\leq 1\%$ of the peak height) and due mainly to the partial absorption processes within the germanium crystal, the effect is considerably enhanced by the multiple Compton scattering in air which takes place principally between the sample and detector (the source block and return collimator are not evacuated in this system).

Initially the resolution function was measured with a weak (~ 1 μCi) ^{241}Am source which could be conveniently positioned some distance in front

of the detector without producing an excessive count rate. However, it was also possible, with careful shielding, to obtain the resolution function directly from the 5 Ci source. By reproducing the correct amounts of beam divergence and by positioning the detector to accept a similar amount of air scattering into it as occured in an actual experiment, it was possible to replicate the experimental conditions of a Compton profile measurement. Fig. 4-8(a) shows the resolution function measured in this way for three air path lengths. The peaks are identical, and even on a logarithmic scale the differences in the tails appear quite small and vanish approximately 4 KeV below the incident energy. In order to judge whether the apparently small differences affect the symmetry of the Compton line, the data for aluminium was processed with each resolution in turn.

The high energy side, as expected, was hardly affected (although J(0) varied by 0.75%), but the low energy side showed marked changes. The profile asymmetry, i.e. J(+q)-J(-q), as a function of J(0) is plotted in Fig. 4-8(b), for the three cases. It is clear from these results that the resolution function with the longest air path over-corrects the low energy side of the profile, while the reverse is true for the one with the shortest air path. The optimum resolution function produces an asymmetry of less than 0.2% of J(0) over the range 2 - 5 a.u. Between 0 and 2 a.u. there is a large asymmetry which may be a result of incorrectly locating the profile centre.

(ii) Location of the Profile Centre

In Fig. 4-8(b) it is apparent that the Compton profile peak has not been properly located. The deficiency in this part of the original processing program led to the more accurate routine involving a quardic fit and location by iteration as described in the previous chapter. In this routine the optimum peak position is found over a limited range of Compton profile data, typically $\pm$ 0.5 a.u. The result for aluminium using the correct resolution function is shown in Fig. 4-9, where the improvement

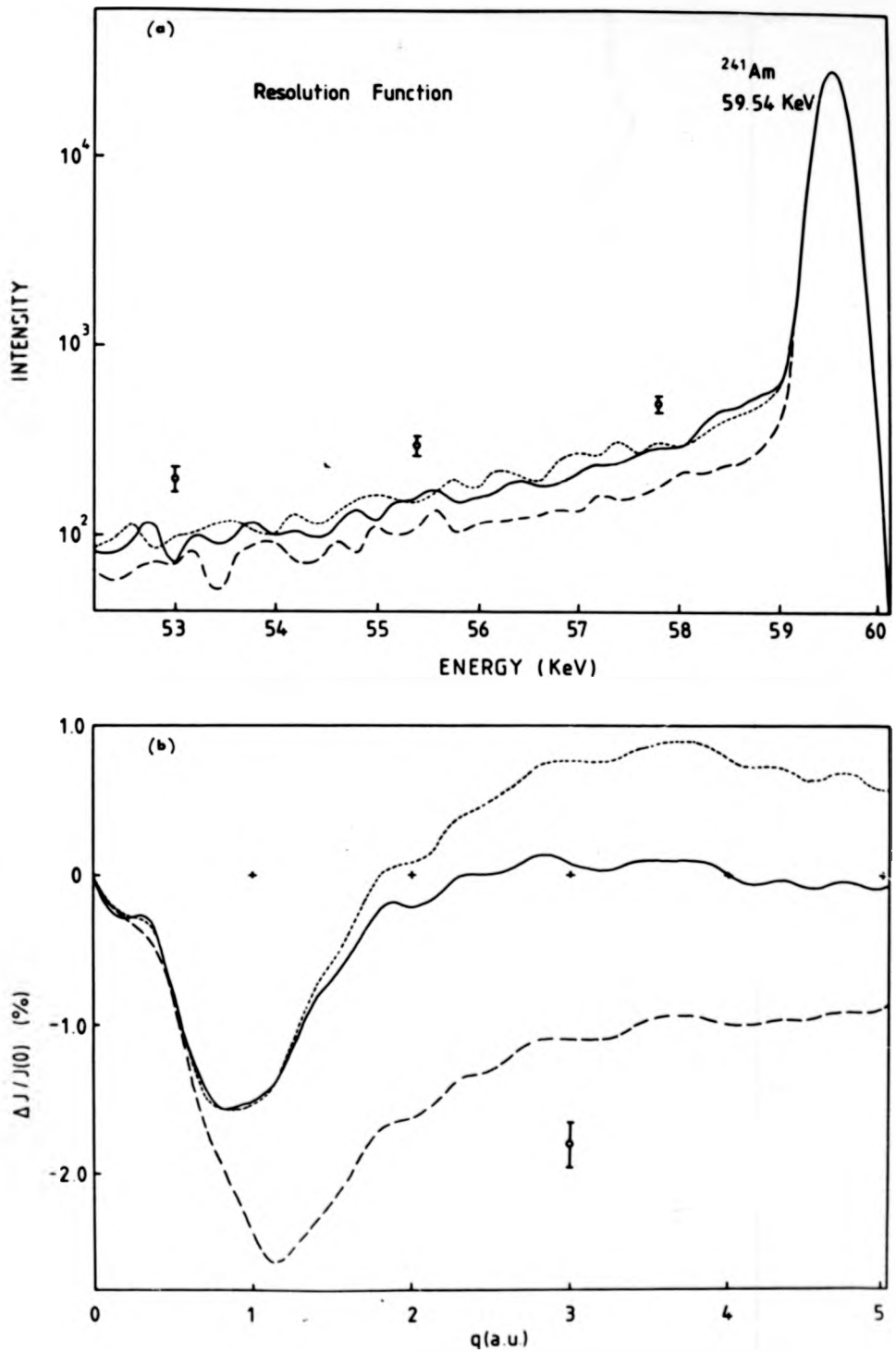

Fig. 4-8: The resolution function measured for three air path lengths, and the corresponding effect on the symmetry of the final Compton profile for aluminium.

22.0 cm (-------), 21.0 cm (———), 19.5 cm (- - - -)

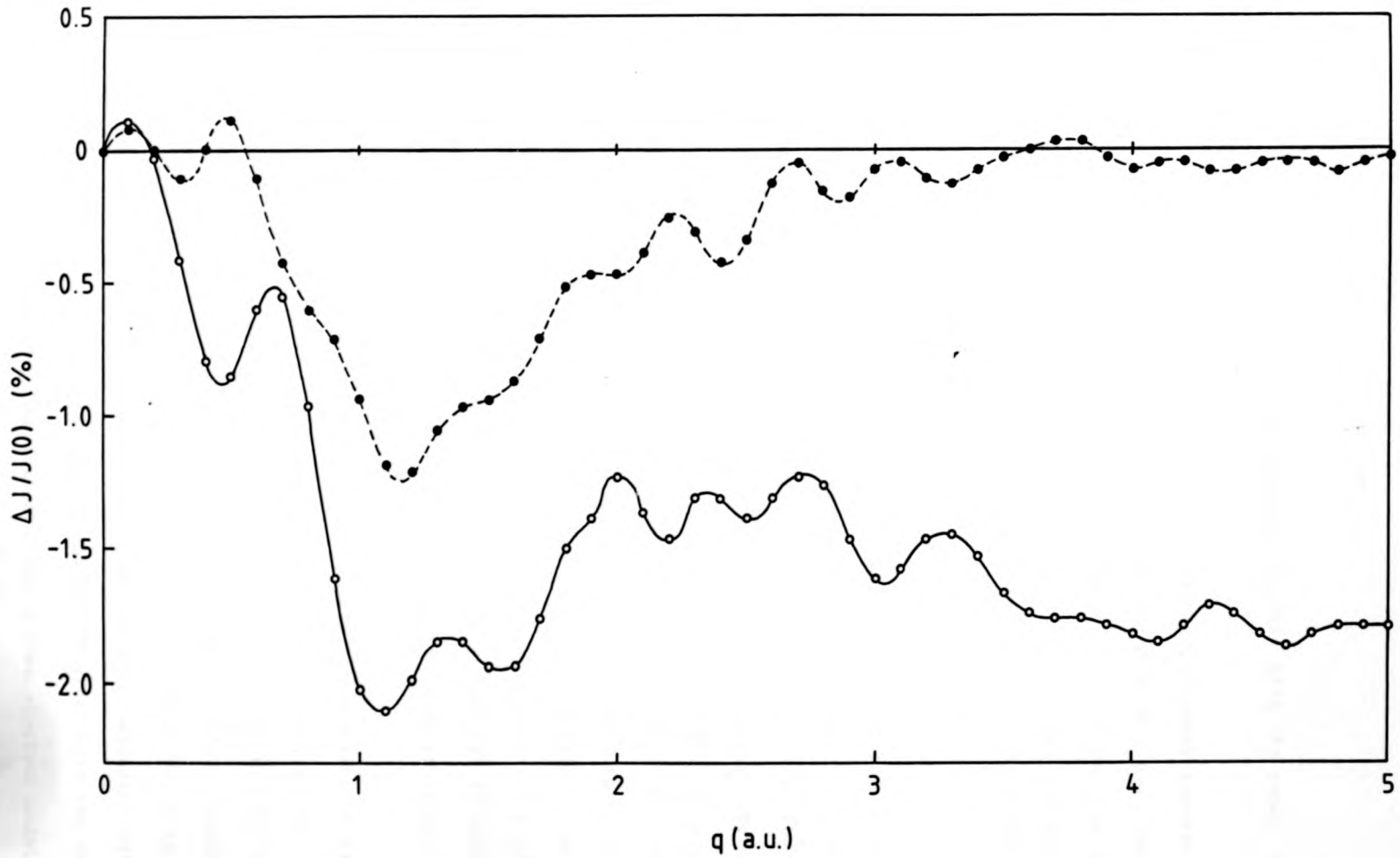

Fig. 4-9: Symmetry of the Compton profile of aluminium after the application of an improved numerical peak fitting routine (••••), compared to the symmetry obtained with the weaker disc source (••••).

in the peak location can be compared directly with the result shown in Fig. 4-8.(b).

Evidently , accurately locating the profile peak appears to affect the symmetry only very slightly. Beyond about 1 or 2 a.u. the symmetry of the profile is hardly affected by small errors in the peak position. Fig. 4-9 also compares the optimum symmetric line obtained in this work with that obtained in a previous study of aluminium using the old system. The result clearly illustrates the significant improvement in symmetry which has been achieved.

The spurious 'bump' between 1 and 2 a.u. has not been observed in other measurements on lighter materials, e.g. hydrocarbons and lithium, where the profile asymmetry is less than 0.2% of J(0) over the range 0 to 5 a.u. However, for metals heavier than aluminium, e.g. iron, vanadium, measurements have resulted in a much larger asymmetry. At present there is no firm experimental explanation although recent unpublished calculations by Mendelsohn (1978) indicate that the Compton profile of M shell electrons in atomic aluminium when studied with 60 KeV radiation is noticeably asymmetric (~3% of J(0) compared with about 1.5% found experimentally). Further examples and a more detailed discussion of the deviations from the impulse approximation have been included in Appendix A.

4.5.3 Qualitative Comparisons

There have recently been six separate measurements of the Compton profile of aluminium using Mo X-rays (Cooper et. al., 1974), ^{241}Am (Manninen et. al., 1974, Pattison et. al., 1974, Halonen et. al., 1975), ^{198}Au (Cooper et. al., 1976) and ^{137}Cs (DuBard, 1978). Provided multiple scattering and instumental resolution effects are properly taken into account, these experimental profiles are in good agreement with one another and with the present experimental results obtained with the annular source. In each case the profiles indicate that a free electron model for the

three conduction electrons is a fairly good first approximation. However, an interacting electron gas model has been developed by Pandey and Lam (1973) in which the effect of orthogonalisation of the conduction electron wavefunction to the core is also included, and this has proved to be a significant improvement on the simpler, free electron model. The present result indicates, in accord with the earlier results, that the interacting electron gas model is clearly better providing a good description of the profile near the Fermi momentum (~1.0 a.u.) where the free electron profile predicts a break which is too sharp.

Summary

The use of a 5 Ci annular ^{241}Am source has shown a very significant improvement in the quality of Compton profile data. The increased source intensity and improved geometry has resulted in a greater statistical accuracy, improved reproducibility and reduced multiple scattering. The rapid acquisition of data almost eliminates electronic drift which has been shown to cause a significant loss in the final accuracy of the Compton data. The use of an intrinsic germanium detector rather than a lithium-drifted germanium detector, and the higher scattering angle provided by the annular arrangement, has led to a large improvement in the momentum resolution from 0.72 a.u. to 0.59 a.u.

Finally, the sensitivity of the profile symmetry to the air scattering contribution contained in the tail of the resolution function was not expected. Fortunately the correct resolution function only has to be determined once, and then in measurements of this accuracy the natural symmetry of the Compton line can then be recovered.

CHAPTER 5

MOLECULAR COMPTON PROFILES

GASEOUS HYDROCARBONS

5.1 Introduction

The first quantitative comparisons between theory and experiment in Compton scattering resulted from the calculations by Hicks (1937) of helium and hydrogen profiles from several variational wavefunctions. The measurements of DuMond and Kirkpatrick (1937) on helium were in excellent agreement with theory, but the hydrogen profile obtained by Kirkpatrick and DuMond (1938) was considerably broader than the calculated one. In 1938 Hughes and Mann (1938) performed the first electron scattering experiments on diatomic gases and simple hydrocarbons CH_4, C_2H_2, C_2H_4 and C_2H_6 (Hughes and Enns, 1941). Unfortunately only the helium results were in agreement with theory. It was later shown by Duncanson (1943) that the poor agreement with theory was due to large multiple scattering effects.

A pioneer study of molecular momentum properties was initiated by Coulson and Duncanson (1941, 1942). In a series of papers they studied the hydrogen molecule-ion and some simple polyatomic molecules, with particular reference to the hydrocarbons. They employed Heitler-London type bond wavefunctions, and despite the elementary nature of their calculations, were able to obtain a number of important qualitative results. Fundamental to their success was the Dirac transformation which they used to convert from a position wavefunction to a momentum wavefunction. Coulson (1941) noted that on transformation the form of a wavefunction is not changed, so that corresponding to every quantity in position space there is a conjugate quantity in momentum space. In this way the position space wavefunction most often employed gave rise to momentum distributions and Compton profiles which were expressible as sums of contributions from

individual one-electron orbitals. Their analysis in terms of chemical notions such as bonds, inner shells, i.e. localised bond orbitals, has become the basis of many recent calculations. Their approach was later refined by Chuang and Hogg (1967) using more accurate wavefunctions in their analysis of positron annihilation studies.

In recent years nearly all calculations of electron momentum density for molecules larger than hydrogen have been carried out within the framework of the self-consistent-field (SCF) approximation (Roothaan, 1951). Although the remaining part of this brief review will deal with this approach, the main emphasis will be on the localised molecular orbital approach since this has received considerable attention in the last ten years.

5.1.1 Self-Consistent-Field Calculations

Henneker and Cade (1968) first used molecular SCF wavefunctions to determine the effects of the quality of the wavefunction on the momentum distribution in atomic and diatomic systems. They found that Hartree-Fock (HF) accuracy is necessary to ensure good agreement with experiment. Unfortunately at that time, SCF studies of molecules containing more than two atoms were almost completely limited to minimum basis set (MBS) wavefunctions, because of computational difficulties. Epstein and Lipscomb (1970) obtained molecular momentum distributions for boron hydrides and hydrocarbons (Epstein, 1970) using MBS wavefunctions. Despite the need for HF accuracy they found good agreement with experiment even for large molecules.

With the rapid development of computer technology, and routines for generating wavefunctions, accurate SCF calculations can now be routinly carried out on small polyatomic systems. Tanner and Epstein (1974) undertook an exhaustive investigation of the effects of SCF wavefunction quality on the electron momentum distribution. These authors calculated

individual one-electron orbitals. Their analysis in terms of chemical notions such as bonds, inner shells, i.e. localised bond orbitals, has become the basis of many recent calculations. Their approach was later refined by Chuang and Hogg (1967) using more accurate wavefunctions in their analysis of positron annihilation studies.

In recent years nearly all calculations of electron momentum density for molecules larger than hydrogen have been carried out within the framework of the self-consistent-field (SCF) approximation (Roothaan, 1951). Although the remaining part of this brief review will deal with this approach, the main emphasis will be on the localised molecular orbital approach since this has received considerable attention in the last ten years.

5.1.1 Self-Consistent-Field Calculations

Henneker and Cade (1968) first used molecular SCF wavefunctions to determine the effects of the quality of the wavefunction on the momentum distribution in atomic and diatomic systems. They found that Hartree-Fock (HF) accuracy is necessary to ensure good agreement with experiment. Unfortunately at that time, SCF studies of molecules containing more than two atoms were almost completely limited to minimum basis set (MBS) wavefunctions, because of computational difficulties. Epstein and Lipscomb (1970) obtained molecular momentum distributions for boron hydrides and hydrocarbons (Epstein, 1970) using MBS wavefunctions. Despite the need for HF accuracy they found good agreement with experiment even for large molecules.

With the rapid development of computer technology, and routines for generating wavefunctions, accurate SCF calculations can now be routinly carried out on small polyatomic systems. Tanner and Epstein (1974) undertook an exhaustive investigation of the effects of SCF wavefunction quality on the electron momentum distribution. These authors calculated

the Compton profile of water using 10 different SCF wavefunctions, including both Slater type orbital (STO) and Gaussian type orbital (GTO) basis functions, and ranging in quality from a MBS to near HF. They found that as the quality of the wavefunction improved, the Compton peak value, J(0) gradually decreased to bring their results into better agreement with the experimental value. This follows from the virial theorem introduced in Chapter 1, where lowering a systems total energy by describing it with an improved wavefunction, results in a higher kinetic energy and hence a shift in momentum density from low momenta to high momenta. Most of the improvement occured in going from a MBS to a double-zeta (DZ) quality basis (where two basis functions are used per MBS orbital). The additional computational effort required in reaching the near HF limit was not balanced by the negligible effect it had on the final Compton profile. Tanner and Epstein (1974) concluded that a DZ basis is adequate, at the present time, for describing the Compton profile of small molecular systems, a conclusion also recently confirmed by Hirst and Liebmann (1975).

The early discrepancies between experimental and theoretical profiles, i.e. measured profiles were generally broader than those predicted from SCF calculations, were attributed to electron-electron correlation (Weiss, 1970). Recently, however, Benesch and Smith (1972), and Smith and Brown (1973) have shown that the inclusion of correlation through configuration interaction (CI) in the calculation yields significant improvement particularly in the valence orbitals, i.e. those orbitals contributing to the profile at low momenta. This has been confirmed by Tawil and Langhoff (1975) in a study of H_2, O_2 and CH_2O molecules. They also found that electron correlation tends to be dominant in momentum regions affected by bonding, i.e. alters J(0) and produces no high momentum tail, where the original discrepancy between theory and experiment was found. At the present time such a discrepancy remains to be resolved.

Most of the computational labour involved in the calculation of the momentum density lies in the first step - the ab initio determination of the orbitals in position space. The accuracy of the calculation is directly dependent on the choice of basis functions, i.e. the number of GTO's, and is thus crucial in finding a balance between accuracy and availability of computing time.

5.1.2 Localised Molecular Orbitals

As the size of the molecule increases, the computational effort in extracting accurate SCF wavefunctions becomes prohibitive. Although the use of GTO's simplifies the calculation of certain molecular integrals, many more GTO's are required to obtain the same accuracy provided by a smaller STO basis. This situation arises because GTO's do not have the correct behaviour for large momentum values (i.e. small r), and many more are needed before they approximate to a single STO. The physical significance of the orbitals resulting from more exact SCF calculations is less clear than the early molecular orbital calculations of say, Coulson and Duncanson (1941), which were easily interpretable in a more 'classical' chemical language involving bonds, inner shells and lone pairs. This picture of localised bond orbitals has been successful in analysing the charge density. Several workers have considered the possibility of analysing momentum densities in terms of the same kind of localised bond orbitals. Such a study of the electronic properties of molecules in momentum space will therefore yield complementary information not only about the properties themselves, but also about the reliability of the particular computational method employed.

The description of molecular electronic structure in terms of localised molecular orbitals (LMO's) in position space has several advantages

(i) The LMO can be used to connect the orbital description with classical chemical concepts such as bonds, unshaired pairs.

(ii) Comparison of the electronic structure of chemically related molecules is easier in the localised one-particle model because chemically identifiable structural units (functional groups) may be consistently described by more or less identical LMO's.

(iii) The LMO of structurally related systems may be transferable, to a certain approximation, from one molecule to another. This makes it possible to use LMO's calculated for small molecules as building blocks in preliminary investigations of larger systems.

(iv) The LMO model can be used for constructing the total wavefunctions of larger, more complex molecules, via (iii).

The transferability between orbitals localised in position space has already been demonstrated in such chemical properties as heats of formation (Franklin, 1949, Schleyer et. al., 1970), magnetic and electric susceptibilities and dipole moments. The application to molecular properties in momentum space was suggested by Hicks (1940). The significance of Hicks' suggestion was that a determination of a small set of Compton profiles should enable the prediction of a Compton profile of a large number of related molecules. The theoretical calculations by Coulson and Duncanson (1941, 1942) on hydrocarbon molecules tended to confirm this suggestion despite the limited accuracy of the wavefunctions used.

Epstein (1970) using SCF molecular orbitals (MBS, STO's) obtained LMO momentum distributions for carbon inner shells, carbon-hydrogen bonds (C-H), and carbon-carbon bonds (C-C). No distinct sigma (σ) and pi (π) orbitals were found in multiple bonds so that a carbon-carbon double bond (C=C) is simply represented by two equivalent C-C bond orbitals. Epstein (1970) found that by transforming the position space density the corresponding momentum density was highly transferable. An indication of the practical use of the LMO approach were the profiles of cyclopropane and decane calculated from methane and ethane LMO's, and compared with an SCF calculation

and an X-ray measurement. The cyclopropane result suggested that even when unusual steric requirements exist, the LMO calculation provided an accurate estimate of the Compton profile. The decane data provided further evidence for good agreement between small molecule LMO and large molecule SCF profiles.

Smith and Whangbo (1974) have carried out calculations (SCF, DZ, GTO's) on the simple hydrocarbons CH_4, C_2H_4 and C_2H_6 to obtain the bond profiles for the C-H, C-C and C=C, where a distinction between carbon single and double bonds was made. They showed, in agreement with experiment, that one can distinguish the momentum space properties of CC single and CC double bonds. Effects of molecular environment on the C-H bond profile and the differences between bonds of hydrogen and sp^3 and sp^2 hybridized carbon atoms were found to be small.

Recently a similar approach has been adopted by Snyder and Weber (1978) in making a distinction between CC single and double bonds. However, these authors calculated the profiles of eight simple hydrocarbons (SCF, DZ, GTO's) to obtain the average bond profiles. These results were in better agreement with the experimentally derived bond profiles of Eisenberger and Marra (1971) than those obtained by Smith and Whangbo (1974).

5.1.3 Experimental Evidence

Experimental evidence for the validity of the LMO concept in momentum space was provided by Eisenberger and Marra (1971) in a series of experiments on small hydrocarbon molecules. Using X-rays they measured the profiles of methane, ethane and ethylene which allowed them to generate empirical valence profiles for the C-H, CC single and CC double bonds. They further showed that their measured profiles of the unstrained hydrocarbons propene, benzene, cyclohexane and normal hexane, could be predicted within the experimental error of 1% at q=0, and 5% at q=2 a.u. An average but unique set of bond Compton profiles was therefore derived which gave an optimum

fit of the observed profiles of all eight molecules. However, the empirical CC single bond Compton profile agreed less well with the observed Compton profile of diamond (Reed et. al., 1974).

In a strict transferable component model, such as those described above, any two stereo, branch or position isomers should have identical total profiles. The relatively close agreement found recently between X-ray measured profiles of the n- and iso-butytric acids (Epstein et. al., 1973) appears to lend considerable support to this view. Moreover, the bond profiles also appear to be rather insensitive to variations in bond angles, or to bond angle strains, a view expressed by Epstein (1970) in his theoretical results for cyclopropane.

X-ray measurements by Inkinen et. al. (1971) on the large molecules hexane and decane have been compared with total profiles obtained from the LMO bond profiles of Eisenberger and Marra (1971) and Smith and Whangbo (1974). Considerable discrepencies exist between these results and both LMO profiles. This is probably due to the large amount of multiple scattering in the experimental results. Almost all of the early experimental work was conducted at a time when multiple scattering was not considered a problem. Unfortunately, the experimental results that were available were treated with some scepticism, since many of the results reported on the same molecule differed by a significant amount. As an example, the peak values of two experimental profiles of benzene reported at that time (Weiss, 1970, Eisenberger and Marra, 1971) differed by almost 10%. It is now clear that multiple scattering was largely responsible for these anomalous results.

Despite the introduction of the gamma-ray technique very few molecular Compton profiles have been reported. ^{241}Am has been used by Epstein et. al. (1975) to measure the profile of decaborane. The same system was used by Manninen et. al. (1975) to measure the molecules formamide and p-benzoquinone.

Correcting the experimental results for multiple scattering and comparing with SCF and LMO profiles, these authors concluded that at the present level of accuracy all theories predict profiles which are in fairly good agreement with experiment. The LMO model, however, underestimates the profiles of formamide and p-benzoquinone at low momenta. Lindner (1977) has commented that the LMO approach is less reliable for these kinds of molecules with important resonance structures.

5.1.4 Aims of the Present Work

With the advent of gamma-ray sources for rapid data accumulation, together with the increased knowledge and availability of computer programs to correct for multiple scattering effects, a renewed series of measurements on hydrocarbon molecules was desirable. The past experimental results and the relative success of the average LMO approach in predicting total profiles does not however, imply bond profile transferability. It may be that there exists significant differences at the component level that either approximately cancel when superimposed, or are so small that they tend to disappear in the total profile, especially when the isotropic average is taken. With present day gamma-ray techniques it may be possible to detect the small deviations from these simple additivity rules and thus provide more interesting chemical and physical information

5.2 Initial Experimental Study

Using the 300 mCi ^{241}Am Compton spectrometer described earlier (section 4.2.), the initial investigation attempted to establish the potential and sensitivity of the low energy gamma-ray technique by looking at isomeric molecules. Undertaking measurements on similar systems and looking at the differences between the profiles, reduces errors arising in the systematic analysis of the data, and like anisotropy data, provides a far more sensitive approach to the study of the low momentum region and the accuracy of the models employed. In the initial study two pairs

of isomeric hydrocarbons were chosen, propene and cyclopropane (C_3H_6) and the cis and trans form of 2-butene (C_4H_8).

There are several reasons why such a comparison is of interest. Firstly, the only previous experimental study of isomeric molecules was undertaken by Epstein et. al. (1973) for dioxane, iso- and n-butytric acids (C_4H_5OH). They found all three profiles to be very similar, a result consistent with the LMO approach employed in the same paper. However, these are rather large molecules, where the considerable number of common bonds is likely to obscure the effects of different bonds in the isomers. It should therefore be more advantageous to look for differences (if any) between smaller molecules where any effects should be more pronounced.

Secondly, if the LMO approach is to serve as the almost invariant building block from which all hydrocarbon momentum densities (for example) may be reconstructed, they must therefore give satisfactory results for molecules with special properties. In this respect the severely strained geometry of cyclopropane might be expected to prevent an accurate representation by average LMO's taken from species with more normal bond angles. Furthermore, it is of interest to see if there is any manifestation of this 'angle strain' in the Compton profile of this molecule.

Thirdly, ab initio calculations have been performed for C_3H_6 and its acyclic isomer (Hirst and Liebmann, 1975), and a similar calculation for C_4H_8 was in progress. It would therefore be possible to obtain valuable information about a small molecule from an LMO and SCF approach and to be able to compare these results with experimental profiles corrected for multiple scattering. Work of this nature would contribute to our understanding of the electronic structure of larger molecules.

Finally, the molecules chosen were gases. The SCF and LMO calculations are performed on isolated, free molecules, so that a more reliable comparison can be made with these theories. Deviations in previous

comparisons may have been due to next-nearest-neighbour contributions to the Compton profile (Cade et. al., 1978)

The molecular geometry of these molecules are shown in Fig. 5-1. Cyclopropane is a highly strained three-membered ring compound where the CCC bond angle deviates significantly from the normal tetrahedral angle of 109.5° to nearer 60°. Propene is the only compound isomeric with it, and contains a CC double bond. A CC double bond is also found in both forms of 2-butene, where the two molecules are distinguished according to the condition that like groups lie on the same side (cis) or opposite side (trans) of the plane of the π bond (i.e. along the CC double bond axis).

5.2.1 Experimental Method

A general description of the experimental method has been given in Chapter 4, and the data processing procedures in Chapter 3. The only modification to the existing equipment was the replacement of the sample chamber by a cylindrical pressure vessel. The vessel, made of steel, was 10 cm in diameter and 0.5 cm thick. The entrance and exit ports for the incident and scattered radiation were covered with a 1 mm thick aluminium sheet, which reduced the intensities by only a few percent. The inside of the vessel was lined with 3 mm thick lead sheet to minimise wall scattering.

The gas samples, supplied by BDH Chemicals, were all of 99% purity. The gas samples inside the pressure vessel were kept close to their critical point in order to maximise the scattered intensity while maintaining the samples in a gaseous state. For the C_3H_6 molecules a pressure slightly in excess of 5 atms was required, whereas for C_4H_8 only 1 atms was necessary.

Each of the measurements, conducted at room temperature, lasted between 240 and 330 hours, during which time over 10^4 counts per channel were accumulated at the Compton peak. In all, eight runs were recorded,

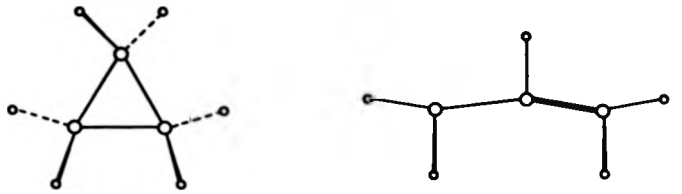

Cyclopropane C_3H_6 Propene

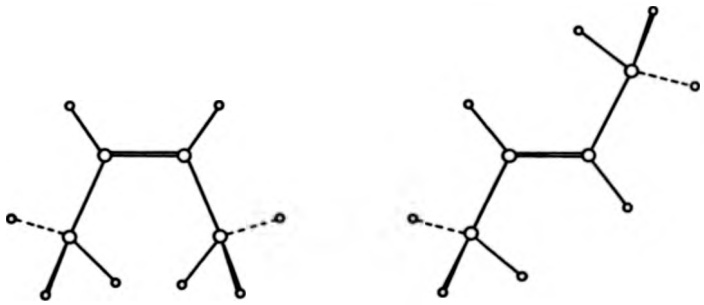

"cis" 2-Butene C_4H_8 "trans"

Fig. 5-1: Molecular structures for cyclopropane, propene and cis- and trans-2-butene.

two on each profile. By repeating the runs a straightforward assessment of the accuracy and reproducibility of the final Compton profile was made possible.

A separate measurement of the background contribution under the profile was made after evacuating the pressure vessel. The calibration of the energy spectrum with a channel spacing of 20 eV (equivalent to approximately 0.03 a.u.) was checked periodically to determine the extent of any drift in the system. During each measurement, the drift never exceeded more than two channels (i.e.~ 0.06 a.u.). The resolution of the Ge(Li) detector was measured with a 1 μCi ^{241}Am source (the same source was also used for calibration purposes). Taking beam divergence effects into consideration and converting from an energy scale to a momentum scale, the final FWHM was 0.72 a.u. for the C_3H_6 measurements, and 0.84 a.u. for the C_4H_8 measurements. The significant loss in resolution for the second set of experiments resulted from the Ge(Li) detector warming up and a subsequent loss of the lithium from the crystal by diffusion.

After correcting the data for background effects and for the energy dependence of absorption in the sample, the data were converted into a Compton profile and placed on a momentum scale. The area under each profile up to 5.0 a.u. was normalised to the free atom value of 11.6643 (C_3H_6) and 14.2213 (C_4H_8) using the tabulated profiles of Biggs et. al. (1975). Finally, the profiles were corrected for multiple scattering effects using the Monte Carlo program. Only double scattering events were considered since higher order multiple scattering was found to be negligible in measurements of this kind. In each profile approximately $5.\ 10^5$ photon paths were followed and only one iteration was necessary. The amount of multiple scattering was about 5% of the total intensity in all cases.

5.2.2 Theoretical Profiles

Following the procedure introduced by Eisenberger and Marra (1971) the total profile was partitioned into core and valence profiles, and the

latter into the localised units C-H, C-C and C=C, i.e.

$$J(q)_{\text{PROPENE}} = 6J(q)_{core} + 12J(q)_{CH} + 2J(q)_{C-C} + 4J(q)_{C=C}$$

$$J(q)_{\text{CYCLOPROPANE}} = 6J(q)_{core} + 12J(q)_{CH} + 6J(q)_{C-C} \qquad 5\text{-}1$$

$$J(q)_{\text{2-BUTENE}} = 8J(q)_{core} + 16J(q)_{CH} + 4J(q)_{C-C} + 4J(q)_{C=C}$$

where $J(q)_{CH}$, $J(q)_{C-C}$ and $J(q)_{C=C}$ are the bond Compton profiles at a momentum value q. Notice that in the LMO approach $J(q)_{CH}$, $J(q)_{C-C}$ and $J(q)_{C=C}$ are the same for all four molecules. The total profiles were therefore constructed using the bond profiles from Smith and Whangbo (1974), Snyder and Weber (1978), Epstein (1970) and the empirical bond profiles of Eisenberger and Marra (1971). In constructing the profiles according to eqn. 5-1 account has been taken of the differences in the various LMO approaches. For example, environmental effects of the $J(q)_{CH}$ profile indicated by Smith and Whangbo (1974) have been included in their total profiles, and Epsteins' (1970) total profiles have assumed the equivalence of the $J(q)_{C=C}$ with $J(q)_{C-C}$ bond profiles.

For all molecules a comparison was also possible with Compton profiles derived from an SCF-MO wavefunction calculation (Hirst and Liebmann, 1975, Holt et. al., 1978). For the C_3H_6 molecules both the LMO and SCF total profiles were convoluted with a Gaussian of width 0.72 a.u., before the comparison was made with the experimental results. For C_4H_8 the profiles were convoluted with a Gaussian of width 0.84 a.u., because of the lower resolution of the detector. The SCF calculations for the C_4H_8 molecules were undertaken by Dr. D.M.Hirst using the ATMOL 3 suite of programs of Saunders and Guest (1975). The areas under the theoretical profiles were normalised to equal the number of electrons in the molecule.

5.3 Results and Discussion

5.3.1 Propene and Cyclopropane

The experimental results for the high energy side of the profile for propene and cyclopropane (corrected for multiple scattering) are given in tables 5-1 and 5-2, respectively. In both tables the results shown are the average of two sets of measurements. Also shown are the SCF and LMO profiles after convolution. The total amount of multiple scattering in each profile did not exceed 5%, and the effect on the peak height after renormalisation was less than 1% of J(0). Thus, any possible errors in the form of the multiple scattering correction will have a very small effect on the differences between the profiles of similar samples.

Fig. 5-2 shows the differences between profiles on the same sample including data from the low energy side. This figure clearly illustrates the accuracy and reproducibility of the results to within ± 0.5% of J(0) (cf. ± 1-2% in an X-ray experiment). Having demonstrated the level of experimental accuracy in this way a difference profile between the propene and cyclopropane profiles was obtained, i.e. $J(q)_{ACYCLIC} - J(q)_{CYCLIC}$, and shown in Fig. 5-3. Also shown on this figure are the SCF and LMO difference results, and all are shown on a 'per electron' basis.

Between 0.6 a.u. and 3.0 a.u. the agreement between experiment and the various SCF, LMO results is extremely good, since all show a shift towards higher momenta with a peak around 1.0 a.u. (beyond 3.0 a.u. all profiles are in good agreement with a free atom model). However, between 0 and 0.6 a.u. there is a small discrepency between the various models and the present results. Although the general trend is consistent, the experimental results show a marked deviation from the expected behaviour. In order to explain these features eqn. 5-1 is used to obtain the above mentioned difference in terms of bond profiles, i.e.

Table 5-1

q (a.u.)	LMO[1]	LMO[2]	LMO[3]	LMO[4]	SCF[5]	Exp[6]
0.0	10.329	10.230	10.036	9.969	10.222	10.190
0.1	10.245	10.149	9.960	9.889	10.140	10.134
0.2	9.997	9.908	9.736	9.652	9.900	9.907
0.3	9.595	9.518	9.373	9.271	9.510	9.516
0.4	9.057	8.998	8.886	8.765	8.989	8.996
0.5	8.406	8.368	8.296	8.157	8.359	8.363
0.6	7.672	7.659	7.628	7.475	7.649	7.633
0.7	6.889	6.901	6.909	6.750	6.890	6.855
0.8	6.091	6.124	6.167	6.011	6.115	6.089
0.9	5.310	5.360	5.431	5.284	5.352	5.347
1.0	4.573	4.634	4.723	4.593	4.629	4.625
1.2	3.305	3.367	3.468	3.387	3.369	3.368
1.4	2.358	2.405	2.490	2.470	2.411	2.465
1.6	1.708	1.735	1.793	1.831	1.742	1.738
1.8	1.285	1.294	1.327	1.406	1.301	1.274
2.0	1.015	1.010	1.025	1.117	1.019	1.023
3.0	0.507	0.496	0.498	0.505	0.502	0.480
4.0	0.298	0.290	0.297	0.300	0.294	0.305
5.0	0.173	0.174	0.174	0.173	0.171	0.196

1. Smith and Whangbo (1974)
2. Snyder and Weber (1978)
3. Epstein (1970)
4. Eisenberger and Marra (1971)
5. Hirst and Liebmann (1975)
6. Estimate of experimental error: q=0,±0.5%, q=1.0,±0.8%, q=2.0,±1.6%, q=5.0,±3.1%.

Experimental and theoretical Compton profiles of propene.

Table 5-2

q (a.u)	LMO[1]	LMO[2]	LMO[3]	LMO[4]	SCF[5]	Exp[6]
0.0	10.217	10.012	10.036	9.680	10.112	10.134
0.1	10.140	9.940	9.960	9.610	10.035	10.029
0.2	9.913	9.728	9.736	9.403	9.807	9.763
0.3	9.541	9.382	9.373	9.067	9.437	9.364
0.4	9.038	8.916	8.886	8.617	8.941	8.852
0.5	8.421	8.346	8.296	8.071	8.340	8.243
0.6	7.715	7.694	7.628	7.451	7.657	7.557
0.7	6.950	6.982	6.909	6.782	6.922	6.824
0.8	6.161	6.238	6.167	6.088	6.165	6.088
0.9	5.379	5.489	5.431	5.395	5.413	5.375
1.0	4.633	4.762	4.723	4.724	4.692	4.686
1.2	3.337	3.461	3.468	3.518	3.421	3.403
1.4	2.363	2.450	2.490	2.564	2.441	2.447
1.6	1.697	1.743	1.793	1.879	1.753	1.760
1.8	1.270	1.284	1.327	1.418	1.300	1.325
2.0	1.003	0.995	1.025	1.112	1.014	1.030
3.0	0.507	0.495	0.498	0.506	0.502	0.528
4.0	0.298	0.290	0.297	0.300	0.293	0.321
5.0	0.173	0.174	0.174	0.173	0.171	0.192

1. Smith and Whangbo (1974)
2. Snyder and Weber (1978)
3. Epstein (1970)
4. Eisenberger and Marra (1971)
5. Hirst and Liebmann (1975)
6. Estimate of experimental error: q=0,±0.5%, q=1.0,±0.8%, q=2.0,±1.6%, q=5.0,±3.1%.

Experimental and theoretical Compton profiles of cyclopropane

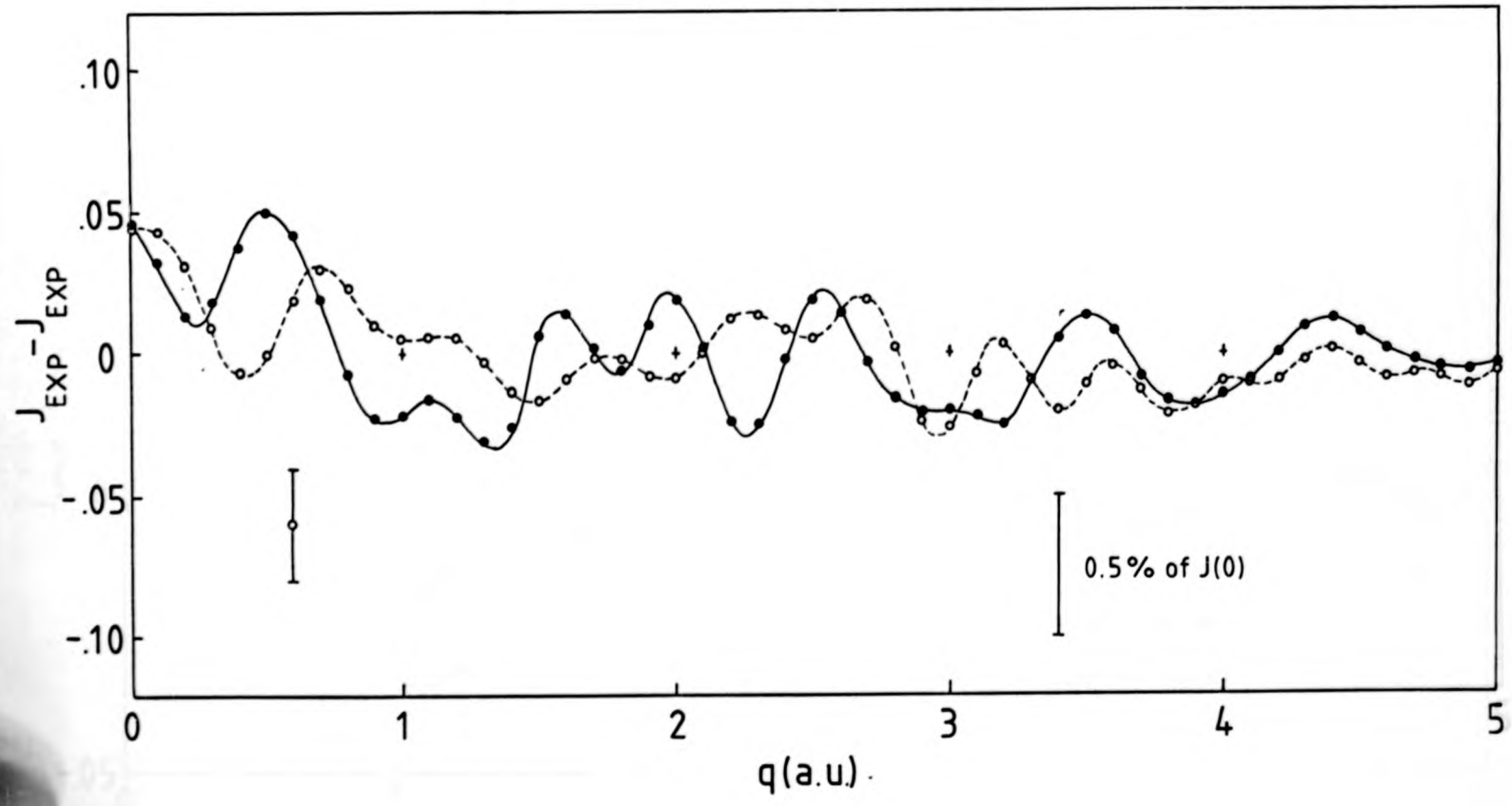

Fig. 5-2: Reproducibility of the Compton profiles of propene (• • •) and cyclopropane (o o o).

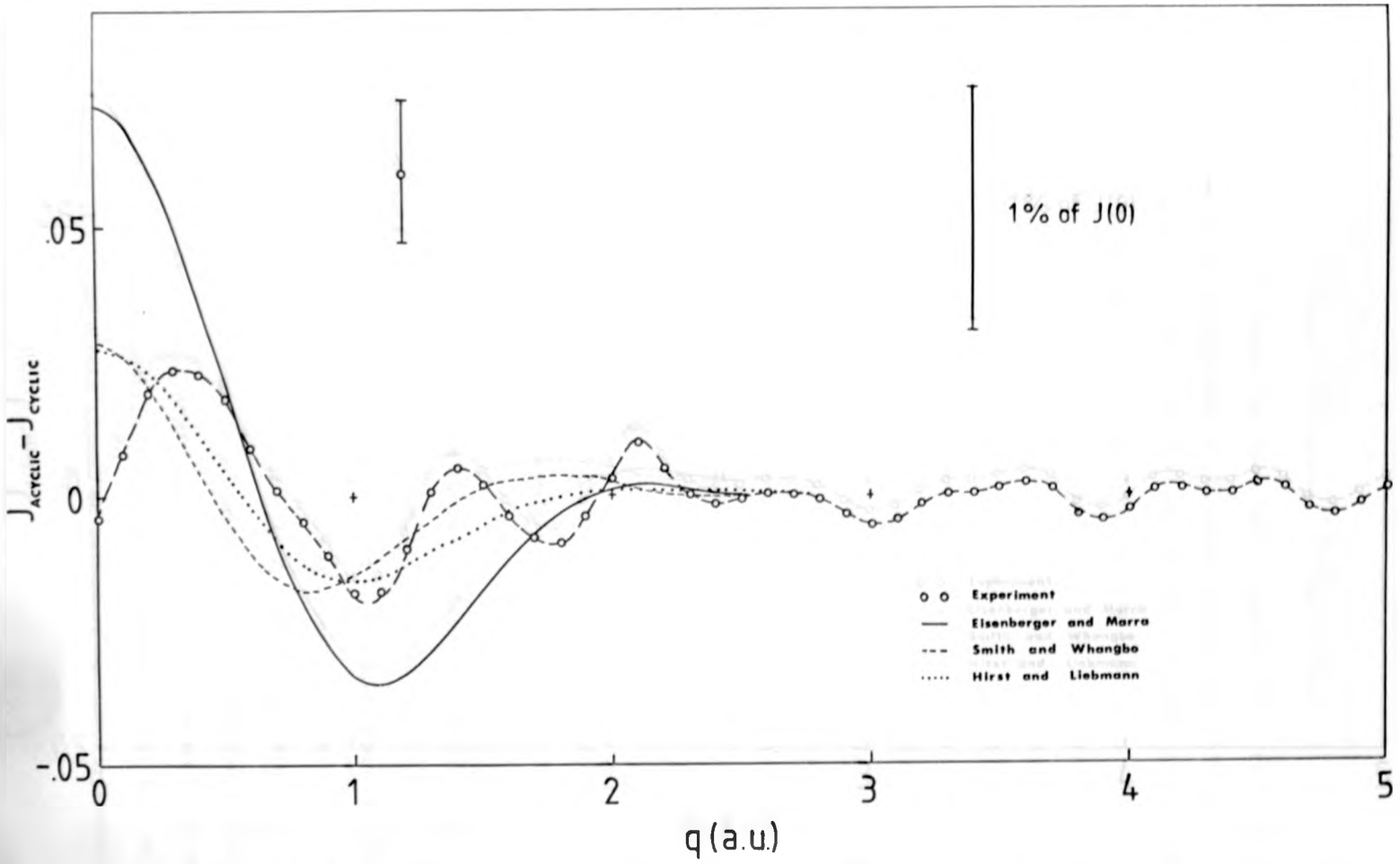

Fig. 5-3: Difference between the Compton profiles of propene and cyclopropane obtained experimentally and from the LCO and SCF descriptions.

$$J(q)_{\text{PROPENE}} - J(q)_{\text{CYCLOPROPANE}} = J(q)_{C=C} - J(q)_{C-C} \qquad 5\text{-}2$$

Eqn. 5-2 expresses the fact that in going from a profile of propene to a profile of cyclopropane an electron (actually 4 electrons are involved) is transfered from the CC double bond to the CC single bond (assuming that the $J(q)_{CH}$ and $J(q)_{C-C}$ bond profiles are identical, and therefore independent of the molecular environment). The experimental results are clearly at varience with the approach used by Epstein (1970) concerning multiple bonds. To explain the results the CC double bond is considered to be constructed from a CC σ and a CC π bond, enabling the LMO to have properties characteristic of both the σ and π bond. Since π bonds are more loosely bound to the nuclei than σ bonds, CC double bonds will have a more expanded charge distribution compared to single bonds. As a consequence of the Fourier transform relation, the Compton profile of CC double bonds will be narrower than that of a CC single bond, and consequently will have a higher J(0) value. Transferring electrons from double to single bonds results in a lowering of the Compton peak accompanied by a general broadening of the profile, particularly around 1 a.u. Such an effect is displayed in the present results albeit with poor statistical accuracy and low resolution.

The difference profile constructed from the empirical profiles of Eisenberger and Marra (1971) is qualitatively similar, with a distinct peak around 1 a.u., but its magnitude is twice that found experimentally. This is directly attributable to multiple scattering effects. To see this more clearly Fig. 5-4 (a) and (b) shows how the resulting profiles differ from the experimental ones for propene and cyclopropane, respectively. In order to avoid the transfer of experimental noise onto the theoretical and empirically reconstructed profiles, the theoretical data by Smith and Whangbo (1974) have been chosen as reference for the difference profiles.

$$J(q)_{\text{propene}} - J(q)_{\text{cyclopropane}} = J(q)_{C=C} - J(q)_{C-C} \qquad 5\text{-}2$$

Eqn. 5-2 expresses the fact that in going from a profile of propene to a profile of cyclopropane an electron (actually 4 electrons are involved) is transfered from the CC double bond to the CC single bond (assuming that the $J(q)_{CH}$ and $J(q)_{C-C}$ bond profiles are identical, and therefore independent of the molecular environment). The experimental results are clearly at varience with the approach used by Epstein (1970) concerning multiple bonds. To explain the results the CC double bond is considered to be constructed from a CC σ and a CC π bond, enabling the LMO to have properties characteristic of both the σ and π bond. Since π bonds are more loosely bound to the nuclei than σ bonds, CC double bonds will have a more expanded charge distribution compared to single bonds. As a consequence of the Fourier transform relation, the Compton profile of CC double bonds will be narrower than that of a CC single bond, and consequently will have a higher J(0) value. Transferring electrons from double to single bonds results in a lowering of the Compton peak accompanied by a general broadening of the profile, particularly around 1 a.u. Such an effect is displayed in the present results albeit with poor statistical accuracy and low resolution.

The difference profile constructed from the empirical profiles of Eisenberger and Marra (1971) is qualitatively similar, with a distinct peak around 1 a.u., but its magnitude is twice that found experimentally. This is directly attributable to multiple scattering effects. To see this more clearly Fig. 5-4 (a) and (b) shows how the resulting profiles differ from the experimental ones for propene and cyclopropane, respectively. In order to avoid the transfer of experimental noise onto the theoretical and empirically reconstructed profiles, the theoretical data by Smith and Whangbo (1974) have been chosen as reference for the difference profiles.

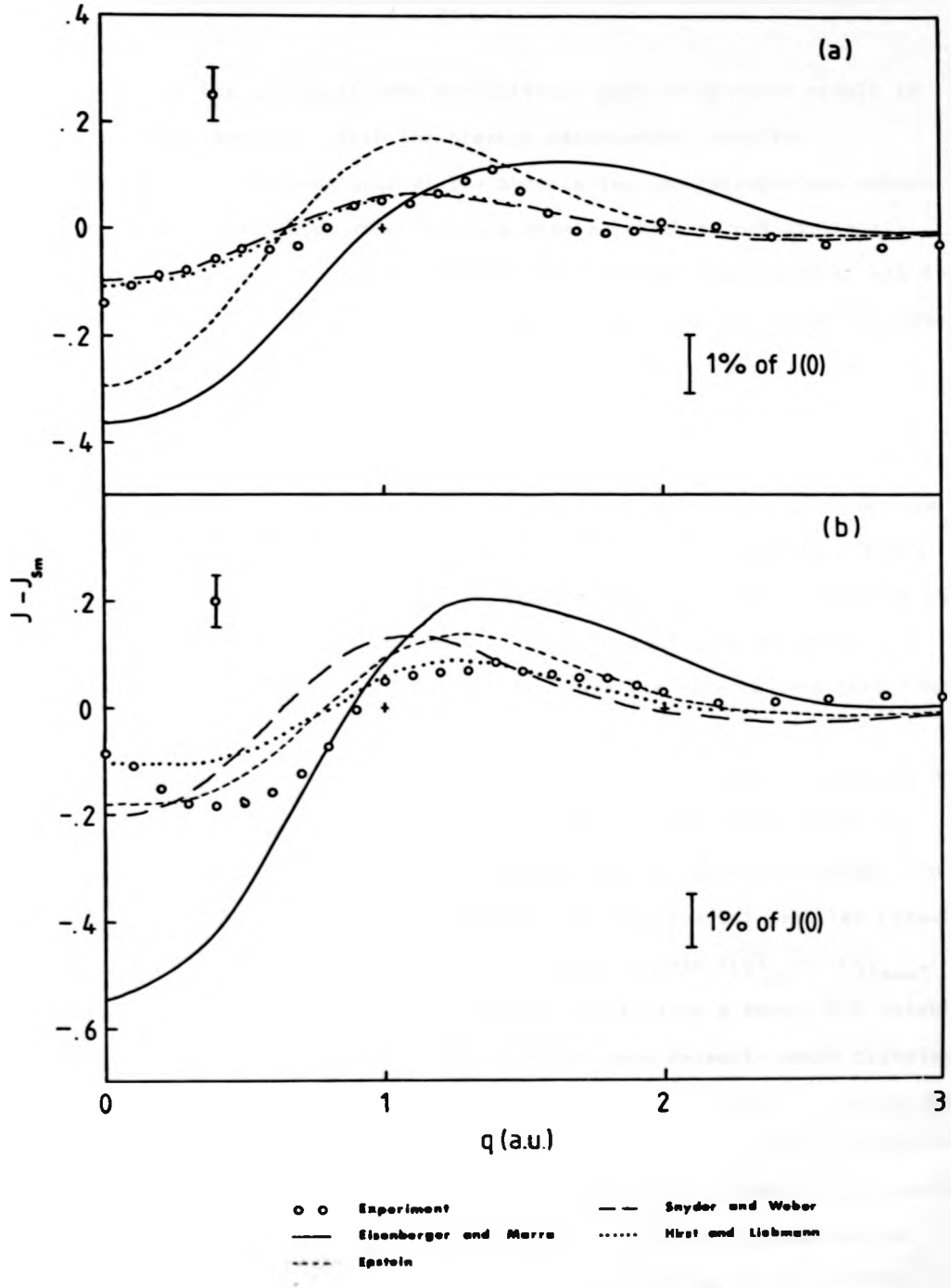

Fig. 5-4: Deviation of the experimental and theoretical profiles of propene (a) and cyclopropane (b) from the LMO profile predicted by Smith and Whangbo (1974).

Correcting the empirical data for multiple scattering would result in much closer agreement with the present experimental results.

The unusual behaviour at low momenta for the cyclopropane molecule may be due to the appearance of ring strain, which is not explicitly taken into account in the SCF calculation, and not considered at all in the LMO approach. However, it is possible that this deviation is associated with next-nearest-neighbour contributions to the Compton profile. Obviously further measurements of this kind are warranted.

The qualitative insensitivity of the calculated profiles with respect to the accuracy of the wavefunctions used is not too surprising as the profile is the result of an integration which tends to smooth out the differences between the various wavefunctions. All theories predict profiles that are in fairly good agreement with experiment with exception to cyclopropane where larger deviations at very low momenta have been found.

5.3.2 2-Butene

In table 5-3 the experimental and theoretical Compton profiles for cis and trans-2-butene are presented. The measured profiles are an average of two sets of readings corrected for multiple scattering. In Fig. 5-5 differences are shown between two experimental profiles (cis-2-butene) together with the difference resulting from $J(q)_{CIS} - J(q)_{TRANS}$, obtained experimentally and also theoretically from a recent SCF calculation. The difference between measurements on the same molecule again illustrates the accuracy and reproducibility of the measured profiles to better than $\pm 0.5\%$ of J(0). The result also shows that there is no significant difference between the two molecules, which is not unexpected considering the spherical averaging and the poor resolution of the measurements. The results also agree with both the SCF calculation and LMO models, including those by Epstein (1970) and Eisenberger and Marra (1971).

Despite the accuracy of the difference profile, a comparison of the total experimental profile with the LMO and SCF profiles on an absolute

Table 5-3

q (a.u.)	LMO[1]	LMO[2]	LMO[3]	LMO[4]	cis-2-butene		trans-2-butene	
					Exp[5]	SCF[6]	Exp[5]	SCF[6]
0.0	13.321	13.215	13.266	12.851	12.650	13.228	12.606	13.243
0.1	13.221	13.117	13.163	12.756	12.534	13.130	12.489	13.145
0.2	12.923	12.828	12.859	12.474	12.238	12.841	12.217	12.854
0.3	12.441	12.359	12.370	12.020	11.804	12.372	11.770	12.382
0.4	11.795	11.731	11.720	11.413	11.274	11.743	11.256	11.749
0.5	11.011	10.969	10.938	10.681	10.639	10.979	10.643	10.982
0.6	10.123	10.107	10.061	9.855	9.880	10.113	9.905	10.112
0.7	9.168	9.177	9.125	8.969	9.028	9.179	9.058	9.176
0.8	8.184	8.216	8.166	8.056	8.169	8.215	8.176	8.210
0.9	7.208	7.259	7.219	7.149	7.341	7.254	7.311	7.248
1.0	6.271	6.336	6.310	6.276	6.527	6.328	6.482	6.322
1.2	4.615	4.687	4.693	4.714	4.973	4.677	4.979	4.671
1.4	3.327	3.387	3.415	3.479	3.720	3.378	3.745	3.375
1.6	2.412	2.450	2.482	2.581	2.704	2.444	2.730	2.442
1.8	1.800	1.815	1.843	1.961	2.025	1.815	2.004	1.814
2.0	1.406	1.401	1.423	1.538	1.507	1.408	1.522	1.407
3.0	0.682	0.664	0.667	0.682	0.651	0.672	0.664	0.672
4.0	0.399	0.388	0.409	0.403	0.444	0.393	0.456	0.393
5.0	0.233	0.232	0.224	0.232	0.247	0.228	0.261	0.228

1. Smith and Whangbo (1974)
2. Snyder and Weber (1978)
3. Epstein (1970)
4. Eisenberger and Marra (1971)
5. Estimate of experimental errors:
   q=0,±0.5%, q=1.0,±0.8%,
   q=2.0,±1.6%, q=5.0,±3.1%.
6. Hirst (1978)

Experimental and theoretical Compton profiles of cis and trans - 2 - butene

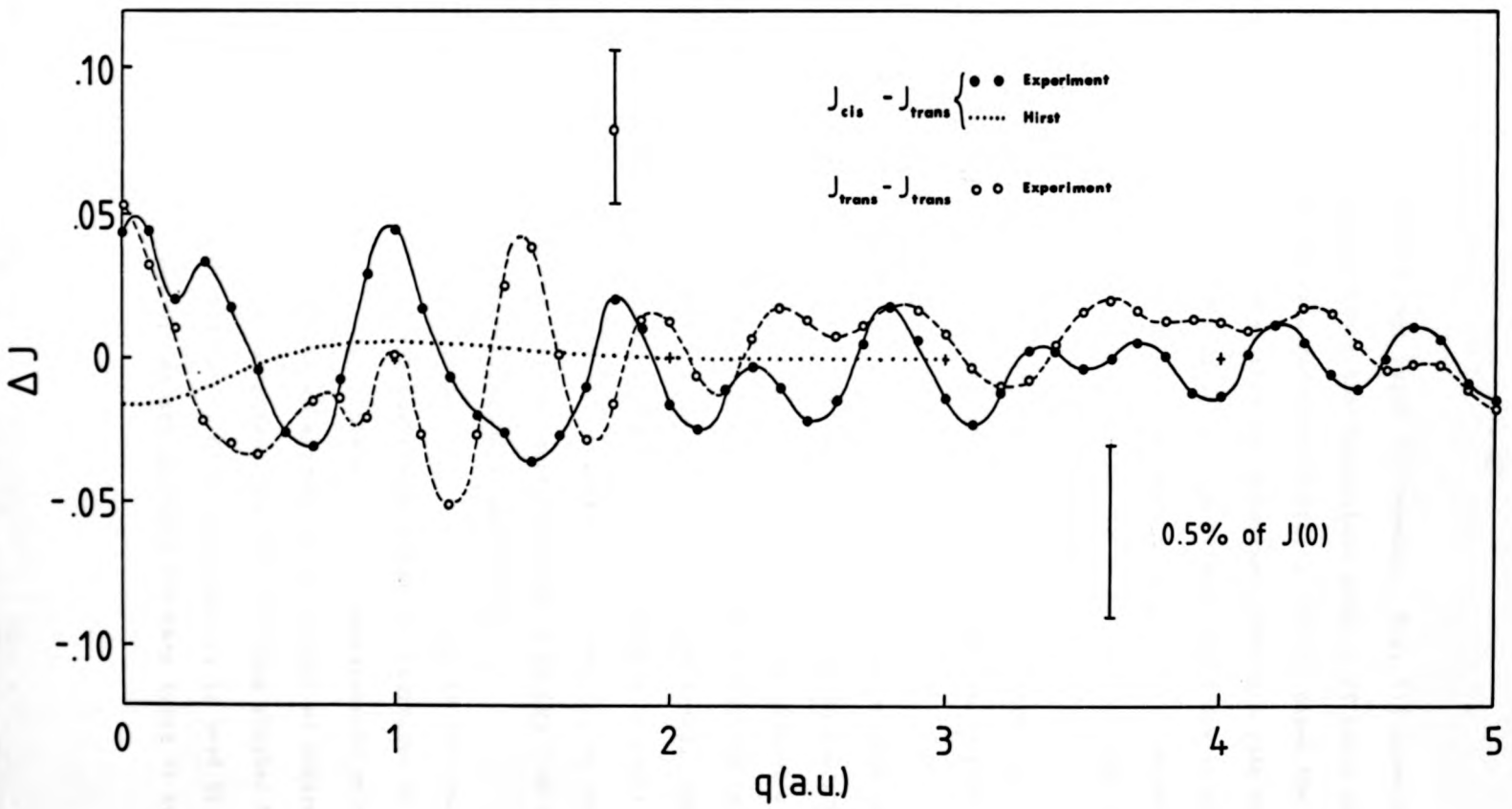

Fig. 5-5: Experimental and theoretical difference curves between cis- and trans-2-butene profiles.

scale displays a very large discrepency. Fig. 5-6 shows this deviation for cis-2-butene where the theoretical profile of Smith and Whangbo (1974) has been chosen as a reference profile. In all cases the calculated profiles are narrower than the experiment having a peak value consistently higher by about 1-5% of J(0). The effect is not due to multiple scattering but may be a consequence of measuring a conjugated diene. In such molecules the electrons tend to be more delocalised with a subsequent shortening of the CC double bond length. Unfortunately, it is difficult to analyse these results based on an isolated measurement, and clearly other measurements on conjugated systems would be helpful.

5.3.3 Conclusions

Although the localised molecular orbital approach can in principle provide a powerful tool for predicting the Compton profiles of large molecules, it should be used with caution. The present experimental results clearly show that the simple notion of bond additivity is incorrect when applied to molecules that possess unusual geometries. Some allowance for differences in molecular geometry should perhaps be built in to the model. Methods for deriving such corrections, for example, as second order effects dependent upon the nonlocal contributions to an LMO from the rest of the molecule, are currently being investigated.

The results presented have however, enabled an accurate assessment of the potential of the low energy gamma-ray technique in studies of molecular systems. Certainly additional measurements on other hydrocarbon isomers are desirable if an attempt is to be made at understanding the nature of these discrepancies. In the following chapter the new Compton spectrometer, utilizing a 5 Ci annular source, is used to obtain a comprehensive set of Compton profiles for many types of hydrocarbon molecules.

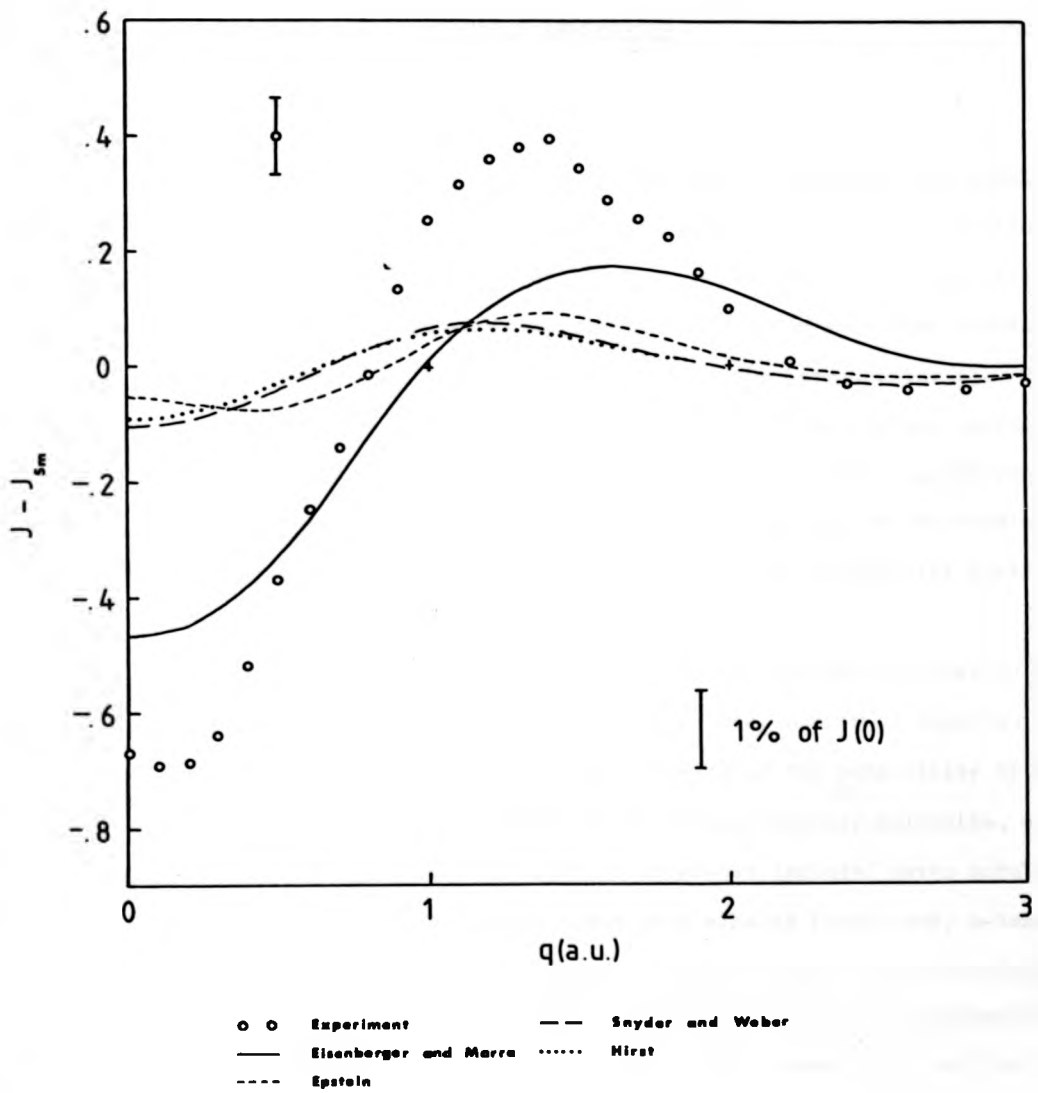

Fig. 5-6: Deviations of the experimental and theoretical profiles of cis-2-butene from the LMO profile predicted by Smith and Whangbo (1974).

CHAPTER 6

MOLECULAR COMPTON PROFILES

LIQUID HYDROCARBONS

6.1 Introduction

The renovation of the ^{241}Am spectrometer to house a 5 Ci annular source, and the purchase of an intrinsic germanium detector, provided an order of magnitude improvement in the quality of the results obtained. The advantages and disadvantages of this new system have been highlighted in measurements on a 'standard' aluminium sample (see Chapter 4). However, the system is also ideal for studying small, light molecules, particularly the hydrocarbons, and the results obtained with the 'old' system confirmed this. Since the scattering vector is not well defined in the annular source arrangement, the molecules that can be studied are necessarily restricted to isotropic systems.

To obtain additional and perhaps more fundamental information about the effects of bonding in momentum space a total number of nineteen liquid hydrocarbon molecules were measured. Because of the sensitivity of the profile to observing subtle differences between similar molecules, e.g. propene and cyclopropane, the list of molecules included seven acyclic-cyclic isomer pairs. A further three were alkanes (n-pentane, n-hexane, n-heptane), and the remaining two were resonant type structures, benzene and cycloheptatriene. The resonant structures are known to possess a highly delocalised set of π electrons which may create difficulties for the LMO description.

In Fig. 6-1 the geometries of some of the fundamental structures are shown schematically. The aromatic molecule, benzene, is also shown structured as cyclohexatriene. A more precise description of each molecule can be found in any standard textbook on organic chemistry.

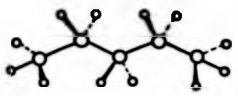

n-Pentane (C_5H_{12})

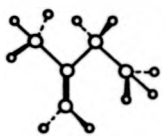

2-Methyl-2-butene (C_5H_{10})

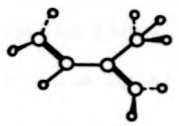

Isoprene (C_5H_8)

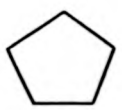

Cyclopentane (C_5H_{10})

Cyclohexane (C_6H_{12})

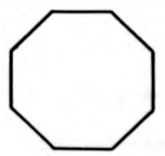

Cyclooctane (C_8H_{16})

Cyclopentene (C_5H_8)

Cyclohexene (C_6H_{10})

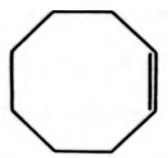

Cyclooctene (C_8H_{14})

Benzene (Cyclohexatriene, C_6H_6)

Cycloheptatriene (C_7H_8)

Fig. 6-1: The molecular structure of some liquid hydrocarbons.

6.2 Experimental Details

A detailed description of the 5 Ci annular source spectrometer has been given in Chapter 4. The only modification necessary was to redesign a sample holder to hold organic liquids. Previous sample holders comprising of a brass ring with two thick mylar windows glued on either side proved to be inadequate, for two reasons. Firstly, the signal-to-noise ratio at the Compton peak deteriorated from 100 to 1, to nearer 10 to 1. The greater incident energy of the 5 Ci source resulted in a considerable increase of scattered intensity, not only from the sample itself but also from the mylar windows. Secondly, many of the hydrocarbon samples reacted with the araldite glue causing excessive sample leakage and eventual loss of signal. After several attempts to find an adequate holder, the final design and construction resulted in a signal-to-noise ratio in excess of 50 to 1 at J(0). The holder is illustrated in Fig. 6-2.

The main brass ring has the dimensions 3.0 cm o.d., 2.5 cm i.d., and 0.3 cm thick. Although rings of differing thickness were available the one chosen represented the optimum compromise between intensity of scattered radiation, signal-to-noise ratio and degree of multiple scattering. The windows were made from 12.5 μm thick aluminium foil and were kept in place by two neoprene, annular pads. In order to achieve the reasonable signal-to-noise ratio of 50 to 1, the scattering chamber was filled with 1 atms. of helium gas, (evacuation of the chamber would have resulted in in the rupture of the aluminium windows). The 50 to 1 ratio represents a mean since the relative densities of the molecules studied varied by only a small amount, typically from 0.5 gm/cc to 0.8 gm/cc. A sketch of the apparatus is shown in Fig. 6-3.

During any measurement period no leakages were found. A measurement of the background was made under identical conditions to those used in an

Fig. 6-2: Illustration of the sample holder.

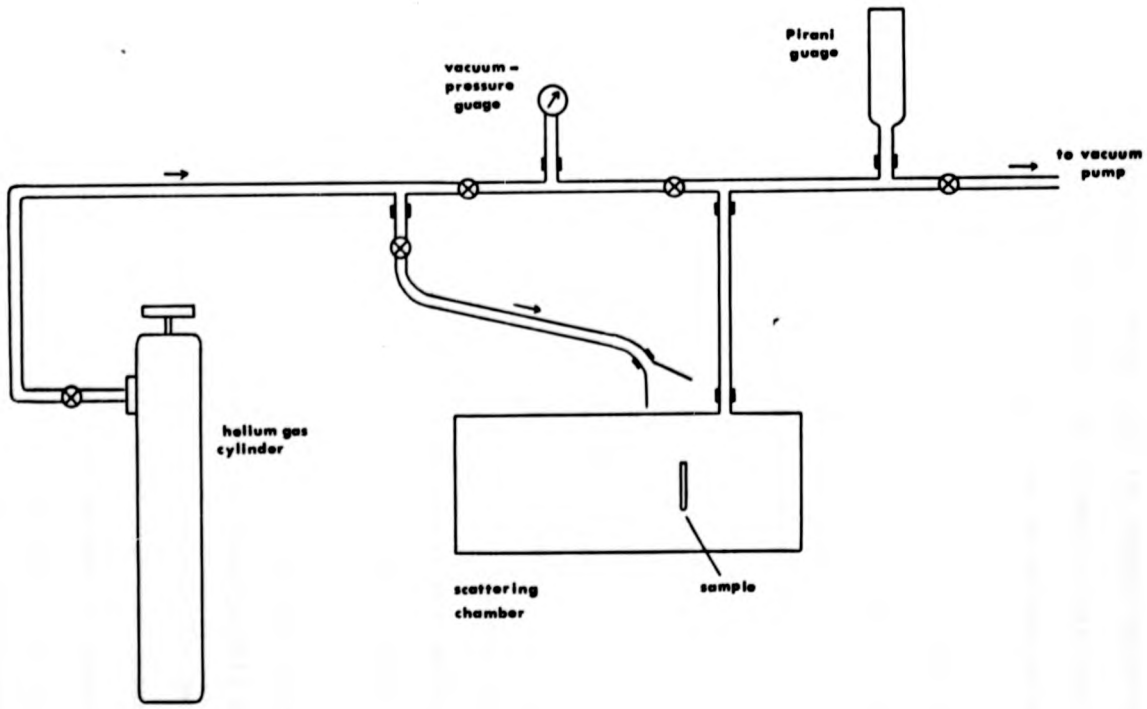

Fig. 6-3: Apparatus used to measure molecular Compton profiles of liquid hydrocarbons.

actual experiment, except that the sample holder was inserted into the scattering chamber empty. No correction was made for the replacement of the liquid sample by helium since the effect on the final profile was regarded as negligible.

For each hydrocarbon sample, approximately 11. 10^4 counts per 20 eV channel (0.03 a.u.) were accumulated in the Compton peak, each measurement taking about 20 hours to complete. Each sample was measured twice in order to assess the reproducibility and accuracy of the final profile. Fig. 6-4 shows a typicelly reproducibility for the n-pentane molecule to better than $\pm$ 0.1% of J(0). The energy-channel relation was determined with the low activity (~1 μCi) ^{241}Am source before and after each experiment. The calibration was checked with the results obtained directly from the energy loss spectrum using the elastic and K_α lead X-ray lines (59.54 KeV, 72.79 KeV and 74.96 Kev, respectively). Due to the rapid accumulation of data, electronic drift was minimized, being typically less than 1 channel over the 20 hour measurement period as indicated from the calibration.

The data from each experiment was then processed according to the procedures detailed in Chapter 3. Each profile was corrected for multiple scattering using the Monte Carlo method. The amount of multiple scattering was approximately 5% of the total scattered intensity, and increased J(0) by 1.5%. Only 5. 10^5 photon paths were followed with one iteration before a statistically significant and accurate profile was returned. The final corrected profiles were normalized to their corresponding free atom value, calculated using the tabulated atomic profiles of Biggs et. al. (1975).

6.3 Bond Compton Profiles

The LMO profiles were constructed from the contributions arising from C-H, CC single and CC double bond profiles taken from the tabulated data of Eisenberger and Marra (1971), Epstein (1970), Smith and Whangbo (1974)

and Snyder and Weber (1978). The number of electrons in each bond profile is dependent on the appropriate molecular structure.

The nature of the measurements undertaken unfortunately does not allow direct access to the contributing bond densities themselves. However, an indirect approach can be used similar to that undertaken on the gaseous hydrocarbon results, where attention is focussed on the differences between the bond profiles, i.e. differences between the Compton profiles of the isomeric molecules. The advantages of this method have already been stated in Chapter 5. The results presented below are not corrected for multiple scattering, for two reasons. Firstly the amount of multiple scattering in profiles of similar molecules is very nearly identical. Therefore subtracting the profiles of similar molecules to obtain a difference curve has the effect of cancelling multiple scattering errors as well as other systematic errors. Secondly, the Monte Carlo program uses a coarse mesh in momentum space which increases as the value of q increases (for computational reasons). Producing a difference curve using the corrected profiles will only enhance the errors arising from this additional correction, and this would be especially apparant in the tails of the profile where the statistical accuracy is necessarily lower.

(i) The LMO Profiles

In the LMO description introduced by Eisenberger and Marra (1971), i.e. distinct C-H, C-C and C=C bond contributions, the difference between acyclic and cyclic isomeric profiles reduces to the simple expression

$$J(q)_{\text{ACYCLIC}} - J(q)_{\text{CYCLIC}} = J(q)_{\text{C=C}} - J(q)_{\text{C-C}} \quad \text{per electron} \qquad 6\text{-}1$$

Eqn. 6-1 is applicable to all seven isomeric pairs of molecules studied here. In deriving this expression it has been assumed that the C-H, C-C and C=C bond profiles are identical in all molecules. This implies that to first order, each bond profile is independent of the molecular environment in which it finds itself.

Although eqn. 6-1 holds for both the empirical and theoretical bond profile data of Eisenberger and Marra (1971) and Snyder and Weber (1978), respectively, the effects of molecular environment on the C-H bond profile has been considered in the LMO approach employed by Smith and Whangbo (1974). The dependence of J_{CH} on the molecular environment burdens the above equation with an additional term involving only J_{CH} contributions from methane, ethane and ethylene. However, preliminary calculations indicated that such a term gives rise to an extremely weak effect on the main difference curve (< 1%) even for systems that have a large J_{CH} bond contribution. Because the effect is small it has been subsequently neglected in all bond difference curves predicted by Smith and Whangbo (1974).

Fig. 6-5 shows the theoretical and empirical difference curves of the form indicated in eqn. 6-1. The curves are shown after convolution with a Guassian of width 0.59 a.u. which is equivalent to the FWHM of the experimental resolution function. The LMO approach of Epstein (1970) (equivalence of multiple bonds) predicts no differences between acyclic and cyclic isomeric profiles.

(ii) Experimental Difference Curves

In a spherically averaged environment large ring molecules should possess very similar Compton profiles to those molecules which are isomeric and structurally similar. Environmental effects on the bonds in such large molecular structures should therefore be small. For isomeric molecules that differ by a single C=C bond, a similar statement concerning environmental effects on the bonds themselves could also be made. Therefore differences between acyclic and cyclic molecules for large systems, e.g. containing eight carbon atoms, should be closely representative of the actual difference between a CC single and a CC double bond, since the common bond contribution should cancel almost exactly. For smaller molecules however, one could expect that environmental effects on the

bond profiles to become increasingly more important. The results of such effects would therefore manifest themselves in a continual distortion from the difference curves predicted for the larger systems.

Evidence for such distortion effects have already been observed in the acyclic-cyclic system of propene and cyclopropane (C_3H_6), albeit with poor statistical accuracy and at low resolution. For this small ring system and also for 4 and 5 membered rings, the carbon atoms lie in a plane, and the deviation of the CCC bond angle from the normal tetrahedral angle angle of 109.5° imposes a strain on the molecule and subsequent instability. For large ring molecules, e.g. 6, 7 and 8 membered rings, angle strain is minimized because the rings are non-planar allowing several possible conformations. Distortion of the $J_{C=C} - J_{C-C}$ difference curve should therefore be minimal for these larger systems.

The difference curves produced from the present set of experimental results are shown in Figs. 6-6 to 6-12 inclusive, in decreasing order of molecular size. The distortion effects described above are clearly apparent in these results.

(a) C_8 Molecules

The C_8H_{16} and C_8H_{14} molecules clearly follow quantitatively the general trend observed by Eisenberger and Marra (1971) despite the conclusions that these earlier profiles contain a substantial amount of multiple scattering. The experimental results are also in reasonable agreement with the recent calculations of Snyder and Weber (1978), although they differ qualitatively with the difference predicted by Smith and Whangbo (1974) LMO model.

(b) C_7, C_6 Molecules

The C_7H_{14}, C_6H_{12} and C_6H_{10} molecules again follow quite closely the difference curve observed for the larger molecules, with however, a

ed molecular

ic - J_{cyclic}.

free atom model.

rence curves

Fig. 6-5: Theoretical and empirical localised molecular orbital difference curves of the form $J_{acyclic} - J_{cyclic}$. Also shown is the difference predicted by a free atom model.

Fig. 6-6, 6-12 inclusive: Experimental difference curves of the form $J_{acyclic} - J_{cyclic}$.

curves

tom model.

cyclic.

ecular

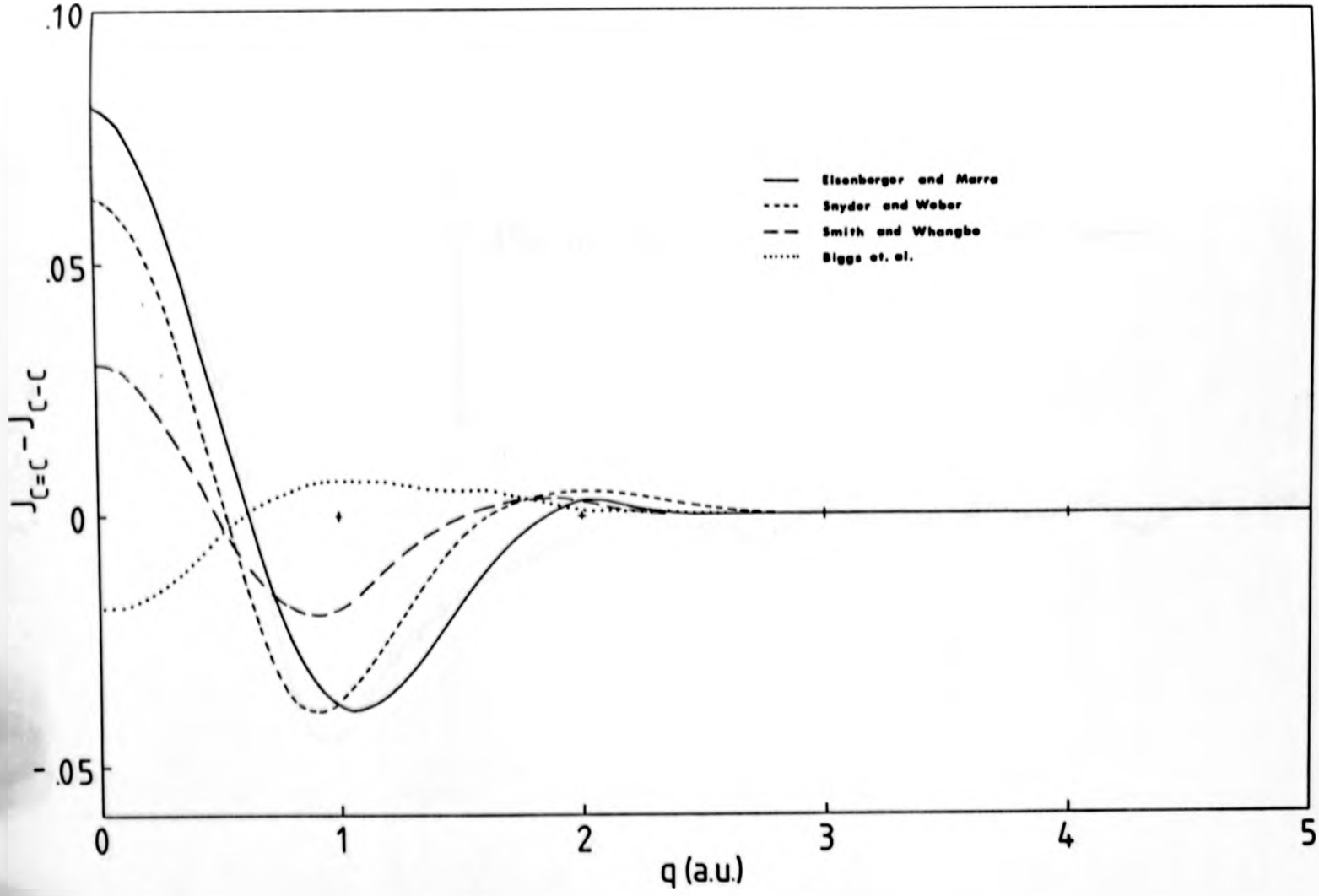

Fig. 6-5

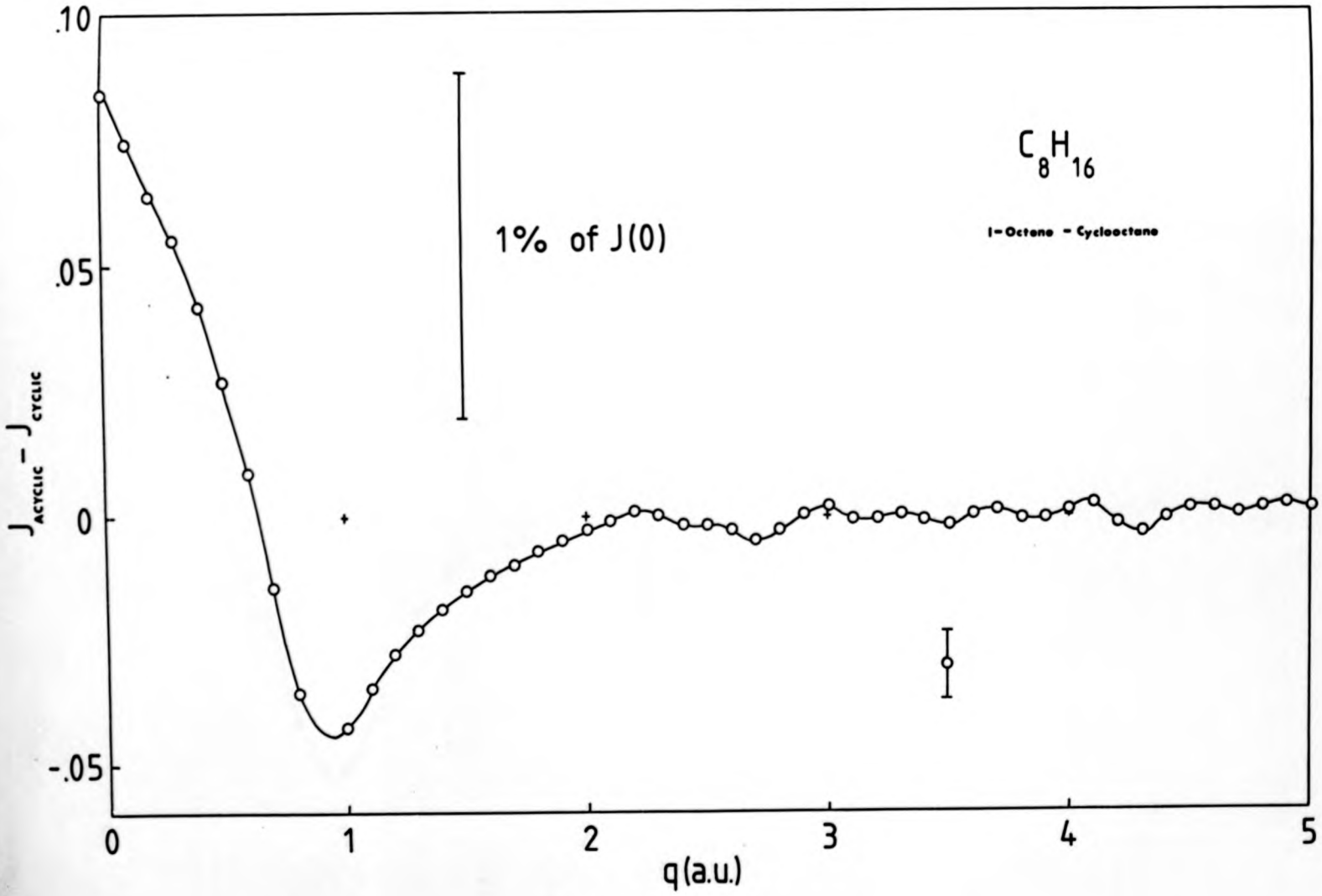
.10
.05
0
-.05
1% of J(0)
C_8H_{16}
1-Octene - Cyclooctane
$J_{ACYCLIC} - J_{CYCLIC}$
0
1
2
3
4
5
q(a.u.)

Fig. 6-6

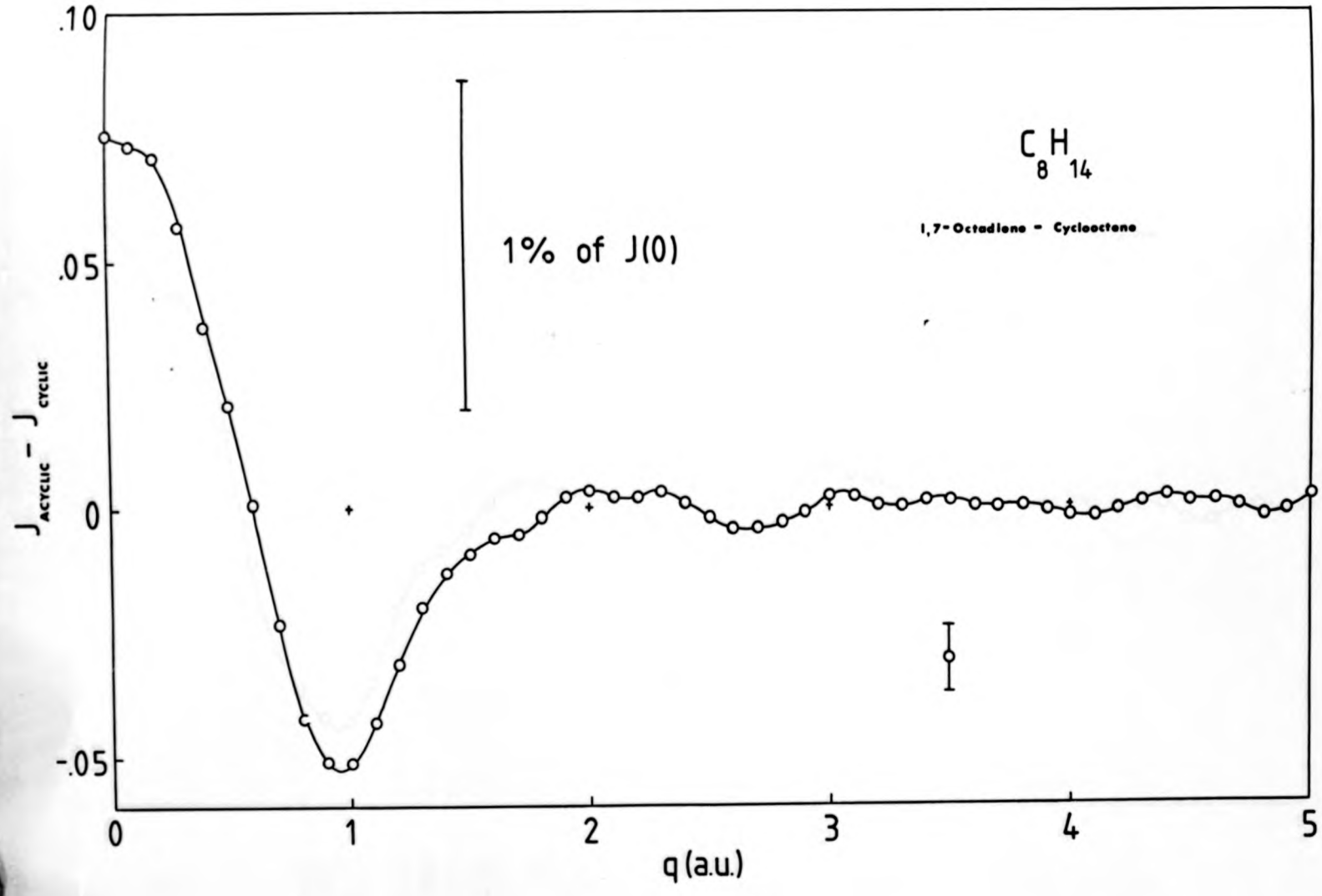
.10
.05
0
-.05
$J_{ACYCLIC} - J_{CYCLIC}$
1% of J(0)
C_8H_{14}
1,7-Octadiene - Cyclooctene
0
1
2
3
4
5
q (a.u.)

Fig. 6-7

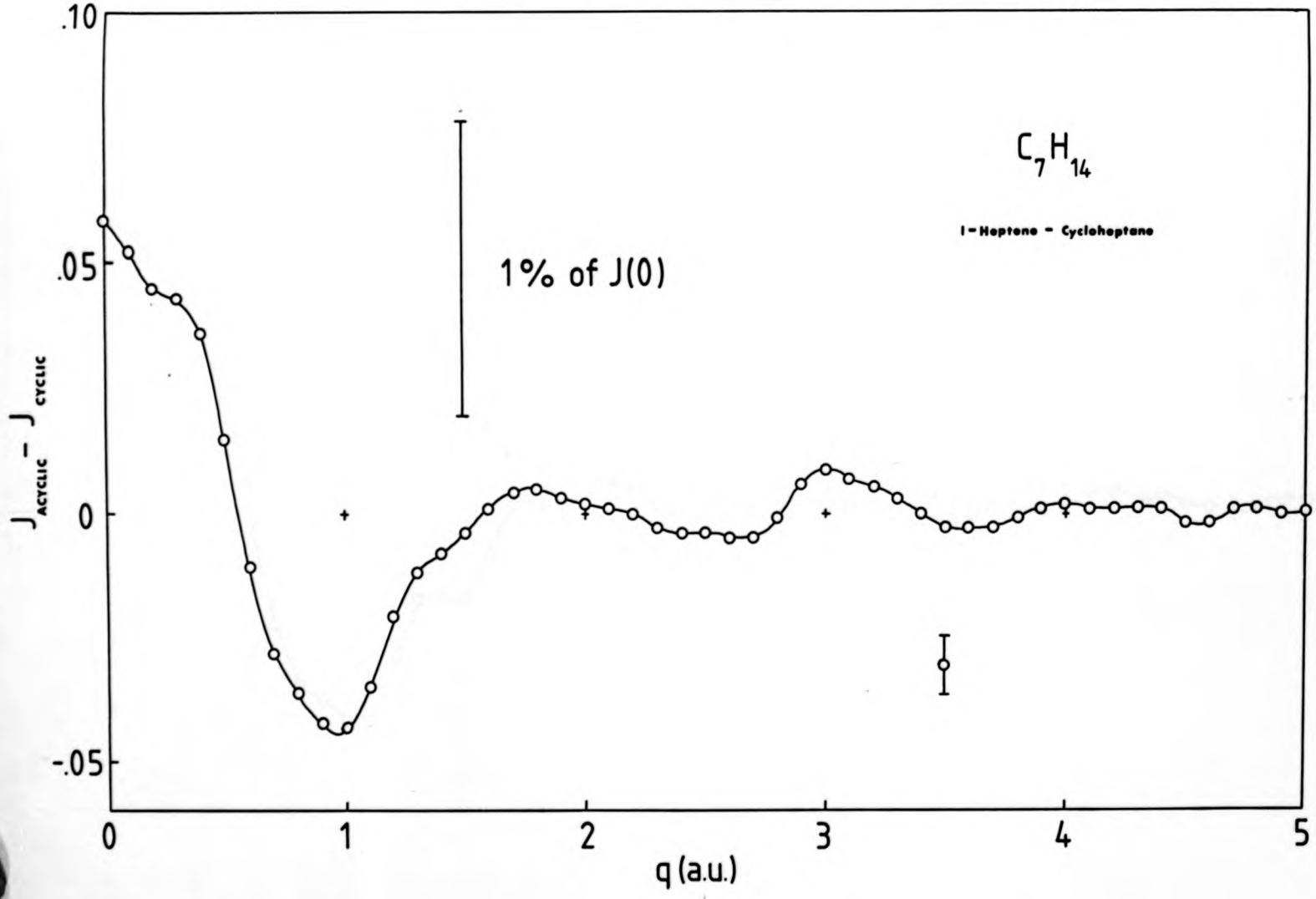
.10
.05
0
-.05
$J_{ACYCLIC} - J_{CYCLIC}$
1% of J(0)
C_7H_{14}
1-Heptene - Cycloheptane
0
1
2
3
4
5
q (a.u.)

Fig. 6-8

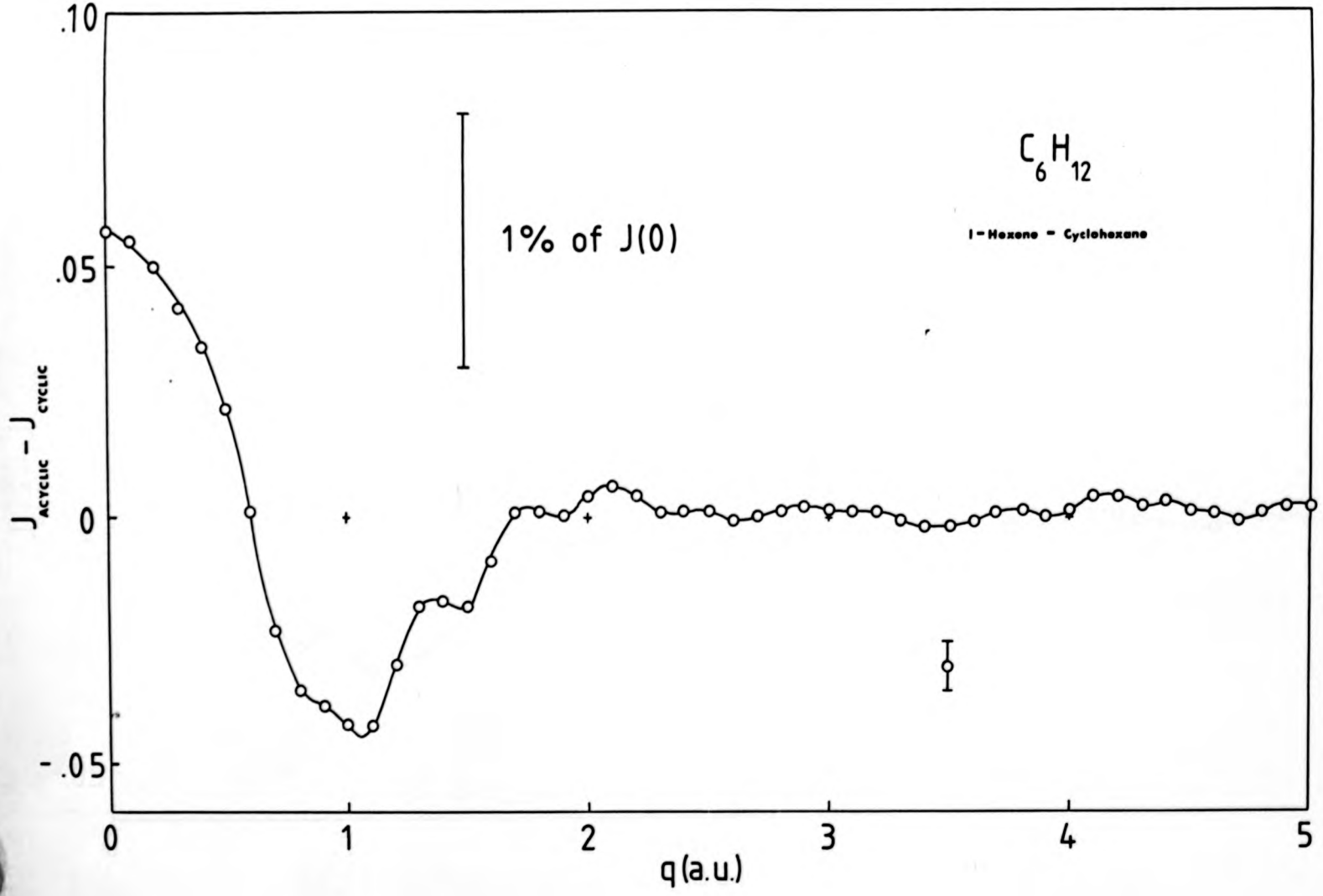
.10
.05
0
-.05
$J_{ACYCLIC} - J_{CYCLIC}$
1% of J(0)
C_6H_{12}
1-Hexene - Cyclohexane
0
1
2
3
4
5
q(a.u.)

Fig. 6-9

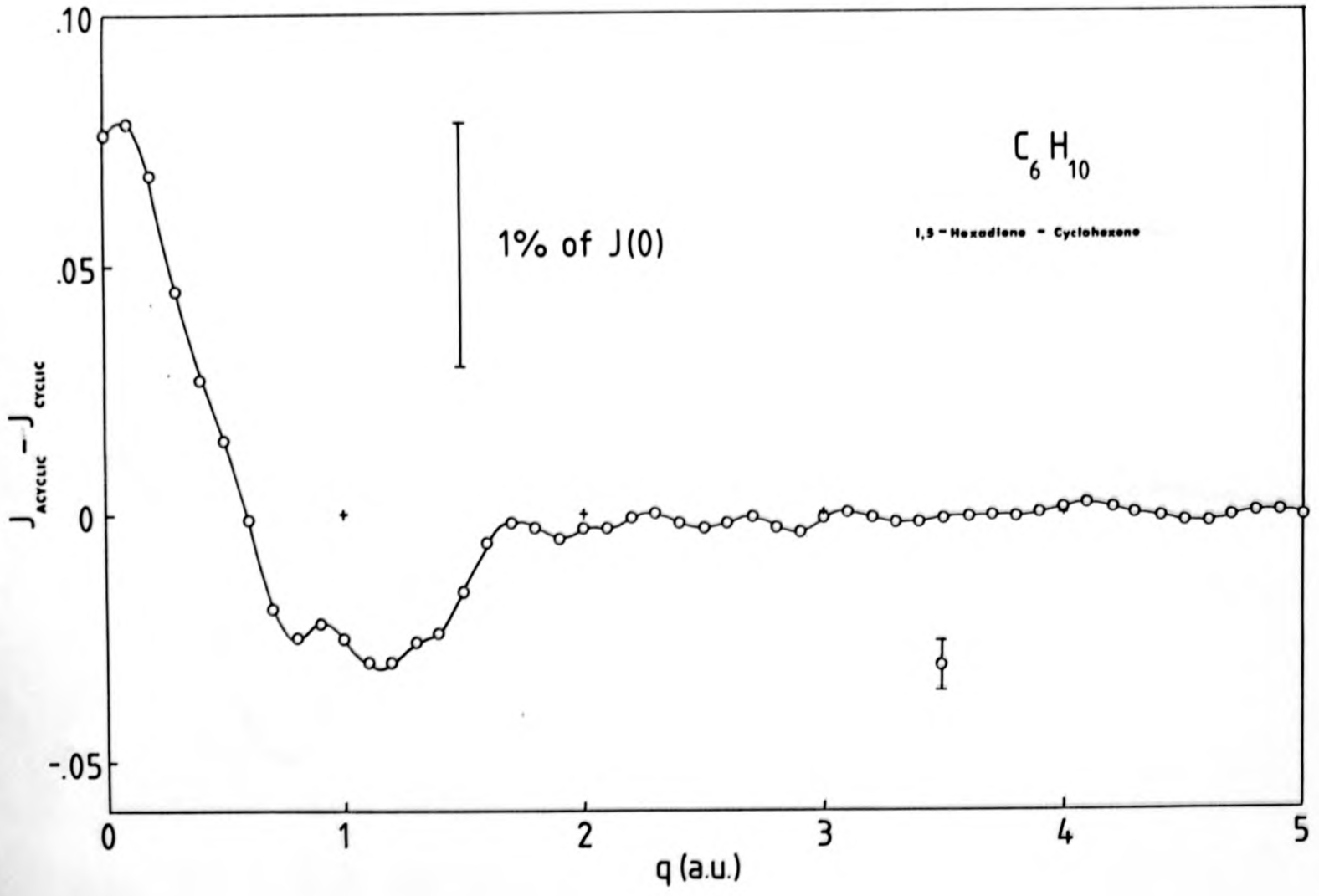
.10
.05
0
-.05
0
1
2
3
4
5
q (a.u.)
$J_{ACYCLIC} - J_{CYCLIC}$
1% of J(0)
$C_6 H_{10}$
1,5 - Hexadiene - Cyclohexene

Fig. 6-10

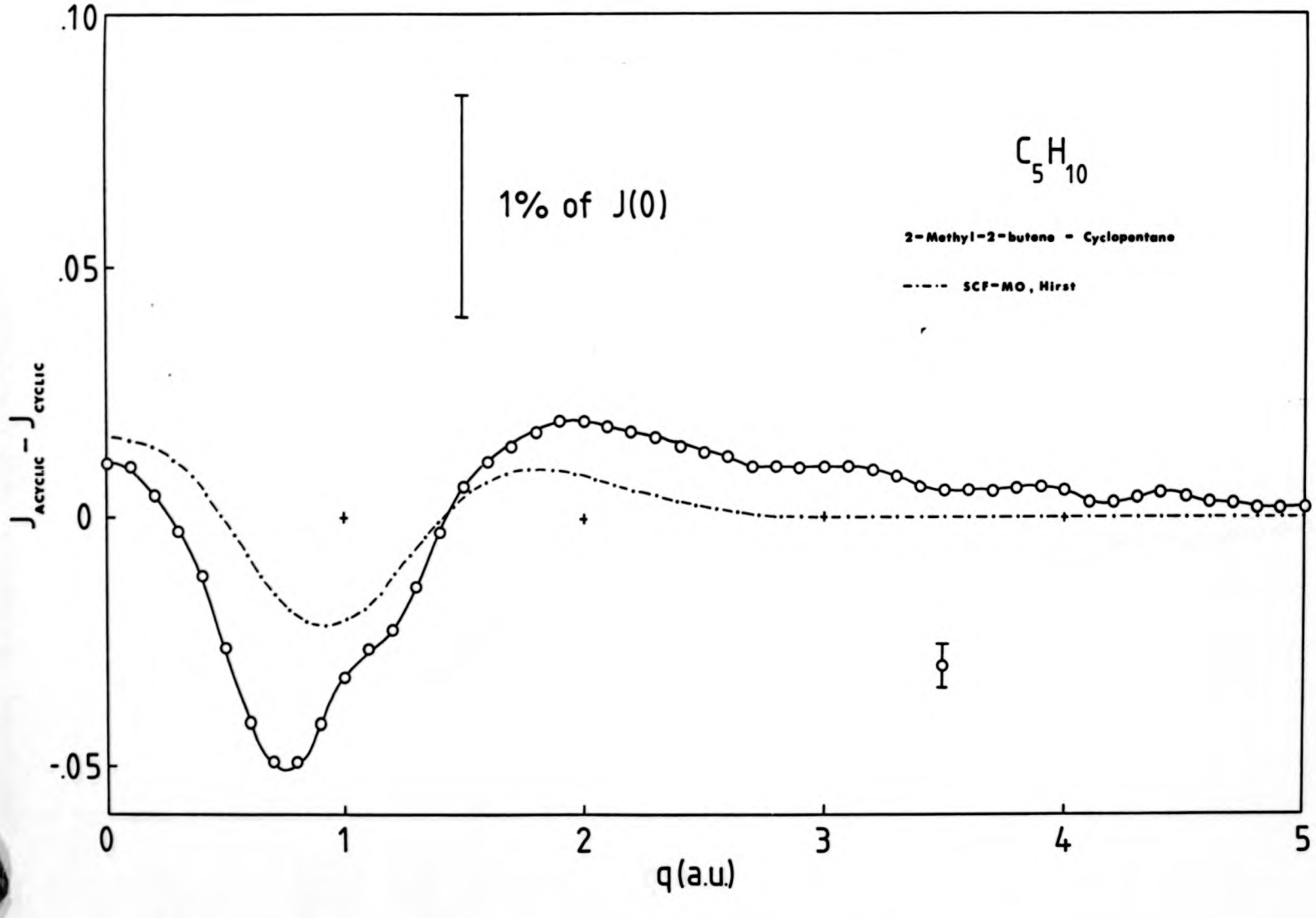
.10
.05
0
-.05
0
1
2
3
4
5
q(a.u.)
$J_{ACYCLIC} - J_{CYCLIC}$
1% of J(0)
C_5H_{10}
2-Methyl-2-butene - Cyclopentane
SCF-MO, Hirst

Fig. 6-11

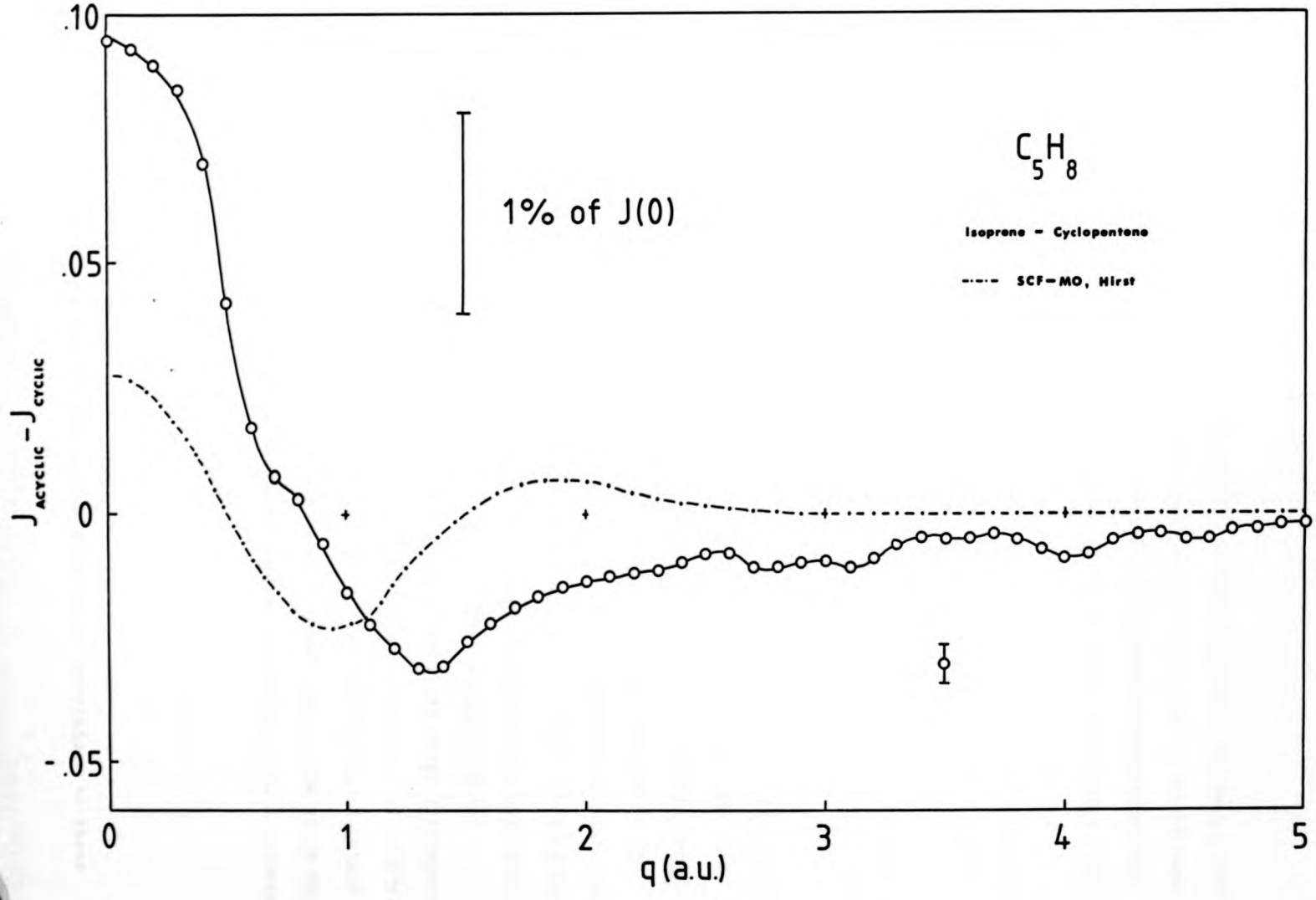
.10
.05
0
-.05
0
1
2
3
4
5
q (a.u.)
$J_{ACYCLIC} - J_{CYCLIC}$
1% of J(0)
C_5H_8
Isoprene - Cyclopentene
SCF-MO, Hirst

Fig. 6-12

deterioration in the relatively smooth varying features. Epstein (1970) in his calculation of the momentum expectation value $\langle p \rangle$ of the CH bond concluded that the value of $\langle p \rangle$ decreases with increasing unsaturation of the carbon atom. The recent calculations by Smith and Whangbo (1974) have also observed that the CH profile is slightly higher for the unsaturated hydrogen. Both of these observations indicate an electronic charge expansion of the CH bond (due to the influence of the CC bonds) which therefore implies that the bonds in general are sensitive to their environment. It is suggested that the results shown indicate the onset of environmental effects on the bond profiles.

(c) C_5 Molecules

The effect of the environment is clearly illustrated in the results for the C_5H_{10} and C_5H_8 molecules where a considerable distortion both at high and low momenta is observed (Figs. 6-11 and 6-12 respectively). Also shown in these figures are the difference curves produced by an SCF-MO calculation using an intermediate basis set similar to that used in the calculations on 2-butene (Hirst 1978) and after convolution with the appropriate Gaussian. Neither of the two experimental curves show good agreement with the theoretical (including an SCF calculation) and empirical difference curves. In order to explain these large discrepancies a closer look at the molecular structures of these systems is necessary.

The two acyclic molecules, isoprene (C_5H_{10}) and 2-methyl-2-butene (C_5H_8) contain the unusual structure of a branched carbon atom which is not found in any of the other measured acyclic molecules, i.e. a structure of the form

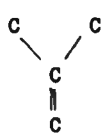

In this structure, the central carbon atom is sp^3 hybridized to three

adjoining carbon atoms. In the LMO approaches employed in the present study such an arrangement of carbon atoms is not included in the calculations. Moreover, both of these acyclic molecules are classified as conjugated dienes, i.e. having alternate single and double CC bonds, and as such deserve special comment. Conjugated dienes are not rigid molecules like the cyclic compounds. In these compounds two π MO embracing only two carbon nuclei can produce a delocalised π MO. The strucure of these molecules coupled with the delocalised MO's they possess may well prevent the molecule from being accurately described by a LMO model based on more usual (i.e. saturated, unsaturated) molecules. Unusual behaviour in conjugated molecules has already been observed for cis and trans 2-butene.

The unusual features observed in these difference curves (shown in Figs. 6-11 and 6-12) may well arise from the cyclic molecules. From energy considerations, it is known that the heat of combustion per CH_2 group in alkanes and cycloalkanes is about 157 Kcal per mole. For cyclopropane this figure is 12 Kcal per mole higher and is attributed almost entirely to the C-C bonds. This distortion in the C-C bond has manifested itself in the poor agreement between the experimental and theoretical profiles at low values of momenta. For cyclopentane, however, this figure is only 1.7 Kcal per mole higher, which indicates a much smaller deterioration in the C-C bond. A similar figure is obtained for cyclopentene despite the presence of the C=C bond. The unusual behaviour of the difference curve does not therefore appear to be due to ring strain effects.

Values of the boiling points of these four liquid hydrocarbons indicate that both the cyclic molecules have higher boiling points and are therefore more stable i.e. have a lower total energy, than their acyclic isomers. One of the unusual features of the present results is the considerable differences at large momentum values ($q \leq 5$ a.u.) which by

the virial theorem (kinetic energy = $\frac{1}{2}\langle p^2 \rangle$) indicate large energy differences. The results for C_5H_8 indicates that the cyclic molecule has a greater second moment and is therefore much more stable than its acyclic isomer, in agreement with the chemical observation of the boiling points. Unfortunately an opposite argument is obtained for the C_5H_{10} system, further complicating the analysis of the results.

(iii) Conclusions

It is apparent from these results that the LMO model is not valid for molecules with unusual molecular structures. The cause of the discrepancy would appear to be due to an inadequate description of the C-C bond. This is perhaps highlighted by the fact that the largest discrepancies between the LMO bond profiles occur for the C-C bond where differences as high as 27% (at J(0)) are found. Finally, the theoretical LMO's have been determined from calculations on isolated, free molecules with complete neglect of intermolecular interactions. Whether such effects are responsible for the results obtained here requires further investigation.

There are three possible sources of improvement that may result in better agreement with the experimental results and help to provide a closer correlation between Compton profiles and chemical properties,

(a) Better quality basis sets

(b) Electron correlation

(c) A reanalysis of the experimental (and theoretical) results.

The first two points, although extremely complicated by the mathematical machinery that surrounds them, are briefly discussed in a later section. The third point is important, since a repartitioning of the momentum density may help to shed more light on the chemical aspect of electron momentum distributions.

6.4 Group Compton Profiles

In the previous section the hydrocarbon Compton profiles were separated into core and valence electron profiles. The valence electron contributions are closely associated with a schematic classical picture of chemical bonds, i.e. CH, C-C and C=C bonds. However, this is not the only method available that may be used to separate the momentum density. Another, perhaps more useful, method is to repartition the molecule into functional groups where emphasis is now placed on the molecular environment. On the basis of this simple model, the linear combinations of the bond Compton profiles, which at each value of q should give the group value, can be written,

$$
\begin{aligned}
J(q)_{C} &= 2J(q)_{C1s} + 2J(q)_{C-C} + 2J(q)_{C=C} \\
J(q)_{CH} &= 2J(q)_{C1s} + 2J(q)_{CH} + 2J(q)_{C=C} + J(q)_{C-C} \\
J(q)_{CH_2} &= 2J(q)_{C1s} + 4J(q)_{CH} + 2J(q)_{C-C} \\
J(q)_{CH_2'} &= 2J(q)_{C1s} + 4J(q)_{CH} + 2J(q)_{C=C} \\
J(q)_{CH_3} &= 2J(q)_{C1_s} + 6J(q)_{CH} + J(q)_{C-C}
\end{aligned}
\qquad 6\text{-}2
$$

where the numbers correspond to the number of electrons in each bond profile. $J(q)_{C1s}$ represents the carbon core profile. Partitioning the molecule in this way has already been used to predict quite accurately the heats of formation of hydrocarbons (Schleyer et. al., 1970). The method also quite naturally takes account of the state of hybridization of the carbon atom and also allows for a distinction between the two types of CH_2 groups, i.e. $=CH_2$ and $>CH_2$, and defined in the above equations as CH_2 and CH_2' respectively. Furthermore, it also considers the carbon branch structure $>C=$ found in the conjugated dienes.

Any reconstruction of a molecular Compton profile using such an LMO method uses the group profiles and not the bond profiles, but since non

have been performed, the above approach should serve as an adequate starting point for such studies. As with bond profile results, it is not possible from an experimental point of view, to study the group profile directly but only to observe the differences between the various groups, e.g. $J_{CH_3} - J_{CH}$. In order to avoid errors arising from the core profile, only differences between molecules containing the same number of carbon atoms were considered. In this way the core profiles subtract exactly, leaving a curve which relates only to the differences in the valence electron distribution. As in the case of the bond profile results, the data are shown without being corrected for multiple scattering. The experimental and theoretical difference curves have been subtracted from the curve predicted by Smith and Whangbo, in order to avoid the transfer of experimental noise onto the theoretical profiles.

(i) $J_{CH_2} - J_{CH_2'}$

Fig. 6-13 shows the difference between the two types of CH_2 groups obtained theoretically and experimentally from a difference between two C_6 and two C_8 molecules, one linear and one cyclic (C_6 represents a hydrocarbon molecule containing six carbon atoms). The experimental results agree extremely well with the empirical difference curve of Eisenberger and Marra, (1971) and with recent calculations of Snyder and Weber, (1978). The curve represents reasonably well the difference between a CC single and CC double bond (similar to results of bond Compton profiles) and emphasises the validity of the approach. It also illustrates more effectively the discrepancies in the Smith and Whangbo (1974) model and the very basic calculations of Epstein (1970).

(ii) $J_{CH_3} - J_{CH_2}$

Fig. 6-14 shows the difference between an alkane and a cycloalkane molecule of sizes C_6 and C_7. The general conclusions reached above

Fig. 6-13, 6-17 inclusive: Deviation of the theoretical and empirical group LMO's (a) and those obtained experimentally (b) from the group LMO profiles predicted by Smith and Whangbo (1974).

Key

Theoretical and empirical group LMO differences

Eisenberger and Marra	———
Snyder and Weber	- - -
Epstein	— —

Experimental Differences

13:	1,5-Hexadiene - Cyclohexene	o o o
	1,7-Octadiene - Cyclooctene	● ● ●
14:	n-Hexane - Cyclohexane	o o o
	n-Heptane - Cycloheptane	● ● ●
15:	2-Methyl-2-butene - Isoprene	o o o
16:	n-Pentane - Cyclopentene	o o o
	n-Hexane - Cyclohexene	● ● ●
17:	Cyclopentane - Cyclopentene	o o o
	Cyclohexane - Cyclohexene	o o o
	Cycloheptane - Cycloheptatriene	□ □ □
	Cyclohexane - Benzene	■ ■ ■
	Cyclooctane - Cyclooctene	▲ ▲ ▲
	Cyclohexene - Benzene	▲ ▲ ▲

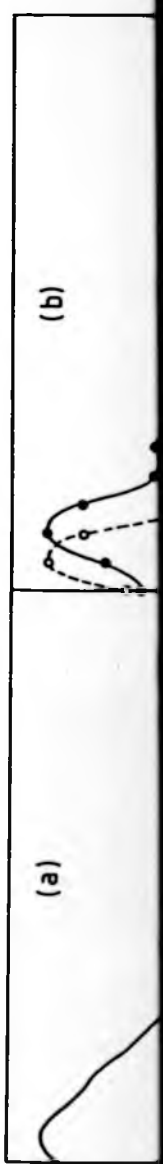

tical and

mentally (b)

Whangbo (1974).

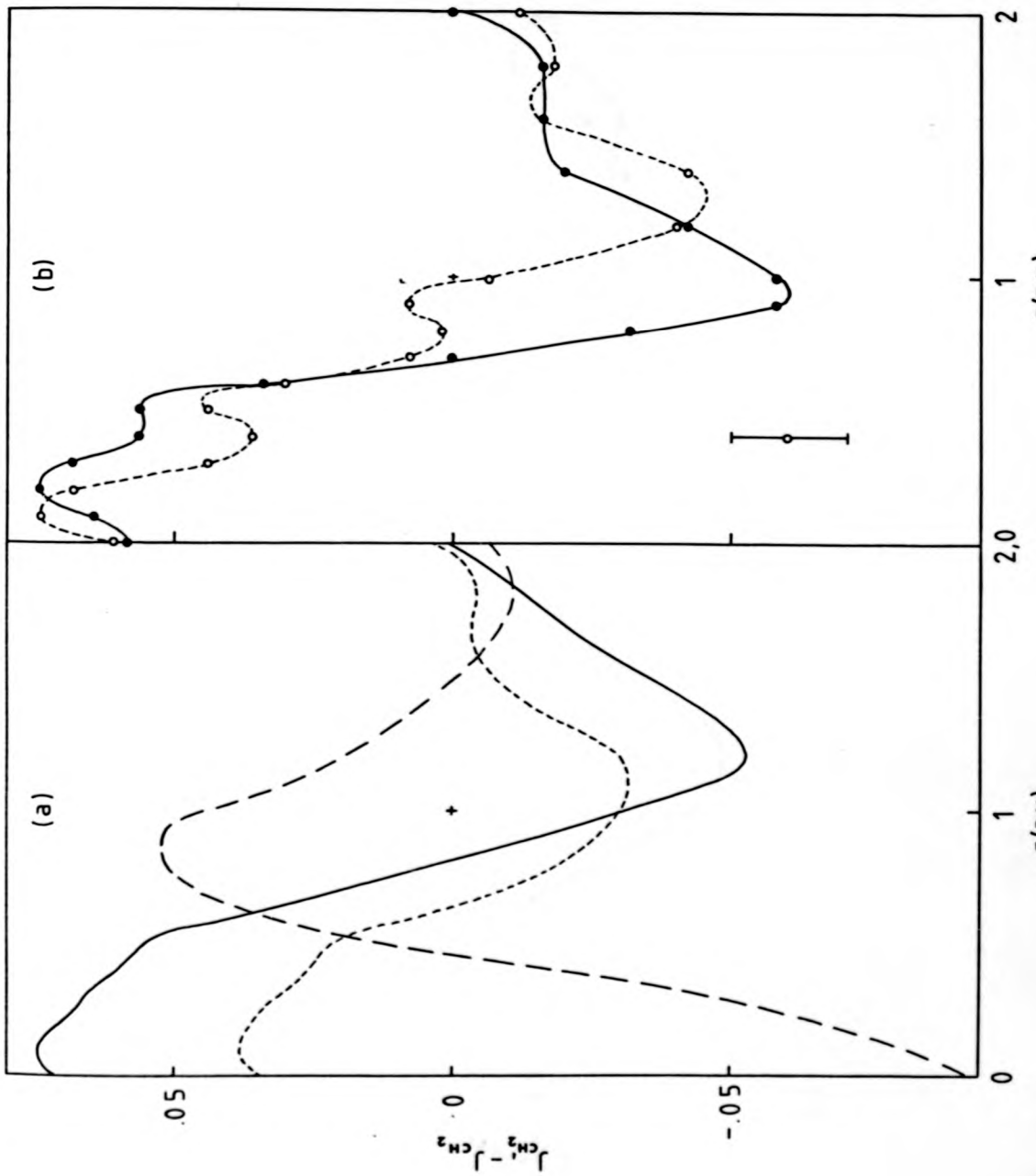

Fig. 6-13

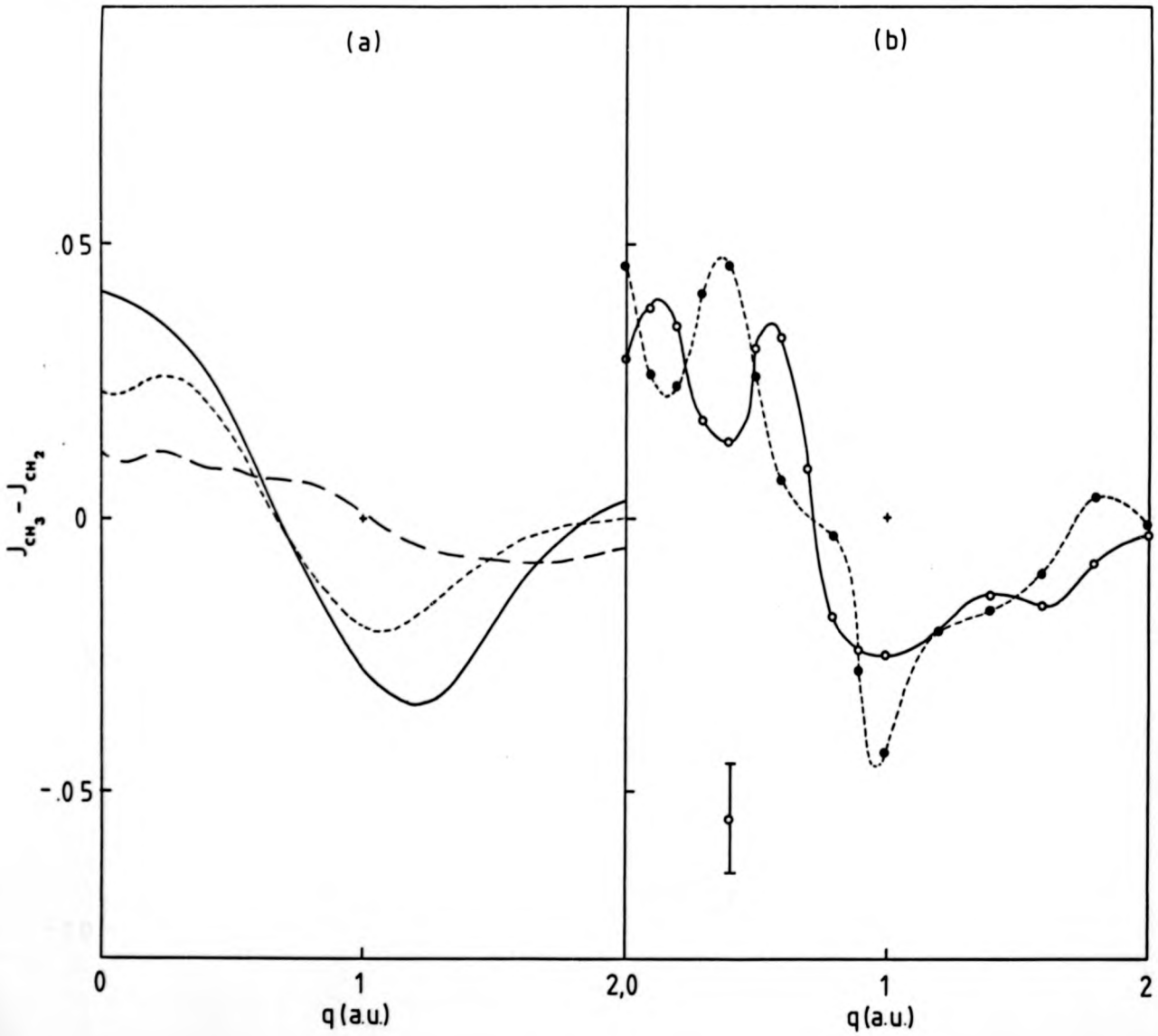

Fig. 6-14

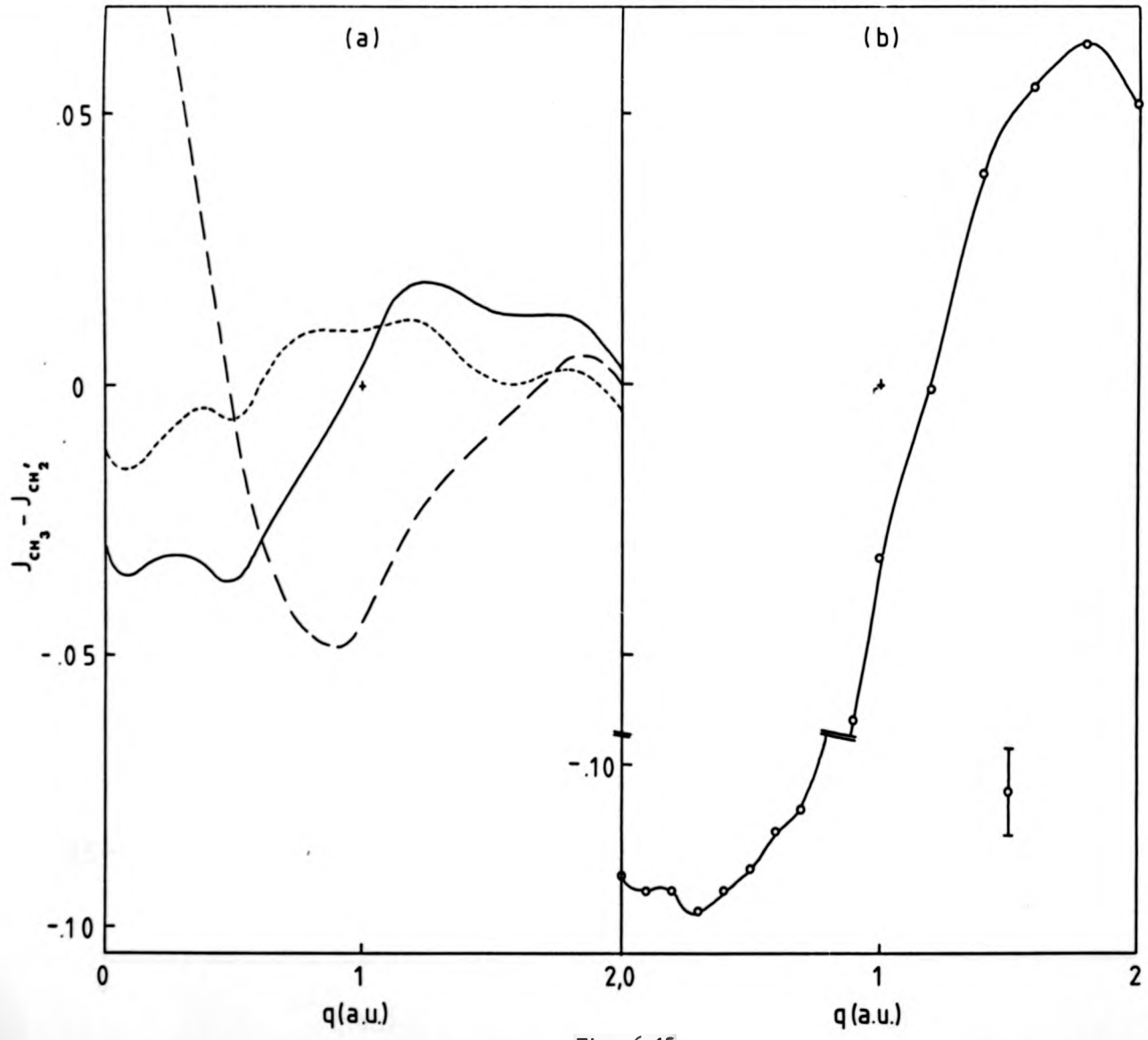

Fig. 6-15

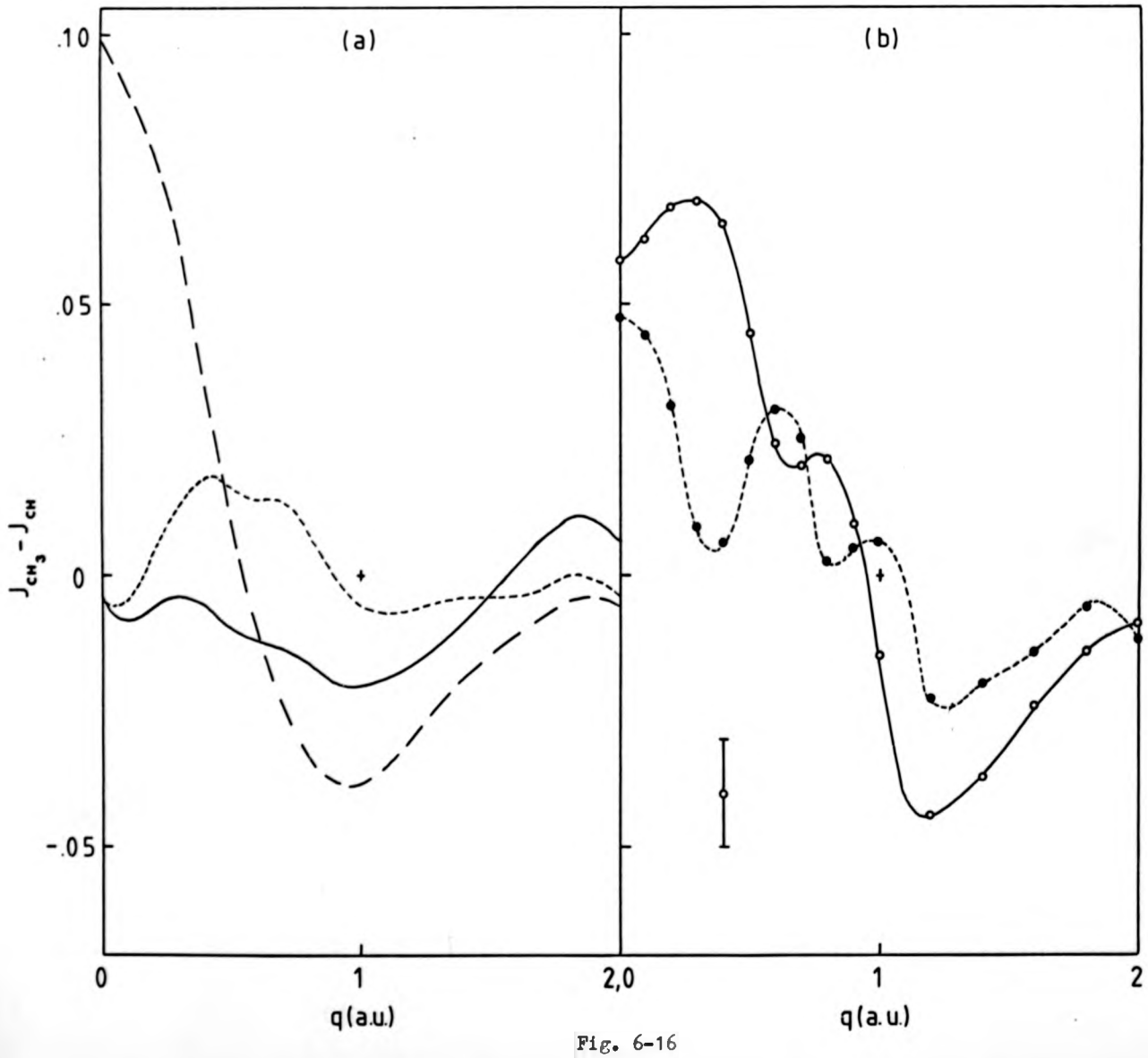

Fig. 6-16

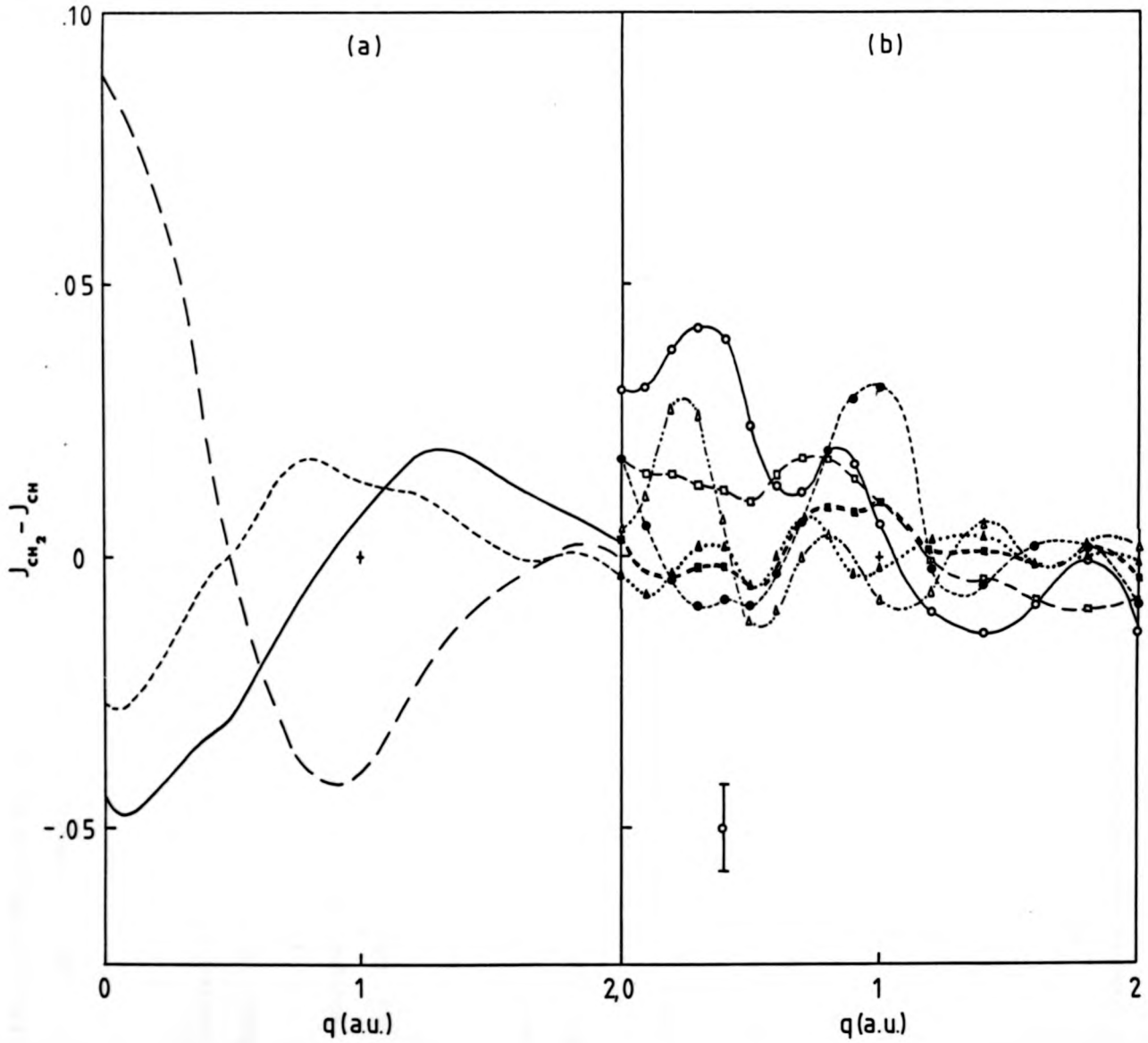

Fig. 6-17

apply equally well in this case with the exception of Epstein's approach which gives a better fit than that predicted by Smith and Whangbo (1974). Since only saturated molecules were considered, this result may be due to the better representation of the C-C bond in Epstein's approach compared to that derived by Smith and Whangbo (1974).

(iii) $J_{CH_3} - J_{CH_2'}$

Considering the previous results for $J_{CH_2} - J_{CH_2'}$ and $J_{CH_3} - J_{CH_2}$, a differnce curve for $J_{CH_3} - J_{CH_2'}$ should follow closely the difference curves predicted by the theoretical and empirical models. The results shown in Fig. 6-15 clearly show that this is not the case. The only hydrocarbons able to produce a $J_{CH_3} - J_{CH_2'}$ curve were isoprene and 2-methyl-2-butene (i.e. the two conjugated dienes). Despite the repartitioning of the momentum density to allow for the unusual molecular structure of conjugated dienes, the delocalized nature of the electronic distribution prevents the difference curve from being adequately described by a localized model. This result adds further support to the conclusions drawn from the results of bond profile measurements.

(iv) $J_{CH_3} - J_{CH}$

The difference curves of the above form are shown in Fig. 6-16, and are obtained from the difference between alkane and cycloalkene profiles of sizes C_5 and C_6. The results are contrary to those obtained by Eisenberger and Narra (1971), but closer to those of Epstein (1970). This may result from a dominance of the J_{CH} group and thus reflect the better representation of the J_{CH} bond by Epstein (1970).

(v) $J_{CH_2} - J_{CH}$

Unfortunately the latter point in the previous argument is not justified in the remaining set of data, which shows the difference curves produced from twelve measurements on acyclic and cyclic molecules,

apply equally well in this case with the exception of Epstein's approach which gives a better fit than that predicted by Smith and Whangbo (1974). Since only saturated molecules were considered, this result may be due to the better representation of the C-C bond in Epstein's approach compared to that derived by Smith and Whangbo (1974).

(iii) $J_{CH_3} - J_{CH_2'}$

Considering the previous results for $J_{CH_2} - J_{CH_2'}$ and $J_{CH_3} - J_{CH_2}$, a differnce curve for $J_{CH_3} - J_{CH_2'}$ should follow closely the difference curves predicted by the theoretical and empirical models. The results shown in Fig. 6-15 clearly show that this is not the case. The only hydrocarbons able to produce a $J_{CH_3} - J_{CH_2'}$ curve were isoprene and 2-methyl-2-butene (i.e. the two conjugated dienes). Despite the repartitioning of the momentum density to allow for the unusual molecular structure of conjugated dienes, the delocalized nature of the electronic distribution prevents the difference curve from being adequately described by a localized model. This result adds further support to the conclusions drawn from the results of bond profile measurements.

(iv) $J_{CH_3} - J_{CH}$

The difference curves of the above form are shown in Fig. 6-16, and are obtained from the difference between alkane and cycloalkene profiles of sizes C_5 and C_6. The results are contrary to those obtained by Eisenberger and Marra (1971), but closer to those of Epstein (1970). This may result from a dominance of the J_{CH} group and thus reflect the better representation of the J_{CH} bond by Epstein (1970).

(v) $J_{CH_2} - J_{CH}$

Unfortunately the latter point in the previous argument is not justified in the remaining set of data, which shows the difference curves produced from twelve measurements on acyclic and cyclic molecules,

including benzene (Fig. 6-17). All the curves are extremely similar, and clearly illustrate a consistency not apparant in the previous difference results on bond profiles. Furthermore, the inclusion of benzene does not appear to perturb this consistency. These results suggest that it may be possible to obtain a set of functional group LMO's which are additive and transferable within say a limited range of cyclic hydrocarbon molecules.

Comparison with theoretical difference curves clearly highlights the present inadequacies of the theoretical models employed. Perhaps calculations of the group profile itself rather than the artificially constructed group profiles used here may help to reduce the serious discrepancies that exist between experiment and theory. In order to judge more accurately the size and nature of the discrepancies, it is necessary to compare absolute experimental profiles (corrected for multiple scattering) with theoretical profiles based on the LMO and SCF descriptions.

6.5 Absolute Compton Profiles

In the following figures, the results for the absolute Compton profiles have been expressed in the form $J(q) - J(q)_{Sm}$, where $J(q)_{Sm}$ represents the Compton profile predicted by Smith and Whangbo (1974) LMO model.

(i) Acyclic Molecules

In Fig. 6-18 the differences between the experimental profiles and those derived by the LMO approach for the alkanes are shown. There is excellent agreement at very low momenta with the recent theoretical profiles of Snyder and Weber (1978), although for higher momentum values this good agreement diminishes. Beyond about 1.0 a.u. the Smith and Whangbo (1974) model describes reasonably well the experimental results. The HBS calculation by Epstein (1970) is not sufficiently accurate to describe the

including benzene (Fig. 6-17). All the curves are extremely similar, and clearly illustrate a consistency not apparant in the previous difference results on bond profiles. Furthermore, the inclusion of benzene does not appear to perturb this consistency. These results suggest that it may be possible to obtain a set of functional group LMO's which are additive and transferable within say a limited range of cyclic hydrocarbon molecules.

Comparison with theoretical difference curves clearly highlights the present inadequacies of the theoretical models employed. Perhaps calculations of the group profile itself rather than the artificially constructed group profiles used here may help to reduce the serious discrepancies that exist between experiment and theory. In order to judge more accurately the size and nature of the discrepancies, it is necessary to compare absolute experimental profiles (corrected for multiple scattering) with theoretical profiles based on the LMO and SCF descriptions.

6.5 Absolute Compton Profiles

In the following figures, the results for the absolute Compton profiles have been expressed in the form $J(q) - J(q)_{Sm}$, where $J(q)_{Sm}$ represents the Compton profile predicted by Smith and Whangbo (1974) LMO model.

(i) Acyclic Molecules

In Fig. 6-18 the differences between the experimental profiles and those derived by the LMO approach for the alkanes are shown. There is excellent agreement at very low momenta with the recent theoretical profiles of Snyder and Weber (1978), although for higher momentum values this good agreement diminishes. Beyond about 1.0 a.u. the Smith and Whangbo (1974) model describes reasonably well the experimental results. The MBS calculation by Epstein (1970) is not sufficiently accurate to describe the

Fig. 6-18, 6-23 inclusive: Deviation of the total theoretical, empirical and present experimental profiles from those predicted by Smith and Whangbo (1974) for :-

(a) alkanes
(b) } alkenes
(c) }
(d) cycloalkanes
(e) cycloalkenes
(f) benzene and cycloheptatriene

Key

Eisenberger and Marra	——
Epstein	- - -
Snyder and Weber	— —
Hirst	·····
This work*	o o o
Bachmann	•-•-•

* The experimental results for C_5H_{12} are also shown before correction for multiple scattering by (• • •).

theoretical,

ose predicted

before

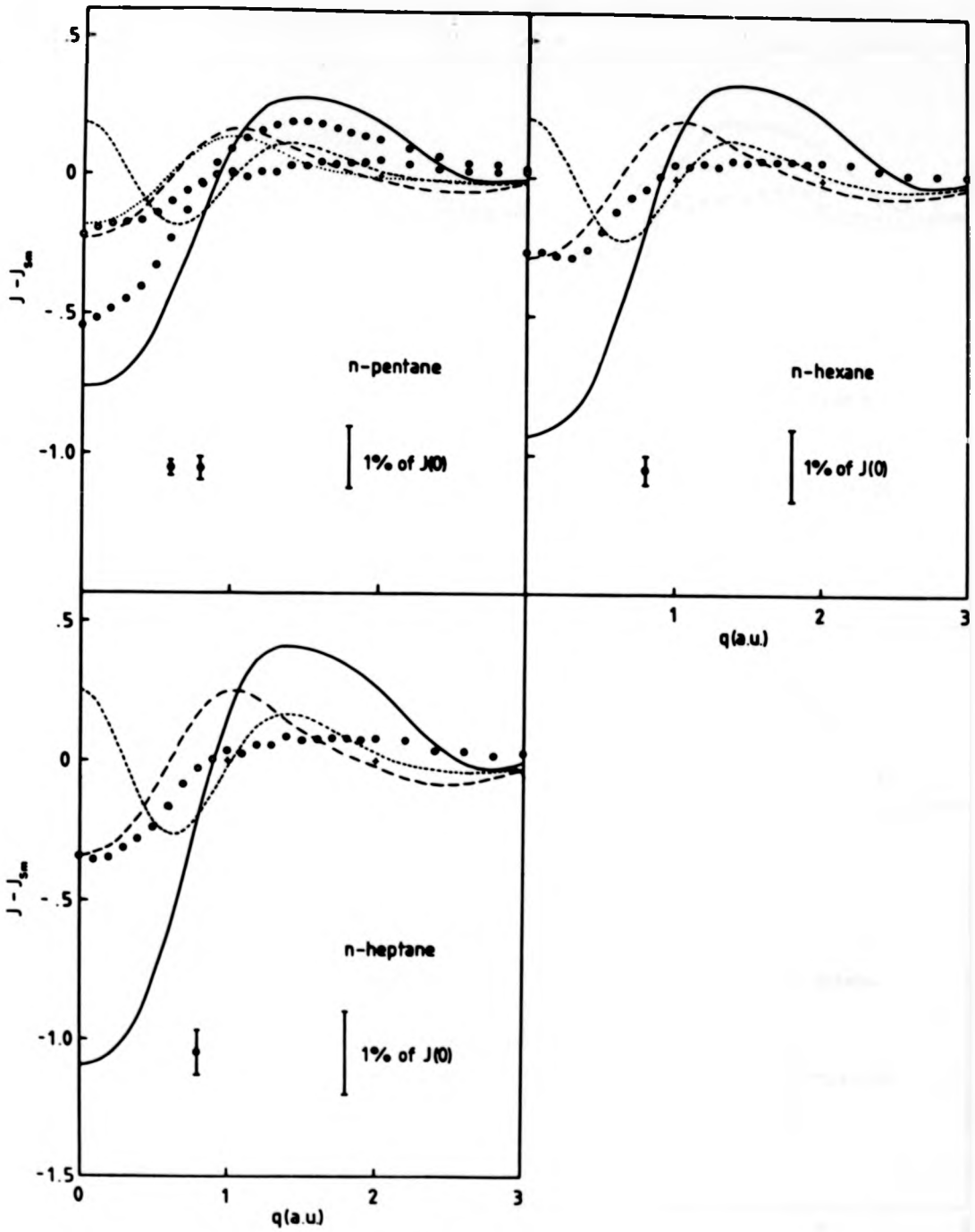

Fig. 6-18: (a) Alkanes

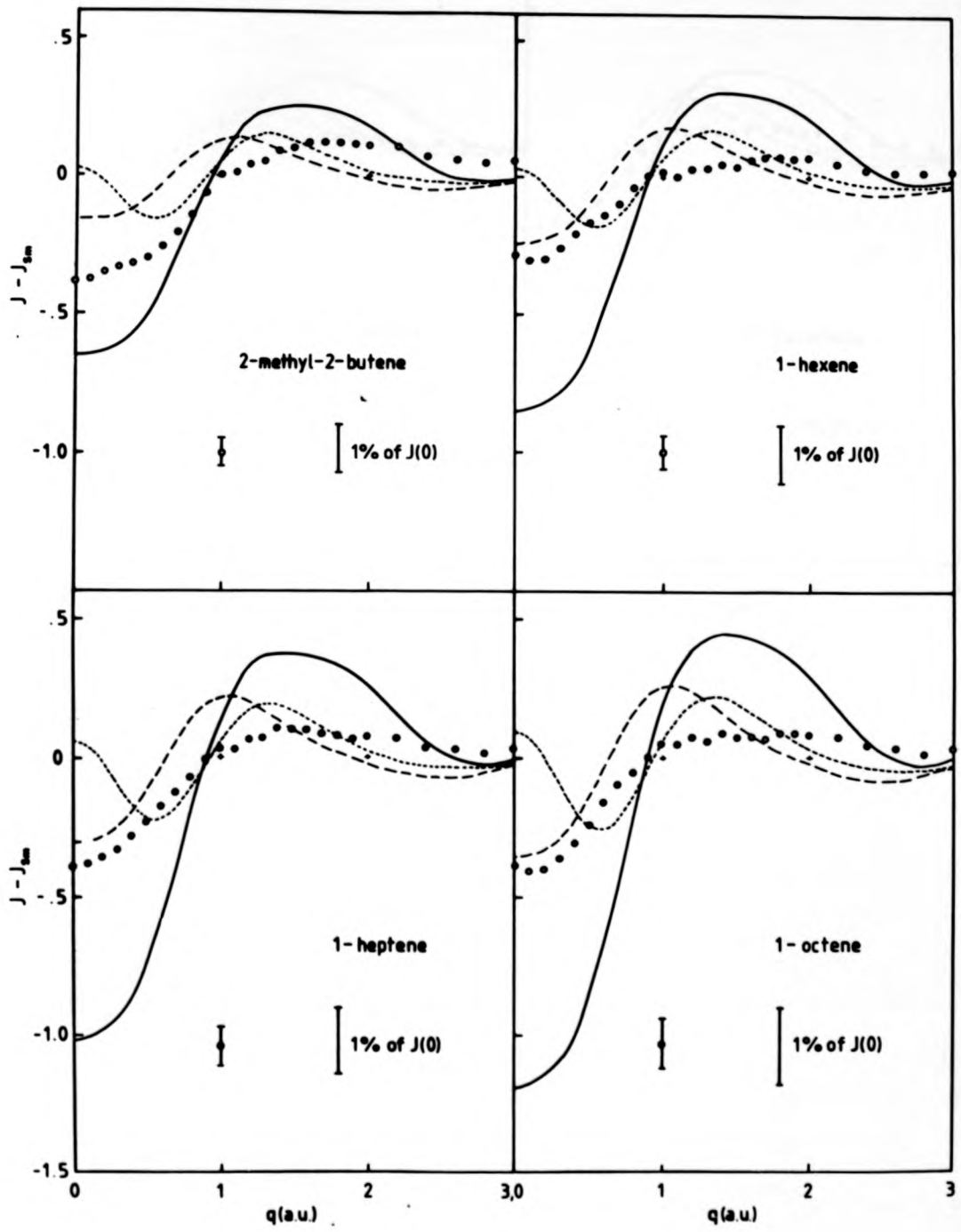

Fig. 6-19: (b) Alkenes

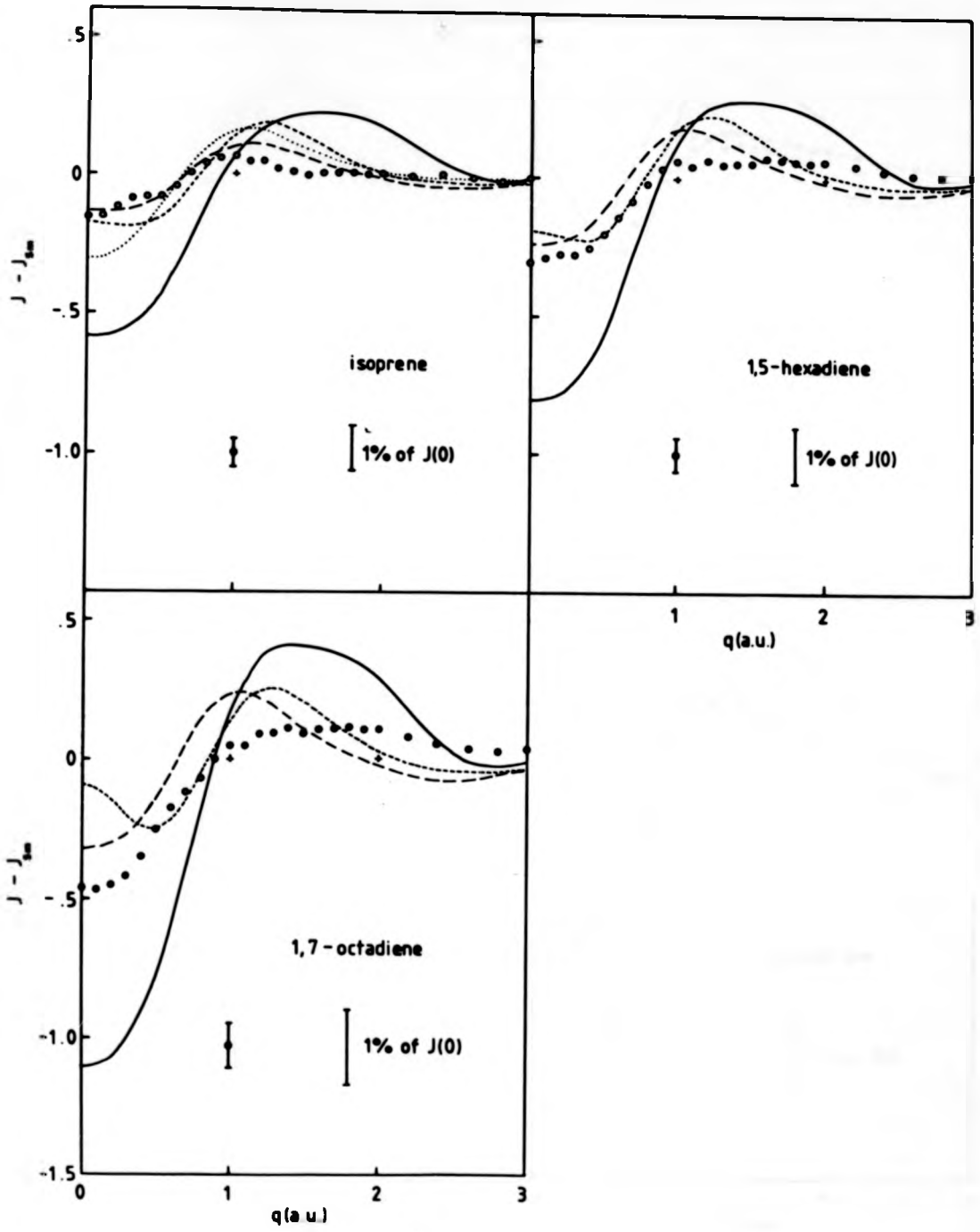

Fig. 6-20: (c) Alkenes

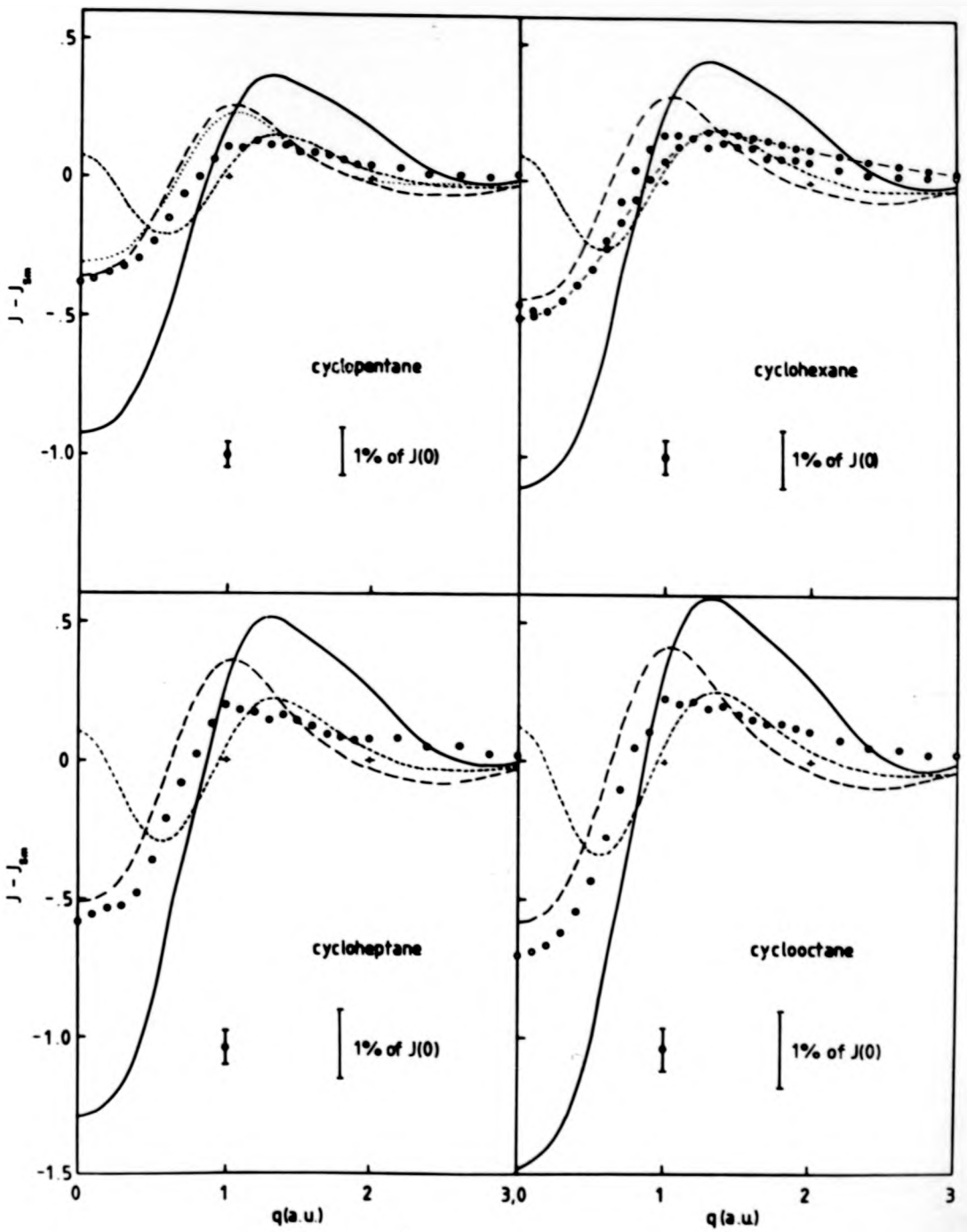

Fig. 6-21: (d) Cycloalkanes

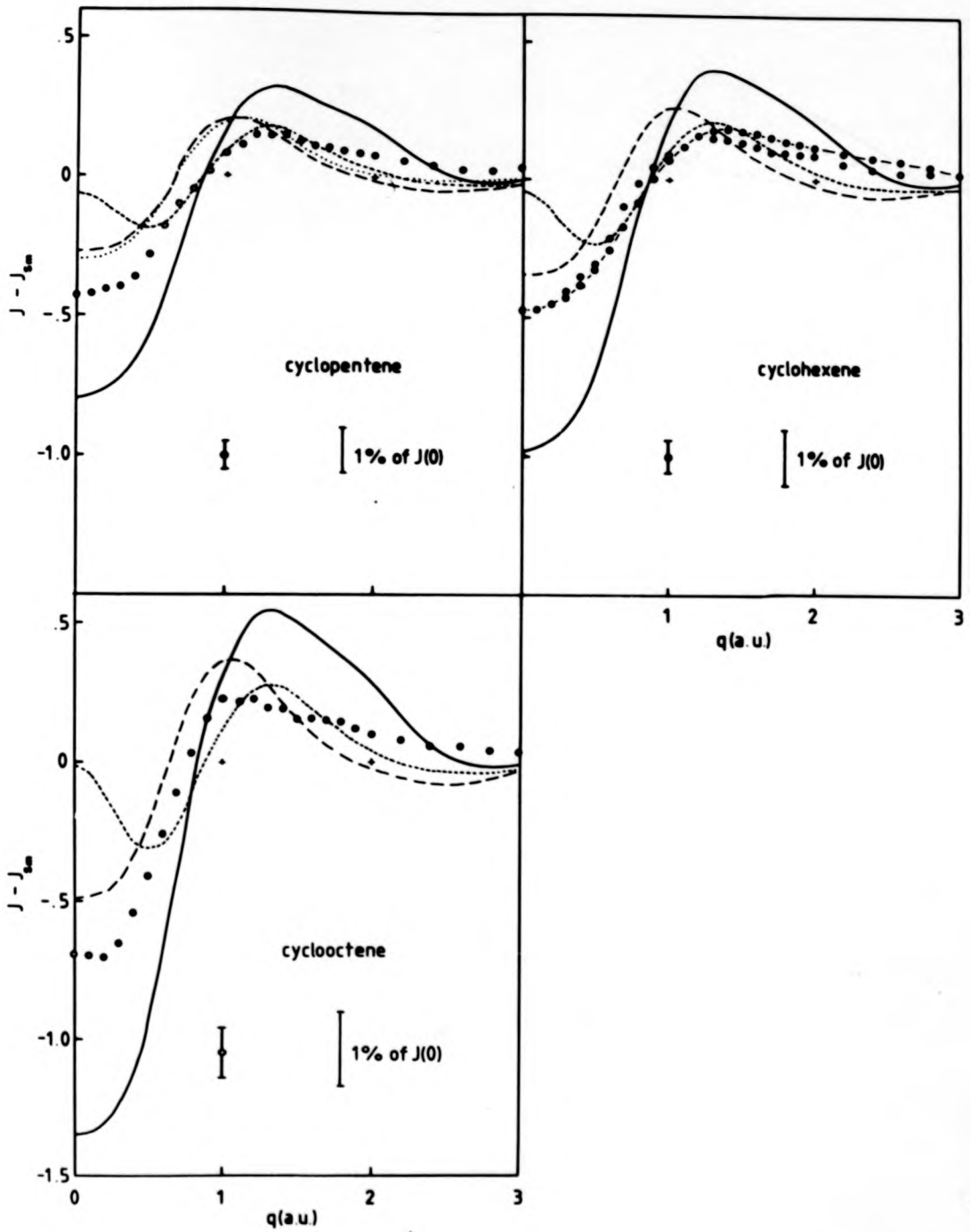

Fig. 6-22: (e) Cycloalkenes

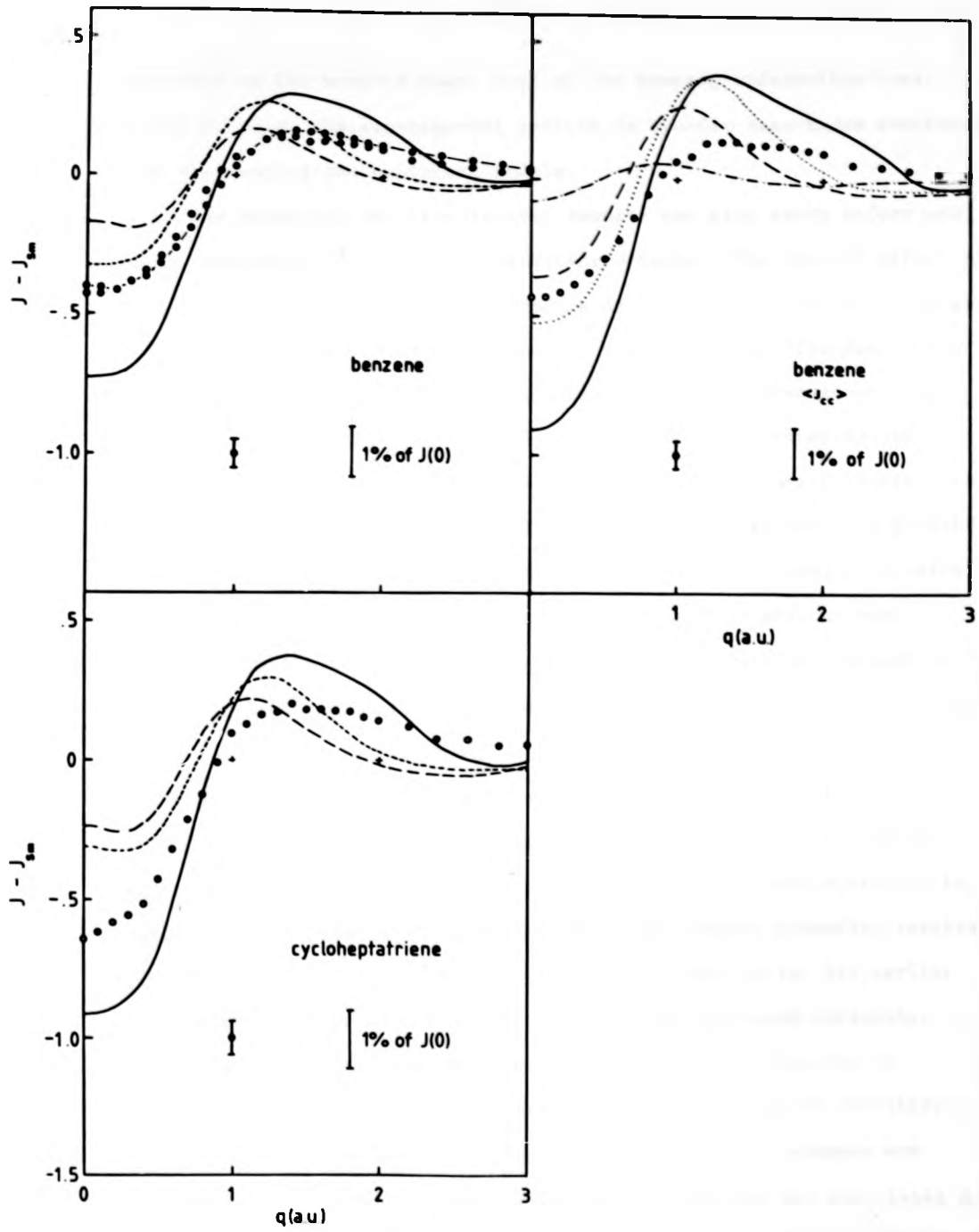

Fig. 6-23: (f) Benzene and Cycloheptatriene

behaviour at low momenta where most of the bonding information lies. Beyond 2.0 a.u. the experimental profile is broader than those constructed from theoretical and empirical models.

For n-pentane the experimental results are also shown before and after correction for multiple scattering effects. The overall effect of this correction is to raise the profile at low momenta (typically between 0 and 1.0 a.u.) and lower the remaining part of the profile due to the normalisation condition. Typically the correction increased J(0) by ~1.5%, thus making the experimental profile lie much closer to the theoretical profiles. The close agreement between the experimental profile before correction for multiple scattering and the reconstructed profile using empirical data of Eisenberger and Marra (1971), clearly illustrates the problems of multiple scattering inherent in this earlier work. Although these authors used thin samples to avoid problems thought to be associated with multiple scattering, the seriousness of the problem and the effect it had on the absolute profile were not well understood. At the present level of accuracy, a small correction of only 1.5% at J(0) makes a considerable difference to the final result. The remaining empirical profiles require a correction of between 1 and 2% of J(0) to bring them into reasonable agreement with the present corrected results. The effect at J(0) indicates that multiple scattering in this earlier work amounted to between 4 and 8% of the total scattered intensity. An indication of the size of these effects was first reported by Bachmann (1975) in his study of cyclic hydrocarbon Compton profiles.

The general observations described above for the alkanes are repeated for the alkenes (Figs. 6-19, 6-20). For the two conjugated dienes isoprene and 2-methyl-2-butene, the results of a recent SCF - MO calculation are also shown. It may be seen from the figures that the recent SCF calculation is very similar to the LMO SCF - MO calculation of

Snyder and Weber (1978) except at very low momenta, where the former predicts a lower J(0) value. For isoprene the experimental result follows quite closely the theoretical profiles, whereas 2-methyl-2-butene is significantly different over the whole momentum range. Such a result confirms the unusual behaviour observed in both the bond and group difference curves.

(ii) Cyclic Molecules

The results obtained for the cyclic molecules are shown in Figs. 6-21 and 6-22 (cycloalkanes and cycloalkenes respectively). The apparent agreement with theory appears to be better for the cycloalkanes than for the cycloalkenes, and the general conclusions reached from an analysis of the acyclic molecules are also valid for the cyclic molecules. For cyclohexane and cyclohexene, the recent experimental results by Bachmann (1975) using a 1 Ci ^{241}Am annular source, and corrected for multiple scattering, are also shown. The excellent agreement between the two sets of experimental data expresses the validity and accuracy of the current state of experimental work on molecular systems. The behaviour of unususal cyclic structures such as aromatic benzene and cycloheptatriene, does not follow the general conclusions reached for the cyclic and acyclic systems, and as such, deserves special comment.

(a) Benzene

Due to the resonant nature of the benzene ring, the bonds are neither C-C or C=C. This is particularly evident from X-ray diffraction studies which show that the six carbon-carbon bond lengths are equal and have a value of 1.39Å. This is less than the 1.54Å of a C-C bond as it occurs in diamond or ethane, but greater than the 1.33Å of a C=C bond as it occurs in ethylene for example.

Using these observations, two LMO profiles of benzene can be constructed. The first model considers benzene to have the structure of

cyclohexatriene, i.e. three single and three double CC bonds. The second model considers the CC bond to be an average of the C-C and C=C bond profiles. Fig. 6-23 shows the comparison of the experimental results with the LMO theory based on these two models. Also shown is the experimental result for benzene obtained by Bachmann (1975) which again shows excellent agreement with the present experimental results. It is apparent from these figures that the model based on average CC bonds is in poorer agreement than the model based on the cyclohexatriene structure. Furthermore, in both sets of results it is clear that none of the theories follow the experimental results well. At low momenta (between 0 and 0.8 a.u.) the SCF calculation of Hirst and Liebmann (1976) agrees reasonably well but shows significant deviation beyond 0.8 a.u.. The MBS profile of Epstein (1970) shows remarkable agreement considering the nature of the calculation. In his calculation, Epstein (1970) found no distinct σ and π electron distributions, concluding that multiple CC bonds are equivalent to single CC bonds with the appropriate number of electrons. Such a model indicates that for benzene the σ and π electron distributions have a non-zero overlap over a significant region of space and therefore provides evidence for a breakdown of total $\sigma - \pi$ separability in momentum space. The close agreement between this model and the experimental results verifies these conclusions.

Further evidence is provided by the poor results obtained using the LMO model of Snyder and Weber (1978) and Smith and Whangbo (1974). However, the conclusions reached by Eisenberger and Marra (1971) although based on a profile containing multiple scattering, are still valid, i.e. the experimental results show the effect of π bonding on delocalizing the bond. In spite of the bond length decreasing in moving from a CC single to a CC double bond, J(0) increases. The delocalization in the plane perpendicular to the bond direction due to the π bonding more

than compensates for the increased localization occurring in the σ part of the bond due to the contraction of the bond length. As with previous results on liquid hydrocarbons the experimental profile is broader at high values of momentum.

(b) Cycloheptatriene

Fig. 6-23 shows the corresponding results for cycloheptatriene. The resonance nature of this molecule is clearly illustrated in the results, which show very similar features to the benzene molecule. Most of the conclusions described above for benzene hold reasonably well for this molecule.

6.6 General Conclusions

If the LMO approach is to serve as the 'almost-invariant' building block from which all hydrocarbon momentum distributions may be constructed, it must give satisfactory results for molecules with special properties. The results of the measurements reported here and in Chapter 5 clearly indicate a breakdown of the LMO approach in three special cases.

(a) The severely strained geometry of cyclopropane, which prevents an accurate representation of this molecule by LMO's taken from molecules with more normal bond angles.

(b) Conjugated molecules, e.g. 2-butene, isoprene and 2-methyl-2-butene which form a set of π delocalized molecular orbitals.

(c) The well known resonance structure of benzene (and cycloheptatriene) with the mobility of its π electrons.

Apart from these three areas, the LMO approach provides a useful tool for predicting the Compton profiles of large molecules for which accurate wavefunction calculations are unfeasible. Some allowance for differences in molecular geometry should be incorporated in the LMO approach and the repartitioning of the molecular structure into functional

groups provides an alternative to the more usual procedure. Further investigations of this repartitioning are now in progress.

For cyclohexane, cyclohexene and benzene, the present experimental results are in excellent agreement with recent gamma-ray Compton profiles obtained by Bachmann (1975). Such a comparison has allowed a critical assessment of the current status of molecular Compton scattering with annular gamma-ray sources. The considerable improvement in the accuracy and quality of the results compared to those obtained with the 'old' system is clearly evident.

The present results also show the considerable amount of multiple scattering contained in the early experimental data of Eisenberger and Marra (1971). Although such effects are not particularly important in the difference curves between similar profiles, it is important in results of absolute profiles. Furthermore, it has recently been shown by Mendlesohn (1978) that the impulse approximation is not valid for individual orbitals, only for total absolute profiles, and that serious breakdown can occur even with 60 KeV radiation. Eisenberger and Marra (1971) used Mo X-rays (17.4 KeV) to measure their hydrocarbon profiles and obtained their bond profiles by subtracting a carbon core contribution. Both of these points should be borne in mind when comparing data with these earlier results.

All of the experimental profiles presented are broader than those calculated for values of momenta in excess of 2.0 a.u.. Such a result is consistent with previous experimental studies of organic molecules. There are several reasons for this discrepancy between the present results and theory. Firstly, it may be due to the failure of the theory to consider the effects of intermolecular interactions. Most of the measurements were made in the liquid phase and most previous comparisons have also used data taken on condensed phases. Such profound effects were not observed in the initial studies made on gaseous hydrocarbons

and suggest that part of the discrepancy may be due to intermolecular interactions. Secondly, the discrepancy could be due in part to an inadequate description of the carbon atom. Improved calculations for this atom, particularly the inner shell orbitals should result in a significant decrease in the total energy. By the virial theorem, a decrease in the total energy must be accompanied by an increase in kinetic energy or by a shift of the momentum density towards higher values of momenta. The addition of polarization functions to the basis set would also make possible an estimate of the importance of this effect on the momentum density. Finally, the effect may be attributable to electron correlation effects similar to those found in metals (Weiss, 1970). However, a series of calculations by Tawil and Langhoff (1975) concluded that the introduction of electron correlation affects only low momenta regions and not the high momenta regions as first suggested. This view has been supported by the SCF calculations of Smith and Whangbo (1974). Close examination of their results reveals that the correlation energies are larger for valence electrons, particularly the CC bonds which have nearly equal energies. The effects of correlation will be more pronounced for the C-C bond because of it's narrower distribution, adding further support to the uncertainties in the C-C bond density. To avoid some of these difficulties, it may well be more appropriate for experimentalists to measure gaseous molecules and compare their results with profiles based on single molecule calculations.

CHAPTER 7

MEASUREMENTS WITH ^{198}Au

7.1 Introduction

During the past decade Compton scattering has risen from an unknown technique into a powerful research tool for the study of the behaviour of the outer electrons in metallic and molecular systems. The introduction of gamma-ray sources, particularly ^{241}Am has extended the range of materials which may profitably be studied, and some of the recent developments and possible applications have been described in this thesis. Over the last few years however, high energy gamma-ray sources, e.g. ^{123m}Te (Eisenberger and Reed, 1972), ^{137}Cs (DuBard, 1978), have been shown to possess many advantages over the lower energy ^{241}Am source.

The particular benefits of an active, high energy source centre around the following areas :-

(a) The study of heavy materials without excessive photoelectric intensity losses which seriously prohibit the scope of the ^{241}Am source.

(b) The large momentum transfers which reduce interpretative problems associated with the failure of the Impulse Approximation.

(c) At a given angle of scattering the momentum resolution can be improved by a factor of two (McIntire, 1976), by increasing the incident photon energy from 60 KeV to 200 KeV. (see also Fukamachi and Hosoya, 1972). Only a slight improvement in momentum resolution is possible by using gamma-rays with energies above 200 KeV.

However, an upper limit of ~500 KeV is imposed. Although a significant improvement in detector resolution is possible for high incident energies

and low scattering angles, it has been shown that these conditions produce angular broadening effects many times as significant as the detector resolution for these cases (McIntire, 1976, DuBard, 1978). Furthermore the shielding problems at these elevated energies are considerable.

Unfortunately there are very few long-lived sources with strong isolated gamma-lines in the range 60 - 500 KeV. ^{137}Cs (ω_1=661 KeV, $T_{1/2}$ = 30 years) has been used (DuBard, 1978), as has ^{123m}Te (ω_1=159 KeV, $T_{1/2}$ = 104 days) despite the cost and inconvenience of periodic reactivation. In fact this latter source has been used considerably because of the significant increase in the momentum resolution over the low energy ^{241}Am sources. There are, however, other possibilities with shorter half-lives. For example ^{57}Cr (ω_1=320 KeV, $T_{1/2}$ = 27 days) and ^{203}Hg (ω_1=279KeV, $T_{1/2}$ = 46 days) are possible sources. On the other hand, sources which have a high specific activity can be used profitably despite their generally shorter half-lives, their location close to a reactor site, and the regular program of reactivation that is required. ^{198}Au (ω_1= 412 KeV, $T_{1/2}$ = 2.7 days) is one source of this type which has been used at the Institute Laue Langevin (ILL), Grenoble, as a gamma-ray diffractometer by Schneider (1974).

The gamma-ray diffractometer at ILL was designed by Schneider for transmission studies of the mosaic structure of neutron monochromators. The high energy, good resolution ($\Delta\omega_1/\omega_1 \sim 10^{-6}$) and small absorption also meant that measurements with targets contained in ovens, cryostats and high pressure devices could be performed. The design of the gamma-ray Compton spectrometer and the initial test profiles were undertaken in 1976 by Cooper et. al. (1976). The results obtained on aluminium (Z = 13) and Germanium (Z = 32) illustrated the viability of the Compton profile measurements made with higher energy gamma-ray sources. Further measurements were therefore undertaken on heavier materials to assess the true potential of the instrument.

7.2 Experimental Technique

7.2.1 Apparatus

The Compton spectrometer was built at ILL and is shown in Fig. 7-1. It is schematically similar to the 'old' 60 KeV ^{241}Am set-up with the disc source but the dimensions are somewhat larger, principally because of the greater shielding problems associated with the higher energy source. The dimensions of the system were fixed by the existing source block size, and the spectrometer was a temporary modification to the diffractometry apparatus already set up.

The source is a piece of gold foil, $0.2 \times 10 \times 4$ mm, which is irradiated in the SILOE reactor at the Centre d'Etudes Nucleares de Grenoble (CENG). After about four days irradiation, a source strength of about 70 Curies is obtained, and the source is then transferred to the large lead block and transported to ILL. In the reactor ^{198}Au is produced by thermal neutron capture. The following reactions can occur,

$$^{197}Au(n,\gamma)\ ^{198}Au \xrightarrow[T_{1/2}=2.7d]{\beta^-}\ ^{198}Hg + \gamma\ (\ 412\ KeV\ )$$
$$^{198}Au(n,\gamma)\ ^{199}Au \xrightarrow[T_{1/2}=3.2d]{\beta^-}\ ^{199}Hg + \gamma \begin{pmatrix} 208\ KeV \\ 158\ KeV \end{pmatrix} \qquad 7\text{-}1$$

Although the decay of ^{198}Au is the dominant reaction, the decay of ^{199}Au also produces gamma-ray lines at lower energies. The total intensities of the 412 KeV, 208 KeV and 158 KeV lines are approximately in the ratio 50:1:5 respectively. The implications of these lower energy lines on the Compton profile measurement is dealt with later in this chapter.

Careful consideration was shown in the shielding which surrounds the source. It was designed to minimize Compton scattering from the source holder, since such parasitic radiation would result in a non-monochromatic beam by producing a large low energy tail on the principal 412 KeV line (Schneider, 1974). To check this, a direct spectrum of the source was taken using a Ge(Li) solid state detector. The measurements were recorded

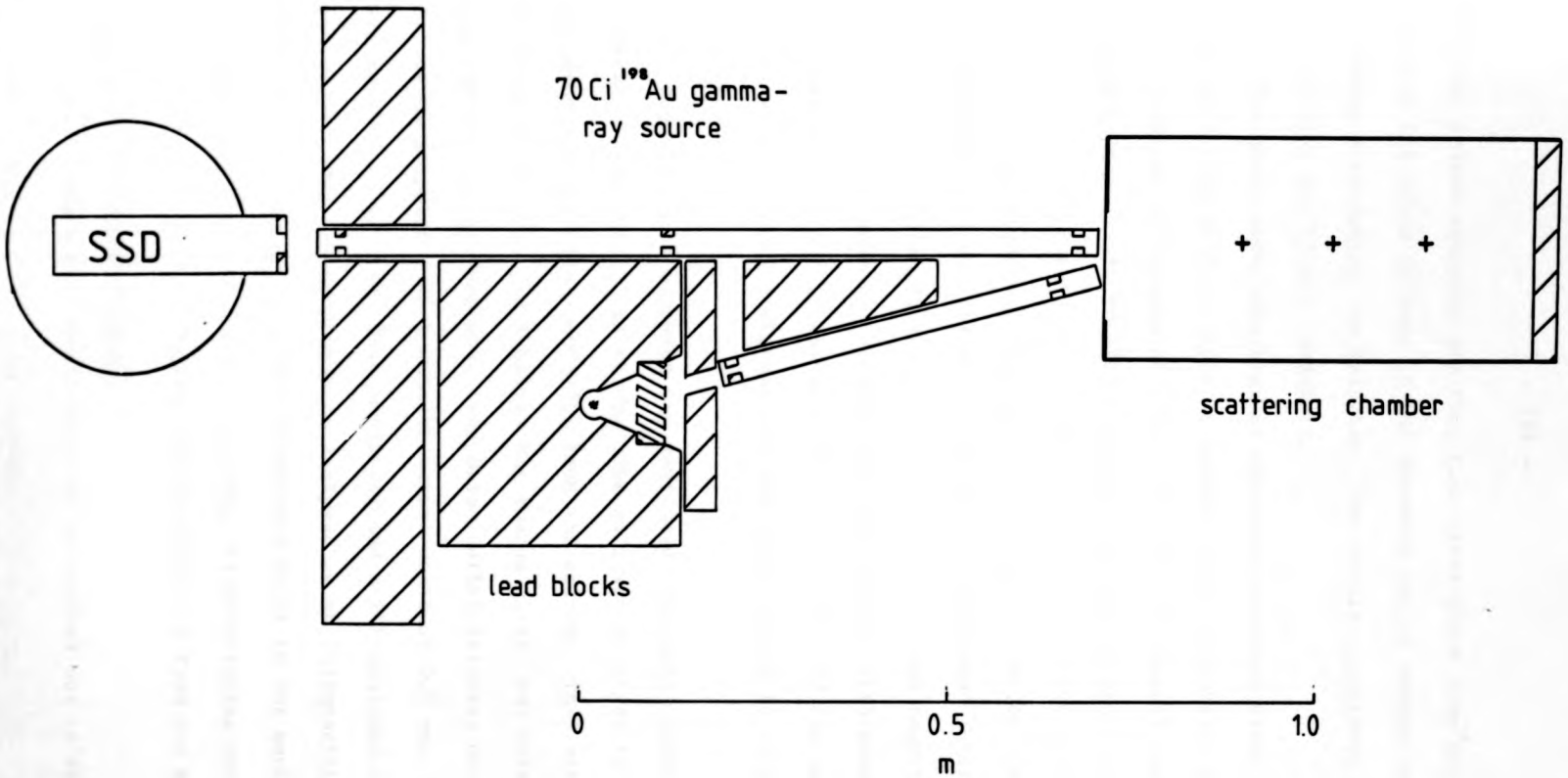

Fig. 7-1: Schematic arrangement of the ^{198}Au Compton spectrometer at ILL.

when the source activity was low, i.e. after about four half-lives, to minimize the pulse pile-up in the detector and to reduce the amount of shielding surrounding the detector. The results confirmed that the 412 KeV line was highly symmetric.

The gamma radiation travels along an evacuated steel tube 50 cm long, which is fitted with a series of annular lead collimators to allow a beam with a maximum divergence of $\pm 0.7^{\circ}$ to enter the sample chamber. The chamber contained the facility to mount the sample under investigation in any one of three positions corresponding to scattering angles of 167°, 169° and 171°. Unfortunately, due to the size of the source block and the amount of shielding that was needed to reduce the background levels, only the lowest scattering angle was possible. The scattered beam travels along a second, similar tube 100 cm long and again fitted with annular lead collimators of 1.6 cm diameter. Both beam tubes and the sample chamber are sealed with thin mylar windows and the whole system is continuously evacuated.

The beam tube carrying the scattered radiation passes through an extensive lead wall 10 cm thick. The wall was required to shield the detector against stray radiation from the source. This was due to the existing equipment, particularly the source block, not being ideal for Compton scattering purposes. The Ortec Ge(Li) detector contains a crystal 1.6 cm in diameter with a nominal active depth of 0.5 cm. The detector was coupled to an Ortec main amplifier and a TRP analogue to digital converter. The recorded data is analysed on an Intertechnique DIDAC 4000 MCA. In order to minimize the electronic drift in the amplification and analogue to digital conversion systems, the electronics were housed in an air-conditioned room, situated approximately 4 m from the spectrometer.

7.2.2. Resolution Measurement

One of the first measurements to be carried out is an accurate

determination of the detector resolution. It has already been seen that the FWHM of the response function of a detector increases approximately with the square root of the incident gamma-ray energy. Usually, i.e. as in the case of the ^{241}Am system, the response function can only be measured at those energies for which a monochromatic source is available. Sometimes it is necessary to extrapolate in order to arrive at the correct resolution function for the particular energy at which the Compton peak appears (Weyrich, 1975). Fortunately, in the present experimental situation with a scattering angle of 167°, the Compton peak falls almost exactly at 159 KeV, (This is very close to the gamma line from ^{199}Au. The intensity of this line is however very small and a more detailed discussion regarding the influence of this line in Compton profile measurements is given in section 7.2.4). This is the same energy as the principal gamma-ray line from ^{123m}Te, and a 10 μCi source of this isotope was therefore used to make a measurement of the detector resolution function.

To achieve optimum resolution and because of the low count rates that may typically be expected in experiments of this type, the time constants on the main, shaping amplifier were set to their maximum value of 10 μsec. Furthermore, the low activity ^{123m}Te source was positioned in front of the detector so as to give a similar count rate to that expected experimentally, since the FWHM of the resolution function depends on the total count rate into the detector. A typical measurement of the resolution produces values of the order 245 eV at 5.9 KeV (^{55}Fe) and 565 eV at 159.0 KeV (^{123m}Te). When the energy scale is converted to a momentum scale, the detector response function has a FWHM of 0.35 a.u. at 159.0 KeV. (cf. 0.58 a.u. at 59.54 KeV, ^{241}Am).

As with the case of low energy gamma-ray sources, account must be taken of the additional contribution to the resolution function arising from beam divergences. These divergencies were deliberately restricted so

determination of the detector resolution. It has already been seen that the FWHM of the response function of a detector increases approximately with the square root of the incident gamma-ray energy. Usually, i.e. as in the case of the ^{241}Am system, the response function can only be measured at those energies for which a monochromatic source is available. Sometimes it is necessary to extrapolate in order to arrive at the correct resolution function for the particular energy at which the Compton peak appears (Heyrich, 1975). Fortunately, in the present experimental situation with a scattering angle of 167°, the Compton peak falls almost exactly at 159 KeV, (This is very close to the gamma line from ^{199}Au. The intensity of this line is however very small and a more detailed discussion regarding the influence of this line in Compton profile measurements is given in section 7.2.4). This is the same energy as the principal gamma-ray line from ^{123m}Te, and a 10 μCi source of this isotope was therefore used to make a measurement of the detector resolution function.

To achieve optimum resolution and because of the low count rates that may typically be expected in experiments of this type, the time constants on the main, shaping amplifier were set to their maximum value of 10 μsec. Furthermore, the low activity ^{123m}Te source was positioned in front of the detector so as to give a similar count rate to that expected experimentally, since the FWHM of the resolution function depends on the total count rate into the detector. A typical measurement of the resolution produces values of the order 245 eV at 5.9 KeV (^{55}Fe) and 565 eV at 159.0 KeV (^{123m}Te). When the energy scale is converted to a momentum scale, the detector response function has a FWHM of 0.35 a.u. at 159.0 KeV. (cf. 0.58 a.u. at 59.54 KeV, ^{241}Am).

As with the case of low energy gamma-ray sources, account must be taken of the additional contribution to the resolution function arising from beam divergences. Those divergencies were deliberately restricted so

that their effect on the final resolution FWHM was small. In fact, following a similar calculation to those already performed with the ^{241}Am systems and described in section 4.3.4, the contribution from beam divergence amounted to only 4% of the detector resolution function, increasing the FWHM to only 0.37 a.u..

7.2.3 Detector Efficiency

Germanium detectors are only 100% efficient over a restricted energy range between ~35 KeV and 60 KeV. Above 100 KeV the efficiency drops rapidly, which means that not only are the count rates reduced but also the spectra must be corrected for the variation of efficiency with energy. The variation in efficiency of the Ge(Li) detector used in the present study was measured by Cooper et. al. using the spectra of two standard, calibrated sources ^{133}Ba and ^{152}Eu.

The measurements made were placed on a common intensity scale and the detector photopeak efficiency η, deduced. Cooper et. al. (1976) found that the efficiency data could be accurately fitted by an analytic function of the form $\eta = \left[1 - \exp(-\mu t)\right]$ where μ is the photoelectric absorption coefficient taken from the tables of McMaster et. al. (1969), and t is the thickness of the germanium crystal. Treating t as a variable parameter they found an optimum value of 0.475 cm, which is slightly less than the nominal value of 0.5 cm, the discrepancy being accounted for by the possibility of a surface dead layer. The fitted curve, together with the efficiencies measured in the range up to 300 KeV are shown in Fig. 7-2.

The significance of this measurement is clearly illustrated in the figure where it is shown that the correction to Compton scattering data is large over the region of interest from 140 KeV to 180 KeV. Deviations of the measured values of efficiency from the fitted curve were quoted as approximately $\pm 2\%$.

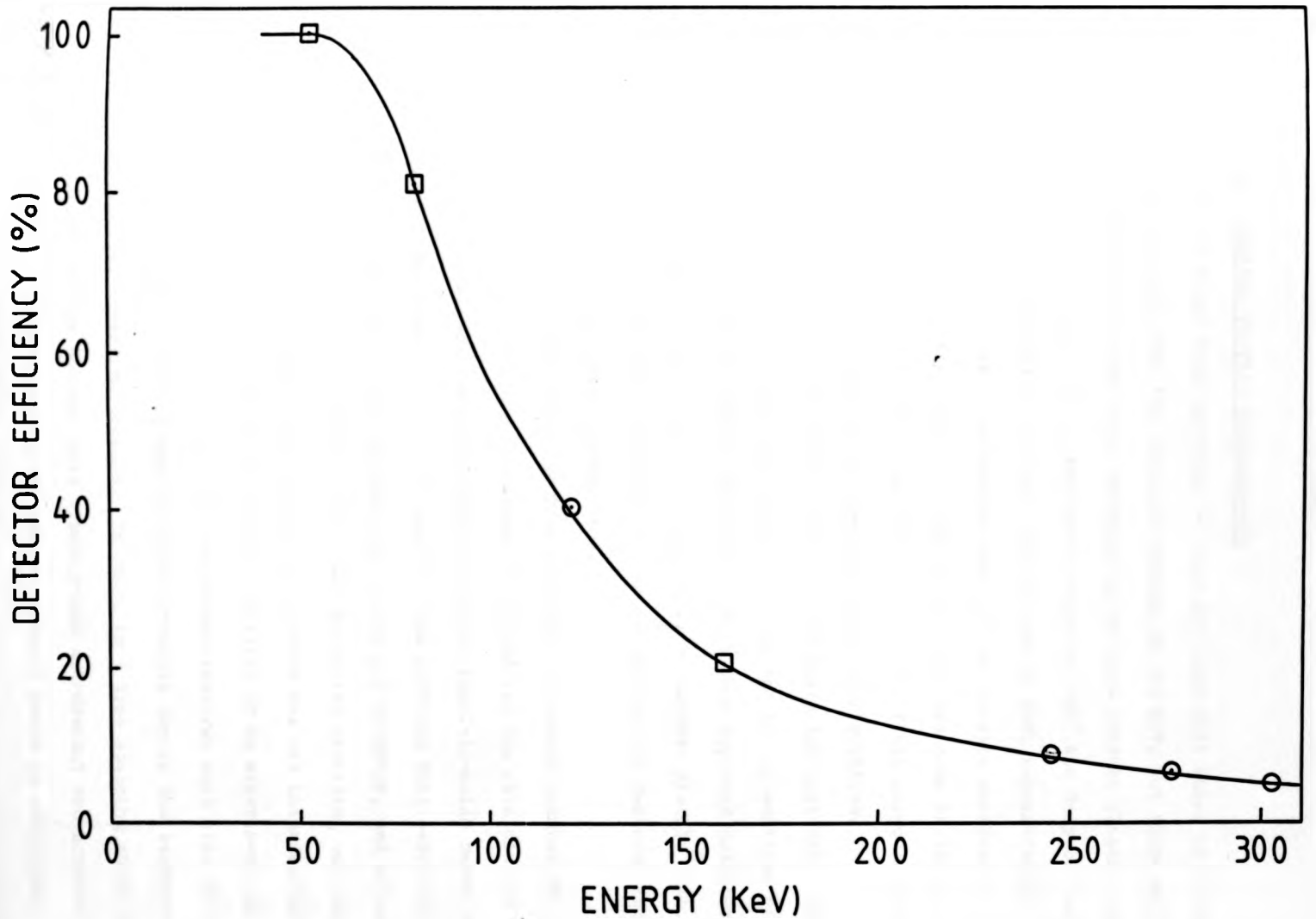

Fig. 7-2: The efficiency spectrum for a Ge(Li) solid state detector.

7.2.4 Compton Profile Measurements

It is clear from equation 7-1 that not only will there be a Compton profile produced from the principle energy of 412 KeV, but there will also be two further Compton lines produced by the less intense elastic lines at 208 KeV and 158 KeV. For a scattering angle of 167° the Compton peak positions are centred at 159 KeV, 115 KeV and 98 KeV, respectively. The gamma-line at 158 KeV is extremely weak and the elastic scattering of this, and all other primary lines, is negligible. The presence of these elastically scattered lines has little or no influence on the final shape or structure of the Compton profiles in the present source configuration.

Fig. 7-3 shows all three Compton lines where the data taken from Cooper et. al. (1976) has been used. Despite the low intensities of the elastic lines the low energy profiles benefit from improved detector efficiency and potentially add a second set of Compton profile data. Such data could, for example, be used to confirm any unusual features found in a measurement of the main Compton line.

The background intensity from an empty, evacuated chamber was normally determined soon after the source was installed and the shielding in position. Previous experience indicated that a typical signal-to-noise ratio of only 50:1 was obtainable at the Compton peak provided that extensive sheilding had been placed between the source and detector, and between the incident and scattered beam tubes. Such extensive shielding was necessary due to the badly constructed source block which was not intended for Compton scattering. Since the typical duration of an experiment was about two half-lives of the source, the background spectrum must also be corrected to take account of the change in source strength during the background and experimental measuring periods. In fact, in a time spanning about three half-lives of the source, both a background measurement and normally two independent measurements on the target material could be completed.

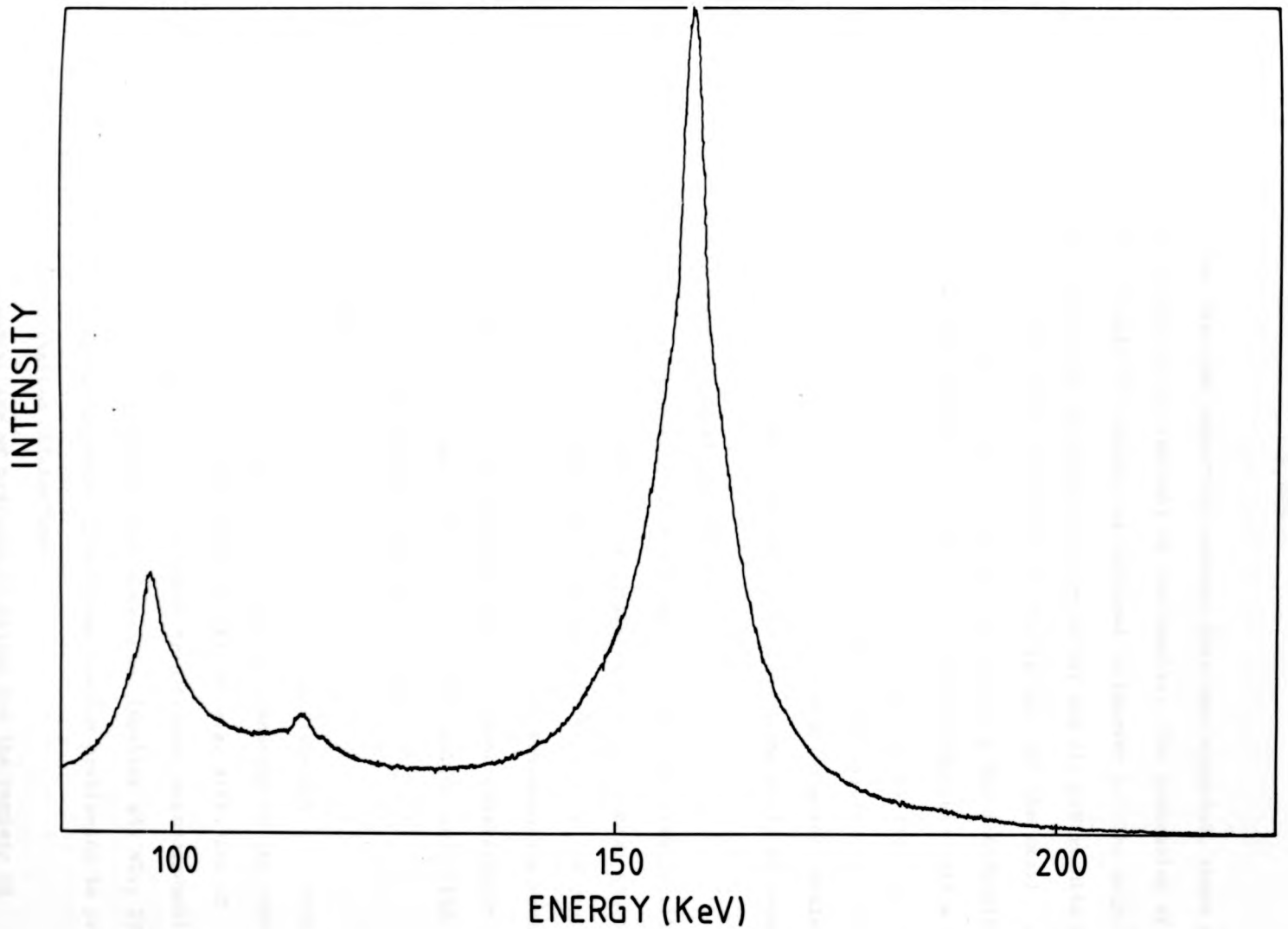

Fig. 7-3: The spectrum of Compton scattering from germanium (data taken from Cooper et. al., 1976)

Once the data and background spectra have been recorded, there only remains the reduction and analysis of the results. The processing of the data follows very closely the procedures outlined in Chapter 3. The only differences between the processing of the 60 KeV and 412 KeV results is the inclusion of an efficiency correction in the latter, and the small modification to the Monte Carlo program. The need for the modification arose from previous results with this system, which indicated that a significant amount of the intensity was due to multiple scattering. Some 20-30% of the intensity was caused not only by double scattering, but also by triple and higher order scatterings. Consequently to obtain self-consistency at least two and sometimes three iterations would be necessary.

7.3 Compton Profiles of Nb and $NbH_{0.76}$

The initial measurements on aluminium and germanium clearly illustrate the advantages of studying heavier materials with a high energy source. However, in order to show more explicitly the sensitivity of the profile to subtle changes in the momentum density, a series of measurements were made on pure niobium and one of its hydrides, $NbH_{0.76}$. These measurements were closely related to a previous study of niobium and niobium deuteride also studied with this source (Pattison et. al., 1976).

(i) Me-H systems

The interest in studying hydrogen in metals stems not only from their potential application but also from the curious phenomena of the behaviour of the light hydrogen in a heavy metallic matrix, e.g. diffusion of hydrogen in metals, gas-liquid-solid phase transitions, superconductivity and the electronic structure of these compounds. (Mueller et. al., 1968). It is the latter of these subjects which allows Compton scattering to provide interesting and detailed information.

The high solubility of hydrogen in metals and the variety of

Me-H bonds formed, provides an enormous range of possibilities for studying the varied electronic properties of these compounds. From this viewpoint the transition and rare-earth metal hydrides are the most interesting. Two alternative models (the anionic and protonic) are used to describe the electronic properties of Me-H compounds. In the anionic model, the hydrogen atom takes electrons from the conduction band to form the negatively charged ion H^-, with bound 1s states. It thus forms a compound which has a predominately ionic character. Conversely, the protonic model is based on the assumption that the hydrogen atom gives up its electron to the conduction band of the metal and is converted into a positively charged proton, which is screened by the rest of the conduction electrons.

The protonic model explains qualitatively many of the phenomena in the Me-H compounds. However, other effects as observed by Knight-shift experiments, NMR and Mossbauer effects (Libowitz, 1965), clearly indicate differing behaviour more in agreement with the ionic model. A measurement of the momentum density by Compton scattering provides an alternative and more direct method of investigating the electronic state of the hydrogen atoms.

(ii) Compton Profiles of Me-H Compounds

The use of the Compton scattering technique to observe these effects arises because the introduction of hydrogen into the metal should substantially modify the band electron density, whilst having little or no effect on the core electron distribution of the host metal. Furthermore, in the case of niobium, the band electron profile has already been calculated using the APW method (Wakoh et. al., 1975). Unfortunately, no similar calculations for the Nb-H system are available and the measurements performed are therefore interpreted on the basis of a rigid band model, where it is assumed that the presence of the hydrogen does not perturb the band structure of the metal.

In an early study of the Compton profile of $VH_{0.45}$ McIntire and Batterman (1974) compared their experimental profile with a free electron-atomic core calculation and concluded that the protonic model is valid for this hydride. In a more recent study Pattison et. al. (1976) measured the Compton profile of Nb and $NbD_{0.6}$ crystals. The results for the deuteride clearly supported the protonic model and should be equally valid for the hydrides. Furthermore, they found that the profiles of the metal and metal hydride were in excellent agreement at high momentum, indicating that the introduction of deuterium into the crystal lattice did not affect the metallic core electrons. In the only other previous study of a niobium hydride, Alexandropoulous and Reed (1977) measured the anisotropy of the Compton profile of the α-phase $NbH_{0.29}$ using ^{123m}Te radiation. Measurements were also made for the (100) and (110) directions in pure Nb. On analysis, the results revealed that the hydrogen atoms donate their electrons to the Nb conduction band and thus provided further and more substantial evidence for the validity of the protonic model. The present measurements on single crystal slices of Nb and $NbH_{0.76}$ in the (100) and (110) directions were designed to provide high resolution results on the hydride system whilst at the same time adding further support to the protonic model. Moreover, the measurements were undertaken with a view to providing a satisfactory qualitative interpretation of the changes in the directional Compton profiles following the introduction of hydrogen into the metal lattice.

7.3.1 Experimental Details

(i) Sample Structure and Preparation

The phase diagram of the Nb-H system is shown in Fig. 7-4. At room temperature hydrogen can be dissolved in the cubic α-phase up to an atomic ratio $H/Nb \sim 0.02$. In this phase the hydrogen atoms are distributed randomly on tetrahedral sites and gives rise to an increase in the lattice

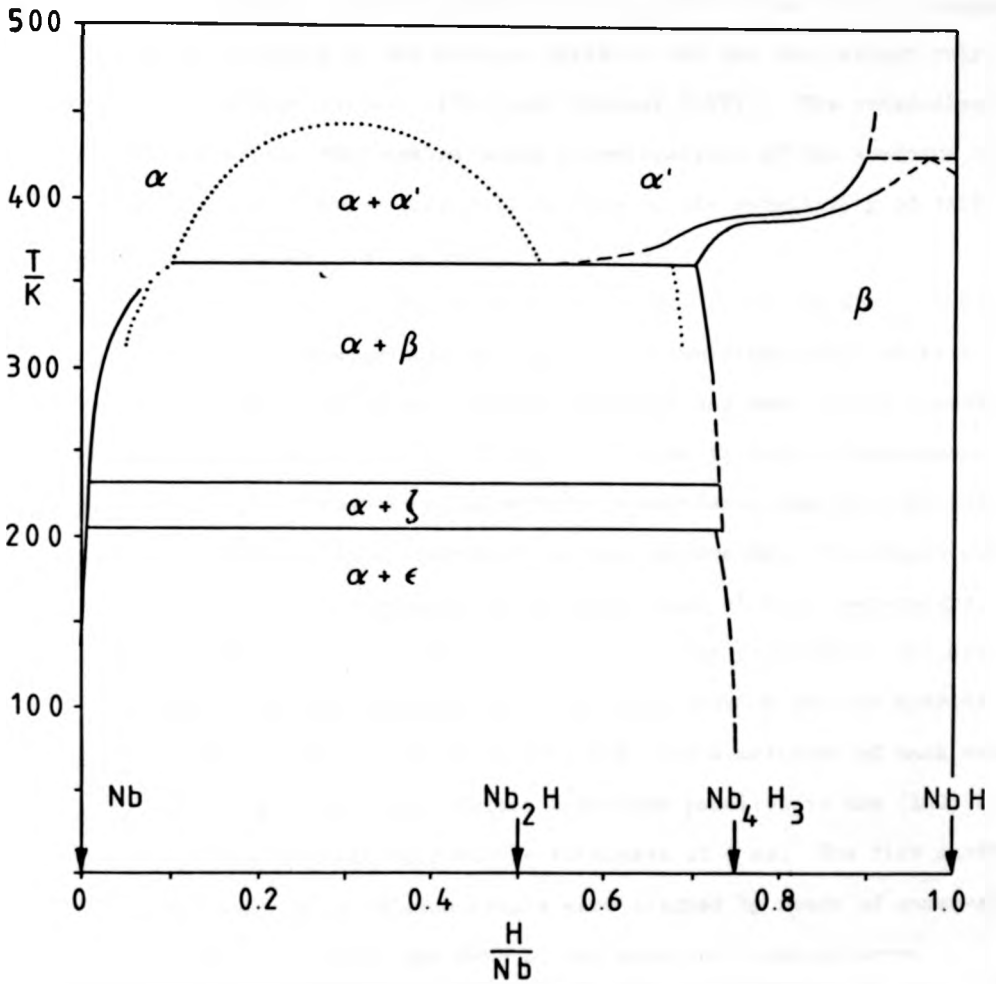

Fig. 7-4: The phase diagram for the Nb-H system.

parameter for $\Delta a/a$ of between $4.5.10^{-4}$ and 7.10^{-4} per % H/Nb. For larger H/Nb ratios a β-phase precipitates which has an orthorhombic structure. The occurrence of a β-metal hydride is responsible for drastic changes in the mosaic structure of the niobium crystals and has been extensively studied by Schober et. al. (1974) and Schober (1975). The order-disorder transitions in the Nb-H system makes investigations of the momentum density by positron annihilation difficult because of the sensitivity of this technique to changes in the defect structure.

The measurements made by Pattison et. al. (1976) on $NbD_{0.6}$ were conducted at room temperature and the sample contained about 25 at.% α-phase and 75 at.% of the β-phase. Alexandropoulous and Reed (1977) undertook their measurements of $NbH_{0.29}$ at 200°C in order to have a homogeneous system. In this phase the niobium hydride maintains the bcc structure of niobium, although with an increased lattice parameter. The single crystals of $NbH_{0.76}$ used in the present study, undertaken at room temperature, contained only the orthorhombic β-phase and were prepared in the Kristallabor of TU, Munich, by Dr. N.Stump. Both the pure niobium and the hydride crystals were built up from two pieces cut from a cylinder of each material. This produced a large, flat surface 25mm×20mm parallel to the (100) and (110) lattice planes, with an approximate thickness of 6 mm. The flat surfaces of the two components of each sample were aligned by means of gamma-ray diffractometry to within the FWHM of the measured rocking-curve.

(ii) Experimental Method and Data Processing

Compton profiles were measured for the (100) and (110) directions for pure niobium and for $NbH_{0.76}$. In each of the four measurements approximately $3.0.10^4$ counts per channel were accumulated at the profile centre. The gain of the main amplifier was adjusted to give a channel spacing of 62 eV (~0.03 a.u.). Each measurement took about one week (~2 half-lives), with a separate measurement of the background recorded at the beginning of the

experiment. The raw data were taken from the MCA and the background subtracted only after the effects for source decay had been taken into account. After background subtraction the data were corrected for detector efficiency and placed on an energy scale. After deconvoluting and filtering the experimental line shape, which left the profile smeared with a Gaussian of width 0.38 a.u., the conversion from an energy scale to a Compton profile was made and the result placed on a momentum scale. Each profile was then normalised to their respective free atom value calculated from the tabulated data of Biggs et. al. (1975). This normalisation took place between the limits 0 and 5 a.u.. For niobium this corresponded to 15.208 electrons, and for $NbH_{0.76}$ 15.488 electrons. Finally the effects of multiple scattering in each profile were removed using the Monte Carlo method. The multiple scattered gamma-ray contribution amounted to about 30% of the total scattered intensity in all cases. The effect on the Compton line shapes was therefore rather large, increasing the peak values by almost 10%. However, the correction was very similar for both Nb and $NbH_{0.76}$, so that any errors in the form of the multiple scattering correction will have only a secondary effect on the difference between the profiles.

7.3.2 Results and Discussion

Fig. 7-5 shows the difference between the experimental Compton profiles of pure niobium along the (100) and (110) directions. Also shown are the anisotropies predicted by the APW calculation of Wakoh et. al. (1975) and the recent experimental results of Alexandropoulous and Reed (1977). Both sets of experimental results are seen to follow the theory well, particularly if the slightly lower resolution in the measurements of Alexandropoulous and Reed (1977) is taken into account. These results therefore verify the calculations of the electronic band structure of the metal. In addition positron annihilation experiments on single crystals of niobium Shiotani et. al., (1975) show quite remarkable agreement with the same

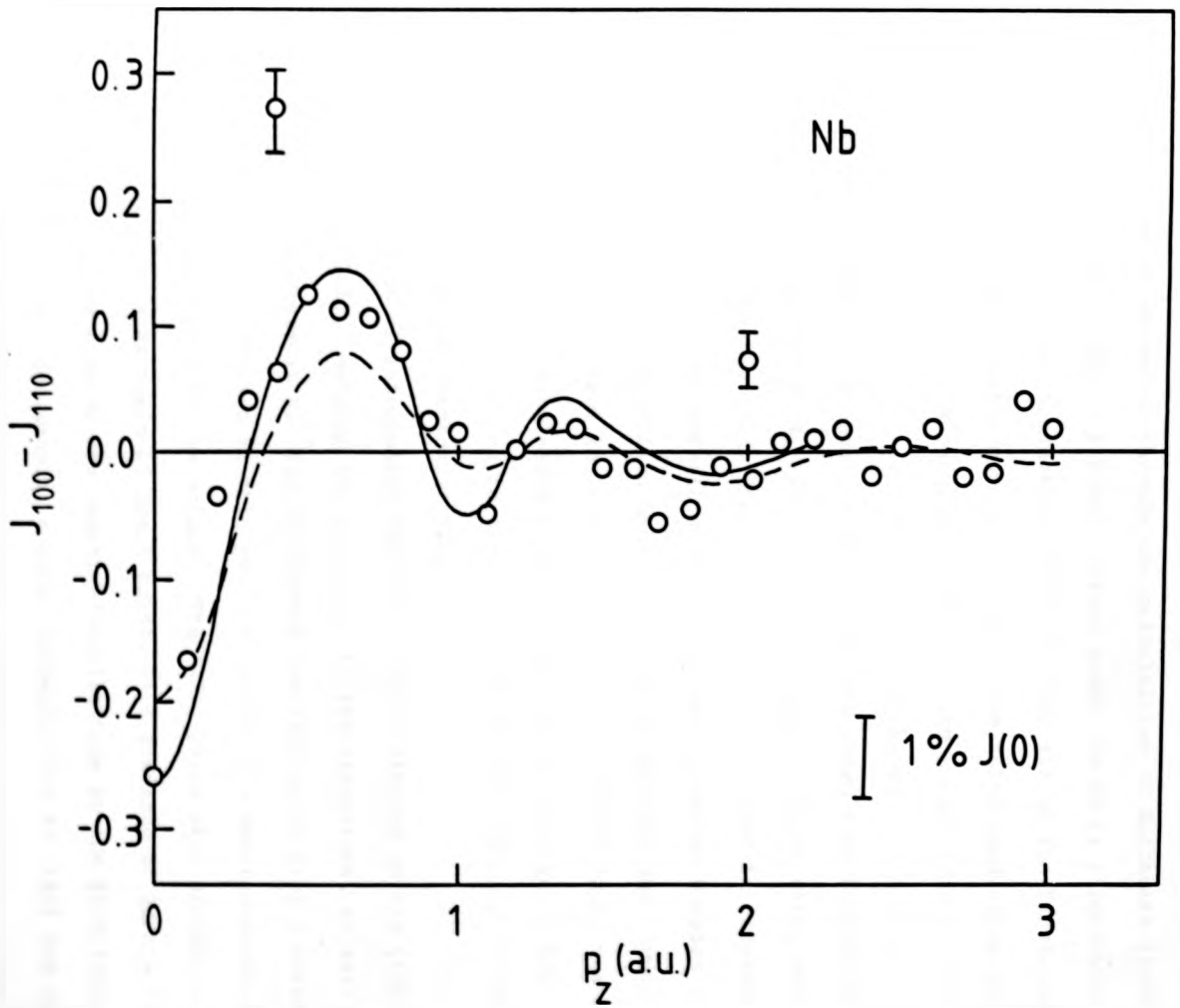

Fig. 7-5: Anisotropy between the Compton profiles of Nb measured along (100) and (110). Present experimental results (o o o), Alexandropoulous and Reed (-----), Wakoh et. al. (——).

band structure calculations.

Having established the close correlation between experiment and theory it is now possible to interpret these curves in terms of the band structure of the metal through the calculations of Mattheiss (1970) and Wakoh et. al. (1975). A Fermi surface model for Nb is illustrated in Fig. 7-6. The five conduction electrons fill all of the first, most of the second and slightly more than half of the third conduction bands. The Fermi surface of the unoccupied portion of the second zone is centred at Γ and has the shape of a rather distorted octrahedron. The Fermi surface which encloses the unoccupied regions of the third zone include distorted ellipsoids centred at N, and a multiply connected sheet which extends from Γ to H in the (100) directions. This open sheet is referred to as the jungle-gym. The overall shape of the band electron Compton profile is determined by the filled band contribution, whereas the structure on the profile comes from the partly filled bands, particularly the third. It is in fact the jungle-gym hole surface that gives rise to most of the finer structure and which in turn contributes most strongly to the anisotropy of the Compton profile.

A plane of integration through Γ perpendicular to the (100) direction (see Fig. 7-6), contains the hole arms in two directions, as well as the hole pockets at N. The relatively low density of filled states over a plane of integration at this position leads to a sharp concave feature in the J_{100} profile at the origin. The (100) plane will encounter the pair of hole arms again at the H point, at a distance of $2\pi/a = 1.01$ a.u. and this gives rise to the negative oscillations in the anisotropy curve at 0 and 1 a.u. Conversely, a plane perpendicular to (110) can contain the hole arms only in one direction, leading to shallower concave depressions in the J_{110} profile at the origin and at $2\pi/a\sqrt{2} = 0.71$ a.u. It is this feature that gives rise to the peak in the anisotropy curve around 0.7 a.u.

band structure calculations.

Having established the close correlation between experiment and theory it is now possible to interpret these curves in terms of the band structure of the metal through the calculations of Mattheiss (1970) and Wakoh et. al. (1975). A Fermi surface model for Nb is illustrated in Fig. 7-6. The five conduction electrons fill all of the first, most of the second and slightly more than half of the third conduction bands. The Fermi surface of the unoccupied portion of the second zone is centred at Γ and has the shape of a rather distorted octrahedron. The Fermi surface which encloses the unoccupied regions of the third zone include distorted ellipsoids centred at N, and a multiply connected sheet which extends from Γ to H in the (100) directions. This open sheet is referred to as the jungle-gym. The overall shape of the band electron Compton profile is determined by the filled band contribution, whereas the structure on the profile comes from the partly filled bands, particularly the third. It is in fact the jungle-gym hole surface that gives rise to most of the finer structure and which in turn contributes most strongly to the anisotropy of the Compton profile.

A plane of integration through Γ perpendicular to the (100) direction (see Fig. 7-6), contains the hole arms in two directions, as well as the hole pockets at N. The relatively low density of filled states over a plane of integration at this position leads to a sharp concave feature in the J_{100} profile at the origin. The (100) plane will encounter the pair of hole arms again at the H point, at a distance of $2\pi/a = 1.01$ a.u. and this gives rise to the negative oscillations in the anisotropy curve at 0 and 1 a.u. Conversely, a plane perpendicular to (110) can contain the hole arms only in one direction, leading to shallower concave depressions in the J_{110} profile at the origin and at $2\pi/a\sqrt{2} = 0.71$ a.u. It is this feature that gives rise to the peak in the anisotropy curve around 0.7 a.u.

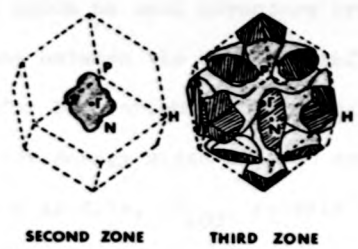

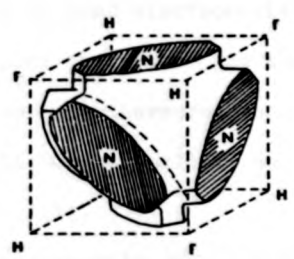

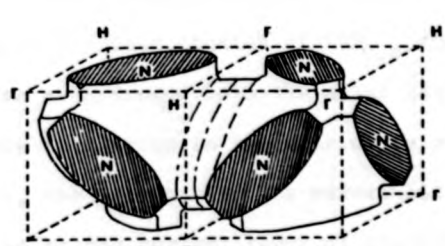

Fig. 7-6: Fermi surface model for Nb.

The experimental and theoretical anisotropy data are clearly in excellent agreement and provides a basis for interpreting the experimental results of the hydride for which no band structure treatment is available.

The difference between the Compton profiles of $NbH_{0.76}$ and Nb are shown in Fig. 7-7 for both orientations. The results shown are an average over the high and low energy sides of each experimental difference profile. The (100) difference profile, ΔJ_{100}, reveals a striking increase at the origin due to the filling up of the sharp concave feature at the peak of the Nb profile in this direction. This is not too unexpected since in this hydride the number of band electrons is raised from 5.0 to 5.76. Therefore, the Fermi hole around the point Γ in the second band of the Nb can be expected to fill up. Furthermore, the closed hole pockets at points N in the third band will become smaller, and the jungle-gym arms along (100) will also begin to fill.

The difference profile, ΔJ_{110} has a much flatter shape resulting from the filling of the shallower concave depressions in the (110) profile of the pure metal. These results support the protonic picture of the hydride in agreement with previous studies of $NbD_{0.6}$ and $NbH_{0.29}$. As a result of the introduction of hydrogen into the metal lattice and the raising of the Fermi level, the anisotropy in the hydride is much smaller than in the metal. In fact, the present results reveal little anisotropy in the Compton profiles at the current level of statistical accuracy and resolution. This is in agreement with the results for $NbH_{0.29}$, and from the qualitative arguments given above for the Fermi topology. Clearly, band structure calculations of these hydrides are required before the directional properties can be fully understood. Further measurements with improved statistical accuracy on these and other transition metal hydrides may

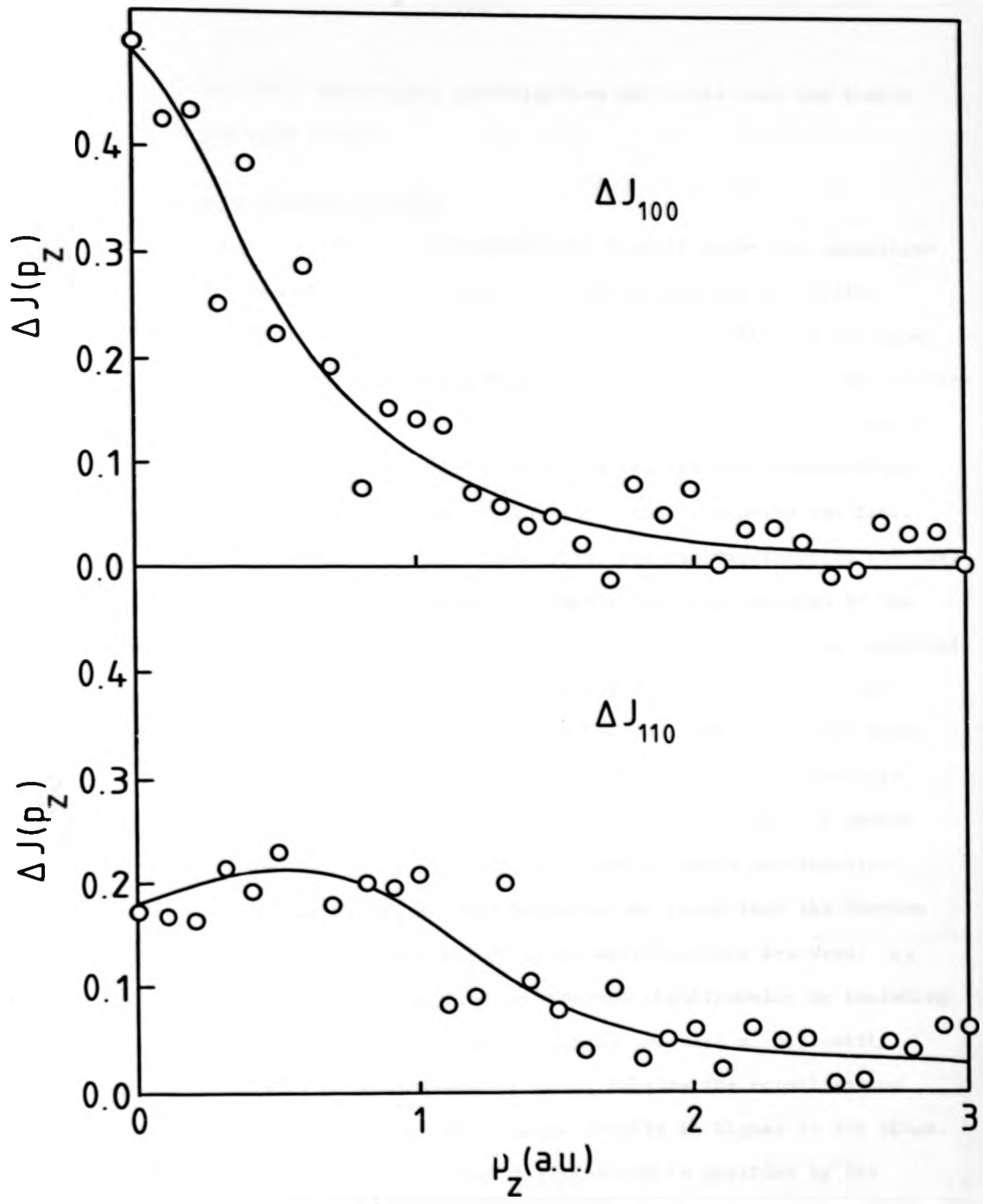

Fig. 7-7: The difference between the Compton profiles of $NbH_{0.7}$ and Nb for profiles measured with the scattering vector along (100) and (110) directions.

prompt a detailed theoretical investigation and could test the limits of the rigid band model.

7.4 Compton Profile of Lead

The previous set of experiments have clearly shown the advantages of using the higher energy sources for studying heavier materials. However, as the size of the atom increases, the velocities of the inner shell electrons become extremely high and relativistic effects become very important. Mendelsohn et. al. (1974) have recently calculated Compton profiles from numerical nonrelativistic and relativistic Hartree-Fock wavefunctions, (HF and RHF respectively) for the rare gases and lead. In general they found that the relativistic spatial wavefunction for low lying s and p orbitals are pulled in towards the nucleus when compared to the wavefunctions obtained from nonrelativistic calculations. They suggested that the effect was due to the mass-velocity effect term (Bethe and Saltpeter, 1957) of the relativistic hamiltonian, which to first order was considered as a perturbing potential term in the nonrelativistic hamiltonian and is attractive in nature. Since a more sharply peaked spatial wavefunction leads to a flatter momentum space wavefunction (Fourier transform principle) they expected and found that the Compton profile is much flatter when relativistic wavefunctions are used. As the inner 1s, 2s and 2p orbitals are affected significantly by including relativistic effects, outer s and p orbitals are also significantly altered because of orthoganalisation. Also, because the normalization condition is maintained the relativistic profile is higher in the wings.

A measure of this relativistic flattening is provided by the percentage decrease in $J_{RHF}(q)$ below $J_{HF}(q)$ at the profile centre, i.e. $q = 0$. For Argon $J(0)$ is decreased by 0.1%, whereas for Krypton $J(0)$ is deceased by 0.71%. Unfortunately, experimental results for heavy atoms are sparse. Eisenberger and Reed (1972) have measured both Ar and Kr

prompt a detailed theoretical investigation and could test the limits of the rigid band model.

7.4 Compton Profile of Lead

The previous set of experiments have clearly shown the advantages of using the higher energy sources for studying heavier materials. However, as the size of the atom increases, the velocities of the inner shell electrons become extremely high and relativistic effects become very important. Mendelsohn et. al. (1974) have recently calculated Compton profiles from numerical nonrelativistic and relativistic Hartree-Fock wavefunctions, (HF and RHF respectively) for the rare gases and lead. In general they found that the relativistic spatial wavefunction for low lying s and p orbitals are pulled in towards the nucleus when compared to the wavefunctions obtained from nonrelativistic calculations. They suggested that the effect was due to the mass-velocity effect term (Bethe and Saltpeter, 1957) of the relativistic hamiltonian, which to first order was considered as a perturbing potential term in the nonrelativistic hamiltonian and is attractive in nature. Since a more sharply peaked spatial wavefunction leads to a flatter momentum space wavefunction (Fourier transform principle) they expected and found that the Compton profile is much flatter when relativistic wavefunctions are used. As the inner 1s, 2s and 2p orbitals are affected significantly by including relativistic effects, outer s and p orbitals are also significantly altered because of orthoganalisation. Also, because the normalization condition is maintained the relativistic profile is higher in the wings.

A measure of this relativistic flattening is provided by the percentage decrease in $J_{RHF}(q)$ below $J_{HF}(q)$ at the profile centre, i.e. $q = 0$. For Argon $J(0)$ is decreased by 0.1%, whereas for Krypton $J(0)$ is deceased by 0.71%. Unfortunately, experimental results for heavy atoms are sparse. Eisenberger and Reed (1972) have measured both Ar and Kr

using ^{123m}Te gamma-rays and compared their experimental profiles with both nonrelativistic and relativistic calculations. Unfortunately the relativistic effects are small and both calculations fall within the experimental error bars. In the case of lead (Z = 82) however, the calculations by Mendlesohn et. al. (1974) reveal a flattening of 5.24% at J(0), although the effects on individual orbitals are much higher. The use of the ^{198}Au source should permit the profile of lead to be measured without too much difficulty, and the present levels of accuracy should be enough to provide conclusive results of relativistic flattening.

7.4.1 Experimental Details and Results

The sample was composed of four slices of pure lead foil, each 10 mm square and 1 mm thick. The sample, mounted on a goniometer head, was aligned in such a manner that no part of the holder could be seen by either the source or the detector. As in all previous measurements with this system, the sample chamber and collimators were continuously evacuated during the measuring period. Within three half-lives of the source a measured energy loss spectrum from the sample and a background run were completed. In the profile approximately 6.10^3 counts were accumulated over the Compton peak with a channel spacing of 48 eV ($\sim$ 0.03 a.u.). The background under the Compton peak amounted to about 2% of the Compton peak intensity.

The energy resolution of the Ge(Li) SSD had slightly deteriorated to a value of 596 eV at 159.0 KeV, measured with a small 10 uCi ^{123m}Te source. Taking beam divergence into account and converting to a momentum scale, the FWHM of the response function was 0.39 a.u.. The data were then processed according to the procedures outlined in section 7.3.1.

In table 7-1 the experimental Compton profile of lead is given, together with the relativistic and nonrelativistic theoretical profiles. In the experimental profile only the high energy side of the profile is

Table 7-1

q (a.u.)	J_{HF}	J_{RHF}	J^{*}_{Exp}
0.0	11.49	10.97	10.65
0.1	11.36	10.88	10.68
0.2	11.00	10.60	10.50
0.3	10.46	10.18	10.21
0.4	9.84	9.67	9.89
0.5	9.21	9.14	9.51
0.6	8.64	8.63	9.02
0.7	8.17	8.18	8.27
0.8	7.80	7.81	7.68
0.9	7.51	7.50	7.40
1.0	7.26	7.23	7.04
1.2	6.83	6.77	6.48
1.4	6.41	6.36	6.13
1.6	5.97	5.93	5.66
1.8	5.51	5.48	5.49
2.0	5.07	5.04	5.31
3.0	3.51	3.51	3.59
4.0	2.84	2.84	2.91
5.0	2.40	2.40	2.60

* Estimate of the experimental error:
q=0,±2.5%, q=1.0,±4.0%,
q=2.0,±8.0%, q=5.0,±15.5%.

Experimental and theoretical Compton profiles of lead.

shown. The low energy suffers from tail effects caused by the resolution function and these will be amplified more than usual because of the relatively poor statistics. (Note that the theoretical profiles given in table 7-1 have now been smeared with a Gaussian of 0.39 a.u. in order to compare the theory with the filtered experimental profiles.). The very large effect of multiple scattering is particularly noticeable in these results. In the region of interest below 5 a.u. the contribution from multiple scattering amounts to over 20% of the total intensity. This in turn gives a correction of 10% to the peak of the profile and over 30% in the tails. Despite the poor statistical accuracy, the profile symmetry i.e. $J(+q) - J(-q)/J(0)$, is in general very good, being within $\pm 2\%$ of $J(0)$ over the range 0 to 5 a.u..

Fig. 7-8 shows more explicitly the difference between the experimental and theoretical profiles. The experimental results clearly favour the relativistic calculation and shows the effect of relativistic flattening on the Compton profile. The relatively poor statistical accuracy, low signal-to-noise ratio, together with the high contribution from multiple scattering merits only a qualitative rather than quantitative interpretation of the results. This result coupled with previous isolated measurements (Cooper et. al., 1976) perhaps highlights a disadvantage of the Compton profile measurements with this source.

7.5 General Discussion

(i) The Present High Energy Spectrometer

The experimental results for niobium and lead, together with previous results with the system for aluminium and germanium illustrate both the advantages and disadvantages of using a high energy, short life-time source for Compton scattering studies. The intensities obtained from both light (Z = 13) and heavy (Z = 41) materials are comparable, indicating

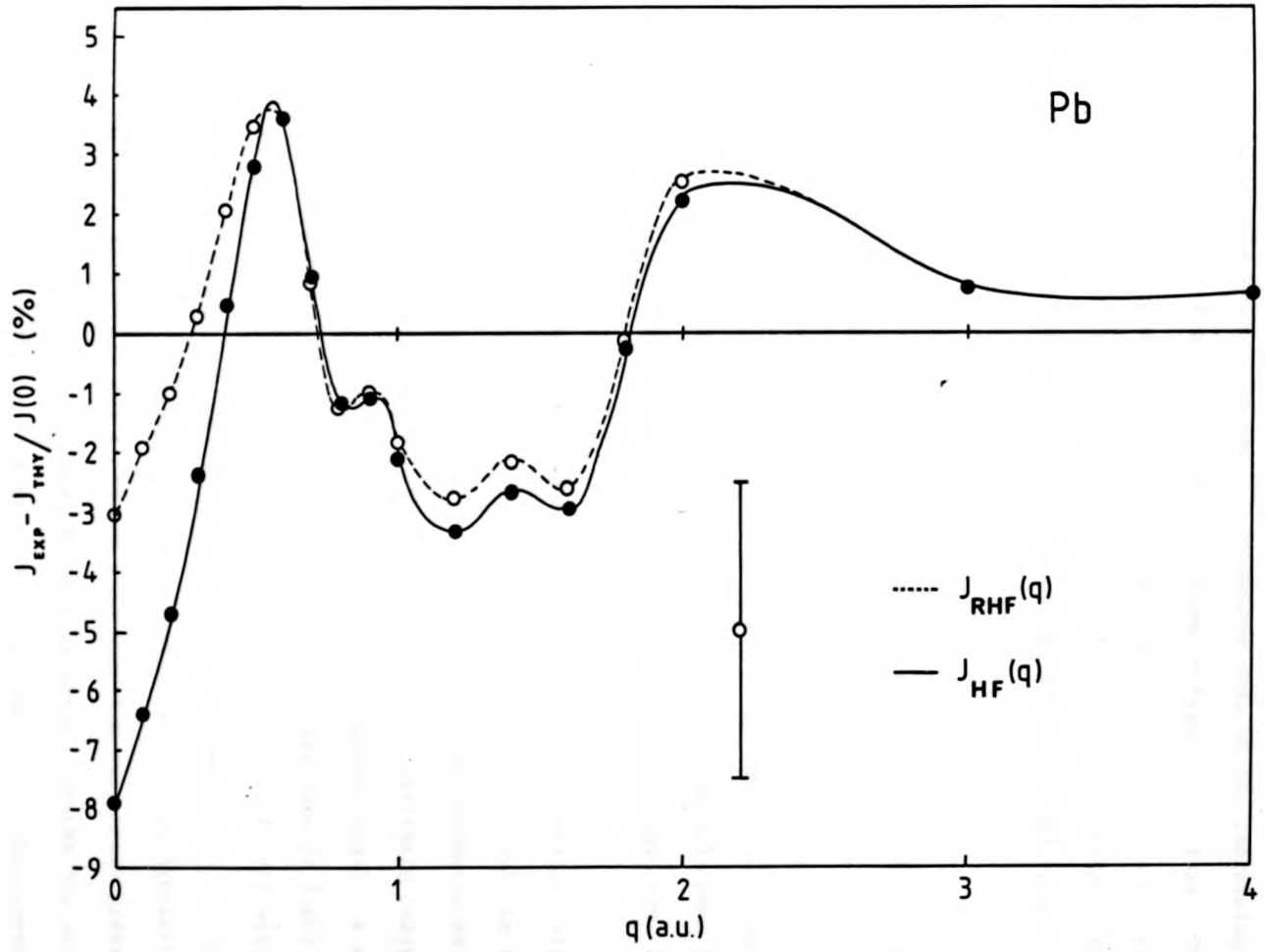

Fig. 7-8: The difference between the experimental and theoretical Compton profiles of lead.

that this experimental technique is not too limited in the same way that experiments with ^{241}Am and ^{123m}Te source are, by the increasing dominance of the photoelectric absorption process in high Z materials. The effects of this are not observed until a very heavy material (Z = 82) is measured, where a drop in intensity of about eight times was recorded. However, experiments with this system on materials in the second transition series should be possible without a prohibitive loss of Compton intensity.

One of the consequences of the short half-life of the source has been the use of relatively thick samples in order to maximize the Compton intensity recorded in the finite life-time of the experiment. This in turn has resulted in a very large multiple scattering contribution of up to 25% of the total scattered intensity. Although the Monte Carlo technique has proved itself versatile enough to cope with such large contributions, it is highly unfortunate that such effects are, in practice, unavoidable.

Although the signal-to-noise ratios are a respectable 50:1 (compared to other gamma-ray systems), a similar ratio has been found in the measurements on all types of samples. Despite the extensive shielding of the detector, inadequate shielding around the remaining parts of the system evidently contributed much to this background level. A measurement of the background has to be undertaken with great care if light elements are being studied. As pointed out by Cooper et. al. (1976) with regard to the aluminium profile, although the signal-to-noise is 50:1 at the Compton peak, it is nearer 1:1 in the tails because the aluminium core contains relatively few electrons with momentum components greater than about 5.0 a.u.. An additional complexity arises because the background is composed of a constant plus a decaying component. The correction is fortunately far less critical for heavier elements (for which the system has been used) because of the much larger core contributions. However,

although the use of the ^{198}Au source enables the core component to be measured out to very high values of momenta, the errors arising from the background correction and the poor signal-to-noise ratios limit the momentum range over which very accurate data can be obtained.

The results obtained on an isolated measurement and those obtained on pairs of measurements, e.g. anisotropy data, also highlights some of the more basic features of this system. It is clearly advisable to avoid the comparison of a single experiment with a single theoretical calculation because of the problem of undisclosed systematic errors. Experiments like those on Nb and $NbH_{0.76}$, where attention is focussed on the difference between two similar measurements, can minimize the effect of systematic errors upon the comparison between experiment and theory. For the ^{198}Au source such a strategy is obviously not only important but essential.

(ii) <u>The Case For an Improved High Energy Spectrometer</u>

Further to the disadvantages outlined above, are a number of other important factors which, collectively, call for a new system to be designed and constructed purely from a Compton scattering point of view. The Institute Laue Langevin is an international centre not only for neutron scattering but also for the many related fields that have grown up with it. The development of a gamma-ray diffractometer by Schneider (1974) was one of these, and which eventually led to the construction of a Compton spectrometer using the same source block. Unfortunately the size of this block and the considerable amount of shielding that had to be placed around it, made it far from ideal for undertaking accurate Compton scattering studies due to the poor signal-to-noise ratio and the weakness of the scattered radiation. This resulted in the use of relatively thick samples and hence a considerable amount of unwanted multiple scattering. Apart from these physical constraints there are a number of experimental difficulties associated with undertaking experiments at a remote location.

The gamma-ray diffractometer was always in continual use, which meant that there was very little preparation time. Moreover, it was usual that only a two week (and sometimes one week) period could be allocated in which to arrange the equipment and complete all the required measurements. With the early departure of Dr. Schneider to the Hahn Meitner Institute, Berlin to build a new gamma-ray diffractometer/Compton spectrometer, it rapidly became desirable to build a complementary system in England.

The new high energy gamma-ray system would be designed primarily for Compton scattering but with the possibility of undertaking some gamma-ray diffractometry. It was hoped that the design of the new system would give rise to a greater scattered intensity, better signal-to-noise ratio, together with the possibility of reducing the excessive amount of multiple scattering. The design, construction and performance of this new high energy system is described in the following chapter.

CHAPTER 8

CONSTRUCTION OF A HIGH INTENSITY 412 KeV COMPTON SPECTROMETER

8.1 Background

The results obtained with the ^{198}Au source at ILL demonstrated that useful information can be extracted from data recorded with a high energy gamma-ray source which not only had an extremely short half-life but also contained several other gamma-ray lines. The disadvantages of this system have been discussed in the previous chapter, with the conclusion that a new ^{198}Au source system in this country would be both beneficial and desirable. Fundamental to the success of this new facility would be a system designed specifically for Compton scattering, but also with the additional feature that it could be used (with little further modification) as a gamma-ray diffractometer. This is precisely the opposite arrangement to that at ILL and also to a recently constructed system at the Hahn Meitner Institute, Berlin. One major advantage of the new ^{198}Au source facility was the possibility of being able to predict, to a reasonable degree of accuracy, the required conditions of operation i.e. the intensity gain, signal-to-noise ratios, probable resolution etc. from the results and experience gained with the original equipment. The actual performance of the system, however, could only be assessed by conducting an actual Compton experiment.

The new facility was designed as a high intensity source for studying materials containing high Z elements. The particular benefits of a 100-200 Ci, 412 KeV source centre around its use in studying these heavy materials without excessive photoelectric losses, or interpretive problems due to the breakdown of the impulse approximation. The strength of the source and the regular program of reactivation that would be required

resulted in the new facility being housed at the Rutherford Laboratory. The reactors at Harwell could then be used to produce the necessary sources. The close proximity of these two establishments reduced the transportation problems considerably and increased the collaboration between them and our own group at Warwick University.

8.2 Design and Constuction Considerations

8.2.1 Compton Scattering Requirements

The main criteria around which the new system was designed (apart from cost limitations) can best be summarized in the following manner.

(i) To make the scattering angle as large as possible for maximum momentum transfer and improved resolution.

(ii) To reduce the incident and scattered beam paths ($1/r^2$ losses).

(iii) To reduce the background levels of radiation by optimising the shielding and to keep the surface activity below 10 mrad/hr

(iv) To increase the Compton scattered intensity.

(v) To produce a flexible system.

Point (iv) is very important if an overall improvement in the system is to be realised. An increase in the intensity can result in :-

(a) A reduction in the time required to conduct an experiment (1 - 2 half-lives).

(b) An increase in the counting statistics.

(c) A reduction in the thickness of the sample, thus minimizing unwanted multiple scattering.

(d) A reduction in the effects of electronic drift caused by long term temperature variations.

If these points are considered in the design then an order of magnitude improvement in the accuracy and reliability of Compton profile data can be visualized. However, the width of a Compton profile, on the scale of scattered gamma-ray energy, and the width of the experimental resolution

function vary with the principal gamma-ray energy and the scattering angle. The optimum resolution criterion is based on the ratio of these two widths. In this system the principal energy is known so that the above criterion rests solely on a precise knowledge of the scattering angle. The smearing of the experimental profile due to the finite range of scattering angles accepted by the radiation collimators has already been dicussed in detail in Chapter 4. Here it is shown that the additional contribution to the resolution arising from geometrical divergence can be examined independently of the electronic instrumental resolution enabling the two effects to be compared and contrasted. The importance of the geometrical resolution in high energy experiments has been emphasised by McIntire (1976) and DuBard (1978). The geometrical energy broadening is given by

$$\Delta\omega_2 = (\omega_2^2/mc^2)\sin\theta\,\Delta\theta \qquad 8\text{-}1$$

Fig. 8-1(a) shows the geometrical energy resolution assuming a deviation of $\pm 1^\circ$ in the scattering angle for 412 KeV radiation together with a higher (^{137}Cs) and lower (^{241}Am) energy source, as a function of the scattering angle. Fig. 8-1(b) shows a similar plot but illustrates the effect in momentum space which is more important in the case of high energy radiation sources. Comparing the two figures, the variation in the geometrical resolution among the three gamma-ray sources shown is slightly smaller in momentum space than in terms of energy. This small variation is due to an improvement in the intrinsic momentum resolution with increasing primary gamma-ray energy. The higher energy sources are however accompanied by a substantial deterioration of the geometrical resolution because of the ω_2^2 term in equation 8-1. These figures clearly illustrate the reasons why scattering angles have a practical lower limit of about 150°. Spectrometers which use low energy sources, as seen before,

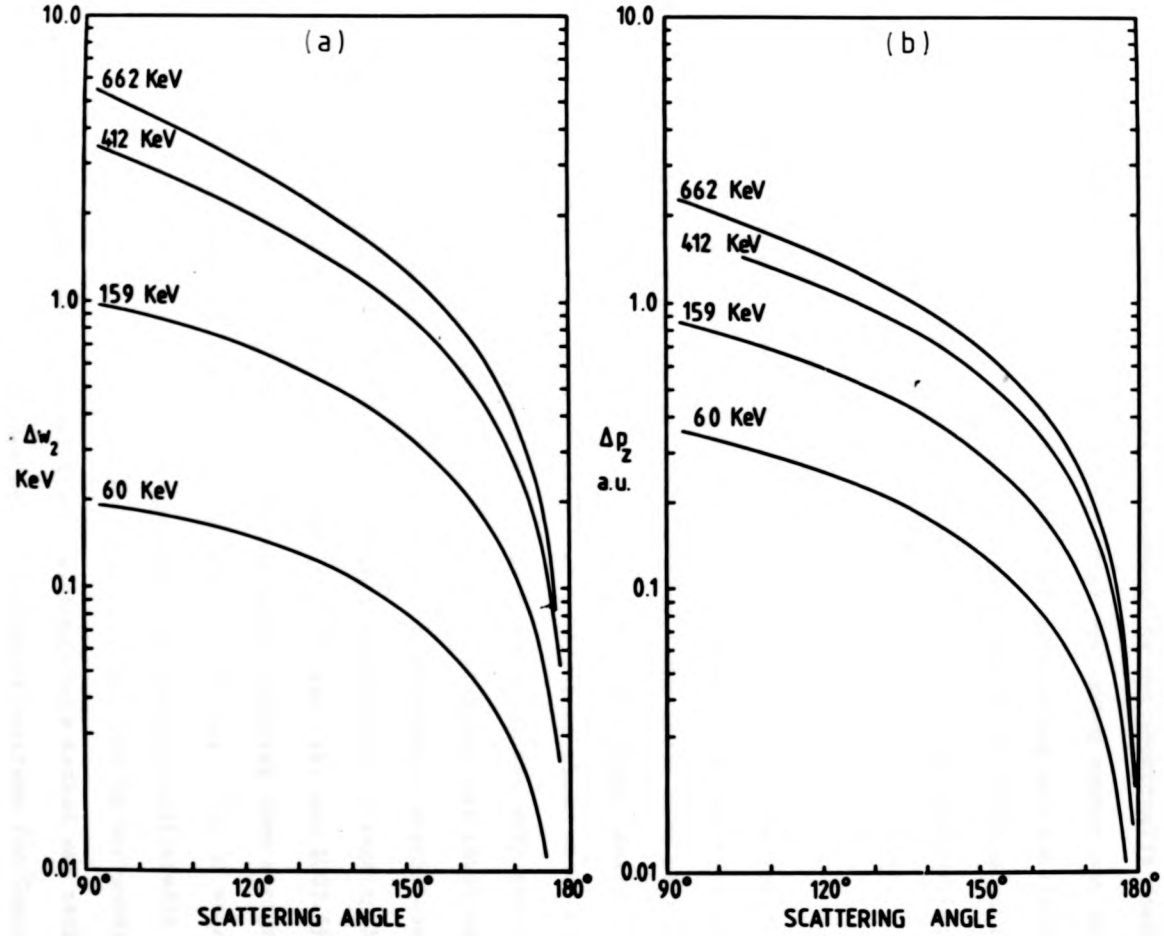

Fig. 8-1: Geometrical spread in the scattered gamma-ray energy (a) and measured electron momentum interval (b), versus the scattering angle for + 1 variation in the scattering angle.

can be constructed with a large scattering angle relatively easily, with a resulting negligible geometrical smearing. Shielding of the primary radiation is comparatively simple allowing excellent peak-to-background ratios. However, such an arrangement is not practically possible with high energy sources since very large scattering angles can not be attained due to the necessary greater bulk of collimating and shielding materials. The design of the spectrometer from a Compton scattering point of view therefore involves some compromise between the geometrical energy resolution, the peak-to-background ratio and the scattered intensity.

8.2.2 Gold Source Spectra

The equations for the decay scheme of ^{198}Au (see equation 7-1) were given to show the principal gamma-ray lines which directly affect the structure of the energy loss spectrum. The lines also help to identify the lines obtained in a Compton scattered spectrum. However, it is with this first transition that special interest is shown since accompanying the 411.8 KeV transition are two other lines which are very much higher in energy. Such higher energy transitions although not involved directly with the Compton scattering process, do contribute significantly to the background. The principal gamma-ray energies and intensity levels for this decay are 411.8 KeV (95.8%), 675.88 KeV (1%) and 1087.69 KeV (0.2%) (Lederer et. al., 1967). The two latter energies have a significant fraction of the total output emanating from say a 100 Ci source, and together with their greater penetration present considerable shielding problems. The ^{198}Au source at ILL overcame this by surrounding the source with large quantities of lead. Although this method was satisfactory for the gamma-diffractometer, it presented problems for Compton scattering that was reflected in the poor signal-to-noise ratio of 50:1. Improvement in this area would be of significance and essentially dependent on the type of shielding materials available.

Recently, however, a second and perhaps more important problem has arisen which directly affects the Compton profiles obtained. It concerns the second of the two expressions given in equation 7-1, and the amount of ^{199}Au. In this reaction the decay of ^{199}Au to ^{197}Au produces two other gamma-ray lines at 208 KeV and 158 KeV. The importance of these two lines in the scattered energy spectrum therefore depends on the ratio of ^{199}Au to ^{198}Au. In Fig. 8-2, a plot is shown of the ratio (as a percentage of ^{198}Au) as a function of the number of days a 0.2 gm ^{197}Au is irradiated by thermal neutrons. The upper curve shows the activity of the ^{198}Au on the same time axis. An important consideration in the design of the source is therefore to obtain a high activity of ^{198}Au whilst at the same time minimizing the ^{199}Au to ^{198}Au ratio. Obviously the previous method used in Grenoble is not an optimum condition. A useful guide to this optimum condition is shown in the figure. A factor of 2 can be gained if the irradiation time is reduced from 3 days to 0.6 days. The activity of ^{198}Au can be recouped by inserting say three pieces of gold foil instead of the usual one.

8.2.3 Shielding Materials

The most common shielding material is lead (ρ = 11.3 gm/cc) because of its low cost and ability to be machined. Fig. 8-3 shows the half-value thickness of lead shielding for several gamma-ray sources as a function of the scattering angle. A transmission factor of 10^{-n} requires 3.322n half-value layers of the absorbing material. For example, a reduction of 10^{3} in the intensity of the primary radiation for say ^{198}Au (412 KeV) requires 28mm of lead, whereas only 1.2 mm are required in the case of ^{241}Am (60 KeV). To adequately shield the high energy gamma-rays (~1 MeV) emitted by ^{198}Au would therefore require a substantial amount of lead. This would not offer a significant gain in the overall size of the system compared to the facility at ILL, if the criteria for the new design were

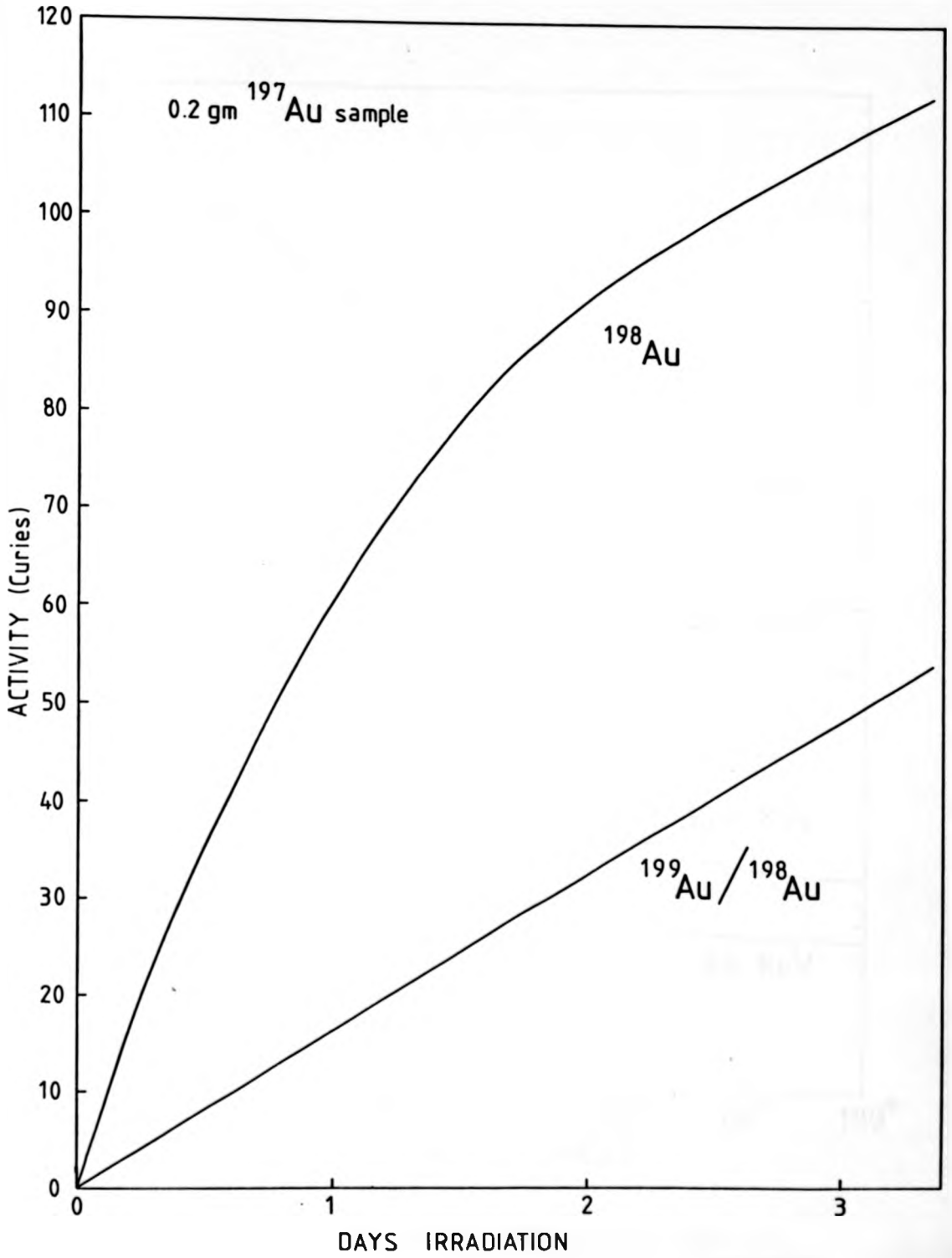

Fig. 8-2: Ratio of ^{199}Au to ^{198}Au, and total ^{198}Au activity as a function of days irradiation to thermal neutrons.

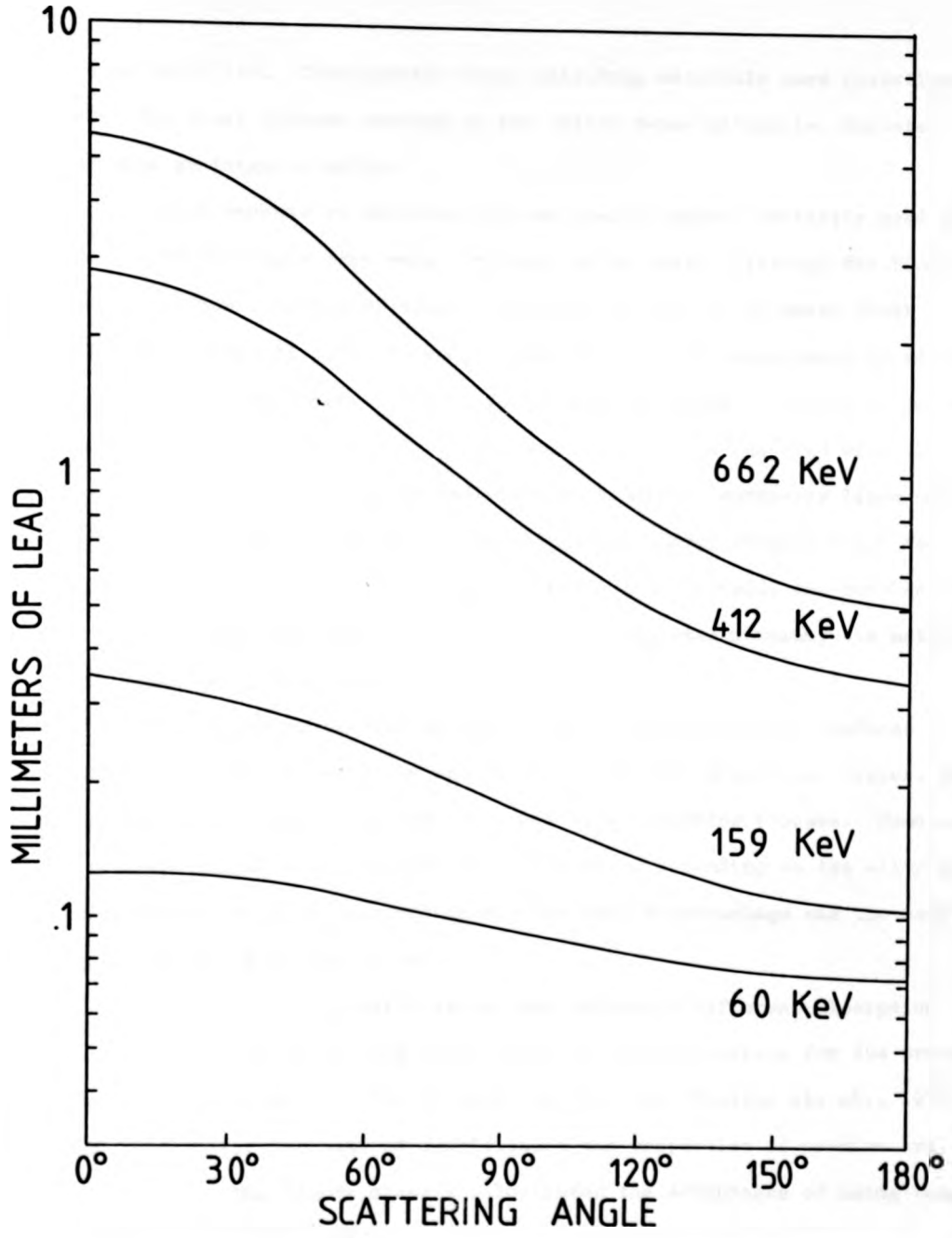

Fig. 8-3: Half-value thickness of lead shielding for several gamma-ray sources as a function of the scattering angle.

to be fulfilled. Consequently other shielding materials were investigated with the final outcome resting on two rather dense materials, depleted uranium or tungsten alloy.

Large amounts of depleted uranium (ρ=22.0 gm/cc) initially used as an accelerator beam stop were available at no cost. Although the blocks had a surface activity of about 2 mrad/cm^2, it was by no means clear that this residual activity would interfere with the experiment if adequate precautions were taken. Several tests were therefore initiated to determine the nature of this activity. Unfortunately, results recorded with the intrinsic germanium detector indicated no prominant gamma-ray lines only a continuous bremsstrahlung background in the energy range 1 - 1.5 MeV. This high energy background would be difficult to shield, and coupled with the restriction imposed on the machining of depleted uranium, the material was reluctantly discounted.

The second of the two materials was a tungsten alloy, produced by GEC-Osram. This material is an alloy of tungsten, nickel and copper, and is produced in various shapes and forms by a sintering process. Densities available ranged from 16.8 gm/cc to 17.5 gm/cc depending on the alloying material and content. Unfortunately the real disadvantage was the cost, approximately £ 15 per 10 cc.

Both lead and tungsten alloy have radically different absorption properties. The broad beam attenuation of these materials for the principal gamma-ray energies of ^{198}Au is shown in Fig. 8-4 (Dunster et. al., 1971, GEC,1964). For the sake of completeness the properties of uranium are also shown. The figure clearly illustrates the advantages of using tungsten alloy as opposed to lead.

As an example of the shielding problems the exposure rate at 1 metre for ^{198}Au is 0.23 Rh^{-1}Ci^{-1} (Dunster et. al., 1971) which for a 100 Ci source at say 8 cm (unshielded) is equivalent to 3590 Rh^{-1}. The facility at ILL

to be fulfilled. Consequently other shielding materials were investigated with the final outcome resting on two rather dense materials, depleted uranium or tungsten alloy.

Large amounts of depleted uranium (ρ=22.0 gm/cc) initially used as an accelerator beam stop were available at no cost. Although the blocks had a surface activity of about 2 mrad/cm^2, it was by no means clear that this residual activity would interfere with the experiment if adequate precautions were taken. Several tests were therefore initiated to determine the nature of this activity. Unfortunately, results recorded with the intrinsic germanium detector indicated no prominant gamma-ray lines only a continuous bremsstrahlung background in the energy range 1 - 1.5 MeV. This high energy background would be difficult to shield, and coupled with the restriction imposed on the machining of depleted uranium, the material was reluctantly discounted.

The second of the two materials was a tungsten alloy, produced by GEC-Osram. This material is an alloy of tungsten, nickel and copper, and is produced in various shapes and forms by a sintering process. Densities available ranged from 16.8 gm/cc to 17.5 gm/cc depending on the alloying material and content. Unfortunately the real disadvantage was the cost, approximately £ 15 per 10 cc.

Both lead and tungsten alloy have radically different absorption properties. The broad beam attenuation of these materials for the principal gamma-ray energies of ^{198}Au is shown in Fig. 8-4 (Dunster et. al., 1971, GEC,1964). For the sake of completeness the properties of uranium are also shown. The figure clearly illustrates the advantages of using tungsten alloy as opposed to lead.

As an example of the shielding problems the exposure rate at 1 metre for ^{198}Au is 0.23 Rh^{-1}Ci^{-1} (Dunster et. al., 1971) which for a 100 Ci source at say 8 cm (unshielded) is equivalent to 3590 Rh^{-1}. The facility at ILL

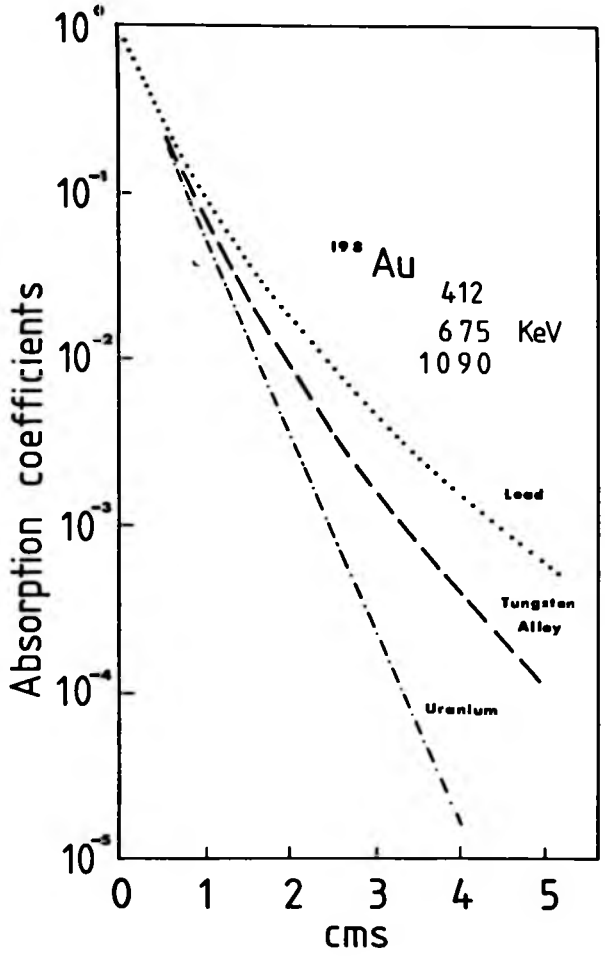

Fig. 8-4: Broad beam absorption coefficients for ^{198}Au as a function of thickness in lead, tungsten-alloy and uranium absorbers.

with an initial source strength of 70 Ci had a surface activity of about 120 mRh^{-1}. In the design of the new system it was hoped that with adequate shielding this figure could be reduced to about 10 mRh^{-1}, with a subsequent increase in the signal-to-noise ratio.

8.3 Details of the Design

The design of the Compton spectometer (gamma diffractometer) which finally resulted was naturally on similar lines to the system at ILL, although on a much smaller scale. Fig. 8-5 illustrates the main features of the system showing the source block, collimators and sample chamber as assembled. Fig. 8-6 shows schematically the approximate layout of the apparatus. In this system a scattering angle of 167° was maintained since there was no real advantage in going to higher angles either from a resolution or intensity point of view. The source block that housed the high activity source was a complex construction which used a combination of lead and tungsten alloy, optimizing on the basis of shielding ability, efficiency and cost. In this section details of the design and construction of each component are described.

8.3.1 The Source Block

(i) Basic Structure

The principal features of the source block design are shown schematically in vertical section in Fig. 8-7. The source block consists of an inner core of tungsten alloy (A) surrounded on three sides by a lead labyrinth. The fourth side contains two thick tungsten alloy plates which were removable thus enabling a second variation of the system to be constructed. This meant that two geometrical arrangements could be envisaged having the same scattering angle and differing only in the path lengths of the incident and scattered beams. The rectangular shape of the core provided more shielding in the scattering plane and thus

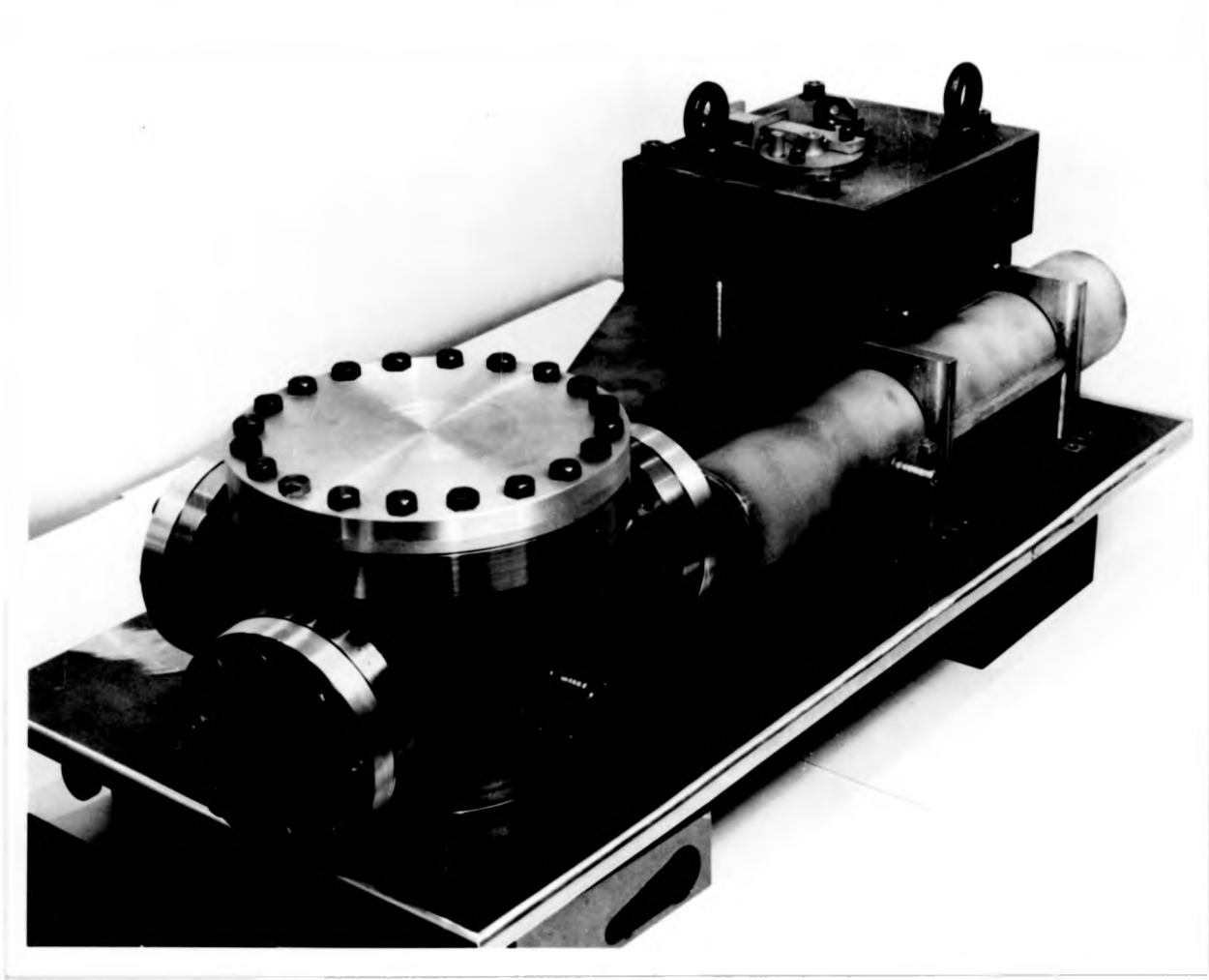

Fig. 8-5: Illustration of the ^{198}Au source facility.

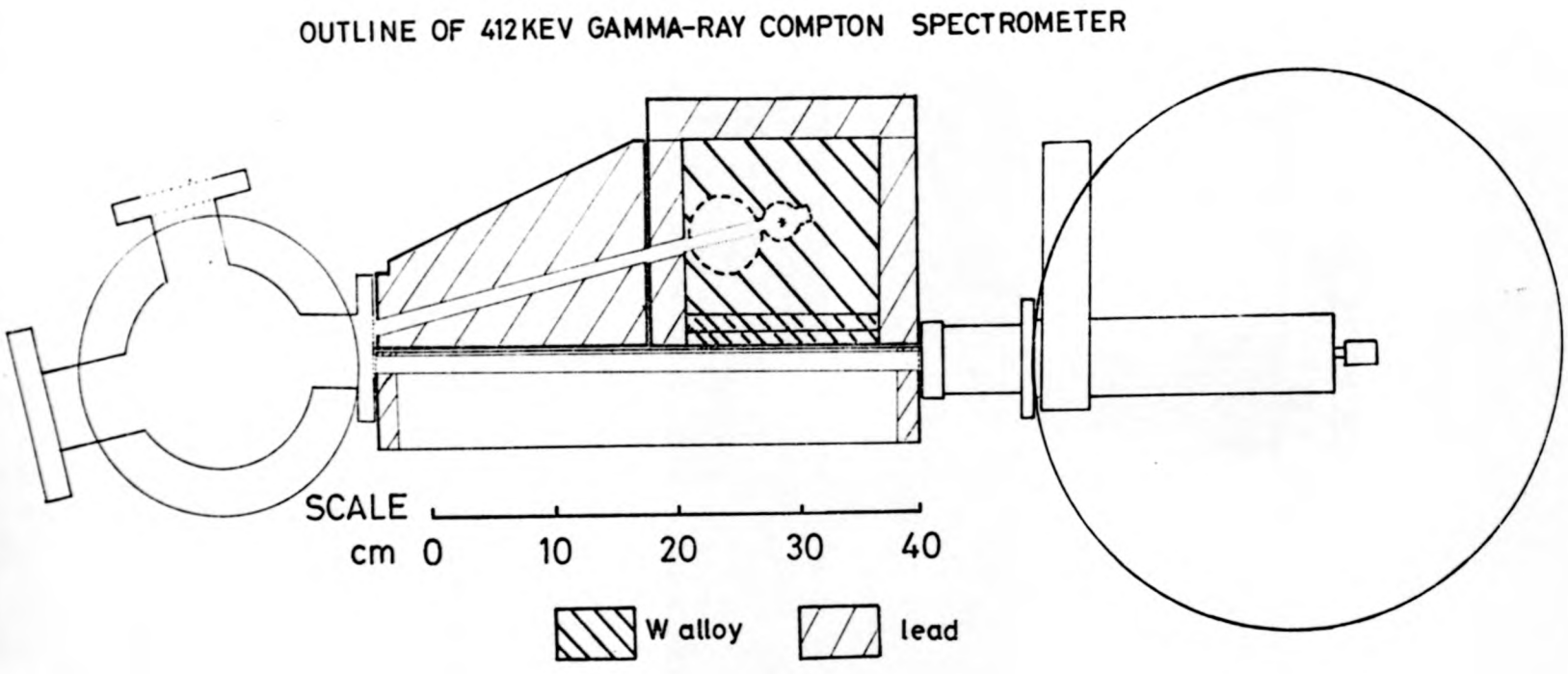

Fig. 8-6: Schematic layout of the ^{198}Au source facility.

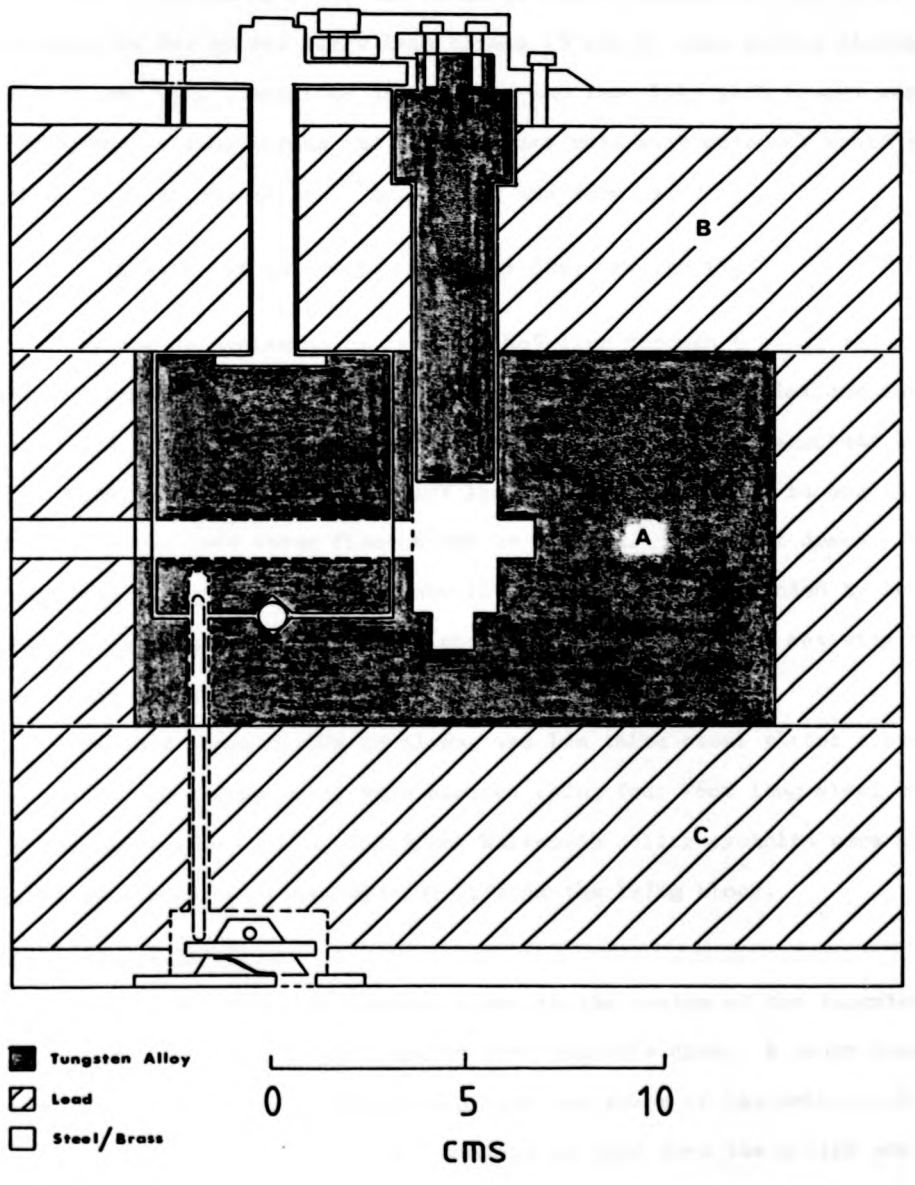

Fig. 8-7: Schematic diagram of the source block shown in vertical section.

adequately protected the detector from direct radiation from the source. The loss of shielding above and below the core (because of the cost) was compensated for by two large lead blocks (B and C) each having dimensions 20×20×8 cm. The dimensions of the core and lead labyrinth blocks were determined by considering the surface dose rate each material would give using a 100 Ci source of ^{198}Au. Using the formula,

$$\text{Activity at 1m} = 0.53 \times \text{Activity (Ci)} \times \text{Energy (MeV)} \qquad 8\text{-}2$$

the computed transmission of the 1.09 MeV line through 8 cm of tungsten alloy gives an exposure rate of 2.26 mRh^{-1}. Similar calculations for the 0.676 MeV line gives a result that is five orders of magnitude lower than this, while for the 411.8 KeV line, the exposure rate is negligible. Obviously for lead these figures can be doubled. The final design therefore consisted of a tungsten alloy core 16×16×8cm thick, surrounded by lead blocks 2cm thick. Such a design should reduce the surface activity to less than 10 mRh^{-1}.

To hold these blocks in place, two 1cm thick steel plates above and below the source block were secured using four 26cm long steel bolts. On the upper steel plate, two ½inch Whitworth collar eyebolts were attached, which were more than adequate for lifting the 127Kg block.

(ii) Source Location

The gold source was located close to the centre of the tungsten alloy core, to gain maximum benefit from the shielding. A major consideration in the design of this stage was the size and shape of the hole required to accomodate the source holder, bearing in mind that the system would also be used as a gamma-ray diffractometer. To assist in the design, the expertise of Dr. J. Schneider was called upon. Dr. Schneider pioneered the first gamma-ray diffractometer at ILL and also assisted in the construction of the ^{198}Au Compton spectrometer. Furthermore, he was

also in the process of building a second, complementary system at the HMI.

The shape of the hole, particularly in the scattering plane, is very critical as it determines the purity and symmetry of the incident beam and hence the symmetry of the Compton profile. In order to minimize backscattering from the walls, a horizontal hole 1cm in diameter and 2cm deep was made in the scattering plane and along the incident beam direction. The removal of tungsten alloy to accomodate the source holder would obviously increase the surface activity. Calculations of this revealed that the surface exposure would increase, at the centre of the faces, by 5 times for a 3cm diameter hole and 3 times for a 2cm hole. The final hole diameter was 2.1cm. The addition of lead surrounding the core would help to alleviate this increase in activity.

(iii) The Window Mechanism

Considerable concern was shown in the design of an adequate window mechanism, since the results for the 'old' system showed excessive leakage of radiation from around the window, even when closed. The resultant design, shown in Fig. 8-7, consisted of a cylindrical window of tungsten alloy 7cm long and 6cm in diameter, pivoted about it's centre on a ball joint. Through the cylinder, parallel to its' faces and centred 2cm from one end, was a tunnel 10mm in diameter. The displaced position of the tunnel together with the accurate location of the window with respect to the core was critical in obtaining the maximum shielding in both the open and closed positions. Furthermore, the outer lead block (on the window side) was modified to include a rotatable lead window. This further reduced the surface activity when the window was in the closed position, e.g. during transit. The window was rotated by means of a brass disc on top of the steel plate.

(iv) Safety Features

To prevent the removal of the source or the removal of the source block when the window was open, a long brass lever was attached to the rotatable disc. In the open position this lever passed through a slit in the steel support structure, on which the whole apparatus was mounted, and could be locked in position. However, such a mechanism did not apply when the window was closed, e.g. during transit. To prevent the removal of the source in this case, a small cylindrical pivot and spring mechanism was imbedded into the lower steel plate. On one side of the pivot was a long steel rod which protuded into a small hole in the base of the window. Only when the source block was positioned over the correct location on the steel support section could the window be unlocked and opened.

8.3.2 The Source Holder

The source holder was made from tungsten alloy to provide adequate shielding in the upward direction. To prevent radiation leakage, the sides of the holder were bevelled, which also allowed easy movement of the holder when being inserted into the source block. Fig. 8-8 shows an illustration of the completed holder. The source was sandwiched in a slot cut into a cylindrical piece of reactor grade graphite 27mm long and 6.5cm in diameter. Graphite was chosen as the support medium because of it's high purity, low atomic number and machinability. A nickel-copper clip was used to connect the graphite to the holder.

Since the precise location of the gold source with respect to the scattering plane was critical, a stainless steel protective cover containing a small spring, was placed around the graphite pin. The spring ensured that the graphite was properly located and also prevented it from being damaged or dislodged during transportation. The bayonet fitting rods on the holder were orientated so that the source was face on in a Compton scattering experiment. A second holder was constructed with these rods

(iv) Safety Features

To prevent the removal of the source or the removal of the source block when the window was open, a long brass lever was attached to the rotatable disc. In the open position this lever passed through a slit in the steel support structure, on which the whole apparatus was mounted, and could be locked in position. However, such a mechanism did not apply when the window was closed, e.g. during transit. To prevent the removal of the source in this case, a small cylindrical pivot and spring mechanism was imbedded into the lower steel plate. On one side of the pivot was a long steel rod which protuded into a small hole in the base of the window. Only when the source block was positioned over the correct location on the steel support section could the window be unlocked and opened.

8.3.2 The Source Holder

The source holder was made from tungsten alloy to provide adequate shielding in the upward direction. To prevent radiation leakage, the sides of the holder were bevelled, which also allowed easy movement of the holder when being inserted into the source block. Fig. 8-8 shows an illustration of the completed holder. The source was sandwiched in a slot cut into a cylindrical piece of reactor grade graphite 27mm long and 6.5cm in diameter. Graphite was chosen as the support medium because of it's high purity, low atomic number and machinability. A nickel-copper clip was used to connect the graphite to the holder.

Since the precise location of the gold source with respect to the scattering plane was critical, a stainless steel protective cover containing a small spring, was placed around the graphite pin. The spring ensured that the graphite was properly located and also prevented it from being damaged or dislodged during transportation. The bayonet fitting rods on the holder were orientated so that the source was face on in a Compton scattering experiment. A second holder was constructed with these rods

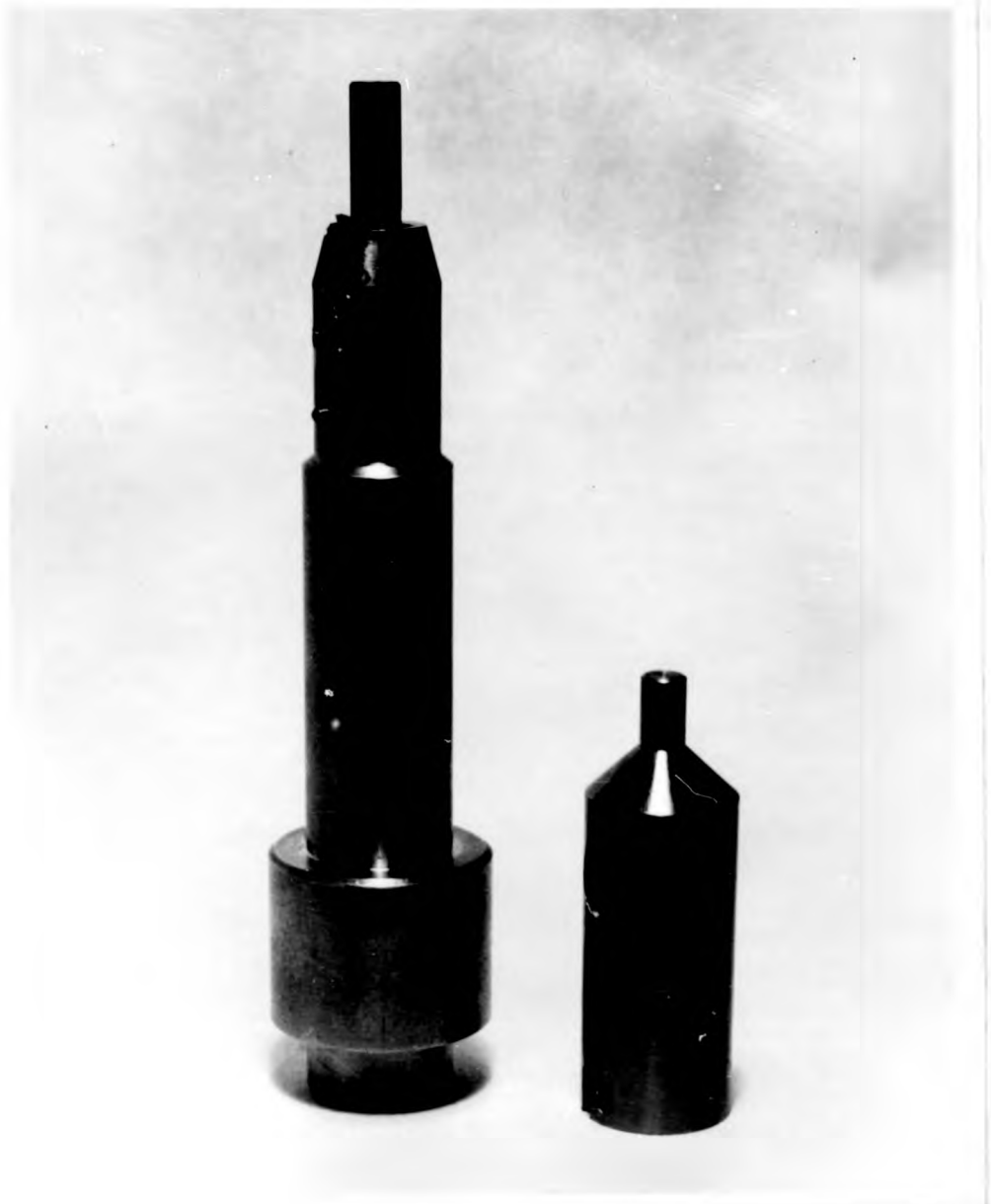

Fig. 8-8: Illustration of the tungsten-alloy source holder.

at right angles to those just described to enable the source to be seen edge on as would be required in gamma-ray diffractometry.

Finally, the source itself is a piece of gold foil, 6.5×6.5×0.25mm i.e. 0.2gm. The size of the foil enables source activities of up to 150 Ci to be easily achieved by thermal neutron irradiation over a four day period in the DIDO reactor at Harwell. The extent to which the neutron flux can achieve these high activities is limited by the type of reactor available and the size of the foil to be irradiated. Usually strong self-absorption of the main 412 KeV radiation is the limiting factor on the foil size. If the foil is too large, then saturation will not be reached (see Fig. 8-2) and self-absorption and multiple scattering in the source will give rise to a deterioration in the symmetry of the incident beam.

8.3.3 Collimators and Shielding

The experience gained with the system at ILL indicated two areas where improved shielding would improve the signal-to-noise ratio. These areas were between the incident and scattered collimators, and between the source block and detector. The objectives of the new system were therefore to improve the shielding whilst at the same time constructing a system which allowed for two different geometrical arrangements. It was hoped that by keeping the same scattering angle, and reducing the incident and scattered beam path lengths, an increase in the scattered intensity of a factor of 3 or so could be realised without a significant deterioration in the momentum resolution. This would involve two separate shielding and collimation conditions.

For the incident beam two large lead blocks were cast from the melt. Each block contained a tunnel 2cm in diameter and two annular collimators positioned to give a beam cross section at the sample position of $1cm^2$. Mylar windows were fixed to each block enabling the tunnels to be evacuated.

The scattered beam collimators were constructed from large diameter brass pipes to minimize wall scattering and low angle scattering, particularly near the detector. Mylar windows were again used to seal and evacuate the collimators. Fig. 8-6 shows the layout of the collimators in the long geometry. The Ge(Li) detector was positioned about 5cm from the end of these collimators. In the short geometry, the two tungsten plates on the side of the source block were removed and the sample chamber repositioned accordingly.

8.3.4 Sample Chamber

The cylindrical sample chamber was made from stainless steel, with an outer diameter of 20.3cms. It contained three standard VG vacuum flanges, one in the direction of the incident radiation, one at right angles to this direction and one that allowed the incident beam to impinge on the sample and the scattered beam to reach the detector. The first port acted as a beam stop and contained a large block of lead. This flange could also be removed and replaced by a long flight tube enabling the system to be used as a gamma-ray diffractometer. At 90° to this was the viewing port containing a lead glass window. This flange could also be removed if minor adjustments to the positioning and orientation of the sample were required. The third flange was covered with 100μm thick mylar to enable the sample chamber to be continuously evacuated.

The inside of the chamber was lined with lead sheet to minimize scatter from the walls. Furthermore, the size of the chamber was such that no part of the wall was within the scattering volume. The large 20 cm flange covering the chamber could be interchanged and modified to suit the needs of a particular experiment, e.g. cryostats, heaters etc.

8.4 Detector and Electronics

The Ge(Li) detector used at ILL was again used in the present system. Its' characteristics were known e.g. efficiency, so that no additional measurements, apart from the resolution were required. The electronic equipment associated with the detector was different than that used previously. Instead of an MCA a PDP8E minicomputer was available that could be programmed to undertake the same functions as those normally found on the MCA. A modified version of DAPHNE II, a BCPL program written for analysis of neutron scattering data, was adapted to run on the PDP8E. The computer was programmed to contain 4000 channels together with the more usual features commonly found on most MCA's. The pulses from the preamplifier were fed to an Ortec spectroscopic amplifier and ADC. The interfacing of the ADC to the computer was undertaken by members of the staff at the Rutherford Laboratory.

During an experiment whether it is a Compton profile spectrum or resolution function measurement, the data is accumulated onto a magnetic tape in blocks. Each block contains all 4000 channels with an upper limit of 3.10^3 counts in any channel. Once a block is filled it is immediately written to a memory core (the upper memory) and a fresh block is released simultaneously to continue the accumulation of data. After completion of a measurement the upper memory (which may contain as many as 10^3 blocks) is transferred to a second tape where it may be read by the main Rutherford computer. A small Fortran program analyses each block and eventually sums the data in each channel, placing the total spectrum (all 4000 channels) onto a magnetic disc. The usual data processing procedures can then be applied as described in the previous chapter.

To reduce the electronic drift particularly in the ADC and less

so in the detector preamplifier, due to long and short term temperature variations, the whole spectrometer system including the computer were housed in an air conditioned room. This is similar to the situation at ILL, and enables a constant temperature (to within $\pm 1.5^{\circ}C$) to be readily maintained.

8.5 Results of Trial Irradiation

The initial test of the new spectometer was aimed at assessing it's performance by comparison with the equipment it replaced and also with Dr. Schneiders complimentary system at the Hahn Meitner Institute (HMI). The tests were further seen as a method for evaluating the special safety features incorporated in the design.

A four day irradiation of one piece of gold foil in the DIDO reactor at Harwell, produced a source with an initial activity of 120 Ci (compared to 70 Ci at ILL). No problems were encountered in assembling the source in its tungsten alloy holder or placing the holder into the source. Moreover, there was little difficulty in transporting the block from the Harwell reactor to the air conditioned room at the Rutherford Laboratory. Measurements of the surface activity with the window closed were typically of the order of 5 mRh^{-1} with a slight increase (~10 mRh^{-1}) on removal of the two alloy plates, as expected. The surface activity was within the limitations imposed by the design criteria.

Problems were, however, encountered with the computer, a situation that could not be resolved in the time alloted (~3 half-lives of the source). Fortunately, an ORTEC 1000 channel MCA was made available, and the measurements reported in this section were obtained with this system. For the first irradiation,Compton scattered intensities and signal-to-noise ratios were of primary interest.

Measurements were conducted on aluminium (the same sample used by Cooper et. al. (1976) in their first experiments with the ^{198}Au source

at ILL) and tin (Z = 50)

The experimental details are similar to those already described in Chapter 7. A small 10 μCi ^{123m}Te source was used to measure the resolution function of the Ge(Li) detector. The FWHM of the resolution function when converted to a momentum scale was 0.38 a.u.. Beam divergence which amounted to $\pm 0.87^{\circ}$ for the extended geometry contributed an additional 60 eV to the FWHM, giving a total width of 0.43 a.u.. The short geometry gives a beam divergence of $\pm 0.92^{\circ}$ and a total width slightly higher at 0.45 a.u.. A low activity ^{123m}Te source and a 1 μCi ^{241}Am source were used to establish the energy-channel relation. The approximate channel spacing corresponded to 182 eV.

The single crystal of aluminium was 0.5 cm thick, and the compressed powder sample of tin was 0.3 cm thick. A typicical energy loss spectrum obtained with this equipment for aluminium is shown in Fig. 8-9. The Compton profiles at 159 KeV, 108 KeV and 96 KeV are clearly distinguishable as are the characteristic X-ray lines from gold. High intensity tungsten fluorescent X-radiation are also visible with the corresponding Compton profiles produced by them. The relative high intensity of these lines is a result of the increased detector efficiency at these lower energies. A calculation of the energy loss arising from the inelastic scattering from these X-ray lines indicates $\sim 90^{\circ}$ scattering. This confirms the expectations that these profiles result from scattering off the walls surrounding the source.

In the extended geometrical configuration a signal-to-noise ratio at the Compton peak of about 1000 to 1 was obtained for aluminium, and a ratio of about 250 to 1 for tin. These figures were obtained only after moderate lead shielding had been placed between the detector and the source block (compared with 10 cm for the ILL system). Extensive shielding would increase the signal-to-noise ratio by a factor of two

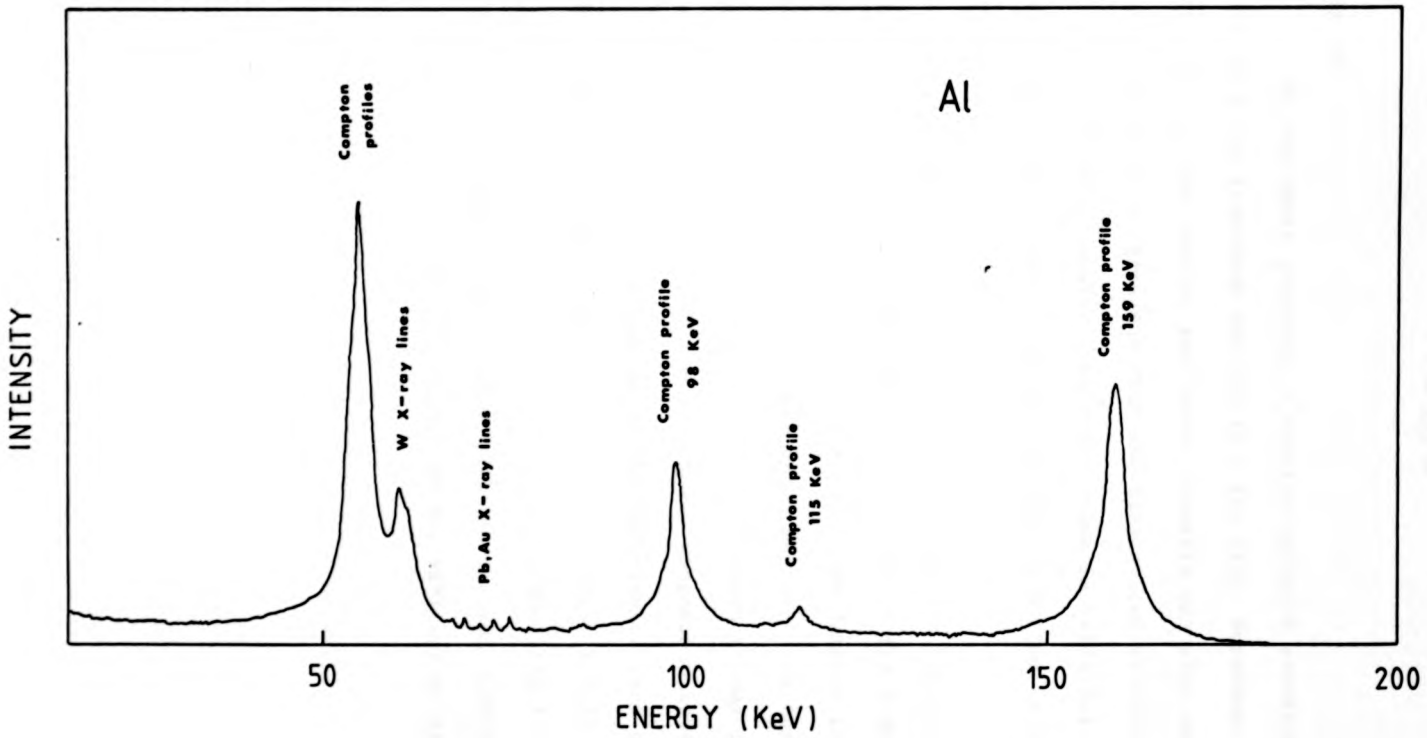

Fig. 8-9: Energy loss spectrum in aluminium using the ^{198}Au source.

or so.

In the short geometry, a similar analysis revealed ratios of 800 to 1 for aluminium and 200 to 1 for tin. Moreover, a factor of two increase in the Compton scattered intensity was also observed, from both samples, in good agreement with the theoretical predictions. A complete summary of the intensity levels are shown in table 8-1, where comparisons with the original system at ILL and the new system at the HMI, are also made.

From the table it is evident that the new system is superior to the original equipment at ILL. An increase in the signal-to-noise ratio of about 20 together with an increase in the Compton intensity of 8 for the long geometry and 16 for the short geometry has been realised. The small deterioration in the momentum resolution arises from the impaired resolution properties of the detector. Comparison between the new system and the complimentary system at the HMI reveals very similar figures despite the differing geometrical arrangments. A full account of the program of work to be undertaken with this facility is given in the following chapter. It is hoped that the initial work will involve close collaboration with Dr. Schneider and Dr. Pattison at the HMI.

	Grenoble-Warwick	Rutherford-Warwick	Hahn-Meitner Institut
Activity (Ci)	70	120	100
Source size (mm)	foil 0.2×10×4	foil 6.5×6.5×0.25	cylinder 2 mm diam.
Scattering angles	167° 169° 171°	167°	165°
Beam divergence	± 0.7°	long ±0.87° short ±0.92°	
Source-sample distance (cm)	50	long 47.6 short 36.3	35
Sample-detector distance (cm)	100	long 59.4 short 48.4	55
Collimator diameter (cm)	1.6	1.12	1.6 - 0.9
Signal-noise ratio	$\frac{Al}{Ge} \sim 50:1$	Al 1000:1 Sn 250:1 (short × .8)	$\frac{Al}{Ge} \geq 1000:1$
Compton intensity cts/50eV/hr	Al 365	Al 2970 Sn 800 (short × 2)	Al 2400(+) Au 542
Resolution (a.u.)	0.37	0.43	0.4 0.6

Table 8-1

Comparison of ^{198}Au source facilities

CHAPTER 9

CURRENT DEVELOPMENTS AND FUTURE EXPERIMENTS

9.1 General Conclusions

Since the revival of Compton scattering in 1965 a considerable amount of progress has been made in understanding electron behaviour in metallic and molecular systems. Much of the recent experimental work has been stimulated by the development of energy sensitive photon detectors and the use of gamma-ray sources. The analysis of the energy spectrum of inelastically scattered gamma-rays with these detectors has led to a considerable reduction in the length of time taken for a Compton profile measurement. Moreover, the range of systems that can be studied is greatly extended to include materials such as the transition metals.

A large part of the authors work has been to develop the gamma-ray technique further by designing and constructing two new gamma-ray Compton spectrometers using ^{241}Am (60 KeV) and ^{198}Au (412 KeV) sources. The application of these techniques to a number of metallic and molecular systems has realised an order of magnitude improvement not only in the accuracy and reproducibility, but also in the quality of the Compton profiles obtained. Table 9-1 gives a summary of these new systems together with a comparison of other sources currently in use to obtain Compton profiles. The considerable improvement in the experimental technique is clearly illustrated. Details of the advantages of the new ^{198}Au system have been given in Chapter 8.

The low energy systems comprising of a 300 mCi disc source and 5 Ci annular source of ^{241}Am radiation, have been used to obtain a comprehensive set of molecular Compton profiles for gaseous and liquid

	X-ray	γ-ray ^{241}Am	γ-ray* ^{241}Am	γ-ray* ^{198}Au	γ-ray ^{137}Cs	synch.
Energy (KeV)	17.4	59.54	59.54	412	662	63.3
Activity		0.3	5	120	200	
Maximum scattering angle (°)	146	150	170.5	167	160	145
Resolution (a.u.)	0.2	0.72	0.55	0.43	0.55	0.95
Compton intensity cts/hr/mm/ 0.03 a.u.	1.4	250	2650	520	210	10750
Peak-background ratio	5:1	2-500:1	70:1	1000:1	25:1	60:1
Detector	crystal analyser	Ge(Li)	intr. Ge	Ge(Li)	Ge(Li)	Si(Li)
Sample range (Z)	8	20	20	90	whole periodic table	25

* This work

Table 9-1

Comparison of sources for Compton scattering

hydrocarbons, respectively. The aims of this work were to extend the range of experimental data on molecular systems, and to investigate the potential of the gamma-ray technique to observe subtle differences in the bonding arrangement of these molecules. Furthermore, it was designed to test the validity of the localised molecular orbital (LMO) and self-consistent-field (SCF) descriptions of the electron momentum density in hydrocarbon systems.

The results, which have been described in detail in Chapters 5 and 6, have shown clearly the inadequacies of the current theoretical models based on single-molecule calculations. It is suggested that an improvement in these models may arise from either extending the basis set; including electron correlation (i.e. configuration interaction); and considering intermolecular interactions. From an experimental point of view measurements on gases would appear to be far more appropriate at the present time for comparison with present calculations.

Despite these effects the results have indicated that the LMO approach can provide a powerful tool for predicting the Compton profile of large molecules for which accurate wavefunction calculations are unfeasible. Such an approach should however, be used with caution since significant discrepancies exist when the Compton profiles of 'special' molecules are constructed. These special molecules have been shown to include:-

(a) highly strained cyclic molecules

(b) conjugated molecules

(c) resonant structures.

For these molecules perhaps a correction term can be incorporated into the LMO model as a second order effect dependent upon the non-local contributions to a LMO from the rest of the molecule. Although investigations of this nature are now in progress it has been suggested

that a repartitioning of the momentum density should be carried out. Exploratory work of this nature has been described in Chapter 6 where the momentum density has been partitioned into functional groups, i.e. C, CH, CH_2 and CH_3. Such localised groups have been shown to be highly transferable within the limited range of molecules studied, excluding groups (a) and (b) above. Although such a method does not solve the problem of comparing Compton profiles it may shed more light on some of the questions which are involved.

The high energy systems comprising of ^{198}Au sources of strengths 70 Ci and 120 Ci have been used to study the Compton profiles of Al, Nb, Sn, Pb and the hydride $NbH_{0.76}$. The use of a high energy source centre around the significant improvement in the momentum resolution and the removal of the limitations arising from photoelectric absorption. Furthermore, it enhances the validity of the impulse approximation which severely restricts the range of materials that can now be profitably studied with ^{241}Am.

Anisotropy measurements on Nb (100 and 110 directions) were found to be in qualitative agreement with a recent APW band structure calculation. The changes in the band electron profile which follows the introduction of hydrogen into the metal lattice have been interpreted quantitatively in terms of the protonic model of the hydride. The sensitivity of the profile to the amount of hydrogen in the metal lattice has invoked further investigations of metal hydride compounds. Future experiments with this source are described later in this chapter.

A Compton profile of lead was also determined with the 70 Ci ^{198}Au source in an attempt to observe the relativistic effects in heavy metals. The results, described in Chapter 7, showed qaulitative agreement with a recent relativistic Hartree-Fock calculation rather than a non-relativistic Hartree-Fock calculation. The experimental profile therefore provided evidence for the flattening of the profile at low values of momenta as

predicted. A more accurate study is proposed using the new 120 Ci ^{198}Au facility that has recently been constructed. Trial irradiations on Al and Sn samples have indicated a significant improvement in the intensity and signal-to-noise ratio (see table 9-1). The results with the ^{198}Au source have concluded that the usefulness of this technique is not in a determination of an absolute profile, but in experiments where interest is focussed on the differences between similar profiles.

In the remaining parts of this chapter the most likely developments in experimentation, not only in gamma-ray Compton scattering but also in the alternative techniques, are described, together with a possible future program of work for the two new gamma-ray systems described in this thesis.

9.2 Developments in Experimentation

9.2.1 Gamma-ray Sources

The development of the gamma-ray technique will probably centre around the use of high energy sources. Fundamental in the development of such systems will be the validity of the impulse approximation. In Appendix A some comments on this approximation and the effect it has on the profile if it is violated are discussed. The premature breakdown of the impulse approximation is one reason for favouring the development of high energy sources. For low energy systems like ^{241}Am this has meant a severe restriction on the elements and hence materials that can be profitably studied: typically $Z \leqslant 20$. Furthermore, other precautions should also be taken if this system is employed. Experience has shown that multiple Compton air scattering between the sample and detector greatly affects the symmetry of the final profile. A fully evacuated experimental arrangement would therefore offer the best chances of minimising errors arising from this effect. It is hoped to implement such an arrangement in the present ^{241}Am annular system. For high energy sources such scattering events are much less of a problem and consequently have little or no effect on the profile symmetry.

High energy sources that have a high specific activity can be profitably used despite their generally shorter half-lives. Although the choice of ^{198}Au appears to have been well founded, a recent study of gamma-ray sources by Cooper (1978) suggests that either of the rhenium isotopes, ^{186}Re (137 KeV) and ^{188}Re (150 KeV) would be other possibilities especially in view of the fact that they have twice the specific activity of gold. ^{203}Hg and ^{57}Cr are also likely candidates. It is not difficult to envisage Compton scattering experiments with initial source strengths of 500 Ci's (cf. 120 Ci ^{198}Au)

The possibility of having an in-situ neutron capture source has also been investigated. Unfortunately the high level of general background, and specific spectral contaminants, dismisses this type of source for Compton scattering studies. However, despite the versatility and advantages of undertaking experiments with high and low energy gamma-ray sources, the future of Compton scattering with them really rests with the development of a higher resolution detector. An order of magnitude improvement in resolution is required to approach the alternative techniques available, and before a wealth of new information can be collected.

9.2.2 X-ray Sources

Despite the superior resolution of the X-ray method very little work has been done to improve the technique from a Compton scattering point of view, although several recent developments have been reported. One such approach has been to eliminate the bremsstrahlung background by using the output of the X-ray tube to excite the characteristic radiation of a metal target by fluorescence; the fluorescence radiation then acts as a source for the experiment (Esslinger et. al., 1974). Although the background is severely reduced the counting rate is still extremely low, and furthermore the incident radiation is still a doublet requiring an $\alpha_1\alpha_2$ separation procedure.

Experiments of this nature call for further investigation, and one

method that could aid its development is to employ more powerful X-ray generators to increase the intensity. Rotating anode X-ray tubes rated at between 30 and 60 kW (cf. Mo X-ray sealed tube 2.4 kW) are now produced commercially. Such instruments should allow the incident X-ray beam to be efficiently monochromated. At present no Compton scattering studies have been made with such equipment although they have been used in the study of extended X-ray absorption fine structure (EXAFS) (Del Cueto and Shevchik, 1978). These recent studies also used a focussing geometry to produce a more brilliant source.

X-ray generators with a power rating of 100 kW are currently being developed, which may offer the possibility of using heavier target elements. Target materials such as tungsten and gold produce characteristic X-ray lines ($K_{\alpha_1\alpha_2}$) at 59.31 KeV, 57.97 KeV, and 68.79 KeV, 66.98 KeV, respectively. With such X-ray tubes a solid state detector may be employed to record the energy loss spectrum albeit at lower resolution.

9.2.3 Synchrotron Radiation

The possibilities of using synchrotron radiation as a source for Compton scattering studies has only recently been reported, following the initial experimental work of Cooper et. al. (1976) and Holt et. al. (1978). Details of the experimental procedure can be found in the authors M.Sc. thesis (Holt, 1976). The synchrotron source has many unique properties and a survey of its main characteristics can be found in Appendix B.

When comparing the synchrotron source properties with those of say an X-ray tube it can be seen that the brilliance of the synchrotron source is several orders of magnitude greater than that attainable from X-ray spectrometers. It is also highly collimated, having a divergence of less than 1 mrad at a wavelength of 1 Å. Such a beam can be efficiently monochromated with silicon or germanium perfect crystals which have rocking curves of similar angular width. In fact a highly collimated beam is an essential pre-requisite in elastic X-ray scattering but not so crucial

in Compton scattering experiments where a more divergent beam can be tolerated. In this case a comparison of the total monochromatic flux available from the synchrotron with that produced by an X-ray spectrometer can be shown to be not so advantageous.

Measurements of the Compton profiles of various metallic and ionic crystals in the energy range 10-80 KeV have been made using the NINA electron-synchrotron at the Daresbury Laboratory. The results have indicated an optimum energy for Compton scattering around 60 KeV where good statistical accuracy has been obtained from thin samples (measurements made at 74.3 KeV are described in Appendix B).

An improvement not only in the stability of the main photon beam but also in the intensity of the incident radiation can be visualised if synchrotron storage rings are used instead of the electron-synchrotron accelerators. To improve the intensity however, at these high energies required by Compton scattering, storage rings with a high characteristic energy ε_c, and operated at maximum electron energy E, are required (both ε_c and E determine the spectral distribution of the emitted radiation, see Appendix B). There are currently three storage rings which have $\varepsilon_c > 30$ KeV, they are Cornell IV (Ithaca, 35 KeV), PEP (Standford, 44 KeV) and PETRA (Hamburg, 75 KeV). The majority of storage rings (including the SRS at the Daresbury Laboratory) are contained within a band where $2 \leqslant \varepsilon_c \leqslant 30$ KeV. If these rings are to be profitably used for Compton scattering, and in order to obtain a high intensity of hard X-rays, it is necessary to use 'wigglers'. Such a device based on superconducting magnets, produces a small local deviation in the otherwise circular orbit, producing a greater acceleration at that point and hence a greater intensity of photon flux at a higher energy (see Suller, 1973). At the present time several types of wigglers are under construction.

A further unique property of synchrotron radiation concerns the state of polarization. In the plane of the electron orbit the radiation is plane polarized. In its full form the photon-electron scattering cross section contains a term in which a circularly polarized component of the radiation couples with the spin of the system. This term is only down by a factor of ω_i/mc^2 on the unpolarized term, which opens up the possibility of studying magnetic effects through Compton scattering. Work involving circularly polarized radiation has already been performed with considerable success despite the extreme experimental difficulties, e.g. cooling the gamma-ray source down to mK temperature (Sakai and Cho, 1977). Unfortunately X-ray sources are unpolarized, which leaves the synchrotron source as the only practical method for obtaining circularly polarized radiation.

The angular distribution of intensity components with the electric vector parallel and perpendicular to the plane of the electron orbit are shown in Fig. 9-1. Linear polarization and circular polarization (from decomposition into left and right circular polarized intensities I_L, and I_R respectively) are also given (ESF, 1977). Circularly polarized radiation only occurs in the weak, off axis direction. However, several experimental techniques are currently being devised, using a combination of a half, or quarter-waveplates, which will reduce the parallel component, and therefore produce a circularly polarized beam much closer to the plane of the electron orbit and at a much greater intensity.

Finally, synchrotron radiation could be employed without a monochromator to excite characteristic radiation in much the same manner as the fluorescence technique from an X-ray tube. Because of the large integrated intensity from a synchrotron such an arrangement should provide a very strong source of characteristic radiation.

A further unique property of synchrotron radiation concerns the state of polarization. In the plane of the electron orbit the radiation is plane polarized. In its full form the photon-electron scattering cross section contains a term in which a circularly polarized component of the radiation couples with the spin of the system. This term is only down by a factor of ω_i/mc^2 on the unpolarized term, which opens up the possibility of studying magnetic effects through Compton scattering. Work involving circularly polarized radiation has already been performed with considerable success despite the extreme experimental difficulties, e.g. cooling the gamma-ray source down to mK temperature (Sakai and Ono, 1977). Unfortunately X-ray sources are unpolarized, which leaves the synchrotron source as the only practical method for obtaining circularly polarized radiation.

The angular distribution of intensity components with the electric vector parallel and perpendicular to the plane of the electron orbit are shown in Fig. 9-1. Linear polarization and circular polarization (from decomposition into left and right circular polarized intensities I_L, and I_R respectively) are also given (ESF, 1977). Circularly polarized radiation only occurs in the weak, off axis direction. However, several experimental techniques are currently being devised, using a combination of a half, or quarter-waveplates, which will reduce the parallel component, and therefore produce a circularly polarized beam much closer to the plane of the electron orbit and at a much greater intensity.

Finally, synchrotron radiation could be employed without a monochromator to excite characteristic radiation in much the same manner as the fluorescence technique from an X-ray tube. Because of the large integrated intensity from a synchrotron such an arrangement should provide a very strong source of characteristic radiation.

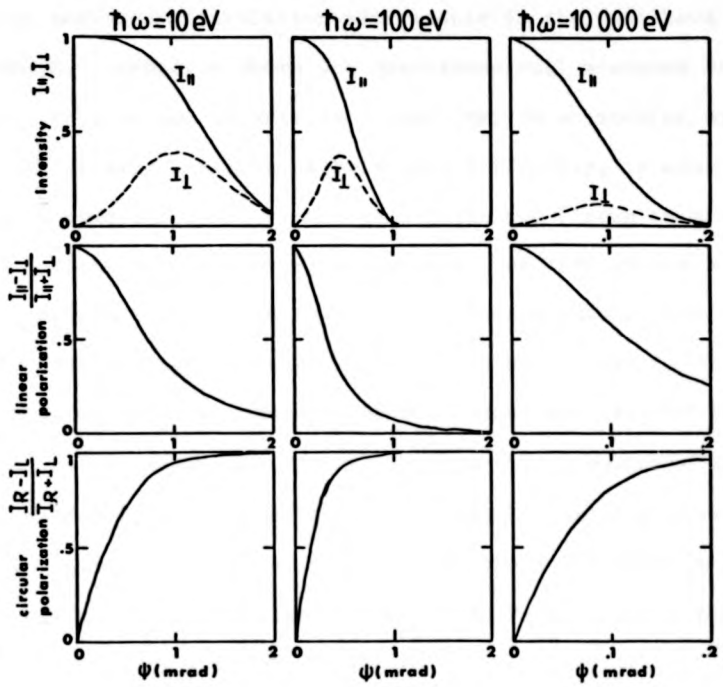

Fig. 9-1: Angular distribution of intensity components with the electric vector parallel and perpendicular to the plane of the electron orbit (data taken from ESF, 1977)

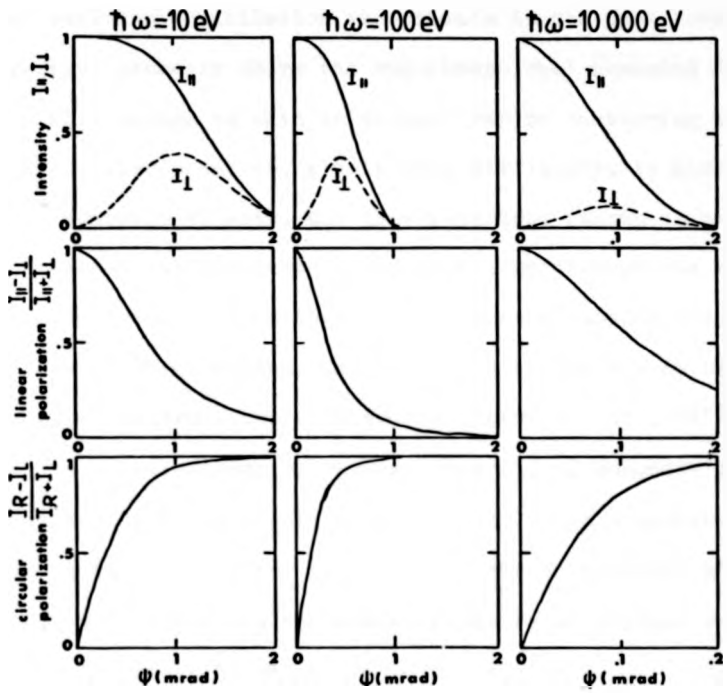

Fig. 9-1: Angular distribution of intensity components with the electric vector parallel and perpendicular to the plane of the electron orbit (data taken from ESF, 1977)

9.2.4 Alternative Techniques

(i) Positron Annihilation

Most positron annihilation experiments in the past have employed the 'long-slit' geometry where the one-dimensional momentum density is measured. This method is akin to photon Compton scattering experiments. However, it is also possible, albeit with difficulty, to measure the two-dimensional momentum density, and this technique (known as either 'crossed-slit' or 'point-slit' geometry) measures a line through the momentum density. Recent advances in this technique have enabled the two-dimensional momentum density of aluminium, and several other metals to be determined, by employing an external positron source (Mader et. al., 1976). The intrinsic low counting rate of the two-dimensional geometry has been compensated for by using a multicounter correlation apparatus. This method appears to be best suited for the study of the Fermi surface in metals and alloys where the changes in the shape of the Fermi surface can be investigated in detail (Berko, 1978).

(ii) HEEIS

The HEEIS technique is best suited for high resolution measurements on gaseous samples. Although it is fast and accurate the requirements of gaseous samples of light elements severely restricts its versatility. The possibility of studying liquid matter either by vapourising them or by using very thin films are currently being investigated, and developments of this nature could ease these restrictions (Wellenstein and Rueckner, 1978).

(iii) (e,2e)

Although this technique is capable of providing detailed information about the momentum density directly and not an integral of the density, the resolution and restriction to gases limits the method. Recent developments in the experimental technique (Coplan, 1978) coupled with the feature that it measures the momentum density of each electron orbital

separately, provides an attractive method for looking in particular at simple molecular systems.

9.3 Future Experiments

Although there has been a significant amount of progress during the last thirteen years, it is only comparatively recently that the technique has evolved into an accurate tool for the determination of electron momentum distributions. This has allowed accurate and detailed comparisons with theoretical wavefunction calculations. The two new Compton spectrometers described in this thesis and the application of them to molecular and metallic systems have given only an indication as to their true potential and capability. The likely developments in some of the present lines of investigations and the future experiments can be divided into two parts depending on the atomic weight of the elements in the sample.

In view of the sensitivity of the Compton profile to subtle changes in the electron density which accompany bond formation, it is now realistic to investigate the bonding in say the simple gaseous hydrocarbons CH_4, C_2H_2, C_2H_4, C_2H_6 etc. using the low energy ^{241}Am source. Such measurements will allow detailed comparisons not only with theoretical calculations but also with profiles obtained from other techniques, such as HEEIS which is necessarily restricted to measurements on gases.

A possible extension to this work is the study of boron hydrides. In these electron deficient materials the normal two-centre bond does not arise because of the shortage of electrons. Instead three-centre bonds are formed in which the three centres are linked by a single orbital. These highly delocalised electron orbitals are akin to free electron behaviour in metals, and the molecules provide a good example of metal-like behaviour in a molecular system. Theoretical profiles for a range of boron hydride molecules are available employing a LMO approach similar to that used in the description of the hydrocarbons (Epstein and Lipscomb, 1970)

Compton scattering measurements on other organic molecules provide an extensive range of systems for study. A particular area in this respect is a study of solutions. Positron annihilation work on metal-ammonia solutions (Varlashkin and Arias-Limonta, 1971) and recent X-ray Compton measurements on a water-methanol mixture (Camp et. al., 1978) suggests that such studies may be quite revealing.

All of the molecular systems so far discussed are isotropic at room temperature, so that a considerable amount of structural information contained in the Compton profile is lost. Measurements on oriented molecules would therefore be much more interesting and this has been shown recently in measurements on a single crystal of urea (Reed et. al., 1978). In this system the H_2NCONH_2 molecules are lined up parallel to the C=O bond. The extremely large anisotropy found in the momentum density arises from the anisotropy in the bonded electron density. Measurements of this kind can usefully complement X-ray diffraction studies of charge densities. To obtain complementary information on other simple organic systems will require a cryostat and some modifications to the low energy system described in Chapter 4.

Changes in electron density which accompany phase transitions in various metals and alloys is another potential area for investigation. So far very little work has been done in this area and possible experiments may include:-

(i) The metal-insulator transition in VO_2. Recent positron annihilation data suggests that the two phases have different momentum distributions (Andreeff and Brauer, 1976).

(ii) Cu-Mn alloys where the transition to an antiferromagnet is accompanied by a tetrahedral distortion.

(iii) The Li-Mg system where there is already some evidence from positron annihilation data for a departure of the momentum

density from that predicted by the sum of the constituents (Brummer et. al., 1973)

The first two points (i and ii) may of course be better suited for study with the 412 KeV ^{198}Au facility. Another material that is particularly suitable for this source is the grey tin - white tin transition which involves a 10% increase in the interatomic spacing. Accurate measurements on heavy metals may also provide further confirmation of the relativistic corrections to the momentum density by studying the Compton profile, and using the facility as a gamma-diffractometer, by studying the form factor at high values of $\sin\theta/\lambda$.

Most of the work with this facility will probably be undertaken on the metallic hydrides. The results described in Chapter 7 have shown that the Compton profile is rather sensitive to the behaviour of hydrogen in metals. Accurate anisotropy measurements on other systems would be particularly useful, and possible experiments may include :-

(i) Cerium and its hydrides across the range of composition and through the metal-semiconductor transition.

(ii) Vanadium and vanadium hydride, for which a band structure calculation of the momentum density for the metal is available.

Such investigations present an attractive extension to the work already performed with the 412 KeV system at ILL.

If the Compton profile of a material is measured in enough different crystal directions, the three-dimensional distribution can be reconstructed (Mijnarends, 1977). In practice however, this means a long series of highly accurate experiments. With the development of more powerful sources and the rapid accumulation of data with good statistical accuracy, such an approach may well prove rewarding.

Finally, a new method of analysing Compton profile data has recently been introduced (Pattison et. al., 1977, Schülke, 1977). The method

involves the Fourier transform, B(z) of the Compton profile $J(p_z)$ to give an auto-correlation function of the wavefunction,

$$B(z) = \int \psi^*(\bar{r})\,\psi(\bar{r}+z)\,d\bar{r} \qquad 9\text{-}1$$

and as such is a close relative of the coordinate space density $\psi^*(\bar{r})\,\psi(\bar{r})$. The procedure was developed to alleviate the problems in the interpretation of the experimental and theoretical Compton profile data and in relating this data to information produced by the more conventional techniques, e.g. electron density in position space. The problems associated with the interpretation of momentum space properties are perhaps highlighted with reference to Fig. 1-2 given in the introduction of this thesis. The familiar landmarks of the two nuclei in position space disappear to give a density map with only a single peak (auxiliary peaks appear as a result of the oscillations arising from the cosine term in the expression for the momentum density). Developments in this area are expected to assist in the significant advances that are likely to evolve during the next decade.

9.1 Summary

The gamma-ray Compton scattering technique has only recently developed from a qualitative study of the nature of momentum distributions into an accurate method for testing current theoretical models of electronic structure. A significant part of the author's work has been to design and construct two gamma-ray Compton spectrometers which have given an order of magnitude improvement in the accuracy and quality of the profiles obtained. The results of this development in the experimental technique and the subsequent application of the techniques to metallic and molecular systems have shown quite clearly that statistically accurate Compton profile measurements can now be reliably interpreted in terms of electron momentum. The subtle differences in the profiles which have been

observed and described in this thesis, have given for the first time a crtical assessment of the potential and reliability of the gamma-ray technique, and has provided a firm basis for the future development of more detailed studies.

REFERENCES

AHLENIUS T. and LINDNER P. (1975) J.Phys.B. 8, 778

ALEXANDROPOULOUS N.G. and REED W.A. (1977) Phys.Rev. B15, 1790

ANDREFF A. and BRAUER G. (1976) Phys.Stat.Sol.(b). 75, K115

BACHMANN P. (1975) Diplomarbeit, Technischen Hochschule, Darmstadt

BARLAS A.D., RUECKNER W. and WELLENSTEIN H.F. (1977) Phil.Mag. 36, 201; (1978) to be published

BECKER P. (1977) Phys.Scripta. 15, 119

BENESCH R. (1978) J.Phys.B. to be published

BENESCH R. and SMITH V.H.Jr. (1972) Phys.Rev. A5, 114

BENESCH R. and SMITH V.H.Jr. (1973) "Wave Mechanics - The First Fifty Years", ed. Price,Chissick and Ravensdale.(Butterworths, London)

BERGGREN K-F. (1972) Phys.Rev. B6, 2156

BERGGREN K-F. and MARTINO F. (1971) Phys.Rev. B3, 1509

BERGGREN K-F., MARTINO F., EISENBERGER P. and REED W.A. (1976) Phys.Rev. B13, 2292

BERKO S. (1978) private communication

BERKO S. and MADER J. (1975) Appl.Phys. 5, 287

BETHE H.A. and SALPETER E.E. (1957) "Quantum Mechanics of One- and Two-Electron Atoms", (Academic Press, N.Y.)

BIGGS F., MENDELSOHN L.B. and MANN J.B. (1975) Atom.Nucl.Data Tables. 16, 202

BLOCH B.J. and MENDELSOHN L.B. (1974) Phys.Rev. A9, 129

BONHAM R.A. and FINK M. (1974) "High Energy Electron Scattering" Ch.5 and 6. (Van Nostrand Reinhold, N.Y.)

BRAUN-KELLER E. and EPSTEIN I.R. (1976) Chem.Phys.Lett. 40, 215

BRUMMER O., BERNDT K. and SCHÜLKE W. (1973) Proc.Int.Conf. on X-ray Processes in Matter (Munchen)., p260

CADE P.E., HENNEKER W.H. and KOSTYLA A. (1978) to be published

CAMP N., EPSTEIN I.R. and WEISS R.J. (1978) Phil.Mag. B37, 43

CARBOTTE J.P. and SALVADORI A. (1967) Phys.Rev. 162, 290

CHENG R., WILLIAMS B. and COOPER M. (1971) Phil.Mag. 23, 115

CHUANG S.Y. and HOGG B.G. (1967) Can.J.Phys. 45, 3895

CLEMENTI E. (1965) I.B.M.J.Res.Dev. 9, 2

COMPTON A.H. (1923) Phys.Rev. 22, 412

COOPER M.J. (1967) Dissertation for the degree of Ph.D., University of Cambridge

COOPER M.J. (1971) Adv.Phys. 20, 453; (1977) Phys.Bulletin.,Oct.(I.O.P.); (1977) Contemp.Phys. 18, 489; (1978) Nucl.Inst.Meth. to be published

COOPER M.J., HOLT R.S. and DuBARD J.L. (1978) J.Phys.E. accepted for publication

COOPER M.J., LEAKE J.A. and WEISS R.J. (1965) Phil.Mag. 12, 797

COOPER M.J., PATTISON P. and SCHNEIDER J.R. (1976) Phil.Mag. 34, 243

COOPER M.J., HOLT R.S., PATTISON P. and LEA K.R. (1976) Comm. on Phys. 1, 159

COOPER M.J., PATTISON P., WILLIAMS B.G. and PANDEY K.C. (1974) Phil.Mag. 29, 1237

COPLAN M.A. (1978) private communication

COULSON C.A. (1973) Mol.Phys. 26, 507

COULSON C.A. and DUNCANSON W.E. (1941) Proc.Camb.Phil.Soc. 37, 55; (1941) Ibid. 37, 67; (1941) Ibid. 37, 74; (1941) Ibid. 37, 406; (1942) Ibid. 38, 100

CRISP R.S. and WILLIAMS S.E. (1960) Phil.Mag. 5, 525

CURRAT R., DeCICCO P.D. and WEISS R.J. (1971) Phys.Rev. B4, 4256

DEL CUETO J.A. and SHEVCHIK N.J. (1978) J.Phys.E. 11, 616

DONIAH S., PLATZMAN P.M. and YUE J.T. (1971) Phys.Rev. B4, 3345

DuBARD J.L. (1978) Phil.Mag. B37, 273; (1978) J.Phys.E. to be published

DuMOND J.W.M. (1929) Phys.Rev. 33, 643

DuMOND J.W.M. (1930) Phys.Rev. 36, 1685

DuMOND J.W.M. and KIRKPATRICK H.A. (1937) Phys.Rev. 52, 419

DUNCANSON W.E. (1941) Proc.Camb.Phil.Soc. 37, 397; (1943) Ibid. 39, 180

DUNSTER H.J., ELLIS R.E., JONES B.E., JONES E.W. and REES J.M. (1971) "Handbook of Radiological Protection". (HMSO., London)

EHRHARDT H., SCHULZ M., TAKAAT T. and WILLMA K. (1969) Phys.Rev.Lett. 22, 89

EISENBERGER P. (1970) Phys.Rev. A2, 1078; (1972) Ibid. A5, 628

EISENBERGER P. and MARRA W.C. (1971) Phys.Rev.Lett. 27, 1413

EISENBERGER P. and PLATZMAN P.M. (1970) Phys.Rev. A2, 415

EISENBERGER P. and REED W.A. (1972) Phys.Rev. A5, 2085; (1974) Ibid. B9, 3237; (1974) Ibid. B9, 3242

EPSTEIN I.R. (1970) J.Chem.Phys. 53, 4425; (1973) Phys.Rev. A8, 160

EPSTEIN I.R. and LIPSCOMB W.N. (1970) J.Chem.Phys. 53, 4418

EPSTEIN I.R. and TANNER A.C. (1977) "Compton Scattering" ed. B.G.Williams, Ch.7.(McGraw-Hill)

EPSTEIN I.R., WILLIAMS B.G. and COOPER M.J. (1973) J.Chem.Phys. 58, 4098

EPSTEIN I.R., PATTISON P., WALLBRIDGE M.G.H. and COOPER M.J. (1975) J.Chem.Soc.Chem.Comm. 567

ESSLINGER D., HOSEMANN R., MULLER A. and WEICK D. (1974) J.Appl.Phys. 45,4100

EUROPEAN SCIENCE FOUNDATION (ESF) (1977) "Synchrotron Radiation a Perspective View for Europe" (Strasbourg) p73

FEINBERG M.J. and RUEDENBERG K. (1971) J.Chem.Phys. 54, 1495

FELSTEINER J. and PATTISON P. (1975) Nucl.Inst.Meth. 124, 449; (1976) Phys.Rev. B13, 2702

FELSTEINER J., FOX R. and KAHANE S. (1970) Phys.Lett. 33A, 442; (1971) Sol.St.Comm. 9, 61

FELSTEINER J., PATTISON P. and COOPER M.J. (1974) Phil.Mag. 30, 537

FRANKLIN J.L. (1949) Ind.Eng.Chem. 41, 1070

FUKAMACHI T. and HOSOYA S. (1970) J.Phys.Soc.Japan. 29, 736; (1972) Tech.Rep.Inst.Sol.St.Phys. A, 529

GENERAL ELECTRIC COMPANY (GEC-OSRAM) (1964) "Heavy Alloy for Industry"

GROSSMAN H. and MENDELSOHN L.B. (1978) to be published

HALONEN V. (1975) Dissertation for the degree of Ph.D., University of Helsinki, Finland

HALONEN V. and WILLIAMS B.G. (1975) Phys.Fenn. 10, 5

HALONEN V., WILLIAMS B.G. and PAAKKARI T. (1975) Phys.Fenn. 10, 107

HENNECKER W.H. and CADE P.E. (1968) Chem.Phys.Lett. 2, 8; (1968) Ibid. 2, 575

HICKS B.L. (1937) Phys.Rev. 52, 436; (1940) Ibid. 57, 665

HIRST D.M. (1978) private communication

HIRST D.M. and LIEBMANN S.P. (1975) Mol.Phys. 30, 1693; (1976) Chem.Phys.Lett. 42, 403

HOLT R.S. (1976) Dissertation for the degree of M.Sc., University of Warwick

HOLT R.S., COOPER M. and HIRST D.M. (1978) Chem.Phys.Lett. 55, 284

HOLT R.S., COOPER M.J. and LEA K.R. (1978) J.Phys.E. 11, 68

HUGHES A.L. and MANN M.M. (1938) Phys.Rev. 53, 50

HUGHES A.L. and ENNS T. (1941) Phys.Rev. 55, 343

INKINEN O., HALONEN V. and MANNINEN S. (1971) Chem.Phys.Lett. 9, 639

JAUCH J.M. and ROHRLICH F. (1955) "Theory of Photons and Electrons" Cambridge, Mass. (Addison-Wesley)

JAUNCEY G.E.M. (1924) Phys.Rev. 24, 204

KAIJSER P. and LINDNER P. (1975) Phil.Mag. 31, 871

KAPPELER H. (1936) Ann.der.Phys. 27, 129

KILBY G.E. (1963) Proc.Phys.Soc. 82, 530

KIRKPATRICK H.A. and DuMOND J.W.M. (1938) Phys.Rev. 54, 802

KITTEL C. (1971) "Introduction to Solid State Physics". (Wiley)

KLEIN O. and NISHINA Y. (1929) Z.Physik. 52, 853

LANGHOFF S.R. and TAWIL R.A. (1975) J.Chem.Phys. 63, 2745

LEDERER C.M., HOLLANDER J.M. and PERLMAN I. (1967) "Tables of Isotopes sixth edition (Wiley, N.Y.)

LIBOWITZ G.G. (1965) "The Solid State Chemistry of Binary Metal Hydrides" (Benjamin, N.Y.)

LINDNER P. (1977) Phys.Scripta. 15, 112

LLOYD H.H. (1969) Am.J.Phys. 37, 329

MADER J., BERKO S., KRAKAUER H. and BANSIL A. (1976) Phys.Rev.Lett. 37, 1232

MAHAN G.D. (1967) Phys.Rev. 163, 612

MANNINEN S., PAAKKARI T. and KAJANTIE J. (1974) Phil.Mag. 29, 167

MANNINEN S., PAAKKARI T., AIKALA O. and MANSIKKA K. (1973) J.Phys.C. 6, L410

MANNINEN S., PATTISON P., COOPER M.J., AHLENIUS T. and LINDNER P. (1975) Chem.Phys.Lett. 36, 92

MARCH N.H. (1954) Proc.Phys.Soc. 67, 9

MATTHEISS L.F. (1970) Phys.Rev. B1, 373

MENDELSOHN L.B. (1978) private communication to M.J.Cooper

MENDELSOHN L.B. and BLOCH B.J. (1975) Phys.Rev. A12, 551

MENDELSOHN L.B. and GROSSMANN H. (1977) "Momentum Wavefunctions"., Am. Inst.Phys.Conf.Proc. *36., ed D.W.Devins., p 249

MENDELSOHN L.B., BIGGS F. and MANN J.B. (1974) Chem.Phys.Lett. 26, 521

MESSIAH A. (1961) "Quantum Mechanics" ., Vol.1. (North Holland, Amsterdam)

MIJNARENDS P.E. (1977) "Compton Scattering" ed. B.G.Williams., Ch. 10. (McGraw-Hill)

MUELLER W.M., BLACKLEDGE J.P. and LIBOWITZ G.G. (1968) "Metal Hydrides" (Academic Press, N.Y.)

McCARTHY I.E., NOBLE C.J., UGABE A. and WEIGOLD E. (1978) to be published

McINTIRE W.R. (1974) Phys.Stat.Sol.(a) 23, 359: (1976) Phys.Rev. B14, 4386

McINTIRE W.R. and BATTERMAN B.W. (1974) Phys.Stat.Sol.(b) 63, 621

McINTYRE J.A., NHA S.K. and MORELAND R.W. (1967) Bull.Am.Phys.Soc. 12, 177

McMASTER W.H., DEL GRANDE N.K., MALLETT J.H. and HUBBELL J.H. (1969) "Compilation of X-ray Cross Sections" UCRL-50174 (unpublished)

McWEENY R. and COULSON C.A. (1949) Proc.Phys.Soc. 62A, 509

OHARA S., FUKAMACHI T., HOSOYA S., TAKEDA T. and TERASAKI O. (1974) Phys.Lett. 49A, 337

PAAKKARI T. (1974) Phys.Fenn. 9, 185

PAAKKARI T., MANNINEN S. and BERGGREN K-F. (1975) Phys.Fenn. 10, 207

PAAKKARI T., BERGGREN K-F., RIBBERFORS R. and HALONEN V. (1976) Phys.Rev. B14. 2301

PAAKKARI T., KOHONEN E-L., AIKALA O., MANSIKKA K. and MIKKOLA S. (1974) Phys.Fenn. 9, 207

PAATERO P., MANNINEN S. and PAAKKARI T. (1974) Phil.Mag. 30, 1281

PANDEY K.C. and LAM L. (1973) Phys.Lett. A43, 319

PATTISON P. (1975) Dissertation for the degree of Ph.D., University of Warwick

PATTISON P. (1978) private communication

PATTISON P., COOPER M.J. and SCHNEIDER J.R. (1976) Zeits.Phys. B25, 155

PATTISON P., WEYRICH W. and WILLIAMS B.G. (1977) Sol.St.Comm. 21, 967

PATTISON P., MANNINEN S., FELSTEINER J. and COOPER M. (1974) Phil.Mag. 30,973

PHILLIPS W.C. and CHIN A.K. (1973) Phil.Mag. 27, 87

PHILLIPS W.C. and WEISS R.J. (1968) Phys.Rev. 171, 790

PLATZMAN P.M. and TZOAR N. (1965) Phys.Rev. 139, 410; (1977) "Compton Scattering" ed. B.G.Williams., Ch. 2. (McGraw-Hill)

POOLE M.W. (1974) Daresbury Laboratory Internal Report, DL/TM 130

REED W.A. (1976) Acta.Cryst. A32, 676; (1978) to be published

REED W.A. and EISENBERGER P. (1972) Phys.Rev. B6, 4596

REED W.A., EISENBERGER P., MARTINO F. and BERGGREN K-F. (1975) Phys.Rev.Lett. 35, 114

REED W.A., EISENBERGER P., PANDEY K.C. and SNYDER L.C. (1974) Phys.Rev. B10, 1507

REED W.A., SNYDER L.C., GUGGENHEIM H.J., WEBER T.A. and WASSERMAN Z.R. (1978) to be published

REINSCH C.H. (1967) Num.Math. 10, 177

RIBBERFORS R. (1975) Phys.Rev. B12, 2067; (1975) Ibid. B12, 3136

ROOTHAAN C.C.J. (1951) Rev.Mod.Phys. 23, 69

ROSS P.A. and KIRKPATRICK P. (1934) Phys.Rev. 46, 668: (1934) Ibid. 45, 223

ROUX M. and EPSTEIN I.R. (1973) Chem.Phys.Lett. 18, 18

SAKAI N. and ONO K. (1977) J.Phys.Soc.Japan. 42, 770

SAUNDERS V.R. and GUEST M.F. (1975) ATMOL 3 Reference Manual, Atlas Computing Division, Rutherford Laboratory, Oxon.

SCHLEYER P.V.R., WILLIAMS J.E. and BLANCHARD K.R. (1970) J.Am.Chem.Soc 98, 2377

SCHNEIDER J.R. (1974) J.Appl.Cryst. 7, 541

SCHOBER T. (1975) Phys.Stat.Sol.(a) 29, 395; (1975) Ibid. 30, 107

SCHOBER T., LINKE U. and WENZL H. (1974) Scripta.Met. 8, 805

SCHULKE W. (1977) Phys.Stat.Sol.(b) 80, 67

SHIOTANI N., OKADA T., MIZOGUCHI T. and SEKIZAWA H. (1975) J.Phys.Soc. Japan. 38, 423

SMITH V.H.Jr. (1977) Phys.Scripta. 15, 147

SMITH V.H.Jr. and BROWN R.E. (1973) Chem.Phys.Lett. 20, 424

SMITH V.H.Jr. and WHANGBO M.H. (1974) Chem.Phys. 5, 234

SNYDER L.C. and WEBER T.A. (1978) to be published

STOKES A.R. (1948) Proc.Phys.Soc. 61, 382

SULLER V.P. (1973) Daresbury Laboratory Technical Memorandum, DL/TM 118

TANNER A.C. and EPSTEIN I.R. (1974) Chem.Phys.Lett. 25, 143; (1976) Phys. Rev. A13, 335; (1976) Ibid. A14, 313; (1976) Ibid. A14, 328

TAVARD C. (1978) private communication to M.J.Cooper

TAWIL R.A. and LANGHOFF S.R. (1975) J.Chem.Phys. 63, 1572

WAKOH S. and YAMASHITA J. (1973) J.Phys.Soc.Japan. 35, 1406

WAKOH S., KUBO Y. and YAMASHITA J. (1976) J.Phys.Soc.Japan. 40, 1043

WAKOH S., FUKUMACHI T., HOSOYA S. and YAMASHITA J. (1975) J.Phys.Soc. Japan. 38, 1601

WEIGOLD E., HOOD S.T. and McCARTHY I.E. (1975) Phys.Rev. A11, 566

WEISS R.J. (1966) Phil.Mag. 14, 403; (1970) J.Chem.Phys. 52, 2237; (1972) Phil.Mag. 26, 153; (1973) Ibid. 27, 1461; (1975) Ibid. 32, 247 (1978) to be published

WEISS R.J., COOPER M.J. and HOLT R.S. (1977) Phil.Mag. 36, 193

WELLENSTEIN H.F. and BONHAM R.A. (1973) Phys.Rev. A7, 1568

WELLENSTEIN H.F. and RUECKNER W. (1978) private communication

WEPFER G.G., EUWEMA N., SURRAT G.T. and WILHITE D.L. (1973) Int. J.Quant. Chem. 7, 613; (1974) Phys.Rev. B9, 2670

WEST R.N. (1973) Adv.Phys. 22, 263

WEYRICH W. (1975) Ber.Bunsenges.Phys.Chem. 79, 1085

WEYRICH W. and PATTISON P. (1975) private communication

WILLIAMS B.G. (1976) Acta.Cryst. A32, 513; (1977) "Compton Scattering" (McGraw-Hill)

WILLIAMS B.G., PATTISON P. and COOPER M.J. (1974) Phil.Mag. 30, 307

APPENDICES

Appendix A. Asymmetry of Compton lines and the Compton defect.

Appendix B. Compton scattering with synchrotron radiation.

APPENDIX A

ASYMMETRY OF COMPTON LINES

AND THE COMPTON DEFECT

In the impulse approximation the Compton profile J(q) is given by

$$J(q) = \frac{1}{2}\int_{q}^{\infty}\frac{1}{p}\left|\chi(p)\right|^2 d^3p \qquad \text{A-1}$$

where $\left|\chi(p)\right|^2$ is the momentum probability distribution in the atom. From this definition of J(q) it is clear that within the impulse approximation the Compton profile is a symmetric monotonic decreasing function of q with increasing q. The maximum of J(q) always occurs at q = 0. Any departure from this symmetry about q = 0 can be classified into two major effects:-

(i) asymmetry of the line

(ii) the defect in the shifted line.

Both signal the breakdown of the impulse approximation. A brief synopsis of the validity of this approximation has already been given in Chapter 2. In this appendix only the very recent work on this problem is covered, in an attempt to explain the asymmetry in the Compton line for relatively high Z materials obtained with 60 KeV radiation.

Mendelsohn and Grossman (1977) have recently undertaken Excited State Hartree-Slater (EHS) calculations on aluminium as a function of increasing photon energy. For s states the defects are typically negative and move toward zero with increasing momentum transfer. For p states the defects are typically positive. Thus both negative and positive defects for the entire atom are possible depending on the number of filled outer s and p orbitals, and the experimental conditions. For aluminium they obtain a total negative defect of -2.5 eV (at 17.4 KeV) compared with experimental values of -10±7 eV (Weiss, 1975) and -12±4 eV (Weiss et. al., 1977).

More recently Grossman and Mendelsohn (1978) have performed calculations using bound state continuum Hartree-Slater wavefunctions in the frozen core approximation. For an outer filled p shell, as found in the rare gases, they expect positive defects. This has been confirmed for neon and krypton using the (e,2e) technique (McCarthy et. al., 1978). Furthermore, the theoretical prediction of a negative defect in helium has also been observed experimentally using the same technique. A more extensive series of measurements with high energy electron scattering by Barlas et. al. (1978) on simple diatomic and inert gases have provided further support to these theoretical calculations.

The validity of the impulse approximation in aluminium has also been investigated theoretically at higher incident photon energies. For 60 KeV radiation Mendelsohn (1978) has determined that such an approximation is valid for the total profile only, and is not valid for individual s and p orbitals. This somewhat surprising result was not expected a priori, and has meant that experimentalists should be aware of presenting valence Compton profiles, where a free atom core profile has been subtracted out. Further calculations are presently underway to determine the validity of the approximation for high Z materials. Fortunately, systems containing light elements e.g. hydrocarbons, do not suffer from such defects and the results presented (total profiles only) are unaffected by this discrepency. Calculations for 159 KeV radiation on aluminium result in a negligible defect in the s and p orbitals with the conclusion that higher energy sources offer the possibility of avoiding impulse approximation problems.

The results of the calculations for aluminium at 17.4 KeV (Mendelsohn and Grossman, 1977) produce a profile that is asymmetric, with the negative q side lying higher than the positive q side, in agreement with the experimental results. If the theoretical profile is centred about

the position to be expected for free electrons, then a maximum in the asymmetry is reached around 0.5 a.u. with a magnitude of about 0.5% of J(0). For 60 KeV radiation preliminary results for the M shell indicates a large asymmetry around 0.5 a.u. of about 3% of J(0) compared with an experimental value of just over 1% for the total profile. Similar experimental asymmetries of greater magnitude have been observed in measurements on vanadium and iron, although non has been found in lithium. An analysis of experiments performed on atomic gases may provide a true test of the accuracy of the EHS method for calculating defects. A gas sample chamber is presently under construction.

the position to be expected for free electrons, then a maximum in the asymmetry is reached around 0.5 a.u. with a magnitude of about 0.5% of J(0). For 60 KeV radiation preliminary results for the M shell indicates a large asymmetry around 0.5 a.u. of about 3% of J(0) compared with an experimental value of just over 1% for the total profile. Similar experimental asymmetries of greater magnitude have been observed in measurements on vanadium and iron, although non has been found in lithium. An analysis of experiments performed on atomic gases may provide a true test of the accuracy of the EHS method for calculating defects. A gas sample chamber is presently under construction.

APPENDIX B

COMPTON SCATTERING WITH SYNCHROTRON RADIATION

(i) Emission Characteristics of Synchrotron Radiation

The important properties of synchrotron radiation can be understood in a qualitative manner by considering the classical picture of an oscillating dipole, and the relativistic transformation of the dipole radiation pattern into the laboratory frame (see Fig. B-1). At relativistic velocities the dipole radiation is strongly peaked in the forward direction in the laboratory frame.

A measure of the useful photon flux from this source $N(\lambda)$ can be expressed in terms of the number of photons emitted per second per milliradian of horizontal angle in the wavelength range $\Delta\lambda$ ($\Delta\lambda$ is the bandwidth where $\Delta\lambda/\lambda \sim 10^{-3}$), i.e.

$$N(\lambda) = \beta \left(\frac{\lambda}{\lambda_c}\right) E G\left(\frac{\lambda}{\lambda_c}\right) \qquad \text{B-1}$$

where λ_c is the characteristic (also called critical) wavelength of the spectrum, β is a constant, G is a universal numerical function and E is the electron energy in GeV. The characteristic wavelength is given by

$$\lambda_c = \frac{4\pi R}{3} \gamma^{-3} \qquad \text{B-2}$$

where $\gamma = E/(mc^2)$, and R is the radius of curvature of the electron orbit (Suller, 1973). Eqn. B-1 shows that $N(\lambda)$ is directly proportional to E, and depends on E and λ/λ_c. Therefore it is possible using eqns. B-1 and B-2 to obtain the spectrum for any accelerator by plotting $N(\lambda)/E$ against λ/λ_c as shown in Fig. B-2. Two important points can be discerned from this figure. Firstly, for $\lambda \gg \lambda_c$ the photon flux is independent of electron

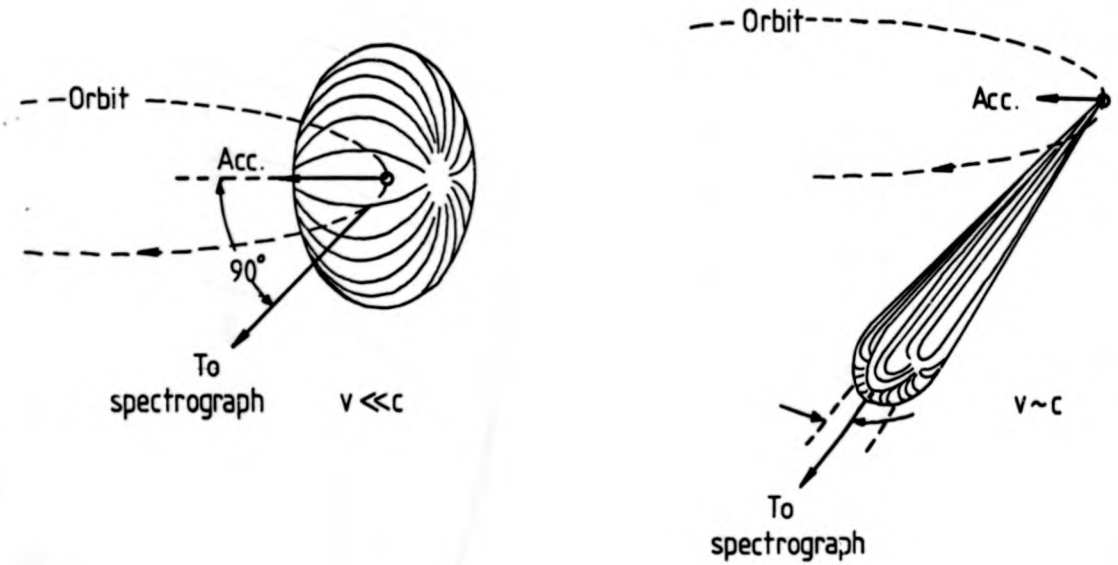

Fig. B-1: Radiation pattern produced by a radially accelerated electron.

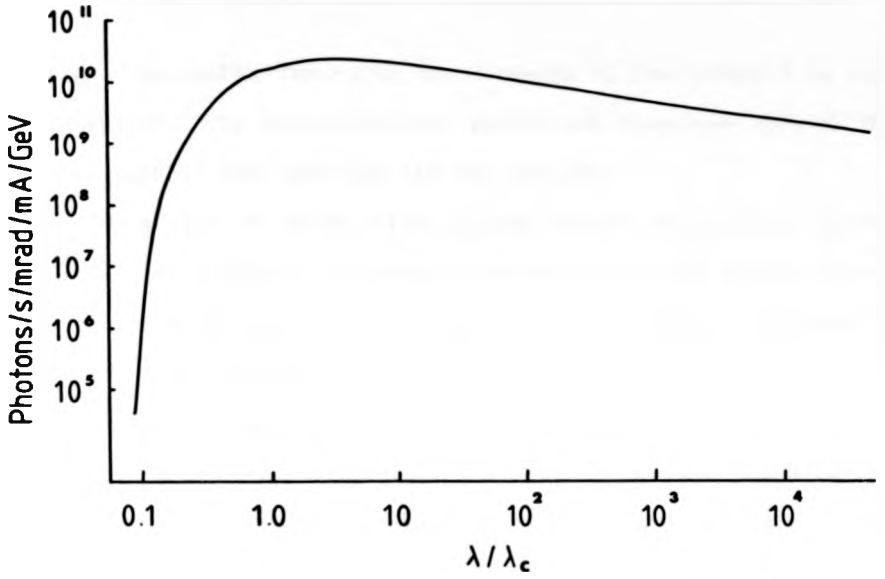

Fig. B-2: The universal spectral curve for synchrotron radiation.

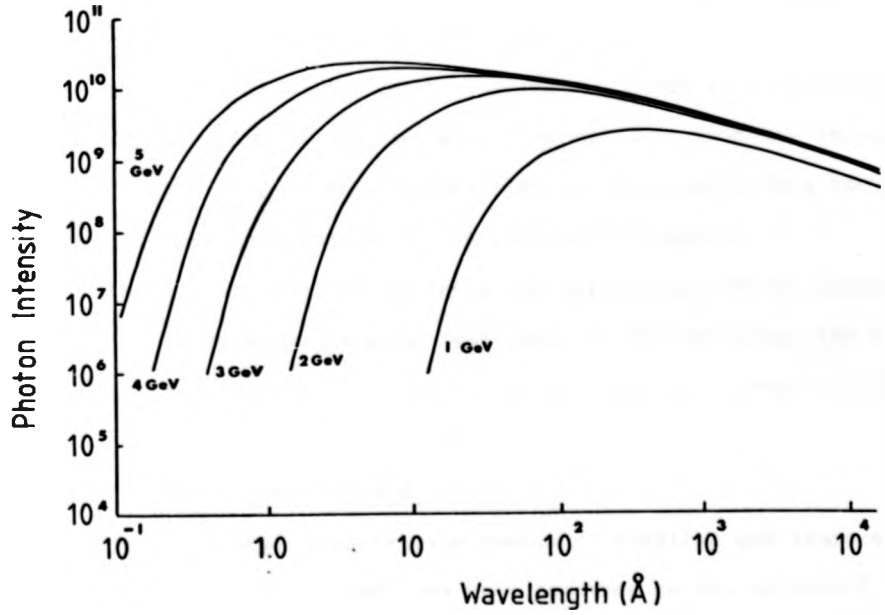

Fig. B-3: Theoretical variation of intensity of synchrotron radiation for various electron energies (Poole, 1974).

energy. Secondly, for $\lambda \ll \lambda_c$ the decrease of flux below λ is approximately exponential. The characteristic wavelength therefore governs the location of the peak of the spectrum and the cut-off.

On a plot of photon flux against actual wavelength, as shown in Fig. B-3, an increase in electron energy causes the curve to move upwards and also towards shorter wavelengths so maintaining a constant flux at a particular wavelength.

(ii) Basic Properties

(a) A continuous spectral distribution which, depending on the maximum energy of the orbiting electrons, may well extend from the infra-red (~10 eV) to the X-ray region (~80 KeV).

(b) A high intensity per wavelength range per unit solid angle.

(c) Relatively small angular size of the effective source about the tangent to the orbit.

(d) A small source size. This, coupled with the small beam divergence, provides a high source brightness.

(e) Pulse structure in the nanosecond range arising from the r.f. acceleration of the electrons and also from the injection procedure. This causes electron bunching within the ring and hence modulation of the radiated intensity.

(f) Almost complete polarization within the orbital plane. As progression is made away from the orbital plane the polarization becomes more elliptical, accompanied by a dramatic loss in intensity (see Fig. 9-1)

(iii) Compton Profile Measurements

Previous measurements on a number of metallic and ionic solids in the energy range 13-63 KeV have been reported in the authors M.Sc thesis. The results reported here at 74.3 KeV are a continuation of the earlier work, and were undertaken to allow a more complete comparison with the ^{241}Am gamma-ray technique.

The measurements were made on the NINA electron-synchrotron at the Daresbury Laboratory. Radiation emitted tangentially from the electron orbit of NINA passed along an evacuated beam pipe 42 m long which was sealed with a beryllium window. The beam was then collimated by specially fabricated, movable lead slits, to an aperture of approximately 1 cm^2. A wavelength was selected by Bragg reflection from the (111) planes of a germanium crystal which diffracted the beam downwards in a verticle plane onto a sample positioned 1.2 m away. The diffracted beam path was pinpointed with the aid of polaroid photographs and the sample and detector positioned accordingly. A short plastic pipe was fixed between the beryllium window and the sample and continuously evacuated to reduce air absorption and minimise air scattering. The Bragg angle used was 1.7° which corresponded to an energy of 74.3 KeV. Because of the small distance between the diffracted beam and the main beam (3.6 cm at 1.2 m), extensive lead shielding was built around both ends of the evacuated pipe. Polaroid photographs showed that the diffracted beam had a cross section of 2 mm by 10 mm.

The incident radiation was scattered through 155° into a Ge(Li) detector linked to a 1024 channel MCA. The calibration of the detector gave an energy per channel of 56.66 eV, indicating a FWHM for the detector of 740 eV ($\sim$0.95 a.u.) at 74.3 KeV. The poor resolution was due to the detector employed. In a measurement period of less than 24 hours, three samples (LiF, NaCl, KCl), as well as a separate background, were recorded. During the acquisition period NINA was operating at maximum energy (5 GeV) and at a mean circulating current of 10 mA.

The results obtained at 74.3 KeV are typified by the raw data illustrated in Fig. B-4 for the NaCl sample. No attempt was made to obtain a final corrected Compton profile because of the poor detector resolution, and the following discussion centres on the count rates achieved. The

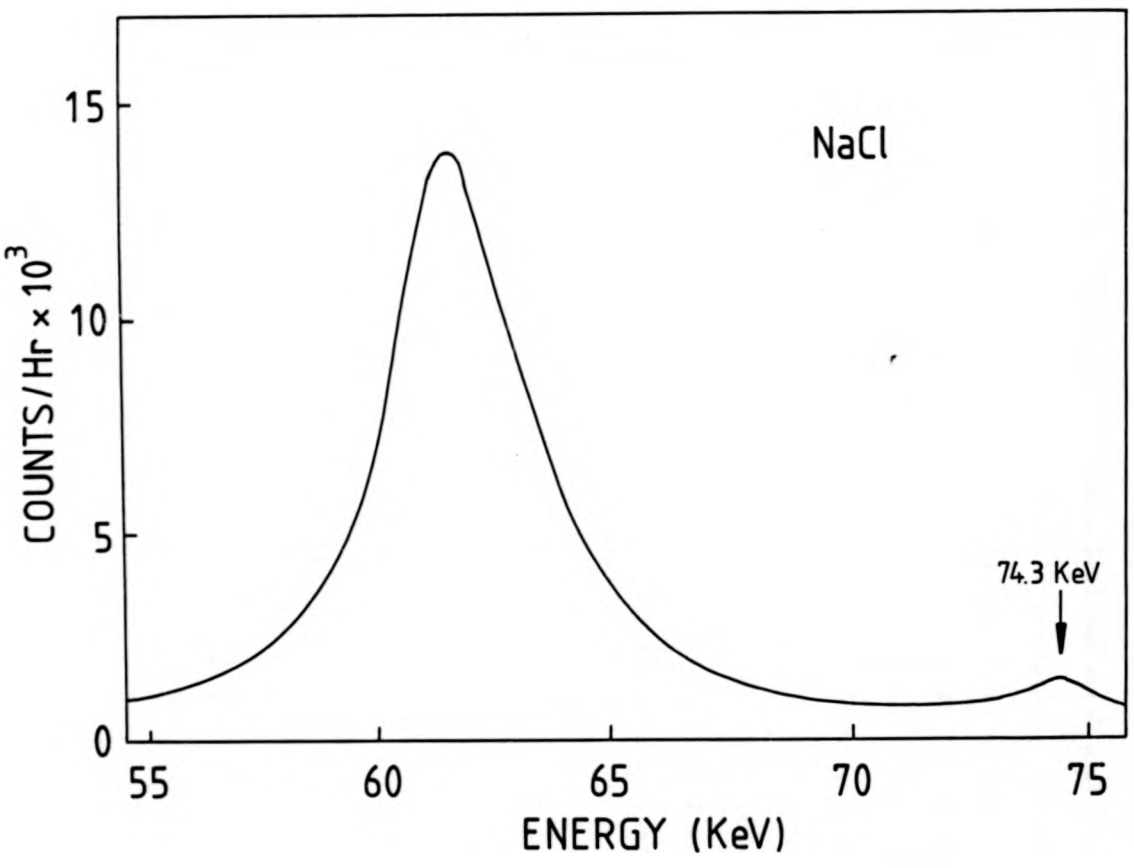

Fig. B-4: Compton scattering spectrum from a sodium chloride crystal.

experiments were carried out at some of the highest X-ray energies produced by NINA. The comparison of the synchrotron results with each other has already been given elsewhere (Cooper et. al., 1976, Holt et. al., 1978). In Chapter 9 (table 9-1) the results at 63.3 KeV have been compared to other Compton scattering techniques. The count rate at 74.3 KeV was, however, down by a factor of six on the 63.3 KeV results despite a similar signal-to-noise ratio at the Compton peak and the use of a germanium detector. It is therefore clearly evident that when NINA is operating at 5 GeV (~10 mA), the optimum energy for undertaking Compton scattering experiments is around 60 KeV, and is therefore competative with the ^{241}Am gamma-ray systems. The synchrotron technique offers real advantages in reducing the persistent problem of parasitic multiple scattering as well as obtaining data with better statistical accuracy.